
TESE DE DOUTORAMENTO

IFT-T.007/19

From micro to Macro: Particle Physics, Gravity and Cosmology

Jéssica Silvano Martins

Orientador

Prof. Dr. Rogério Rosenfeld

Co-orientador

Prof. Dr. Eduardo Pontón Bayona

Dezembro de 2019

M386f Martins, Jéssica Silvano
 From micro to macro: particle physics, gravity and cosmology / Jéssica
 Silvano Martins. – São Paulo, 2019
 149 f. : il.

 Tese (doutorado) - Universidade Estadual Paulista (Unesp), Instituto de
Física Teórica (IFT), São Paulo
 Orientador: Rogério Rosenfeld
 Coorientador: Eduardo Pontón Bayona

 1. Cosmologia. 2. Matéria escura (Astronomia). 3. Partículas (Física
nuclear). I. Título

To my family

“Yes, there is happiness to be found in the mere contemplation of the deepest mysteries.”

John Archibald Wheeler

*“Nobody ever figures out what life is all about, and it doesn’t matter. Explore the world.
Nearly everything is really interesting if you go into it deeply enough.”*

Richard P. Feynman

Agradecimentos

É injusto tentar, em apenas uma página, agradecer as pessoas que me ajudaram e me apoiaram nessa jornada até aqui. É muito difícil falar de todos, então já deixo aqui minhas desculpas aos não mencionados.

Gostaria de agradecer primeiramente a minha família por tudo que tem feito por mim nesses últimos anos, apesar da distância física. Agradeço a minha mãe, Cilineide, pelo carinho e por sempre ter me estimulado a ler e estudar; a meu pai, Jorge, por me apoiar, desde o início, a estudar Física, e por sempre ser um exemplo de determinação e ousadia; e a meu irmão, Jansen, pelos debates sobre ciência e por sempre me apoiar a seguir em frente.

Devo um agradecimento especial ao meu querido Heliudson, pois sem ele eu não sei se teria chegado até aqui. Obrigada pela paciência, carinho e por ser sempre “Yang” quando eu começava a ser “Yin” demais. Espero que ainda possamos rir muito juntos, conversar muito sobre ciência e nos aventurar pelo mundo. Afinal, o fim de uma jornada é sempre o início de outra.

Na parte acadêmica, meus estudos aprofundados na Física começaram na Universidade de Brasília, então agradeço primeiramente a seus professores, por terem sido a base dessa formação. Devo um agradecimento especial ao Prof. Dr. Arsen Melikyan, pois sua ajuda e conselhos foram de inestimável valor. Agradeço também o Instituto de Física Teórica e sua equipe de professores, por proporcionar, desde o mestrado, o suporte que eu precisava para estudar e aprender, e a CAPES, pelo auxílio financeiro sem o qual esse doutorado não poderia ter sido feito.

Aqui eu deixo um agradecimento, feliz e triste, ao Prof. Dr. Eduardo Pontón. Quando minha carreira estava sem rumo você se ofereceu para me ajudar, por mais adversas que fossem suas condições. Mesmo tendo me orientado por pouco tempo, seus ensinamentos foram profundos e me mostraram o valor de pensar mais claramente e entender tudo nos mínimos detalhes. Tenho certeza que o eco da sua, mesmo que breve, existência ainda vai reverberar por muito tempo.

Agradeço também ao Prof. Dr. Farinaldo Queiroz e ao Prof. Dr. Ilya Shapiro, por também me ajudarem quando eu precisava e se tornarem importantes colaboradores improváveis, ao me inserirem em áreas da Física até então inexploradas por mim.

Também sou grata ao meu orientador Prof. Dr. Rogério Rosenfeld por me dar liberdade de procurar outras áreas da Física com que eu tivesse mais afinidade, e a Prof. Dr. Flávia Sobreira que desde o meu mestrado me ajuda e apoia.

Por fim, agradeço a todos aqueles que direta ou indiretamente ajudaram na minha formação acadêmica.

Resumo

Nessa tese revisaremos o conteúdo de partículas do nosso Universo e sua evolução cósmica e mostraremos algumas buscas de nova física nessas áreas. Na Parte I apresentamos limites na escala de energia de nova física e acoplamentos de um possível novo bóson de calibre usando experimentos em baixas energias que envolvem a teoria electrofraca. Na Parte II nós revisamos teoria quântica de campos em espaço-tempo curvos e aplicamos alguns resultados em cosmologia na Parte III. Nessa última parte também mostramos limites na massa da matéria escura morna que podem ser obtidos a partir de catálogos de galáxias fotométricos.

Palavras Chaves: Nova física, violação de paridade, experimentos de baixas energias, cosmologia, inflação, matéria escura

Áreas do conhecimento: Física de Partículas e Cosmologia

Abstract

In this thesis we review the particle content of our Universe and its cosmic evolution and show some new physics searches in these two areas. In Part I we present bounds on the energy scale of new physics and couplings of a possible new neutral gauge boson using low energy experiments in the electroweak sector. In Part II we review quantum field theory in curved spacetime and apply some results in cosmology in Part III. In this last part we also show bounds on warm dark matter mass from photometric galaxy surveys.

Key Words: New physics, Parity Violation, low energy experiments, Cosmology, inflation, dark matter

Areas of Knowledge: Particle Physics, Cosmology

List of Figures

4.1	Diagrams of major contributions to parity violation in atoms. N labels the nucleus and e^- the atomic electrons. $A_{e,N}$ stands for an axial-vector current and $V_{e,N}$ for a vector current. (a) Z boson exchange between electron axial-vector and nucleon vector currents, the leading contribution to APV; (b) Z boson exchange between nucleon axial-vector and electron vector currents; (c) Electromagnetic interaction of atomic electrons with nucleus anapole moment, shown as a dark circle; (d) Combined effect of (a) with the hyperfine interaction.	33
4.2	Scale dependence (gray curve) of $\sin^2 \theta_W$ [1, 2] compared with measurements (colored points) from APV [3] and E158 [4] as well as the future experiments, Qweak [5, 6], P2 [7], Mesa [8], Moller [9], Solid [10], where the error bars are projected sensitivity and the points are on arbitrary positions.	35
4.3	Bound on the couplings between the electron neutrino and up-quark (f_{Vu}/Λ^2) and electron neutrino and down quark (f_{Vd}/Λ^2) as defined in Eq. (4.31). The green area is the region allowed by the COHERENT data. The CHARM constraint stems from $\nu_e - N$ inelastic scattering data [11]. The LHC bound results from missing energy searches [12]. Collectively these different data sets restrict new physics to live inside the overlapping region, which roughly implies that $ f_{Vq}^{eff}/\Lambda^2 < 10^{-6}$. See the text for details. For comparison we show with a red circle the region which is consistent with APV, which is clearly more restrictive.	38
4.4	Bounds of the experiments E158, Qweak, Moller, P2 and SoLID on the mixing between Z and Z' with respect to the mass of the new light neutral gauge boson following the relations on the table. In each plot the mixing parameter δ is changing logarithmically from $\delta = 10^{-4}$ to $\delta = 1$, so we can also visualize the dependence of ϵ with this parameter.	44
5.1	One-loop corrections to the mass of a scalar field in curved spacetime. Figure from [13].	51
5.2	One-loop corrections to the vacuum energy from a scalar field in curved spacetime. Figure from [13].	52
6.1	Cosmic Microwave Background Radiation measured by Planck satellite. It depicts the temperature variation across the background. Figure of ESA/Planck Collaboration [14].	65

6.2	SDSS map of the Universe. The Earth is in the middle of the image and each point is a galaxy. Figure from [15].	67
6.3	The horizon problem in Λ CDM model. All events that we currently observe are on our past light cone. The intersection of our past light cone with the spacelike slice labelled <i>recombination</i> corresponds to two opposite points in the observed CMB. Their past light cones don't overlap before they hit the singularity, $a_i = 0$, so the points appear never to have been in causal contact. Figure from [16].	72
6.4	The spectral index and tensor-to-scalar ratio measured by Planck using CMB data. The figure also shows several models of inflation, with n_s and r calculated with $N = 50$ and $N = 60$. TT stands for temperature power spectrum from CMB, EE the polarization spectrum and TE the temperature-polarization spectrum, BAO for baryonic acoustic oscillations and BK15 are B-mode polarization data. Figure from [17].	82
6.5	The potential $U(\chi)$ of Starobinsky inflation perturbed by non-polynomial terms, induced by scalars coupled to fermions of mass 10^{15} GeV (green, dashed) and 10^{16} GeV (blue dotted), together with the pure R^2 term (black).	88
7.1	Linear matter power spectrum at $z = 0$ inferred from different cosmological probes, together with the Λ CDM prediction in black. We can see how well the Λ CDM model fits observations. Figure from [14].	94
7.2	Fourier transform of the normalized Navarro-Frenk-White density profile, shown for some different mass values.	102
8.1	Linear matter power spectrum at $z = 0$ for WDM particle masses of $m_{\text{wdm}} = 2.0$ keV (dashed) and $m_{\text{wdm}} = 0.5$ keV (dot-dashed), together with the linear power spectrum for CDM. The vertical lines indicate the half-mode scale for each mass.	110
8.2	Jenkins mass function (first), concentration-mass parameter (second), NFW density profile (third) and Tinker halo bias (fourth) for CDM (solid lines), $m_{\text{wdm}} = 2.0$ keV (dashed) and $m_{\text{wdm}} = 0.5$ keV (dot-dashed).	112
8.3	Left: Power spectrum from Viel (dotted) and from modified Halo model (dashed) for $m_{\text{wdm}} = 0.5$ keV, together with CDM halofit (solid line) at $z=0.5$. Right: Difference between non-linear power spectrum from modified halo model for WDM particle masses of $m_{\text{wdm}} = 0.5$ keV (dashed) and $m_{\text{wdm}} = 2.0$ keV (dotted) and CDM at $z=0.5$	113
8.4	Left: C_ℓ s computed for different WDM particle masses at $z=0.5$. Right: percentage difference between C_ℓ s for $m_{\text{wdm}} = 1$ keV and CDM $= m_{\text{wdm}} = 100$ MeV.	116
8.5	Left: C_ℓ s computed at 4 different redshifts for $m_{\text{wdm}} = 0.1$ keV (Dashed lines) and CDM (Solid lines). Right: Percentage difference between C_ℓ s for $m_{\text{wdm}} = 0.1$ keV and CDM at 2 redshifts.	116

8.6	Top left: normalized likelihoods of m_{wdm}^{-1} marginalized over Ω_{m} and b_{g} . The dashed line shows the probability function for calculations done with l until 1000. We see that decreasing the non-linear regime in the computations has a great impact in error estimation (see Section 8.3). Top right: likelihood of Ω_{m} with m_{wdm}^{-1} and b_{g} marginalized. Bottom: the expected error ellipsis for Ω_{m} and m_{wdm}^{-1} with b_{g} marginalized. The light blue and dark blue curves represent a 2σ and 1σ confidence region, respectively. All plots are DES forecasts. . . .	118
8.7	Top left: normalized likelihoods of m_{wdm}^{-1} marginalized over Ω_{m} and b_{g} . Top right: likelihood of Ω_{m} with m_{wdm}^{-1} and b_{g} marginalized. Bottom: the expected error ellipse for Ω_{m} and m_{wdm}^{-1} with b_{g} marginalized. The light green and dark green curves represent a 2σ and 1σ confidence region, respectively. All plots are LSST forecasts. . . .	119
8.8	Left: Comparison between DES (blue line) and LSST (green dashed) 1σ error ellipse. Right: 1σ error ellipse for LSST (green line) and combined result with shear power spectra from EUCLID (blue dashed). . . .	119
8.9	1σ (dark red) and 2σ (light red) error ellipse for LSST using Viel non-linear fitting formula. . . .	120

Contents

Resumo	iii
Abstract	v
List of Figures	v
1 Introduction	1
I The Standard Model of Particle Physics	5
2 A Standard Model Overview	7
2.1 Lorentz group and Spinors	9
2.1.1 The (0,0) representation	10
2.1.2 The $(\frac{1}{2}, 0)$ representation	10
2.1.3 The $(0, \frac{1}{2})$ representation	10
2.1.4 The $(\frac{1}{2}, \frac{1}{2})$ representation	11
2.1.5 Dirac and Majorana spinors	11
2.2 The particle content	12
2.3 The Lagrangian	14
2.4 The Higgs Mechanism	16
2.4.1 Fermions masses	17
2.4.2 Bosons masses	18
3 Electroweak Theory	21
3.1 Charged-current of fermions interactions	21
3.2 Neutral-current of fermions interactions	23
3.3 Four fermions interaction and effective theories	24
3.4 Discrete symmetries	26
3.4.1 Parity	26
3.4.2 Charge conjugation	27
3.4.3 Time reversal	28

4	Low energy experiments	29
4.1	Atomic Parity Violation	29
4.2	Polarized Electron Scattering	32
4.3	Neutrino-Nucleus coherent scattering	34
4.4	New Physics probes from Atomic Parity Violation, Polarized Electron Scattering and Neutrino-Nucleus coherent scattering	34
4.4.1	New physics with APV	35
4.4.2	New physics with ν NCS	37
4.4.3	New physics with PeS	39
4.4.4	Models	41
4.5	Conclusions	43
II	Semiclassical Gravity	45
5	Quantization of Field Theories in Curved Spacetime	47
5.1	Einstein's gravity	48
5.2	Matter fields in curved spacetime	49
5.3	Effective action in curved spacetime	52
5.3.1	Renormalization group equations	57
5.4	Effective potential	58
5.4.1	Sterile scalar and massive fermions with Yukawa interaction	59
III	The Standard Model of Cosmology	61
6	Early Universe	63
6.1	The Friedmann-Lemaître-Robertson-Walker Universe	66
6.1.1	Friedmann equations	67
6.2	Flatness and horizon problems	71
6.3	Inflation	71
6.3.1	Inflationary observables	74
6.4	Higgs inflation	77
6.5	Starobinsky inflation	79
6.6	Starobinsky inflation with sterile scalar coupled to massive fermions	82
7	Large scale structure formation	89
7.1	Linear perturbation theory	89
7.1.1	Adiabatic perturbations	91
7.1.2	Vector perturbations	93
7.2	The matter power spectrum	93
7.3	Halo Model	96
7.3.1	Spherical Collapse	96

7.3.2	Dark matter halos properties	98
7.3.3	Structure formation with halos	102
8	Forecasts for Warm Dark Matter from photometric galaxy surveys	107
8.1	Warm dark matter and structure formation	109
8.1.1	Linear regime	109
8.1.2	Non-linear regime: Halo Model modifications for WDM	111
8.1.3	Non-linear fitting formula for WDM	112
8.2	Forecasting constraints for WDM particle mass from photometric surveys . .	113
8.2.1	Angular power spectrum	114
8.2.2	Fisher matrix analysis	115
8.2.3	Combined result with weak lensing	120
8.3	Discussion	121
9	Conclusions	123
	Bibliography	125

1

Introduction

In this thesis we will review some aspects of fundamental physics and present results of the search for new physics in three different areas. For this reason the thesis is divided in three parts, respectively, particle physics, semiclassical gravity and cosmology, and they are all connected by fundamental physics.

The first part is about particle physics. All the matter we know in the Universe is made of quanta of fundamental fields and their bound states. These fundamental building block are the fermions leptons and quarks. The matter particles can interact with each other in four different ways, three of them are the weak force, strong force and electromagnetism. These forces are also mediated by fundamental particles: the weak interaction is mediated by three gauge bosons W^+ , W^- and Z ; the strong interactions by the gluons, which are exchanged only by quarks; and electromagnetism by the photons. We also have another particle, called Higgs boson, which gives mass to the massive particles. This matter content is bound together in the Standard Model of Particle Physics.

The Standard Model fermions are chiral, and only their left-handed counterparts take place in electroweak interactions, the unified version of electromagnetism and weak force. This end up by causing parity, the spatial coordinates inversion transformation, to be violated in the electroweak sector. Parity violating low energy experiments are a good probe to search for physics beyond the Standard Model, in particular, we can compare measurements of the weak angle θ_W to the Standard Model predictions. We used Atomic Parity Violation, polarized electron scattering and neutrino-nucleus coherent scattering experiments to put bounds on the existence of a new neutral boson Z' . The motivation for searching for such extra boson lies within several Standard Model extensions that contains a new $U(1)$ gauge group and attempt to solve some issues within the Standard Model, as neutrino masses and baryogenesis.

The last chapter of Part I is strongly based on the work: *New Physics Probes: Atomic Parity Violation, Polarized Electron Scattering and Neutrino-Nucleus Coherent Scattering*, J  ssica Martins, Farinaldo S. Queiroz, Giorgio Arcadi, Manfred Lindner, arXiv:1906.04755, (in process of publication) [18].

There is another way particles can interact that is not contained in the Standard Model, which is through gravity. The attempts to treat gravity as a quantum fundamental field like the other forces still don't give reasonable results at high energies, and the best description we have of gravity is classical General Relativity, in which gravity is not a force but an effect of the spacetime geometry. However, we do know that at least matter should be made of quantum fields, which takes us to second part of the thesis.

In the second part we show general results of quantizing scalars, fermions and vector bosons in curved spacetime. To get a renormalizable theory of such fields in four-dimensions the classical, bare action should contain a non-minimal coupling between the scalar field and curvature Ricci scalar. Furthermore, the vacuum energy receives contributions from divergent quantum corrections of the matter fields that can be ignored in flat, but not in curved spacetime, as this energy interacts with the gravitational background. In order to deal with such divergences, the classical action must also contain higher-derivatives terms in the metric, besides the GR Einstein-Hilbert term. In the end of Part II we show the induced gravitational action that is generated by an sterile scalar coupled to massive fermions. These massive fermions could be beyond the Standard Model particles, like the right-handed neutrinos, and the main motivation for introducing a sterile scalar comes from cosmological inflation, and that leads us to the third and last part of the thesis.

In Part III we review the Standard Cosmological model at early and late times. In order to cure fine-tuning problems in the Universe initial conditions we can use an early inflationary era of accelerated expansion, driven by a scalar field, the inflaton. There are several models of inflation that agree with observations, one of the most natural and successful of them being Starobinsky inflation. In Section 6.6 we show that the model of a sterile scalar coupled to massive fermions in curved spacetime can drive a Starobinsky inflation with a perturbation coming from non-polynomial terms in the curvature. This section is a preliminar result of the work of J  ssica Martins, Ana Romero, Fl  via Sobreira, Ilya Shapiro and Alexei Starobinsky, to appear [19].

The quantum fluctuations of the inflaton field generate the initial perturbations on the matter density fields that at late times grow and form the structure we observe in the Universe. But this structure cannot be explained with Standard Model particles only. In order to match the observations that go from the comic microwave background radiation power spectrum to galaxies velocity rotation curves, we need much more matter. In fact, it seems that $\sim 80\%$ of the matter of the Universe is not made of the Standard Model content. This new matter can only interact very weakly with the known particles, and its effect has been seen until now only through gravitational interaction. It is also non-relativistic, and by all this "known" characteristics we named it cold dark matter.

However, despite of fitting great well the cosmological observations at large scales, the cold dark matter paradigm still faces some issues at smaller scales. When we compare cold

dark matter simulations with observational data at few Mpc, the cold dark matter scenario in general predicts more structure than we actually observe. This mismatching could be ameliorated if, instead of cold, we consider dark matter to be warm. In the last chapter of the Part III we show constraints on the warm dark matter particle mass that can be obtained using the photometric galaxy surveys DES and LSST.

This last chapter is strongly based on the work: *Forecasts for warm dark matter from photometric galaxy surveys*, J  ssica Martins, Fl  via Sobreira, Rog  rio Rosenfeld, MNRAS, Volume 481, Issue 1, November 2018, Pages 1290 – 1299 [\[20\]](#).

Then, we conclude by stating some general remarks of each work.

Part I

The Standard Model of Particle Physics

2

A Standard Model Overview

The question of what is matter had intrigued philosophers and physicists for millennia. The idea that everything we see around us is made of fundamental indivisible building blocks named atoms date from Democritus 400 BC. However, the discovery of the electron in 1897 by Thomson [21] and of the nucleus in 1911 by Rutherford [22] started to show that atoms, that were believed to be the fundamental blocks of matter, are actually made of other particles. At that time, electromagnetism and gravity were the known ways that matter could interact and electromagnetic theory was already developed consistently with special relativity. During the 20's it became clear that Nature is quantum, and all matter particles and interactions should also play by quantum mechanics rules.

The first proposal for the existence of weak interactions was in 1933 by Fermi to explain the beta decay [23], which also gave a hint on the existence of neutrinos, and a few years later it was applied to the recent discovered muon decay [24, 25]. In 1935, Yukawa developed the first theory of strong interactions [26] as a proposal for explaining the force that keeps the protons and neutrons together inside the nucleus. In the late 40's the four fundamental interactions and a bunch of particles were known, but a theory was lacking in order to combine everything in a consistent way.

Paul Dirac, in 1927, built a quantum theory for electrons using as fundamental objects, not particles, but quantum fields that live in a Minkowski spacetime [27]. It was a starting path for what later became known as quantum electrodynamics (QED), in which the electromagnetic field is also quantum. After that it became widely accepted that the fundamental constituents of matter and interactions are fields and the particles are their excitations. Another important feature of QED is that the electromagnetic interaction arises in the theory due to the invariance under local gauge transformations of the $U(1)$ group. Therefore, we

start with the electron, and the photon emerge due to gauge symmetry as a gauge boson. This became a general guiding principle to build theories: one starts with the matter content, chooses the underlying symmetries and compare the resulting interactions with Nature. Yang and Mills in 1954 [28] applied this procedure to build a gauge theory based on the non-Abelian gauge group $SU(2)$ and the result was used later in the 60's by Weinberg, Glashow, Salam and Ward [29–31] to unify the electromagnetic and weak forces into the electroweak (EW) theory, which gauge group is $SU(2) \times U(1)$. Therefore, EW theory predicted the existence of three gauge bosons related to weak forces (named Z , W^+ and W^-) and the photon. It was only in 1983 that the existence of the heavy Z and W bosons was experimentally confirmed [32, 33].

It was in 1973 that Fritzsch, Leutwyler and Gell-Mann used the $SU(3)$ gauge group to finish developing the theory of strong interactions [34] that describes quarks, which form protons, neutrons and other bound states known at the time, and have a strong charge called *color*. Because of that, the theory of strong interactions, which gauge bosons are called gluons, was named quantum chromodynamics (QCD), and it was greatly confirmed experimentally afterwards.

The predictions from QED and QCD (at high energies) were always calculated using perturbation theory. However, Oppenheimer pointed out in 1930 [35] that higher-order perturbative calculations in QED always resulted in infinite quantities, which suggested that the computational methods at the time could not deal with interactions involving photons with high momenta. It was only around 50's that a method for eliminating infinities was developed by Schwinger, Feynman, Dyson, and Tomonaga [36–42]. The main idea was to replace the initial parameters in the Lagrangian such as mass and coupling constants, which have no physical meaning, by their finite measured values. To cancel the apparently infinite parameters, one has to introduce additional, infinite, counterterms into the Lagrangian. This procedure is known as renormalization and can be applied to arbitrary order in perturbation theory. Renormalization also became a guiding principle for building theories, and a general Lagrangian should in principle contain all renormalizable operators in the given number of spacetime dimensions. Using renormalization techniques, Gross, Wilczek and Politzer showed, in 1973 [43, 44], that non-Abelian gauge theories are asymptotically free, which means that the coupling strength between quarks and gluons decreases with increasing energy. This helped to enlighten why free quarks are not seen in Nature, and it is said that QCD is confining, as it confines quarks inside bound states [45].

The last piece of the puzzle was how to give mass to the weak force mediators gauge bosons. Before detecting the weak bosons, the short-rangeness of the weak interactions were an indication that the mediators were very heavy particles. But invariance on gauge transformations forbids the inclusion of quadratic mass terms for the gauge bosons. In 1964, Higgs, Brout and Englert proposed that the gauge symmetry $SU(2)$ could be broken by a mechanism called spontaneous symmetry breaking, through which massless gauge bosons could acquire mass [46, 47]. This became known as the Higgs mechanism. Then, in 1967, Weinberg and Salam combined the electroweak theory with the Higgs mechanism [48, 49], and this theory was later proved to be renormalizable by t'Hooft [50]. The EW theory was then combined with the QCD to what is known today as the Standard Model of Particle Physics, and it is

the best description we have of what the Universe is made of and how its constituents interact. It does not contain gravity, as the gravitational force mediator, the graviton, leads to a perturbatively non-renormalizable theory [51–57]. One of the Standard Model predictions was the scalar field Higgs boson, which was observed experimentally in 2012 at the Large Hadron Collider [58, 59].

We shall now go through a quick review of the Standard Model construction in the next sections, where we show the particle content and interactions. For a more detailed view see [60–65] and references therein.

Throughout the thesis we use natural units ($M_P = 1 = \hbar$) and the Minkowski spacetime metric as $\eta_{\mu\nu} = \text{diag}(-1, 1, 1, 1)$, unless stated otherwise.

2.1 Lorentz group and Spinors

In order to build a covariant physical theory we need Lorentz invariant quantities, that is, objects that live in a Minkowski spacetime and that do not transform under the Lorentz group.

The Lorentz group is a group which transformations leave the quantity $ds^2 = -dt^2 + dx^2 + dy^2 + dz^2$ unchanged. Its proper subgroup consists of rotations in space and time directions and boosts in space directions, and it is denoted by $SO(1, 3)$. The Lorentz group is completely determined in terms of its generators and commutation relations:

$$\begin{aligned} [J_i, J_j] &= i\epsilon_{ijk}J_k, \\ [J_i, K_j] &= i\epsilon_{ijk}K_k, \\ [K_i, K_j] &= -i\epsilon_{ijk}J_k, \end{aligned} \tag{2.1}$$

where J_i , $i = \{0, 1, 2, 3\}$, are the generators of rotations and K_i of boosts. A general Lorentz transformation with boost parameter ϕ (that depends on the velocity β of the frame) and rotation parameter θ is written as

$$\Lambda = e^{i\mathbf{J}\cdot\theta + i\mathbf{K}\cdot\phi}. \tag{2.2}$$

Now, let's consider the following linear combination of the generators:

$$N_i^\pm = \frac{1}{2}(J_i \pm iK_i). \tag{2.3}$$

In terms of this generators the commutation relations become

$$\begin{aligned} [N_i^+, N_j^+] &= i\epsilon_{ijk}N_k^+, \\ [N_i^-, N_j^-] &= i\epsilon_{ijk}N_k^-, \\ [N_i^-, N_j^+] &= 0. \end{aligned} \tag{2.4}$$

This choice of generators revealed that the Lorentz group is made of two copies of $SU(2)$. Representations of $SU(2)$ are specified by a value j that can be an integer or a half-integer. Therefore, representations of the Lorentz group will be specified by the doublet (j, j') , where j corresponds to the $SU(2)$ generated by the N_i^+ and j' to the one generated by N_i^- .

2.1.1 The (0,0) representation

The smallest representation of the Lorentz group is given by $(j, j') = (0, 0)$. These are just 1×1 matrices, or scalars, and don't change under Lorentz transformations.

2.1.2 The $(\frac{1}{2}, 0)$ representation

In the representation $(\frac{1}{2}, 0)$ only the N_i^+ generators are used, therefore

$$N_i^- = \frac{1}{2}(J_i - iK_i) = 0 \Rightarrow J_i = iK_i. \quad (2.5)$$

This leads to

$$N_i^+ = iK_i = \frac{1}{2}\sigma_i, \quad (2.6)$$

where σ_i are the Pauli matrices

$$\sigma_1 = \begin{pmatrix} 0 & 1 \\ 1 & 0 \end{pmatrix}, \quad \sigma_2 = \begin{pmatrix} 0 & -i \\ i & 0 \end{pmatrix}, \quad \sigma_3 = \begin{pmatrix} 1 & 0 \\ 0 & -1 \end{pmatrix}. \quad (2.7)$$

So, the rotations and boosts generators are

$$K_i = -i\frac{1}{2}\sigma_i, \quad J_i = \frac{1}{2}\sigma_i. \quad (2.8)$$

Therefore, an object in the $(\frac{1}{2}, 0)$ representation will transform under rotations R and boosts B as,

$$R(\theta) = e^{i\theta \cdot \mathbf{J}} = e^{\frac{i}{2}\theta \cdot \sigma}, \quad (2.9)$$

$$B(\phi) = e^{i\phi \cdot \mathbf{K}} = e^{\frac{1}{2}\phi \cdot \sigma}. \quad (2.10)$$

This representation will be called left-handed spinor representation.

2.1.3 The $(0, \frac{1}{2})$ representation

Now, in the $(0, \frac{1}{2})$ representation only the N_i^- part is used, so

$$N_i^+ = \frac{1}{2}(J_i + iK_i) = 0 \Rightarrow J_i = -iK_i. \quad (2.11)$$

Then,

$$N_i^- = -iK_i = \frac{1}{2}\sigma_i. \quad (2.12)$$

So,

$$K_i = i\frac{1}{2}\sigma_i, \quad J_i = \frac{1}{2}\sigma_i. \quad (2.13)$$

Therefore, the general transformations in this representation are

$$R(\theta) = e^{i\theta \cdot \mathbf{J}} = e^{\frac{i}{2}\theta \cdot \boldsymbol{\sigma}}, \quad (2.14)$$

$$B(\phi) = e^{i\phi \cdot \mathbf{K}} = e^{-\frac{1}{2}\phi \cdot \boldsymbol{\sigma}}. \quad (2.15)$$

This representation is named right-handed spinor representation. We see that the left and right-handed representations transform identically under rotations but with a different sign under boosts.

2.1.4 The $(\frac{1}{2}, \frac{1}{2})$ representation

The $(\frac{1}{2}, \frac{1}{2})$ representation is nothing but the familiar vectors, that now will be written as 2×2 matrices. If we denote the left-handed indices transforming under N_i^+ without a dot and the right-handed indices that transform under N_i^- with a dot, we can define an object in the $(\frac{1}{2}, \frac{1}{2})$ representation as $\nu^{\dot{a}b}$. As both N_i^+ and N_i^- generators are Hermitian, we can write $\nu^{\dot{a}b}$ as

$$\nu^{\dot{a}b} = \nu^\mu \sigma_\mu^{\dot{a}b}, \quad (2.16)$$

where σ_0 is the identity matrix and $\sigma_i^{\dot{a}b}$ for $i = 1, 2, 3$ are just the Pauli matrices. The dotted and undotted indices transform separately under boosts and rotations as the right and left-handed representations

$$\nu^{\dot{a}b} \rightarrow \nu'^{\dot{c}d} = (e^{\frac{i}{2}\theta \cdot \boldsymbol{\sigma} - \frac{1}{2}\phi \cdot \boldsymbol{\sigma}})_{\dot{a}}^{\dot{c}} (e^{\frac{i}{2}\theta \cdot \boldsymbol{\sigma} + \frac{1}{2}\phi \cdot \boldsymbol{\sigma}})_b^d \nu^{\dot{a}b}. \quad (2.17)$$

2.1.5 Dirac and Majorana spinors

We can group the two left-handed and two right-handed spinors into a 4-component object. One way of doing that is through the Dirac spinor, where the two upper components transform as left-handed spinors and the last two components as right-handed spinors:

$$\psi = \begin{pmatrix} \psi_{L1} \\ \psi_{L2} \\ \psi_{R1} \\ \psi_{R2} \end{pmatrix}. \quad (2.18)$$

The Dirac spinor ψ transforms under Lorentz transformations as,

$$\psi \rightarrow \psi e^{\frac{1}{2}\omega_{\mu\nu} S^{\mu\nu}}, \quad (2.19)$$

where $\omega_{\mu\nu}$ are the parameters of the transformation and $S^{\mu\nu}$ is

$$S^{\mu\nu} = \frac{1}{4}[\gamma^\mu, \gamma^\nu], \quad (2.20)$$

where the γ^μ matrices satisfy the Clifford algebra

$$\{\gamma^\mu, \gamma^\nu\} = 2\eta^{\mu\nu}. \quad (2.21)$$

In components they read,

$$\gamma^0 = \begin{pmatrix} 0 & -i \\ -i & 0 \end{pmatrix} \equiv -i\beta, \quad \gamma_k = \begin{pmatrix} 0 & -i\sigma_k \\ i\sigma_k & 0 \end{pmatrix}. \quad (2.22)$$

It is useful to define the matrix

$$\gamma_5 = \begin{pmatrix} -I & 0 \\ 0 & I \end{pmatrix} \equiv i\gamma^0\gamma^1\gamma^2\gamma^3, \quad (2.23)$$

and we also have that

$$(\gamma^0)^2 = -1 = -(\gamma^i)^2, \quad \gamma^0\gamma_5 = -\gamma_5\gamma^0. \quad (2.24)$$

Then, we can project the left-handed or right-handed components of the Dirac spinor using the following projectors:

$$\psi_L = \frac{1}{2}(1 - \gamma_5)\psi \equiv P_L\psi = \begin{pmatrix} \psi_L \\ 0 \end{pmatrix}, \quad (2.25)$$

$$\psi_R = \frac{1}{2}(1 + \gamma_5)\psi \equiv P_R\psi = \begin{pmatrix} 0 \\ \psi_R \end{pmatrix}. \quad (2.26)$$

It is also convenient to define the Dirac conjugate of a spinor,

$$\bar{\psi} \equiv \psi^\dagger\beta, \quad (2.27)$$

so that we can form Lorentz invariant objects like $\bar{\psi}\psi$.

There is also another 4-component spinor we can work with called Majorana spinor. Its upper and lower two components are not independent

$$\psi_M = \begin{pmatrix} \xi \\ \epsilon\xi^* \end{pmatrix}, \quad (2.28)$$

where the matrix ϵ is defined as

$$\epsilon \equiv i\sigma_2 = \begin{pmatrix} 0 & 1 \\ -1 & 0 \end{pmatrix}. \quad (2.29)$$

Note that, as $\epsilon\sigma_i^* = -\sigma_i\epsilon$, the quantity $\epsilon\xi^*$ transforms as a right-handed spinor if ξ is left-handed.

Now we are ready to write the Standard Model Lagrangian and analyse the interactions of the particles in nature.

2.2 The particle content

The Standard Model of Particle Physics (SM) describes three of the four fundamental interactions. The electromagnetic, weak and strong forces are mediated by spin-one gauge

bosons, which are exchanged by the spin-half particles we use to describe matter. The symmetry gauge group of the Standard Model is $SU(3)_c \times SU(2)_L \times U(1)_Y$ and its generators are associated with the observed gauge bosons. The subscript “ c ” is to indicate that fields that transform under the $SU(3)_c$ group are charged by the quantum number called *color*. The Standard Model fermions particles are chiral, that is their right-handed and left-handed counterparts couples differently with the other SM fields, and the subscript “ L ” of $SU(2)_L$ is to indicate that only the left-handed fermions transforms under this gauge group. Finally, the subscript “ Y ” is meant to distinguish the weak hypercharge Y under the gauge group $U(1)_Y$ from the most commonly used electric charge Q from electromagnetism $U(1)_{\text{em}}$.

The gauge group $SU(3)_c$ has eight generators and the associated gauge boson are denoted as $G_\mu^\alpha(x)$, $\alpha = 1, \dots, 8$, and they are called gluons. These are the mediators of the strong force and are massless. The gauge group $SU(2)_L$ has three generators W_μ^a , $a = 1, 2, 3$ and the group $U(1)_Y$ has only one generator B_μ . Together, the four give rise to the three massive bosons mediators of the weak force, W^+ , W^- and Z , and the massless photon, A_μ .

The known matter content of our Universe is made of fundamental spin-half fermions and their interactions are characterized by the way these fermions transform under the $SU(3)_c \times SU(2)_L \times U(1)_Y$ gauge group.

The quarks take part on all interactions and form several bound states called hadrons, as the proton and the neutron. Up to date there are six known quarks, up (u), down (d), top (t), bottom (b), charm (c), strange (s), all denoted collectively as q , and they can be grouped into three generations of up-type quarks and down-type quarks that are ordered with respect to increasing particle mass:

$$\begin{aligned} u_m, & \quad u_1 = u, \quad u_2 = c, \quad u_3 = t, \\ d_m, & \quad d_1 = d, \quad d_2 = s, \quad d_3 = b. \end{aligned} \tag{2.30}$$

The left-handed counterpart of each generation of up-type quark and down-type form a doublet under the $SU(2)_L$ gauge group:

$$Q_m = \begin{pmatrix} P_L u_m \\ P_L d_m \end{pmatrix}. \tag{2.31}$$

The leptons are the fundamental matter particles that don’t take part in the strong interactions. There are six known leptons, the electron (e), the muon (μ) and the tau (τ), and their respective neutrinos, ν_e , ν_μ and ν_τ . They can also be grouped into three generations with increasing mass,

$$\begin{aligned} e_m, & \quad e_1 = e, \quad e_2 = \mu, \quad e_3 = \tau, \\ \nu_m, & \quad \nu_1 = \nu_e, \quad \nu_2 = \nu_\mu, \quad \nu_3 = \nu_\tau. \end{aligned} \tag{2.32}$$

The left-handed part of each generation of lepton with their respective neutrino also form a $SU(2)_L$ doublet:

$$L_m = \begin{pmatrix} P_L \nu_m \\ P_L e_m \end{pmatrix}. \tag{2.33}$$

There hasn't been an observation of a right-handed neutrino so far, so the right-handed leptons $P_R e$, $P_R \mu$ and $P_R \tau$ are singlets under $SU(2)_L$.

For the sake of notation, the lower case letters ($e, \mu, \tau, u, c, t, d, s, b$) are Dirac spinors. For example, the electron field is denoted as $e(x)$, which has left-handed and right-handed counterparts:

$$e = \begin{pmatrix} e_L \\ e_R \end{pmatrix}. \quad (2.34)$$

On the other hand, capital letters (L, E, D, U, Q) or script letters ($\mathcal{E}, \mathcal{U}, \mathcal{D}$) are Majorana spinors. For example, in the Standard Model lagrangian the electron is represented by two Majorana fields, $\mathcal{E}(x)$ and $E(x)$, defined as:

$$\mathcal{E} = \begin{pmatrix} e_L \\ \epsilon e_L^* \end{pmatrix}, \quad E = \begin{pmatrix} -\epsilon e_R^* \\ e_R \end{pmatrix}. \quad (2.35)$$

Such that,

$$e = P_L \mathcal{E} + P_R E. \quad (2.36)$$

The same applies to the other leptons and the quarks, so that we can write the doublets,

$$L_m = \begin{pmatrix} P_L \nu_m \\ P_L \mathcal{E} \end{pmatrix}, \quad Q_m = \begin{pmatrix} P_L \mathcal{U} \\ P_L \mathcal{D} \end{pmatrix} \quad (2.37)$$

in terms of Majorana fermions.

The standard model also contains a boson scalar field, called Higgs (ϕ), which is a doublet under the $SU(2)_L$ gauge group and has a non-trivial ground state under the symmetry $SU(2)_L \times U(1)_Y$. This happens to spontaneously break the symmetry, which allows the fermions and bosons to acquire mass in a gauge invariant way, as we will see in following sections. For sake of completeness, the Higgs field and its complex conjugate are written as:

$$\phi = \begin{pmatrix} \phi^+ \\ \phi^0 \end{pmatrix}, \quad \tilde{\phi} \equiv \begin{pmatrix} \phi^{0*} \\ -\phi^{+*} \end{pmatrix} = \epsilon \phi^*. \quad (2.38)$$

2.3 The Lagrangian

We are now in position to write the Lagrangian for the Standard Model of Particle Physics. The Lagrangian has to be invariant under Lorentz transformations and renormalizable in four dimensions. We also require it to be invariant under the gauge transformations of the group $SU(3)_c \times SU(2)_L \times U(1)_Y$. The most general Lagrangian density we can write to describe our observed matter fields, with such conditions is:

$$\mathcal{L}_{\text{SM}} = \mathcal{L}_{fg} + \mathcal{L}_{\text{Higgs}}, \quad (2.39)$$

where,

$$\begin{aligned}\mathcal{L}_{fg} = & -\frac{1}{4}G_{\mu\nu}^\alpha G^{\alpha\mu\nu} - \frac{1}{4}W_{\mu\nu}^a W^{a\mu\nu} - \frac{1}{4}B_{\mu\nu}B^{\mu\nu} - \frac{g_3^2\Theta_3}{64\pi^2}\epsilon_{\mu\nu\lambda\rho}G_{\mu\nu}^\alpha G^{\alpha\lambda\rho} \\ & - \frac{g_2^2\Theta_2}{64\pi^2}\epsilon_{\mu\nu\lambda\rho}W_{\mu\nu}^a W^{a\lambda\rho} - \frac{g_1^2\Theta_1}{64\pi^2}\epsilon_{\mu\nu\lambda\rho}B_{\mu\nu}B^{\lambda\rho} - \frac{1}{2}\bar{L}_m\not{D}L_m - \frac{1}{2}\bar{E}_m\not{D}E_m \\ & - \frac{1}{2}\bar{Q}_m\not{D}Q_m - \frac{1}{2}\bar{U}_m\not{D}U_m - \frac{1}{2}\bar{D}_m\not{D}D_m,\end{aligned}\quad (2.40)$$

in which the field-strengths of the gauge fields are given by:

$$G_{\mu\nu}^\alpha = \partial_\mu G_\nu^\alpha - \partial_\nu G_\mu^\alpha + g_3 f_{\beta\gamma}^\alpha G_\mu^\beta G_\nu^\gamma, \quad (2.41)$$

$$W_{\mu\nu}^a = \partial_\mu G_\nu^a - \partial_\nu G_\mu^a + g_2 \epsilon_{abc} W_\mu^b G_\nu^c, \quad (2.42)$$

$$B_{\mu\nu} = \partial_\mu B_\nu - \partial_\nu B_\mu. \quad (2.43)$$

We used that $\not{D} = \gamma^\mu D_\mu$, $f_{\beta\gamma}^\alpha$ are the structure constants of the $su(3)$ algebra and the covariant derivatives are,

$$D_\mu L_m = \partial_\mu L_m + \left[\frac{i}{2}g_1 B_\mu - \frac{i}{2}g_2 W_\mu^a \tau_a \right] P_L L_m + \left[-\frac{i}{2}g_1 B_\mu + \frac{i}{2}g_2 W_\mu^a \tau_a^* \right] P_R L_m, \quad (2.44)$$

$$D_\mu E_m = \partial_\mu E_m + i g_1 B_\mu (P_R E_m) - i g_1 B_\mu (P_L E_m), \quad (2.45)$$

$$\begin{aligned}D_\mu Q_m = & \partial_\mu Q_m + \left[-\frac{i}{2}g_3 G_\mu^\alpha \lambda_\alpha - \frac{i}{2}g_2 W_\mu^a \tau_a - \frac{i}{6}g_1 B_\mu \right] P_L Q_m \\ & + \left[\frac{i}{2}g_3 G_\mu^\alpha \lambda_\alpha^* + \frac{i}{2}g_2 W_\mu^a \tau_a^* + \frac{i}{6}g_1 B_\mu \right] P_R Q_m,\end{aligned}\quad (2.46)$$

$$D_\mu U_m = \partial_\mu U_m + \left[-\frac{i}{2}g_3 G_\mu^\alpha \lambda_\alpha - \frac{2i}{3}g_1 B_\mu \right] P_R U_m + \left[\frac{i}{2}g_3 G_\mu^\alpha \lambda_\alpha^* + \frac{2i}{3}g_1 B_\mu \right] P_L U_m, \quad (2.47)$$

$$D_\mu D_m = \partial_\mu D_m + \left[-\frac{i}{2}g_3 G_\mu^\alpha \lambda_\alpha + \frac{i}{3}g_1 B_\mu \right] P_R D_m + \left[\frac{i}{2}g_3 G_\mu^\alpha \lambda_\alpha^* - \frac{i}{3}g_1 B_\mu \right] P_L D_m. \quad (2.48)$$

In these equations, g_i , $i = 1, 2, 3$ are the gauge couplings, the λ_α , $\alpha = 1, \dots, 8$ are the 3×3 Gell-Mann matrices related to the $SU(3)_c$ generators T_α as $T_\alpha = \frac{1}{2}\lambda_\alpha$ [66], and τ_a are the Pauli matrices when acting on $SU(2)_L$ indices.

Finally, the Higgs Lagrangian is given by,

$$\begin{aligned}\mathcal{L}_{\text{Higgs}} = & -(D_\mu \phi)^\dagger (D^\mu \phi) - V(\phi^\dagger \phi) \\ & - \left(f_{mn} \bar{L}_m P_R E_n \phi + h_{mn} \bar{Q}_m P_R D_n \phi + g_{mn} \bar{Q}_m P_R U_n \tilde{\phi} + \text{h.c.} \right),\end{aligned}\quad (2.49)$$

where f, h, g are Yukawa couplings and,

$$V(\phi^\dagger \phi) = \lambda \left[\phi^\dagger \phi - \frac{\mu^2}{2\lambda} \right]^2. \quad (2.50)$$

is the Higgs potential allowed by renormalizability and invariance under $SU(2)_L \times U(1)_Y$. To guarantee stability of the potential λ has to be positive¹. The covariant derivative is given

¹In fact, loop quantum corrections can make the self coupling λ to run to negative values [67–71], making the electroweak minimum of the potential to become a local one. From the measured values of the top quark and Higgs mass we have today (which impact the most the running of λ) we can conclude that the Higgs potential is meta-stable, though the local minimum life-time before decaying to the unbounded region is much larger than the age of the Universe.

by,

$$D_\mu \phi = \partial_\mu \phi - \frac{i}{2} g_2 W_\mu^a \tau_a \phi - \frac{i}{2} g_1 B_\mu \phi. \quad (2.51)$$

We see that the Standard Model Lagrangian written so far has only massless particles, which is a consequence of the $SU(3)_c \times SU(2)_L \times U(1)_Y$ required invariance. However, the leptons, quarks and weak interactions mediators we observe in nature are massive. As mentioned before, the Higgs field allows mass terms for the fermions and bosons by spontaneously breaking the $SU(2)_L \times U(1)_Y$ symmetry. We shall look into that in more detail in the next section.

2.4 The Higgs Mechanism

Let's go back to the Higgs Lagrangian (2.49):

$$\begin{aligned} \mathcal{L}_{\text{Higgs}} &= -(D_\mu \phi)^\dagger (D^\mu \phi) - V(\phi^\dagger \phi) + \text{Yukawa}, \\ V(\phi^\dagger \phi) &= \lambda \left[\phi^\dagger \phi - \frac{\mu^2}{2\lambda} \right]^2. \end{aligned} \quad (2.52)$$

If $\mu^2 < 0$ the minimum of the potential is $|\phi|^2 = 0$ and we have a $SU(2)_L \times U(1)_Y$ invariant vacuum. However, if $\mu^2 > 0$ the potential is minimized by the field configuration $|\phi|^2 = \frac{\mu^2}{2\lambda}$ and the theory has an infinite number of vacuums, one for each point in the circle $|\phi|^2 = \frac{\mu^2}{2\lambda}$. So, the vacuum of the theory is not gauge invariant anymore and we say the symmetry is spontaneously broken. We can use the freedom of the local gauge groups to choose a vacuum by hand and make not only this vacuum, but also the field ϕ to be real. This is called unitary gauge and with this choice we can expand the field ϕ around its true vacuum:

$$\phi = \begin{pmatrix} 0 \\ \frac{1}{\sqrt{2}}(v + H(x)) \end{pmatrix}, \quad (2.53)$$

where the field $H(x)$ is the real scalar field representing fluctuations around the vacuum expectation value we chose as

$$v^2 \equiv \frac{\mu^2}{\lambda}. \quad (2.54)$$

The Higgs potential then becomes:

$$\begin{aligned} V &= \frac{\lambda}{4} \left[(v + H)^2 - \frac{\mu^2}{\lambda} \right]^2 \\ &= \lambda v^2 H^2 + \lambda v H^3 + \frac{\lambda}{4} H^4. \end{aligned} \quad (2.55)$$

Writing the pauli matrices explicitly we can express the covariant derivative as,

$$D_\mu \phi = \frac{1}{\sqrt{2}} \begin{pmatrix} 0 \\ \partial_\mu H \end{pmatrix} - \frac{i}{2\sqrt{2}} \begin{pmatrix} g_2 W_\mu^3 + g_1 B_\mu & g_2 W_\mu^1 - i g_2 W_\mu^2 \\ g_2 W_\mu^1 + i g_2 W_\mu^2 & -g_2 W_\mu^3 + g_1 B_\mu \end{pmatrix} \begin{pmatrix} 0 \\ v + H \end{pmatrix}, \quad (2.56)$$

so that the scalar field kinect term becomes:

$$\begin{aligned}
-(D_\mu \phi)^\dagger (D^\mu \phi) &= -\frac{1}{2} \partial_\mu H \partial^\mu H - \frac{1}{8} (v + H)^2 g_2^2 (W_\mu^1 - i W_\mu^2)(W^{1\mu} + i W^{2\mu}) \\
&\quad - \frac{1}{8} (v + H)^2 (-g_2 W^{3\mu} + g_1 B^\mu)(-g_2 W_{3\mu} + g_1 B_\mu).
\end{aligned} \tag{2.57}$$

The Yukawa couplings can be expanded in the same way:

$$\begin{aligned}
\bar{L}_m P_R E_n \phi &= \frac{1}{\sqrt{2}} \begin{pmatrix} \bar{\nu}_m \\ \bar{\mathcal{E}}_m \end{pmatrix}^T P_R E_n \begin{pmatrix} 0 \\ v + H \end{pmatrix} \\
&= \frac{1}{\sqrt{2}} (v + H) \bar{\mathcal{E}}_m P_R E_n,
\end{aligned} \tag{2.58}$$

and in a similar way for Q and D , and

$$\begin{aligned}
\bar{Q}_m P_R U_n \tilde{\phi} &= \frac{1}{\sqrt{2}} \begin{pmatrix} \bar{\mathcal{U}}_m \\ \bar{\mathcal{D}}_m \end{pmatrix}^T P_R U_n \begin{pmatrix} v + H \\ 0 \end{pmatrix} \\
&= \frac{1}{\sqrt{2}} (v + H) \bar{\mathcal{U}}_m P_R U_n.
\end{aligned} \tag{2.59}$$

Putting everything together gives the final expression for the Higgs Lagrangian:

$$\begin{aligned}
\mathcal{L}_{\text{Higgs}} &= -\frac{1}{2} \partial_\mu H \partial^\mu H - \lambda v^2 H^2 - \lambda v H^3 - \frac{\lambda}{4} H^4 \\
&\quad - \frac{1}{8} g_2^2 (v + H)^2 |W_\mu^1 - i W_\mu^2|^2 - \frac{1}{8} (v + H)^2 (-g_2 W_\mu^3 + g_1 B_\mu)^2 \\
&\quad - \frac{1}{\sqrt{2}} (v + H) [f_{mn} \bar{\mathcal{E}}_m P_R E_n + \text{h.c.}] - \frac{1}{\sqrt{2}} (v + H) [g_{mn} \bar{\mathcal{U}}_m P_R U_n + \text{h.c.}] \\
&\quad - \frac{1}{\sqrt{2}} (v + H) [h_{mn} \bar{\mathcal{D}}_m P_R D_n + \text{h.c.}].
\end{aligned} \tag{2.60}$$

2.4.1 Fermions masses

The fermion masses can be read off quite easily from the quadratic terms in the fermion fields of the Yukawa interaction part of the Lagrangian (2.60):

$$\mathcal{L} = -\frac{1}{\sqrt{2}} v (f_{mn} \bar{\mathcal{E}}_m P_R E_n + g_{mn} \bar{\mathcal{U}}_m P_R U_n + h_{mn} \bar{\mathcal{D}}_m P_R D_n + \text{h.c.}). \tag{2.61}$$

In terms of Dirac spinors e_m , d_m and u_m

$$\begin{aligned}
e_m &\equiv P_L \mathcal{E}_m + P_R E_m, \\
d_m &\equiv P_L \mathcal{D}_m + P_R D_m, \\
u_m &\equiv P_L \mathcal{U}_m + P_R U_m,
\end{aligned} \tag{2.62}$$

it has a simple form, as

$$\bar{\mathcal{E}}_m P_R E_n + \text{h.c.} = \bar{\mathcal{E}}_m P_R E_n + \bar{E}_m P_L \mathcal{E}_n = \bar{e}_m e_n, \tag{2.63}$$

and similar for the up-type quarks and down-type quarks. Then, the quadratic terms become:

$$\mathcal{L} = -\frac{1}{\sqrt{2}}v(f_{mn}\bar{e}_m e_n + g_{mn}\bar{u}_m u_n + h_{mn}\bar{d}_m d_n). \quad (2.64)$$

The mass terms induced by the Yukawa coupling between the Higgs and the fermions need not to be diagonal in the generation indices m, n in general. But they can be diagonalized if we do redefinitions of the fermions fields:

$$e_m = U_{mn}^{(e)} e'_n, \quad u_m = U_{mn}^{(u)} u'_n, \quad d_m = U_{mn}^{(d)} d'_n, \quad (2.65)$$

and then choose $U^{(e)}, U^{(u)}, U^{(d)}$ to ensure we have diagonal mass matrices in the end:

$$\begin{aligned} U_{mj}^{(e)\dagger} f_{jk} U_{kn}^{(e)} &= \text{diag}(f_e, f_\mu, f_\tau), \\ U_{mj}^{(u)\dagger} g_{jk} U_{kn}^{(u)} &= \text{diag}(g_u, g_c, g_t), \\ U_{mj}^{(d)\dagger} h_{jk} U_{kn}^{(d)} &= \text{diag}(h_d, h_s, h_b). \end{aligned} \quad (2.66)$$

The resulting mass terms then become

$$\mathcal{L} = -\frac{1}{\sqrt{2}}v(f_m\bar{e}_m e_m + g_m\bar{u}_m u_m + h_m\bar{d}_m d_m). \quad (2.67)$$

If we compare it to standard mass terms, $-m\bar{\psi}\psi$, we find the fermion masses to be:

$$m_n^{(e)} = \frac{1}{\sqrt{2}}f_n v, \quad m_n^{(u)} = \frac{1}{\sqrt{2}}g_n v, \quad m_n^{(d)} = \frac{1}{\sqrt{2}}h_n v. \quad (2.68)$$

It is worth emphasizing that all Yukawa couplings f_n, g_n and h_n are different for each fermion generation.

2.4.2 Bosons masses

The mass of the Higgs boson can be read off from the quadratic term in H of (2.60) when compared to a standard scalar field mass term of the form $-\frac{1}{2}m_H^2 H^2$, which gives

$$m_H^2 = 2\lambda v^2 = 2\mu^2. \quad (2.69)$$

Recent measurements of the Higgs mass give $M_H = 125.10 \pm 0.14$ GeV [65].

For the gauge bosons the relevant terms are:

$$\mathcal{L}_{\text{Higgs}}^{(2)b} = -\frac{1}{8}g_2^2 v^2 |W_\mu^1 - iW_\mu^2|^2 - \frac{1}{8}v^2 (-g_2 W_\mu^3 + g_1 B_\mu)^2. \quad (2.70)$$

The first term gives:

$$-\frac{1}{8}g_2^2 v^2 (W_\mu^1 W^{1\mu} + W_\mu^2 W^{2\mu}), \quad (2.71)$$

so that the bosons W_μ^1 and W_μ^2 appear only in this combination and don't mix with other fields. Therefore, their masses can be immediately found by comparing this terms to $-\frac{1}{2}M_1^2 W_\mu^1 W^{1\mu} - \frac{1}{2}M_2^2 W_\mu^2 W^{2\mu}$:

$$M_1^2 = \frac{g_2^2 v^2}{4} = M_2^2. \quad (2.72)$$

It's useful to write W_1 and W_2 as the real and imaginary parts of a complex, charged field:

$$W_\mu^\pm \equiv \frac{1}{\sqrt{2}}(W_\mu^1 \mp iW_\mu^2). \quad (2.73)$$

The mass term for such a field is

$$-M_W^2 W_\mu^+ W^{-\mu}, \quad (2.74)$$

where,

$$M_W = M_1 = M_2 = \frac{g_2 v}{2}. \quad (2.75)$$

The mass of the W bosons is measured to be $M_W = 80.363 \pm 0.020$ GeV [65].

The remaining fields appearing in Eq. (2.70), B_μ and W_μ^3 appear only in the combination

$$g_1 B_\mu - g_2 W_\mu^3. \quad (2.76)$$

Then, we can normalize this combination to write another boson field:

$$Z_\mu \equiv \frac{-g_1 B_\mu + g_2 W_\mu^3}{\sqrt{g_1^2 + g_2^2}} \quad (2.77)$$

$$\equiv W_\mu^3 \cos \theta_W - B_\mu \sin \theta_W. \quad (2.78)$$

The last equation introduces the weak-mixing angle, or Weinberg angle, θ_W , which is defined as,

$$\cos \theta_W = \frac{g_2}{\sqrt{g_1^2 + g_2^2}}, \quad (2.79)$$

$$\sin \theta_W = \frac{g_1}{\sqrt{g_1^2 + g_2^2}}. \quad (2.80)$$

The mass term with respect to this field then becomes:

$$-\frac{1}{8}v^2(g_1^2 + g_2^2)Z_\mu Z^\mu, \quad (2.81)$$

from which the mass can be read to be:

$$M_Z^2 = \frac{1}{4}(g_1^2 + g_2^2)v^2, \quad (2.82)$$

and its measured value is $M_Z = 91.1876 \pm 0.0021$ GeV [65].

The last mass eigenstate is the combination of B_μ and W_μ^3 that is orthogonal to Z_μ , which we call A_μ

$$A_\mu \equiv W_\mu^3 \sin \theta_W + B_\mu \cos \theta_W = \frac{g_1 W_\mu^3 + g_2 B_\mu}{\sqrt{g_1^2 + g_2^2}}. \quad (2.83)$$

This term doesn't appear in the Lagrangian (2.70) and therefore is a massless eigenstate. The masslessness of A_μ is related to the fact that we still have a remaining symmetry in the theory. For instance, the combination $T_3 + Y$ annihilates the vacuum:

$$(T_3 + \frac{1}{2}Y)\langle\phi\rangle_0 = \frac{1}{2} \left[\begin{pmatrix} 1 & 0 \\ 0 & -1 \end{pmatrix} + \begin{pmatrix} 1 & 0 \\ 0 & 1 \end{pmatrix} \right] \begin{pmatrix} 0 \\ \frac{v}{\sqrt{2}} \end{pmatrix} = 0 \quad (2.84)$$

where we have used that $T_3 = \frac{\tau_3}{2}$, the Higgs charge under $U(1)_Y$ is $1/2$ (as can be read off from Eq. (2.51)) and we denoted as $\langle\phi\rangle_0$ the Higgs vacuum expectation value.

The combination $Q \equiv T_3 + Y$ is what we call electric charge and its associated symmetry is unbroken even if $v \neq 0$. Thus, we started with the gauge symmetry $SU(2)_L \times U(1)_Y$ that got spontaneously broken by the Higgs vev , and we are left with the electromagnetic gauge invariance, $U(1)_{\text{em}}$. As Q is the electric charge, the field A_μ is expected to have the same couplings as the usual photon.

The gluons remain massless as the Higgs field does not transform under the $SU(3)_c$ gauge group, and thus it left this symmetry intact.

The neutrinos masses in the Standard Model are also identically zero, as we cannot introduce their masses in the same way we did for the other leptons because this would require a right-handed neutrino, which has not been observed so far. But, we observe neutrino oscillations (change of flavor during propagation) [72–74], and the most simple explanation for this phenomena would be that neutrinos have mass. The simplest way to include neutrino masses would be to extend the Standard Model to include right-handed neutrinos, N_m , singlet under $SU(3)_c \times SU(2)_L \times U(1)_Y$. This would allow another Yukawa coupling between L and N like $j_{mn} \bar{L}_m P_R N_n \phi$. As not forbidden, we could also include a mass term for the right-handed neutrinos of the form $m_m \bar{N}_m N_m$. In principle, such right-handed neutrinos could exist and be very heavy [75].

3

Electroweak Theory

The Standard Model Lagrangian contains several interactions between the particle spectrum. For the Higgs field we have cubic and quartic self interactions; couplings of the form HWW , $HHWW$, HZZ , $HHZZ$ with the W^+ , W^- and Z bosons; and Yukawa interactions with all the twelve Standard Model fermions. Concerning strong interactions, we have gluons self-coupling and interactions between the gluons and all the quarks. We also have self interactions between the electroweak bosons, like $WW\gamma$, WWZ , $WWWW$, $WWZZ$, $WW\gamma\gamma$ and $WWZ\gamma$. We won't discuss in more detail these interactions and for the rest of the work we turn our attention only to the electroweak sector with fermions interactions.

3.1 Charged-current of fermions interactions

The couplings between the gauge fields W_μ^a and B_μ and the fermions arise from the fermions kinetic terms in Eq. (2.40):

$$\mathcal{L} = -\frac{1}{2}\bar{L}_m \not{D} L_m - \frac{1}{2}\bar{E}_m \not{D} E_m - \frac{1}{2}\bar{Q}_m \not{D} Q_m - \frac{1}{2}\bar{U}_m \not{D} U_m - \frac{1}{2}\bar{D}_m \not{D} D_m. \quad (3.1)$$

As these interactions always involve the projection operators P_L and P_R , we can replace the Majorana fermions by the Dirac fermions. After writing the explicit form of each covariant

derivative, the Lagrangian takes the form:

$$\begin{aligned}\mathcal{L}_{\text{ew}} = & \frac{i}{4} \begin{pmatrix} \bar{\nu}_m & \bar{e}_m \end{pmatrix} \gamma^\mu P_L \begin{pmatrix} -g_1 B_\mu + g_2 W_\mu^3 & g_2(W_\mu^1 - iW_\mu^2) \\ g_2(W_\mu^1 + iW_\mu^2) & -g_1 B_\mu - g_2 W_\mu^3 \end{pmatrix} \begin{pmatrix} \nu_m \\ e_m \end{pmatrix} \\ & + \frac{i}{4} \begin{pmatrix} \bar{u}_m & \bar{d}_m \end{pmatrix} \gamma^\mu P_L \begin{pmatrix} \frac{1}{3}g_1 B_\mu + g_2 W_\mu^3 & g_2(W_\mu^1 - iW_\mu^2) \\ g_2(W_\mu^1 + iW_\mu^2) & \frac{1}{3}g_1 B_\mu - g_2 W_\mu^3 \end{pmatrix} \begin{pmatrix} u_m \\ d_m \end{pmatrix} \\ & + \frac{i}{3} g_1 B_\mu \bar{u}_m \gamma^\mu P_R u_m - \frac{i}{6} g_1 B_\mu \bar{d}_m \gamma^\mu P_R d_m - \frac{i}{2} g_1 B_\mu \bar{e}_m \gamma^\mu P_R e_m + \text{h.c.}\end{aligned}\quad (3.2)$$

Remembering that we defined $W_\mu^\pm \equiv \frac{1}{\sqrt{2}}(W_\mu^1 \mp iW_\mu^2)$, we can easily see from the Lagrangian the couplings between the fermions and the charged bosons W^+ and W^- . These couplings are called *charged-current* interactions and are given by:

$$\mathcal{L}_{\text{cc}} = \frac{ig_2}{2\sqrt{2}} \left[W_\mu^+ (\bar{\nu}_m \gamma^\mu P_L e_m + \bar{u}_m \gamma^\mu P_L d_m) + W_\mu^- (\bar{e}_m \gamma^\mu P_L \nu_m + \bar{d}_m \gamma^\mu P_L u_m) \right]. \quad (3.3)$$

Notice, however, that this Lagrangian is diagonal in the generation indices the way we had in Eq. (2.40) before doing the field redefinitions in Eq. (2.65) to get a diagonal mass term. To see how the charged-current are in the mass basis we have to do the field redefinitions (2.65) here as well:

$$\mathcal{L}_{\text{cc}} = \frac{ig_2}{2\sqrt{2}} [W_\mu^+ (\bar{\nu}'_m \gamma^\mu P_L e'_m + \bar{u}'_m U_{mk}^{(u)\dagger} \gamma^\mu P_L U_{kn}^{(d)} d'_m) \quad (3.4)$$

$$+ W_\mu^- (\bar{e}'_m \gamma^\mu P_L \nu'_m + \bar{d}'_m U_{mk}^{(d)\dagger} \gamma^\mu P_L U_{kn}^{(u)\dagger} u'_m)]. \quad (3.5)$$

Defining,

$$V_{mn} = (U^{(u)\dagger} U^{(d)})_{mn}, \quad (3.6)$$

introducing the parameter e_W ,

$$e_W \equiv \frac{g_2}{2\sqrt{2}}, \quad (3.7)$$

and dropping the primes on the fields, we find the charged-current interaction in the mass basis:

$$\mathcal{L}_{\text{cc}} = ie_W [W_\mu^+ (\bar{\nu}_m \gamma^\mu (1 - \gamma_5) e_m + V_{mn} \bar{u}_m \gamma^\mu (1 - \gamma_5) d_m) \quad (3.8)$$

$$+ W_\mu^- (\bar{e}_m \gamma^\mu (1 - \gamma_5) \nu_m + V_{mn}^\dagger \bar{d}_m \gamma^\mu (1 - \gamma_5) u_m)]. \quad (3.9)$$

The matrix V_{mn} is a 3×3 unitary matrix called Cabbibo-Kobayashi-Maskawa (CKM)-matrix. Its arguments depend on physical parameters that have to be measured experimentally [65].

It is useful to define:

$$J_\mu^+ = i \bar{\nu}_m \gamma^\mu (1 - \gamma_5) e_m + i V_{mn} \bar{u}_m \gamma^\mu (1 - \gamma_5) d_n, \quad (3.10)$$

$$J_\mu^- = i \bar{e}_m \gamma^\mu (1 - \gamma_5) \nu_m + i V_{mn}^\dagger \bar{d}_m \gamma^\mu (1 - \gamma_5) u_n, \quad (3.11)$$

so that,

$$\mathcal{L}_{\text{cc}} = e_W [W_\mu^+ J_\mu^+ + W_\mu^- J_\mu^-]. \quad (3.12)$$

3.2 Neutral-current of fermions interactions

To analyse the couplings of the fermions to the B_μ and W_μ^3 bosons is useful to rewrite Eq. (3.2) as

$$\begin{aligned}\mathcal{L}_{\text{ew}} = & \frac{1}{2} \begin{pmatrix} \bar{\nu}_m & \bar{e}_m \end{pmatrix} \gamma_\mu P_L \begin{pmatrix} i g_1 B_\mu Y_L + i g_2 W_\mu^3 T_3 & \frac{1}{2} i g_2 (W_\mu^1 - i W_\mu^2) \\ \frac{1}{2} i g_2 (W_\mu^1 + i W_\mu^2) & i g_1 B_\mu Y_L + i g_2 W_\mu^3 T_3 \end{pmatrix} \begin{pmatrix} \nu_m \\ e_m \end{pmatrix} \\ & + \frac{1}{2} \begin{pmatrix} \bar{u}_m & \bar{d}_m \end{pmatrix} \gamma_\mu P_L \begin{pmatrix} i g_1 B_\mu Y_L + \frac{1}{2} i g_2 W_\mu^3 T_3 & \frac{1}{2} i g_2 (W_\mu^1 - i W_\mu^2) \\ \frac{1}{2} i g_2 (W_\mu^1 + i W_\mu^2) & i g_1 B_\mu Y_L + i g_2 W_\mu^3 T_3 \end{pmatrix} \begin{pmatrix} u_m \\ d_m \end{pmatrix} \\ & + \frac{i}{2} g_1 B_\mu Y_R \bar{u}_m \gamma^\mu P_R u_m + \frac{i}{2} g_1 B_\mu Y_R \bar{d}_m \gamma^\mu P_R d_m + \frac{i}{2} g_1 B_\mu Y_R \bar{e}_m \gamma^\mu P_R e_m + \text{h.c.} \end{aligned} \quad (3.13)$$

where T_3 is the charge under the $SU(2)_L$ generator $T_3 = \tau_3/2$ and Y_L is the hypercharge of the left-handed fermion and Y_R of the right-handed one. For the right-handed fermions the electric charge is the same as the hypercharge, as $T_3 = 0$ for this particles. So, $T_3 + Y_L = Q = Y_R$. We see that the interactions of the fermions with the B_μ and W_μ^3 bosons is flavor-diagonal and can be rewritten more simply as,

$$\mathcal{L}_{\text{nc}} = \sum_f [\bar{f} \gamma^\mu P_L (i g_2 W_\mu^3 T_3 + i g_1 B_\mu Y_L) f + \bar{f} \gamma^\mu P_R (i g_1 B_\mu Y_R) f]. \quad (3.14)$$

We can use that,

$$\begin{pmatrix} W_\mu^3 \\ B_\mu \end{pmatrix} = \begin{pmatrix} \cos \theta_W & \sin \theta_W \\ -\sin \theta_W & \cos \theta_W \end{pmatrix} \begin{pmatrix} Z_\mu \\ A_\mu \end{pmatrix}, \quad (3.15)$$

to work out the expression in Eq. (3.14) we shall define J_μ :

$$\begin{aligned}J_\mu & \equiv P_L g_2 W_\mu^3 T_3 + P_L g_1 B_\mu Y_L + P_R g_1 B_\mu Y_R \\ & = P_L g_2 W_\mu^3 T_3 + P_L g_1 B_\mu (Q - T_3) + P_R g_1 B_\mu Q \\ & = T_3 P_L [g_2 (Z_\mu \cos \theta_W + A_\mu \sin \theta_W) - g_1 (A_\mu \cos \theta_W - Z_\mu \sin \theta_W)] \\ & \quad + g_1 (A_\mu \cos \theta_W - Z_\mu \sin \theta_W) Q. \end{aligned} \quad (3.16)$$

We can simplify this expression using relations among the coupling constants:

$$g_2 = \cos \theta_W \sqrt{g_1^2 + g_2^2}, \quad g_1 = \sin \theta_W \sqrt{g_1^2 + g_2^2}, \quad (3.17)$$

so that

$$g_1 \cos \theta_W = g_2 \sin \theta_W \equiv e, \quad (3.18)$$

and

$$g_2 \cos \theta_W + g_1 \sin \theta_W = \sqrt{g_1^2 + g_2^2} = \frac{e}{\sin \theta_W \cos \theta_W}. \quad (3.19)$$

Using this relations in J_μ we have,

$$J_\mu = \frac{e}{\sin \theta_W \cos \theta_W} [T_3 P_L - Q \sin^2 \theta_W] Z_\mu + e Q A_\mu. \quad (3.20)$$

Plugging it back on Eq. (3.14) gives,

$$\mathcal{L}_{\text{nc}} = \sum_f i \bar{f} \gamma^\mu \left(\frac{e}{\sin \theta_W \cos \theta_W} [T_3 P_L - Q \sin^2 \theta_W] Z_\mu + e Q A_\mu \right) f. \quad (3.21)$$

We can read off from this Lagrangian the photon-fermion coupling as being,

$$\mathcal{L}_{\text{em}} = e J_{\text{em}}^\mu A_\mu, \quad J_{\text{em}}^\mu = i Q \sum_f \bar{f} \gamma^\mu f. \quad (3.22)$$

where the sum is taken over all fermion types but the neutrino, which is electrically neutral. We see that e indeed plays the role of electromagnetic coupling constant.

The remaining coupling, with the Z_μ boson, is given by

$$\mathcal{L}_{\text{nc}} = \frac{ie}{\sin \theta_W \cos \theta_W} \sum_f Z_\mu \bar{f} \gamma^\mu [T_3 P_L - Q \sin^2 \theta_W] f, \quad (3.23)$$

and is called *neutral-current* of fermions interactions. We can write it also as

$$\mathcal{L}_{\text{nc}} = \frac{ie}{\sin \theta_W \cos \theta_W} \sum_f Z_\mu \bar{f} \gamma^\mu [g_V - \gamma_5 g_A] f, \quad (3.24)$$

where we defined

$$g_V = \frac{1}{2} T_3 - Q \sin^2 \theta_W, \quad g_A = \frac{1}{2} T_3. \quad (3.25)$$

Introducing,

$$J_\mu^3 = i \sum_f \bar{f} \gamma^\mu T_3 \left(\frac{1 - \gamma_5}{2} \right) f, \quad (3.26)$$

so that,

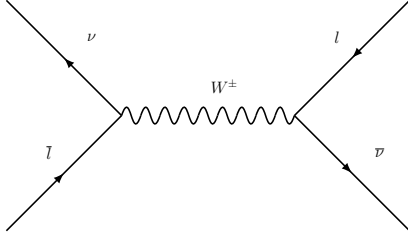
$$J_\mu^Z = J_\mu^3 - \sin^2 \theta_W J_\mu^{\text{em}}, \quad (3.27)$$

we get for all weak interactions Lagrangian:

$$\mathcal{L}_{\text{in}} = e_W [W_\mu^+ J_\mu^+ + W_\mu^- J_\mu^-] + \frac{e}{\sin \theta_W \cos \theta_W} Z_\mu J_\mu^Z + e A_\mu J_\mu^{\text{em}}. \quad (3.28)$$

3.3 Four fermions interaction and effective theories

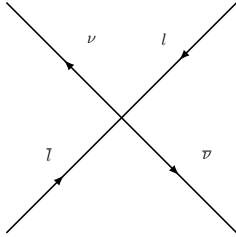
Several years before having an electroweak theory, physicists could already give very accurate predictions of the weak interactions phenomena. Low energy measurements gave indications that the bosons W and Z should be very heavy, and also indicated that the theory of weak interactions should involve vector currents like $\bar{\psi} \gamma^\mu \psi$ and axial vector currents such as $\bar{\psi} \gamma^\mu \gamma_5 \psi$. The description of low energy interactions between leptons was achieved with the non-renormalizable 4-fermion theory. To find the 4-fermion theory we will do a top-down approach and compute the leptons weak interactions at three level:



The diagram shows a lepton line (l) and a neutrino line (ν) interacting via a W boson (W±) exchange. The lepton line enters from the bottom left and exits from the top right. The neutrino line enters from the top left and exits from the bottom right. A wavy line representing the W boson connects the two vertices. The label W± is placed above the wavy line.

$$\sim e_W^2 (\bar{e}_m \gamma_\mu (1 - \gamma_5) \nu_m) \times \frac{-i \left(\eta^{\mu\nu} - \frac{p^\mu p^\nu}{m_W^2} \right)}{p^2 - m_W^2} (\bar{\nu}_m \gamma_\nu (1 - \gamma_5) e_m) \quad (3.29)$$

At the low energy regime $p^2 \ll m_W^2$, so we can approximate the exchange of a boson by a local four fermions interaction:



The diagram shows a contact interaction between a lepton line (l) and a neutrino line (ν). The lepton line enters from the bottom left and exits from the top right. The neutrino line enters from the top left and exits from the bottom right. The two lines cross each other at a central point, representing a local interaction.

$$\sim -\frac{e_W^2}{m_W^2} [(\bar{e}_m \gamma^\mu (1 - \gamma_5) \nu_m) \times (\bar{\nu}_m \gamma_\mu (1 - \gamma_5) e_m)] \quad (3.30)$$

We can also define the quantity

$$\frac{G_F}{\sqrt{2}} = \frac{e_W^2}{m_W^2} = \frac{g_2^2}{8m_W^2} = \frac{1}{2v^2}. \quad (3.31)$$

G_F can be inferred by experiments to be $G_F = 1.166 \times 10^{-5} \text{ GeV}^{-2}$ [65] and from its value we find the electroweak vev to be

$$v = 247 \text{ GeV}. \quad (3.32)$$

We could have done the same analysis for a Z boson exchange between leptons and quarks in the low energy limit and we would find the same G_F . Therefore, G_F works as a low energy universal coupling strength between leptons and quarks. Hence, the full 4-Fermi theory can be written as

$$\mathcal{L}_{4F} = -\frac{G_F}{\sqrt{2}} \left[J_\mu^+ J^{-\mu} + 8(J_\mu^Z)^2 \right]. \quad (3.33)$$

This is a complete description of the electroweak interactions when the interacting particles have energies much smaller than the boson masses. It is an example of an effective field theory (EFT) and it is valid up to $\approx 80 \text{ GeV}$ (W^\pm mass). Beyond this energy scale contributions coming from the boson propagator start becoming important and we have to correct our Lagrangian. Formally, to build an EFT we have to integrate out all heavy degrees of freedom of the theory and in the end we will be left with the low energy ones and free parameters that have to be fixed by experimental measurements. In this way we are able to explore and

make predictions about low energy physics without having to worry about what happens in the UV. This is a very useful tool in physics, and in fact all theories we have to describe nature are effective theories, as we still don't have a complete consistent description of all fundamental interactions and matter that is valid in all energy scales.

3.4 Discrete symmetries

The Standard Model is built with the continuous gauge symmetries $SU(3)_c$, $SU(2)_L$ and $U(1)_Y$ and is important to keep track of continuous global symmetries, as they are associated with conserved quantities. But there are also three important discrete transformations that arise in a general relativistic quantum mechanical system. They are the space and time inversions, that are improper Lorentz transformations, and charge conjugation, that transforms a particle into its antiparticle. These are presented in the following subsections. For a more detailed discussion, see [76–78].

3.4.1 Parity

The unitary parity transformation, \mathcal{P} , inverts all spatial coordinates, and consequently the momenta, by reflecting through the origin:

$$\mathcal{P}\psi(\vec{r}) = \psi(-\vec{r}). \quad (3.34)$$

Applying parity operation twice makes you go back to the original state, so $\mathcal{P}^2 = 1$.

We say that a wavefunction is even if $\mathcal{P}\psi(\vec{r}) = \psi(\vec{r})$, and it is odd if $\mathcal{P}\psi(\vec{r}) = -\psi(\vec{r})$. In spherical polar coordinates, $(r, \theta, \phi) \rightarrow (r, \pi - \theta, \pi + \phi)$ under a parity transformation, and for a wavefunction that depends on a product of a radial function $f(r)$ and the spherical harmonics $Y_l^m(\theta, \phi)$ we have,

$$\mathcal{P}\psi(r, \theta, \phi) = (-1)^l \psi(r, \theta, \phi), \quad (3.35)$$

where l is the orbital angular momentum. Then, a parity of some state will depend on the parity of its constituents.

It is interesting to see how parity is greatly connected to handedness. For instance, let us consider the two sets of transformation laws for the left and right-handed spinors under the Lorentz group Eqs. (2.10),(2.15). We saw that these transformations are different only for the boosts equation. Let's take first the left-handed boosts transformations:

$$B(\phi) = e^{\frac{1}{2}\phi \cdot \sigma} \quad (3.36)$$

The angles of the Lorentz boosts are related to the frame speed, and under parity they all change by a minus sign. Then, we have

$$\mathcal{P}B(\phi) = \mathcal{P}e^{\frac{1}{2}\phi_x\sigma_x + \frac{1}{2}\phi_y\sigma_y + \frac{1}{2}\phi_z\sigma_z} = e^{-\frac{1}{2}\phi_x\sigma_x - \frac{1}{2}\phi_y\sigma_y - \frac{1}{2}\phi_z\sigma_z} = e^{-\frac{1}{2}\phi \cdot \sigma}. \quad (3.37)$$

Comparing these with the boosts transformations for the right-handed spinors in Eq. (2.15) we see that they are exactly the same. Therefore, parity transforms left-handed into right-handed spinors. For a Dirac fermion with left and right-handed components $\psi = \begin{pmatrix} \psi_L \\ \psi_R \end{pmatrix}$ is easy to see that the same transformation can be achieved by multiplying the fermion by the matrix:

$$\mathcal{P} \equiv \begin{pmatrix} 0 & I \\ I & 0 \end{pmatrix}, \quad \mathcal{P}\psi = \begin{pmatrix} \psi_R \\ \psi_L \end{pmatrix}. \quad (3.38)$$

Notice that this matrix is exactly the same we defined before as $\beta = i\gamma^0$.

Now we can see that some interactions we have found before in the Standard Model violate parity, more precisely the electroweak interactions. For instance, let's consider the quantities $j_V^\mu \equiv \bar{\psi}\gamma^\mu\psi$ and $j_A^\mu \equiv \bar{\psi}\gamma^\mu\gamma_5\psi$ and see how they transform under parity. We know that, $\mathcal{P}\psi \equiv \psi' = i\gamma^0\psi$, and therefore,

$$\bar{\psi}' = \overline{i\gamma^0\psi} = (\psi^\dagger\gamma^0(-i))i\gamma^0 = \psi^\dagger. \quad (3.39)$$

Then, we have

$$\bar{\psi}'\gamma^\mu\psi' = \psi^\dagger\gamma^\mu i\gamma^0\psi = \begin{cases} \bar{\psi}\gamma^0\psi, & \mu = 0 \\ -\bar{\psi}\gamma^i\psi, & \mu = i \end{cases} \quad (3.40)$$

where we have used that $\gamma^i\gamma^0 = -\gamma^0\gamma^i$. Thus, j_V^μ behaves as a normal vector as only its spatial part changes under parity. Now, for $\bar{\psi}\gamma^\mu\gamma_5\psi$, since $\gamma_5\gamma^0 = -\gamma^0\gamma_5$, we have

$$\bar{\psi}'\gamma^\mu\gamma_5\psi' = -\psi^\dagger i\gamma^\mu\gamma^0\gamma_5\psi = \begin{cases} -\bar{\psi}\gamma^0\gamma_5\psi, & \mu = 0 \\ +\bar{\psi}\gamma^i\gamma_5\psi, & \mu = i \end{cases} \quad (3.41)$$

which changes in the opposite way of a vector, and the spatial components don't change sign under a parity transformation. This structure is called pseudo-vector, or axial-vector. A term of this type appears in the charged and neutral-currents (3.24), which causes the electroweak interactions to violate parity. More precisely, it is the mixture of vector and axial-vector terms that causes parity violation. When calculating the amplitude of weak interaction processes like Eq. (3.29) or the 4-fermion interaction Eq. (3.30) one roughly gets $\sim j_V^\mu j_{\mu V} + j_A^\mu j_{\mu A} - 2j_V^\mu j_{\mu A}$, and under parity this transforms to $\sim j_V^\mu j_{\mu V} + j_A^\mu j_{\mu A} + 2j_V^\mu j_{\mu A}$, so the amplitude is not invariant under parity.

The parity violation effect was observed in nature for the first time by Wu et al. in 1957 in the beta decay of Co^{60} [79], in which almost all electrons are emitted with the same angle with respect to the nucleus angular momentum.

3.4.2 Charge conjugation

Charge conjugation is the discrete symmetry that changes a particle by its anti-particle. It reverses the sign of the particle's charge, not only electric, but magnetic moment, color,

hypercharge, baryon and lepton number. If a particle has no quantum number, then it is its own anti-particle. Like the parity operator, the charge operator obeys $C^2 = 1$ and can be represented by the charge conjugation matrix.

$$C = \begin{pmatrix} -\epsilon & 0 \\ 0 & \epsilon \end{pmatrix} = \gamma^2 \beta. \quad (3.42)$$

Then,

$$C^\dagger = -C, \quad C\beta = -\beta C, \quad C\gamma_5 = \gamma_5 C. \quad (3.43)$$

3.4.3 Time reversal

Time reversal is the act of reversing the time coordinate $t \rightarrow -t$. This leaves the positions of all particles unchanged but reverses their motions and spins $p \rightarrow -p$, $J \rightarrow -J$.

In general these discrete symmetries may be individually violated by Standard Model interactions, but the *CPT* theorem [80–82] states that all quantum field theories must be invariant under the three combined. It also enables us to relate combinations of two discrete symmetries in terms of the others:

$$CP \leftrightarrow T, \quad CT \leftrightarrow P, \quad PT \leftrightarrow C. \quad (3.44)$$

4

Low energy experiments

In general when comes to the subject of getting precision measurements of particle physics predictions and its parameters one usually thinks that the higher the energy we can probe (the energy we use to smash poor particles against each other in huge colliders) the better, but this is not always the case.

Low energy experiments can lead to very precise values of some of the Standard Model parameters, like the $\sin \theta_W$. Comparison of these precise measurements with what the Standard Model predicts allows us to say something about physics beyond the Standard Model. In the next sections we will review examples of such low energy experiments, namely atomic parity violation, neutrino-nucleus scattering and polarized electron scattering, and then present bounds on the existence of a new neutral boson by using measurements of the $\sin \theta_W$. For extense reviews on the low energy experiments, see [83–88].

This chapter is based on the work [18].

4.1 Atomic Parity Violation

For decades it was assumed that the laws of nature preserved parity, but the seminal paper of Lee and Yang in 1956 gave rise to a different perspective [89]. This was indeed confirmed in 1957 in the realm of weak interactions, via the beta decay in Cobalt [79] and muon decay [90]. In 1959 the possibility of observing parity violation in atomic physics, which involves a Z boson exchange as the atom stays stable with the same particles, was contemplated by Zeldovich [91] for the Hydrogen atom, but he concluded that the effect was too small to be of experimental significance. To see why, let's consider the left-right asymmetry A_{LR} that arises from the interference between an odd contribution under space

reflections coming from the amplitude of processes with a Z exchange, A_W , and an amplitude from electromagnetic processes, A_{em} , in electric dipole transitions in the atom, defined as:

$$A_{LR} = \frac{P_L - P_R}{P_L + P_R}, \quad (4.1)$$

where, for $P_{L,R} = |A_{em} \pm A_W|^2$ we have,

$$A_{LR} = 2Re \left(\frac{A_W^{odd}}{A_{em}} \right), \quad (4.2)$$

where A^{odd} denotes an odd parity amplitude. If q is the four-momentum transfer between the lepton and the hadron, A_{em} and A_W are given, respectively, by

$$A_{em} \propto \frac{e^2}{q^2}, \quad A_W \propto \frac{g^2}{q^2 + M_Z^2}. \quad (4.3)$$

For atoms, we expect q to be of the order of the Bohr radius $q \sim \hbar/m_e\alpha$, so we arrive in an estimate for the left-right asymmetry:

$$A_{LR} \sim \alpha^2 \frac{m_e^2}{m_Z^2} \sim 10^{-15}. \quad (4.4)$$

This estimation, though naive, seemed to give no hope for the observation of such an effect. But further investigations in the late 70's by the Bouchiat and others [92–95] showed that there is in fact an enhancement on the atomic parity violation (APV) on heavy atoms, of order Z^3 [96]. Since then, the APV has been successfully observed in Pb, Tl, Yb and Cs, where the parity violating effects are enhanced by a factor of $10^5 - 10^6$ over those of hydrogen atoms, by detection of radiation emitted by these atoms in frequencies associated to transitions forbidden by electromagnetic interactions only.

To write down the interaction Hamiltonian for APV processes, let's first write the parity violating terms of the effective Lagrangian (3.33), with a Z boson interaction,

$$\begin{aligned} -\mathcal{L}_{\text{eff}}^{\text{PV}} = \frac{8G_F}{\sqrt{2}} & \left[\frac{1}{2} \bar{e} \gamma^\mu T_{3e} e \left(-\frac{1}{2} \bar{q} \gamma_\mu \gamma_5 T_{3q} q \right) - \frac{1}{2} \bar{e} \gamma^\mu \gamma_5 T_{3e} e \left(\frac{1}{2} \bar{q} \gamma_\mu T_{3q} q \right) \right. \\ & \left. - \frac{1}{2} \bar{e} \gamma^\mu \gamma_5 T_{3e} e (-\bar{q} \gamma_\mu Q_q \sin^2 \theta_W q) + \frac{1}{2} \bar{e} \gamma^\mu Q_e \sin^2 \theta_W e \bar{q} \gamma_\mu \gamma_5 T_{3q} q \right], \end{aligned} \quad (4.5)$$

which simplifies to,

$$\begin{aligned} -\mathcal{L}_{\text{eff}}^{\text{PV}} = \frac{8G_F}{\sqrt{2}} & \left[-\frac{1}{2} \bar{e} \gamma^\mu e \left(\frac{T_{3e}}{2} - Q_e \sin^2 \theta_W \right) \bar{q} \gamma_\mu \gamma_5 q T_{3q} \right. \\ & \left. - \frac{1}{2} \bar{e} \gamma^\mu \gamma_5 T_{3e} e \left(\frac{T_{3q}}{2} - Q_q \sin^2 \theta_W \right) \bar{q} \gamma_\mu q \right]. \end{aligned} \quad (4.6)$$

Taking $T_{3e} = -1/2$, $Q_e = -1$, $T_{3u} = 1/2$, $Q_u = 2/3$, $T_{3d} = -1/2$, $Q_d = -1/3$, as the values of the charges of the electron, up and down quarks, we find,

$$\begin{aligned}
-\mathcal{L}_{\text{eff}}^{\text{PV}} = \frac{8G_F}{\sqrt{2}} & \left[-\frac{1}{2} \bar{e} \gamma^\mu e \left(-\frac{1}{4} + \sin^2 \theta_W \right) \bar{u} \gamma_\mu \gamma_5 u \left(\frac{1}{2} \right) \right. \\
& - \frac{1}{2} \bar{e} \gamma^\mu \gamma_5 e \left(-\frac{1}{2} \right) \left(\frac{1}{4} - \frac{2}{3} \sin^2 \theta_W \right) \bar{u} \gamma_\mu u \\
& - \frac{1}{2} \bar{e} \gamma^\mu e \left(-\frac{1}{4} + \sin^2 \theta_W \right) \bar{d} \gamma_\mu \gamma_5 d \left(-\frac{1}{2} \right) \\
& \left. - \frac{1}{2} \bar{e} \gamma^\mu \gamma_5 e \left(-\frac{1}{2} \right) \left(-\frac{1}{4} + \frac{1}{3} \sin^2 \theta_W \right) \bar{d} \gamma_\mu d \right]. \quad (4.7)
\end{aligned}$$

As the quantity $\sin^2 \theta_W \simeq 1/4$, we see that the second and fourth terms are dominating, i.e. Z boson exchange between the electron axial-vector and nucleon vector currents. Using this expression we can write the interaction Hamiltonian as

$$H_{\text{eff}}^{\text{PV}} \Big|_{\text{int}} = \frac{2G_F}{\sqrt{2}} \sum_q (C_q^{(1)} \bar{e} \gamma_\mu \gamma_5 \bar{q} \gamma^\mu q + C_q^{(2)} \bar{e} \gamma_\mu e \bar{q} \gamma^\mu \gamma_5 q), \quad (4.8)$$

where the interactions and constants can be further combined into couplings to protons and neutrons inside the nucleus:

$$C_p^{(1,2)} = 2C_u^{(1,2)} + C_d^{(1,2)}, \quad (4.9)$$

$$C_n^{(1,2)} = C_u^{(1,2)} + 2C_d^{(1,2)}. \quad (4.10)$$

In terms of the Weinberg angle θ_W the couplings are written as

$$C_u^{(1)} = \frac{1}{4} - \frac{2}{3} \sin^2 \theta_W, \quad C_u^{(2)} = \frac{1}{4} - \sin^2 \theta_W, \quad (4.11)$$

$$C_d^{(1)} = -\frac{1}{4} + \frac{1}{3} \sin^2 \theta_W, \quad C_d^{(2)} = -\frac{1}{4} + \sin^2 \theta_W. \quad (4.12)$$

Therefore,

$$C_p^{(1)} = \frac{1}{4} (1 - 4 \sin^2 \theta_W), \quad (4.13)$$

$$C_n^{(1)} = -\frac{1}{4}, \quad (4.14)$$

$$C_p^{(2)} = -C_n^{(2)} = \frac{1}{4} - \sin^2 \theta_W. \quad (4.15)$$

To work out the dominant term of the Hamiltonian (4.8) we need to define the weak charge, Q_W^{SM} , which is an analogous of the electromagnetic charge, but with the Z boson playing the role of mediator between the atomic electron and nucleus interactions instead. Q_W^{SM} is the sum of the weak charges of all constituents of the atomic nucleus, $Q_W^{\text{SM}} = (2Z + N)Q_W(u) + (Z + 2N)Q_W(d)$, where N is the number of neutrons and Z the number of protons (not to be confused with the Z boson) inside the nucleus. Therefore,

$$ZC_p^{(1)} + NC_n^{(1)} = \frac{1}{4} (Z(1 - 4 \sin^2 \theta_W) - N) \equiv \frac{1}{4} Q_W^{\text{SM}}. \quad (4.16)$$

up to radiative corrections. Then, we see that a precise measurement of the weak charge ($\sin^2 \theta_W$) and a comparison to theoretical predictions can be used to constrain new physics using APV.

We want to write down a Hamiltonian that describes electrons subject to a potential sourced by a heavy nucleus. To do that let's step back and remember that in the non-relativistic regime, after a Fourier transform the propagator of the Z boson becomes,

$$\frac{1}{m_Z^2 - q^2} \rightarrow \frac{e^{-m_Z |\vec{r}|}}{4\pi |\vec{r}|} = \frac{1}{m_Z^2} \frac{m_Z^2 e^{-m_Z |\vec{r}|}}{4\pi |\vec{r}|}, \quad (4.17)$$

and when $m_Z^2 \rightarrow \infty$ we get,

$$\frac{1}{m_Z^2} \frac{m_Z^2 e^{-m_Z |\vec{r}|}}{4\pi |\vec{r}|} \rightarrow \frac{\delta(\vec{r})}{m_Z^2}. \quad (4.18)$$

Therefore, the Hamiltonian for the dominant electron axial-vector nucleus vector current interaction is

$$H_{\text{eff}}^{\text{PV}_{dom}} \Big|_{\text{int}} = \frac{G_F}{2\sqrt{2}} Q_W^{\text{SM}} e^\dagger \gamma_5 e \delta(r). \quad (4.19)$$

The sub-leading contributions to the parity violation Hamiltonian depend on the nucleus spin and can be parametrized as [97]

$$H_{\text{eff}}^{\text{PV}_{sub}} \Big|_{\text{int}} = \frac{G_F}{\sqrt{2}} (\eta_{\text{axial}} + \eta_{\text{NAM}} + \eta_{\text{hf}}) (\alpha \cdot \mathbf{I}) \rho(r), \quad (4.20)$$

where η_{axial} comes from the axial-vector nucleus and electron vector current interaction; η_{NAM} parametrizes the nuclear anapole moment, that is, the exchange of a Z boson between quarks inside the nucleus; η_{hf} comes from the hyperfine interaction; $\alpha = \gamma_0 \gamma^i$, \mathbf{I} is the nuclear spin and $\rho(r)$ the nuclear density.

All the parity violating interactions for an atom are illustrated by the diagrams in Figure (4.1).

4.2 Polarized Electron Scattering

Another parity violation observable that also constitutes an important laboratory to new physics searches is the polarized electron scattering (PeS) [98]. In these experiments a beam of polarized electrons is scattered by a steady target like a hadron and, as the electrons in a polarized beam have their spin aligned with the direction of motion, part of the electrons behave as left-handed and part as right-handed fermions. Again, the left-right asymmetry due to the weak interactions is the key observable. It describes the relative difference between scattering cross sections with right-handed electrons σ_R and left-handed electrons σ_L . The cross sections, in turn, can be calculated using the effective 4-Fermi Lagrangian Eq. (3.33) and the parity violating terms will be the same as in the APV case. For deep inelastic scattering

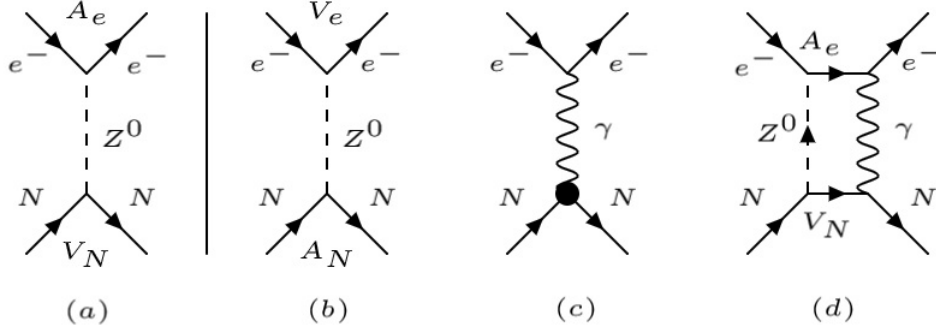


Figure 4.1: Diagrams of major contributions to parity violation in atoms. N labels the nucleus and e^- the atomic electrons. $A_{e,N}$ stands for an axial-vector current and $V_{e,N}$ for a vector current. (a) Z boson exchange between electron axial-vector and nucleon vector currents, the leading contribution to APV; (b) Z boson exchange between nucleon axial-vector and electron vector currents; (c) Electromagnetic interaction of atomic electrons with nucleus anapole moment, shown as a dark circle; (d) Combined effect of (a) with the hyperfine interaction.

processes of the type $e_{L,R}N \rightarrow eX$, the left-right asymmetry can be expressed, in the quark model and in the limit of zero nucleon mass, in a relatively simple form¹

$$A_{LR} = \frac{\sigma_L - \sigma_R}{\sigma_L + \sigma_R} \approx -\frac{G_F Q^2}{4\sqrt{2}\pi\alpha} [a_1(x)Y_1(x) + a_2(x)Y_2(x)], \quad (4.21)$$

where Q is the four-momentum of the mediator particle, the coefficients a_1, a_2 depends on the axial-vector coupling between the electron and quarks, which depend on $\sin^2 \theta_W$, $Y_{1,2}(x)$ are kinematic functions of the fraction energy transfer x from the electron to the hadrons and α is the fine-structure constant. Detailed expressions for a_1, a_2 and $Y_{1,2}$ can be found, for example, in [99, 100].

Thus, a measurement of A_{LR} translates into a measurement of $\sin^2 \theta_W$ at a given momentum Q . It is well-known that photon exchange diagrams conserve parity but processes mediated by the Z do not, since the latter does not interact with left-handed and right-handed fermions in the same way. In a similar vein, eventual additional massive vector bosons from new physics models might also contribute to the left-right asymmetry. Therefore, if the measurement of A_{LR} , in other words, $\sin^2 \theta_W$, agrees with the Standard Model prediction one can use this information to constrain new physics effects that induce parity violation and hence contribute to the left-right asymmetry. We can parametrize the new physics contributions to A_{LR} by a shift on $\sin^2 \theta_W$ and consequently constrain new physics effects (see e.g. [1, 2, 101, 102] for a previous analysis along this line).

¹In the case of electron positron scattering or the so-called Moeller scattering (scattering of electrons), the Q^2 dependence of the asymmetry is more complicated and is parametrized by a form factor.

4.3 Neutrino-Nucleus coherent scattering

The aforementioned observables depend on the interactions between electrons and quarks. Hence they lead to relevant bounds on the corresponding couplings. That has been the whole story up to now, but with the observation of neutrino-nucleus coherent scattering new information came into light [103]. Strictly speaking, neutrino-nucleus coherent scattering (ν NCS) and parity violation probes are sensitive to different interactions, the former between electron and quarks, the latter between neutrinos and quarks. Nevertheless, using $SU(2)$ invariance, one can potentially correlate the signal in neutrino-nucleus coherent scattering to the one appearing in parity violation observables. In other words, they are complementary to one another.

The ν NCS is the process by which a neutrino interacts with a nucleus and the nucleus recoils as a whole. The initial and final states are identical, though the process happens through the exchange of a Z boson. Such scattering can be calculated from the Lagrangian (3.33) for neutrino-quarks interaction through the neutral-current:

$$\mathcal{L}_{\nu-q} = -\frac{8G_F}{\sqrt{2}} [\bar{\nu}\gamma^\mu(g_V^\nu - \gamma_5 g_A^\nu)\nu] [\bar{u}\gamma^\mu(g_V^u - \gamma_5 g_A^u)u + \bar{d}\gamma^\mu(g_V^d - \gamma_5 g_A^d)d]. \quad (4.22)$$

We show in Figure 4.2 an illustration of the expected energy scale dependence of $\sin^2 \theta_W$ (see e.g. [1, 2] for details) together with different measurements of $\sin^2 \theta_W$ see also [102].

In the next section we will present new physics bounds from APV, electron scattering and neutrino-nucleus scattering. We will carry out this study using effective field theory and later concentrate on vector mediators. We highlight that this work adds to the previous ones done in the literature because instead of focusing on one observable we explore the complementarity between ν NCS, APV and polarized electron scattering. Moreover, we apply our findings to existing models in the literature.

4.4 New Physics probes from Atomic Parity Violation, Polarized Electron Scattering and Neutrino-Nucleus coherent scattering

New physics parity violation effects can be described through effective field theory, with the Lagrangian discussed before for the Standard Model, plus a possible new effect [104, 105],

$$\begin{aligned} -\mathcal{L}_{\text{eff}}^{\text{PV}} &= \frac{2G_F}{\sqrt{2}} \bar{e}\gamma^\mu\gamma^5 e \left[\left(\frac{1}{4} - \frac{2}{3} \sin^2 \theta_W \right) \bar{u}\gamma_\mu u + \left(-\frac{1}{4} + \frac{1}{3} \sin^2 \theta_W \right) \bar{d}\gamma_\mu d \right] \\ &\quad + \frac{1}{\Lambda^2} \bar{e}\gamma^\mu\gamma^5 e \left[f_{V_u} \bar{u}\gamma_\mu u + f_{V_d} \bar{d}\gamma_\mu d \right], \end{aligned} \quad (4.23)$$

where we encode the new physics effects with three parameters namely, Λ which represents a new energy scale, and the couplings f_{V_u} and f_{V_d} that quantify how new physics interact with electrons and quarks.

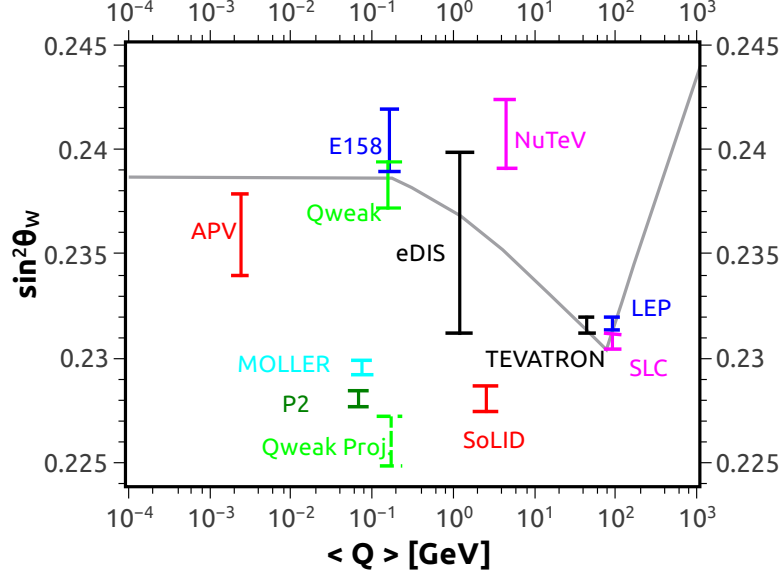


Figure 4.2: Scale dependence (gray curve) of $\sin^2 \theta_W$ [1, 2] compared with measurements (colored points) from APV [3] and E158 [4] as well as the future experiments, Qweak [5, 6], P2 [7], Mesa [8], Moller [9], Solid [10], where the error bars are projected sensitivity and the points are on arbitrary positions.

Now we can link effective field theory approach to new physics to atomic parity violation.

4.4.1 New physics with APV

In order to relate parity violation to APV, we need to define the weak charge of a nucleus which enters into the Hamiltonian of the electron field [105]. This weak charge, Q_W^{eff} is the sum of both Standard Model and new physics contributions. The former was defined in Eq. (4.16):

$$Q_W^{\text{SM}} = (Z(1 - 4 \sin^2 \theta_W) - N). \quad (4.24)$$

In analogy we can define a new physics contribution by combining the couplings of the vector currents:

$$\begin{aligned} Q_W^{\text{NP}} &= Z \left(2 \frac{f_{Vu}}{\Lambda^2} + \frac{f_{Vd}}{\Lambda^2} \right) + N \left(\frac{f_{Vu}}{\Lambda^2} + 2 \frac{f_{Vd}}{\Lambda^2} \right) \\ &= \frac{3}{\Lambda^2} f_{Vq}^{\text{eff}} (Z + N), \end{aligned} \quad (4.25)$$

where the effective coupling is defined as,

$$f_{Vq}^{\text{eff}} = \frac{f_{Vu}(2Z + N) + f_{Vd}(Z + 2N)}{3(Z + N)}. \quad (4.26)$$

Hence, we can write an effective Hamiltonian in terms of the new effective charge. By doing an analogous calculation as we did in Eqs. (4.17 - 4.19) we arrive that the effective Hamiltonian describing Atomic Parity Violation can be written in terms of the weak charge of the nucleus as:

$$\begin{aligned}
H_{\text{eff}}^{PV} \Big|_{\text{int}} &= -\mathcal{L}_{\text{eff}}^{PV} \Big|_{\text{int}} \\
&= e^\dagger \gamma^5 e \left[\frac{G_F}{2\sqrt{2}} Q_W^{\text{SM}} + \frac{3}{\Lambda^2} f_{Vq}^{\text{eff}}(Z+N) \right] \delta(r) \\
&= e^\dagger \gamma^5 e \frac{G_F}{2\sqrt{2}} \left[Q_W^{\text{SM}} + \frac{2\sqrt{2}}{G_F} Q_W^{\text{NP}} \right] \delta(r) \\
&= e^\dagger \gamma^5 e \frac{G_F}{2\sqrt{2}} Q_W^{\text{eff}}(Z, N) \delta(r).
\end{aligned} \tag{4.27}$$

We can define the variation of the effective charge, with respect to the SM expectation, as:

$$\Delta Q_W = Q_W^{\text{eff}} - Q_W^{\text{SM}} = \frac{2\sqrt{2}}{G_F} \frac{3}{\Lambda^2} f_{Vq}^{\text{eff}}(Z+N). \tag{4.28}$$

This should be compatible with experimental observation. But to compare the observations with a prediction one has to do very precise theoretical calculations of the atomic structure. As the effect of APV is larger in heavier atoms this can be quite challenging. That is why the Cesium atom is a perfect candidate for measuring APV, as it has a heavy Xe-like core with only one valence electron, which makes the calculations easier. At the moment, by transitions on stable isotope $^{133}_{78}\text{Cs}$, we can determine the following bound, at 90% confidence level:

$$|\Delta Q_W| < |Q_W^{\text{exp}} - Q_W^{\text{th}}| = 0.23. \tag{4.29}$$

Inserting $G_F = 1.17 \times 10^{-5} \text{ GeV}^{-2}$, $Z = 55$, $N = 78$, we constrain the ratio effective coupling over the energy scale,

$$\frac{f_{Vq}^{\text{eff}}}{\Lambda^2} < 2.38 \times 10^{-9} \text{ GeV}^{-2}. \tag{4.30}$$

The EFT description illustrated above is valid as long as the new degrees of freedom associated to the New Physics scale Λ are heavy with respect to the typical energy/momentum transfer of parity violation experiments, the simplest option being $\Lambda \equiv m_{Z'}$ with Z' being a new spin-1 boson (we will briefly illustrate some concrete models in section (4.4.4)). If this is not the case, namely $m_{Z'} \lesssim 100 \text{ MeV}$ [105], atomic parity violation effects are damped by a form factor $K(m'_{Z'}) < 1$, which should be included in Eq. (4.28), accounting for the propagator of the new boson. We will not consider explicitly this case here. An effective complementary probe for light bosons is represented by polarized electron scattering. Before discussing this we will compare bounds from APV with the ones stemming from neutrino-nucleus coherent scattering.

4.4.2 New physics with ν NCS

The Lagrangian that dictates the APV discussion, Eq. (4.23), has the form $\bar{e}\gamma_\mu\gamma_5 e\bar{q}\gamma_\mu q$ with $q = u, d$. From $SU(2)$ invariance, whatever new physics that interacts with electrons should also interact with neutrinos. Therefore we can write the effective Lagrangian:

$$-\mathcal{L}_{\text{eff}} = \frac{f'_{Vu}}{\Lambda^2}(\bar{\nu}_L\gamma^\mu\nu_L)(\bar{u}\gamma_\mu u) + \frac{f'_{Vd}}{\Lambda^2}(\bar{\nu}_L\gamma^\mu\nu_L)(\bar{d}\gamma_\mu d), \quad (4.31)$$

which can provide a microscopic description of neutrino-nucleus scattering processes. The latter can be probed, for example, by the COHERENT experiment [106–108]. Given the agreement with the Standard Model prediction we can use the COHERENT data to constrain new physics effects. In the EFT framework under consideration this constraint can be expressed through the following relation [109, 110]:

$$Z(g_p^V + 2\epsilon_{Vu} + \epsilon_{Vd}) + N(g_n^V + \epsilon_{Vu} + 2\epsilon_{Vd}) = \pm(Zg_p^V + Ng_n^V), \quad (4.32)$$

where $g_{p,n}^V$ are the couplings of the SM Z -boson with the proton and the neutron:

$$g_p^V = \left(\frac{1}{2} - 2\sin^2\theta_W\right), \quad g_n^V = -\frac{1}{2}, \quad (4.33)$$

while:

$$\epsilon_{Vu} = \frac{\sqrt{2}}{G_F} \frac{f'_{Vu}}{\Lambda^2}, \quad \epsilon_{Vd} = \frac{\sqrt{2}}{G_F} \frac{f'_{Vd}}{\Lambda^2}. \quad (4.34)$$

This equation is solved for:

$$\epsilon_{Vu} = -\frac{A+N}{A+Z}\epsilon_{Vd}, \quad (4.35)$$

or

$$\epsilon_{Vu} = -\frac{A+N}{A+Z}\epsilon_{Vd} - \frac{2(Zg_p^V + Ng_n^V)}{A+Z}. \quad (4.36)$$

Consequently, the allowed regions from the COHERENT data would appear as linear band in the bidimensional plane $\left(\frac{f'_{Vd}}{\Lambda^2}, \frac{f'_{Vu}}{\Lambda^2}\right)$. Assuming, for simplicity, $f'_{Vu} = f_{Vu}$, $f'_{Vd} = f_{Vd}$, we can compare the sensitivity of the coherent experiments with APV. This kind of comparison is shown in Figure (4.3). The green area is the allowed region in the f_{Vu} vs f_{Vd} plane [110].

We remark again that the solution illustrated above is valid as long as the new physics scale Λ is sensitively above the typical momentum transfer q in the neutrino scattering processes. If this is not the case one should explicitly consider the new BSM mediator of the interactions between neutrinos and SM quarks and hence consider the following redefinition:

$$\frac{\sqrt{2}}{G_F} \frac{f'_{Vq}}{\Lambda^2} \rightarrow \frac{\sqrt{2}}{G_F} \frac{f'_{Vq}}{m_{Z'}^2 + q^2}, \quad (4.37)$$

where f'_{Vq} should be now interpreted as the product of the couplings of the mediator with neutrinos and up/down quarks.

In order to compare the sensitivity of ν NCS and APV, we need to compute f_{Vq}^{eff} , as defined in Eq. (4.26) with $N = 78$ and $Z = 55$. The APV observable is related to the coupling

between electrons and quarks. Assuming, for simplicity, that the couplings in Eq. (4.31) are equal to the ones responsible for APV, we can pick the pairs f_{Vu}, f_{Vd} inside the overlapping region in Fig. (4.3). The green band delimits the region allowed by the COHERENT data, whereas the blue one comes from the CHARM experiment based on the observation of $\nu_e - N$ inelastic scattering [11]. The LHC bound results from missing energy searches [12]. Collectively these different data sets restrict new physics to live inside the overlapping region, which roughly implies that $|f_{V_q}^{eff}/\Lambda^2| < 10^{-6}$. Therefore, if couplings involved in APV and neutrino-nucleus coherent scattering processes for some reason are similar, APV clearly constitutes a more promising probe. Be that as it may, we emphasize that the couplings involved in these processes can be quite different depending on the model.

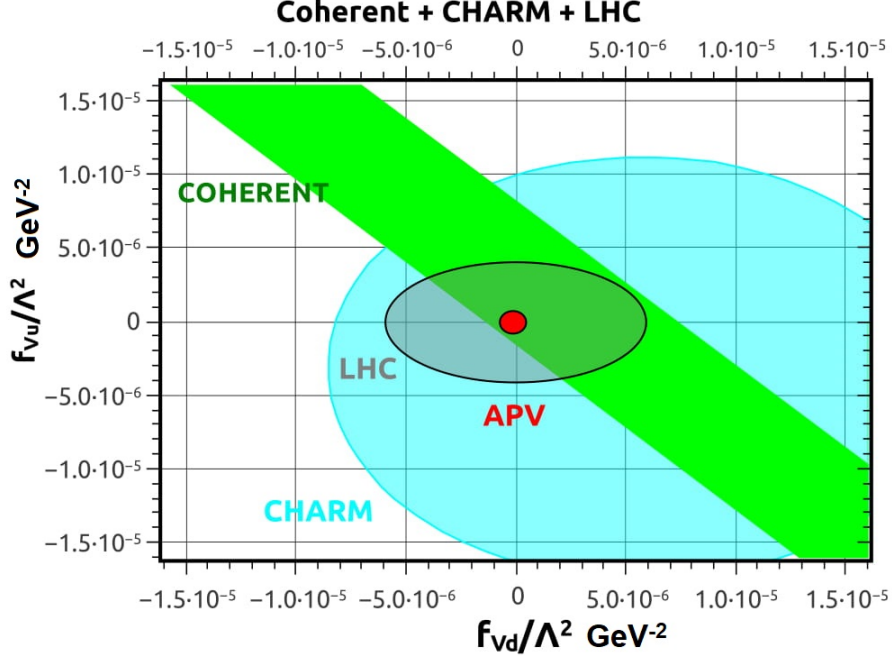


Figure 4.3: Bound on the couplings between the electron neutrino and up-quark (f_{Vu}/Λ^2) and electron neutrino and down quark (f_{Vd}/Λ^2) as defined in Eq. (4.31). The green area is the region allowed by the COHERENT data. The CHARM constraint stems from $\nu_e - N$ inelastic scattering data [11]. The LHC bound results from missing energy searches [12]. Collectively these different data sets restrict new physics to live inside the overlapping region, which roughly implies that $|f_{V_q}^{eff}/\Lambda^2| < 10^{-6}$. See the text for details. For comparison we show with a red circle the region which is consistent with APV, which is clearly more restrictive.

Anyway, it is exciting to see that COHERENT, a 14 kg detector, can already place important bounds on new physics. This fact has triggered several new physics sensitivity studies using COHERENT data and other nuclei [111–113, 113–122]. There are upcoming experiments that aim at probing ν NCS at different energies and precision which will be certainly important to improve the overall sensitivity to new physics [123–125].

We have parametrized the new physics effect in terms of the effective couplings and the energy scale Λ . This parametrization is valid in the regime which the new physics scale is much heavier than the typical energy scale involved. However, new physics can also appear as light mediators (Z') with masses much below the Z mass and light mediators alter the Standard Model prediction for $\sin\theta_W$ at low energies. The deviation can be observed using polarized electron scattering as we explore below.

4.4.3 New physics with PeS

Atomic Parity Violation is an important probe to test new physics, but if new physics surface at low energy polarized electron scattering becomes an ideal laboratory, specially in the presence of kinetic and mass mixing terms between the Z and Z' gauge boson. Indeed, low energy scattering of polarized electrons on electrons and other targets are very sensitive to parity violation effects at low energy, and consequently to the presence of light mediators. In other words, they are very sensitive to the parity violation effects that are proportional to $1 - 4\sin^2\theta_W$, and in this way constrain $\sin\theta_W$. Generally, additional parity violation sources rise from both kinetic and mass $Z - Z'$ mixings. The former originates from a Lagrangian term of the form:

$$\mathcal{L} \supset \frac{\epsilon}{2\cos\theta_W} B^{\mu\nu} Z'_{\mu\nu}. \quad (4.38)$$

For what concern mass mixing we will adopt a generic parametrization of the form:

$$M^2 = \begin{pmatrix} m_Z^2 & -\delta m_Z m_{Z'} \\ -\delta m_Z m_{Z'} & m_{Z'}^2 \end{pmatrix}, \quad (4.39)$$

where $0 \leq \delta < 1$, if the Z' is light compared to Z we can write,

$$M^2 = \begin{pmatrix} 1 & -\epsilon_Z \\ -\epsilon_Z & \frac{m_{Z'}^2}{m_Z^2} \end{pmatrix} m_Z^2, \quad (4.40)$$

with

$$\epsilon_Z = \delta \frac{m_{Z'}}{m_Z}. \quad (4.41)$$

The cross-term (4.38) can be rotated away leading to the following redefinition of the Z and photon fields:

$$\begin{aligned} A_\mu &\rightarrow A_\mu + \epsilon Z'_\mu, \\ Z_\mu &\rightarrow Z_\mu - \epsilon \tan\theta_W Z'_\mu, \end{aligned} \quad (4.42)$$

inducing, in turn, the following interactions for the Z' boson:

$$\mathcal{L} = - \left(e\epsilon J_\mu^{\text{em}} - \frac{g}{2\cos\theta_W} \epsilon_Z J_\mu^Z \right) Z'^\mu. \quad (4.43)$$

These terms induce weak currents that can be accounted for by redefining the $\sin\theta_W$ as [126, 127],

$$\sin^2\theta_W \rightarrow \kappa_d \sin^2\theta_W, \quad \kappa_d = 1 - \frac{\epsilon}{\epsilon_Z} \delta^2 \frac{\cos\theta_W}{\sin\theta_W} f(Q^2/m_{Z'}^2), \quad (4.44)$$

where $f(Q^2/m_{Z'}^2)$ is the propagator effect given by [128–131],

$$f(Q^2/m_{Z'}^2) = \frac{1}{1 + Q^2/m_{Z'}^2}. \quad (4.45)$$

Using equations (4.44) and (4.45) we can write the change of the weak angle due to the mixing between Z and Z' as,

$$\Delta \sin^2 \theta_W \simeq -0.42\epsilon\delta \frac{m_Z}{m_{Z'}} f(Q^2/m_{Z'}^2), \quad (4.46)$$

and so we can put bounds on the mixing ϵ given the difference between measurements and prediction of the weak angle,

$$\begin{aligned} \epsilon^2 &\simeq \frac{5.67}{\delta^2} (\Delta \sin^2 \theta_W)^2 \left(\frac{m_{Z'}}{m_Z} \right)^2 (1 + Q^2/m_{Z'}^2)^2 \\ &\simeq \frac{5.67}{\delta^2} (\Delta \sin^2 \theta_W)^2 \left(\frac{m_{Z'}^2 + Q^2}{m_Z m_{Z'}} \right)^2. \end{aligned} \quad (4.47)$$

The bounds obtained using the existing and expected precision in the measurement of $\sin^2(\theta_W)$ by some future experiments are written in the Table 4.1. From Table 4.1 we notice that the bounds on ϵ become stronger for large values of δ which accounts for the mass mixing. We exhibited these bounds for several values of δ in Figure (4.4). Since the experiments run at different energies they are sensitive to different Z' masses. In particular, SoLID is very sensitive to Z' masses around 1 GeV. It is remarkable the precision aimed by Moller at JLab planning to measure $\sin^2(\theta_W)$ to ± 0.00029 at $\langle Q \rangle = 75$ MeV, followed by the P2 experiment with precision of ± 0.00033 in $\sin^2(\theta_W)$ for $\langle Q \rangle = 67$ MeV. Looking either at the Table 4.1 or Figure (4.4) one can see that if the mass mixing parameter δ is of the order of 10^{-2} precise measurements on $\sin^2 \theta_W$ give rise to stringent bounds on ϵ , namely $\epsilon^2 < 10^{-4}$.

Notice that in the regime $m_{Z'}^2 \gg Q^2$ bounds from atomic parity violation are also effective in our framework. These can be straightforwardly accounted by the following rescaling in the parameters of the weak interaction lagrangian:

$$\begin{aligned} G_F &\rightarrow \rho_d G_F, \\ \sin^2 \theta_W &\rightarrow \kappa_d \sin^2 \theta_W, \end{aligned} \quad (4.48)$$

where:

$$\begin{aligned} \rho_d &= 1 + \delta^2 \frac{m_{Z'}^2}{m_{Z'}^2 + Q^2}, \\ \kappa_d &= 1 - \frac{\epsilon}{\epsilon_Z} \delta^2 \frac{1}{\tan \theta_W} \frac{m_{Z'}^2}{m_{Z'}^2 + Q^2}. \end{aligned} \quad (4.49)$$

Similarly to what was done for atomic parity violation we would like to compare the limits stemming from $\sin^2 \theta_W$ to those from neutrino-nucleus coherent scattering. This task

Lab	$\langle Q \rangle$	$\sin^2 \theta_W (m_Z)$	Light Mediator (90% CL)
E158	160 MeV	0.2329(13)	$\epsilon^2 < \frac{1.54 \times 10^{-5}}{\delta^2} \left(\frac{m_{Z'}^2 + 160^2}{m_Z m_{Z'}} \right)^2$
Qweak	170 MeV	± 0.0007	$\epsilon^2 < \frac{2.78 \times 10^{-6}}{\delta^2} \left(\frac{m_{Z'}^2 + 170^2}{m_Z m_{Z'}} \right)^2$
Moller	75 MeV	± 0.00029	$\epsilon^2 < \frac{4.77 \times 10^{-7}}{\delta^2} \left(\frac{m_{Z'}^2 + 75^2}{m_Z m_{Z'}} \right)^2$
P2	67 MeV	± 0.00033	$\epsilon^2 < \frac{6.17 \times 10^{-7}}{\delta^2} \left(\frac{m_{Z'}^2 + 67^2}{m_Z m_{Z'}} \right)^2$
SoLID	2.5 GeV	± 0.0006	$\epsilon^2 < \frac{2.04 \times 10^{-6}}{\delta^2} \left(\frac{m_{Z'}^2 + 2500^2}{m_Z m_{Z'}} \right)^2$

Table 4.1: 90% confidence level bounds on the kinetic mixing parameter for light mediators for different experiments that aim at measuring $\sin^2 \theta_W$ at low energies. All masses are in MeV units.

is, however, not trivial because in the generic description we are considering of the different, in principle independent parameters, namely $\epsilon, \epsilon_Z, \delta$. We will then compare bounds from polarized electron scattering and neutrino-nucleus coherent scattering for some specific models, illustrated in the next section, where it is possible to establish relations between these parameters.

4.4.4 Models

In this section we will interpret the bounds from parity and atomic parity violation, expressed until now, in terms of generic parameters, within a collection of anomaly free models proposed in the literature.

Dark Z

One of the simplest models which can be probed by parity violation phenomena and neutrino elastic scattering is dark Z model proposed in [127, 132, 133]. It is an extension of the photon model which includes a free parameter, δ , to account for the existence of a mass mixing term between the Z and Z' gauge bosons as we have done in Eq. (4.41). Such Z' field arises from the presence of a new abelian gauge group. If the Standard Model fermions are uncharged under this new $U(1)$ gauge group, the Z' interactions with fermions appear through the presence of kinetic and mass mixing [134]. On top of that, the scalar sector is not specified, thus δ is a free parameter. Looking at Table 4.1 we get $\epsilon^2 < 10^{-7}$ for $m_{Z'} \sim 100$ MeV and $\delta \sim 10^{-2}$, using the P2 projected sensitivity. Notice this limit is slightly stronger than the one achieved using *BaBar* data [135] which is the relevant experiment at this mass range. One can notoriously find stronger bounds from larger values of δ . A study of COHERENT data on neutrino-nucleus coherent scattering yields $\epsilon^2 < 10^{-6}$ [112]. Therefore, we conclude that our bounds are stronger. Our bounds are also applicable to the $U(1)_N$ model discussed in [134, 136].

Two Higgs Doublet Model

A UV complete version of the dark photon model has been discussed in the context of a Two Higgs Doublet Models (2HDM) augmented by an Abelian symmetry, $U(1)_X$, [134]. In this case, the Z' mass depends on the scalar sector of the model and consequently the parameter δ is no longer a free parameter. Many $U(1)_X$ extensions were discussed in the context 2HDM, in any case we find $m_{Z'} = g_X v \cos \beta^2 / \delta$, where $\tan \beta = v_2 / v_1$, $v_2(v_1)$ being the vacuum expectation value of the scalar doublets in the model, and g_X the gauge coupling. The parameter δ is a function of the $U(1)_X$ charges of the scalars fields and their vacuum expectation values (See Eq.C3 in [134]). For most $U(1)_X$ models we find $\delta \sim 10^{-2}$ assuming $\tan \beta \sim 50$. Taking $\delta \simeq 10^{-2}$ we find the bound $\epsilon^2 < 10^{-7}$ for $m_{Z'} \simeq 100$ MeV using the P2 experiment. One can easily recast this limit using the Table 4.1.

In the heavy mediator regime, we can apply our effective field theory approach taking $f_{V_u} \sim f_{V_d}$ we get $g_X^2 / m_{Z'}^2 \leq 4.38 \times 10^{-9}$ GeV. Consequently, $m_{Z'} \geq 1.5 g_X \times 10^4$ GeV. This bound is applicable under the assumption that axial-vector couplings between the electrons are present as occurs for many models discussed in [134]. Having in mind that LEP bound on vector mediators roughly reads, $m_{Z'} > 7 g_X \times 10^3$ GeV [137], we conclude that APV provides a stronger bound. This limit from LEP was derived for the B-L model where only vectorial interactions are present but it is roughly applicable to other models [138, 139]. Anyway, our conclusion stands, APV gives rise to a more restrictive bound on the Z' mass. One may wonder about LHC lower mass bounds on such vector bosons. It has been shown that many of these models predict a large Z' width. This feature weakens LHC sensitivity. Analyzing LHC data it has been found that $m_{Z'} > 1 - 2$ TeV for many models taking $g_X = 0.1$ [140], which is again weaker than APV. In summary, APV seems to be the most promising laboratory for such models as far as the Z' mass is concerned.

3-3-1 Model

3-3-1 models are based on the $SU(3)_c \otimes SU(3)_L \otimes U(1)_N$ gauge group [141, 142]. They explain the number of replication of fermion generations in the Standard Model and are able to address neutrino masses and dark matter. The presence of the $U(1)_N$ group gives rise to heavy Z' whose mass is set the energy scale at which the 3-3-1 symmetry is broken down to the Standard Model gauge group. The Z' does have axial-vector couplings to electrons and therefore might leave imprints on APV, although the Z' couplings to fermions are suppressed, of the order of 10^{-2} . Using Table V of [143] where the vector and axial-vector couplings are provided, we can compute $f_{V_q}^{\text{eff}}$ and consequently find a lower mass bound on the Z' that reads $m_{Z'} > 1.7$ TeV for the *model A* with $\beta = \sqrt{3}$. We point out that the parameter β defines the vector and axial-vector couplings in the model according to Table V in [143]. However, this limit is sub-dominant when compared to existing bounds stemming from dijet and dilepton searches at the LHC which impose $m_{Z'} > 4$ TeV [144–147]. There are other bounds rising from other observables such as from flavor physics but they are not as relevant [148–153]. We highlight that there are possible extensions of this model via the inclusion of right-handed neutrinos which can weaken the LHC bounds by decreasing the Z' branching ratio into charged

leptons and quarks [154]. In that case our bounds could become competitive.

Light Z' Models

It has been recently proposed a model which successfully accommodates neutrino masses within the type II seesaw while hosting a light Z' gauge boson [155]. The mass of the Z' comes from the vacuum expectation value of the scalar doublets and therefore the Z' must be light, for this reason we will focus on polarized electron scattering which constitutes a great probe for light species. Again the mass mixing parameter δ depends on the scalar spectrum which is set by anomaly cancellation requirements. For the $U(1)_{Y'}$ presented in Table 1 of [155] we get $\delta \sim 10^{-1}$. For such a large value of delta we find $\epsilon^2 < 10^{-10}$ for $m_{Z'} \simeq 100$ MeV using the P2 experiment, and $\epsilon^2 < 10^{-7}$ for $m_{Z'} \simeq 1$ GeV using SoLID projection. These bounds are much stronger than those derived using The Heavy Photon (HPS) Search Experiment and Belle projections shown in [155].

Models based on the $L_\mu - L_\tau$ gauge symmetry have recently brought a lot of attention due to some flavor anomaly [156–162]. The Z' boson can be quite light and has no interactions with quarks at tree-level. At loop level, one could nevertheless generate the neutrino-nucleus coherent scattering and the parity-violating observables discussed here. Albeit, there are already stringent bounds rising from neutrino-trident production and meson mixings [163, 164], making our assessment of 1-loop induced parity violation effects not relevant, in agreement with [112].

4.5 Conclusions

We have reviewed the theoretical aspects of parity violation and put it in context with other relevant observables. We treated Atomic Parity Violation using effective field theory and showed how one can constrain new physics via precise measurements of the Cesium weak charge. Moreover, we have discussed neutrino-nucleus coherent scattering and shown that Atomic Parity Violation leads to a more restrictive bound on the new physics scale under the assumption that the new physics particle couples to electrons and neutrinos with similar strength. This conclusion is also valid to heavy vector mediators with masses at the TeV scale, for instance. Shifting the discussion to light mediators we have parametrized new physics effects in polarized electron scatterings in terms of the $\sin \theta_W$ and explored the sensitivity of new measurements on $\sin \theta_W$ to derive bounds on the kinetic mixing between the Z and Z' gauge bosons as a function of the Z' mass. Lastly, we applied our constraints to models previously proposed in the literature and showed that our findings constitute, in some cases, the strongest limits on the kinetic mixing parameter, highlighting the importance of our reasoning.

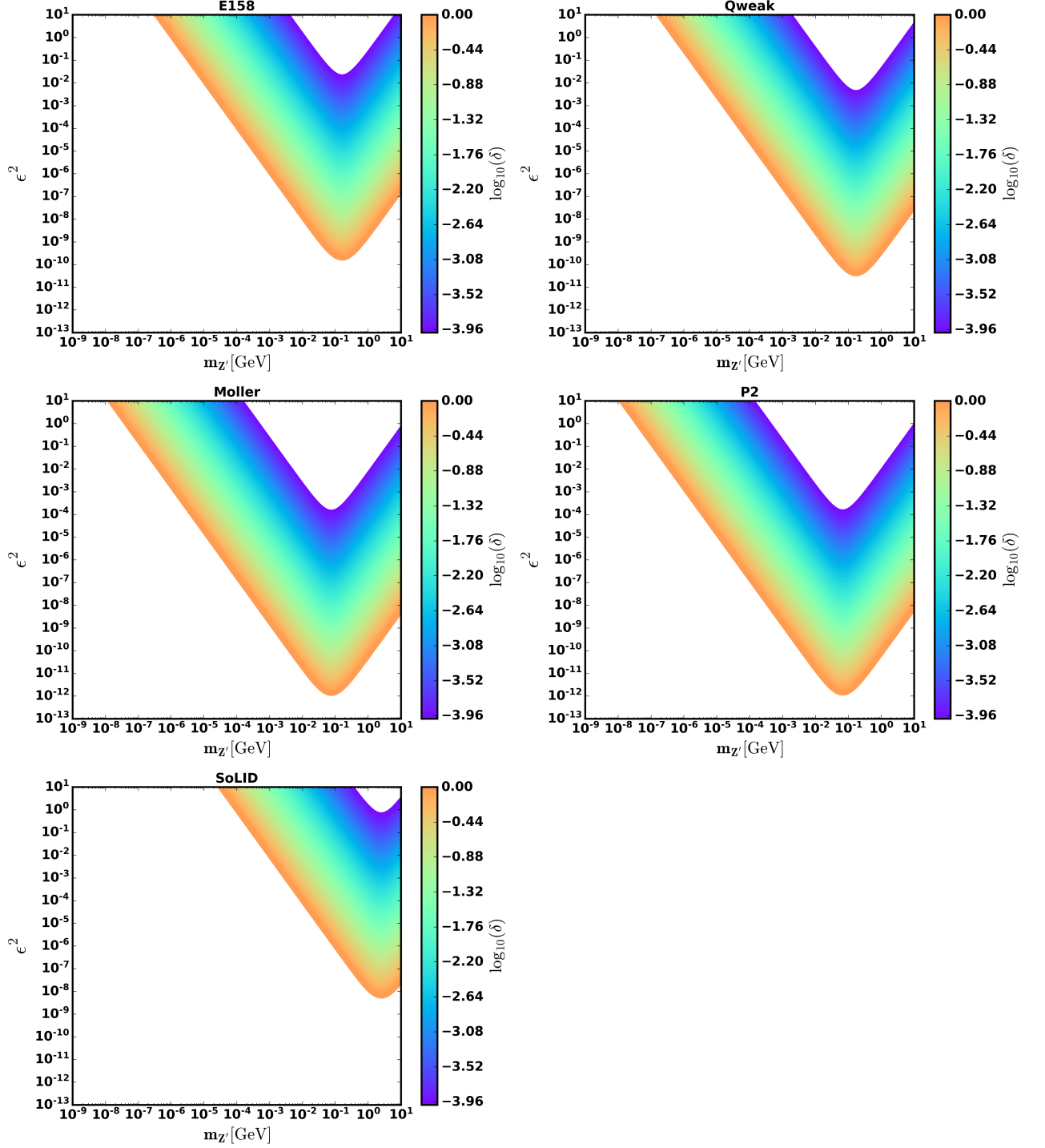


Figure 4.4: Bounds of the experiments E158, Qweak, Moller, P2 and SoLID on the mixing between Z and Z' with respect to the mass of the new light neutral gauge boson following the relations on the table. In each plot the mixing parameter δ is changing logarithmically from $\delta = 10^{-4}$ to $\delta = 1$, so we can also visualize the dependence of ϵ with this parameter.

Part II

Semiclassical Gravity

5

Quantization of Field Theories in Curved Spacetime

In Part I we saw briefly the Standard Model of Particle Physics that describes quarks and leptons and their interactions through the strong, weak and electromagnetic interactions. But that is another way matter can interact, which is through gravity.

The best description we have of gravity was formulated in 1915 by Einstein [165] and it is known as General Relativity. In the theory of General Relativity gravity is not a force mediated by some particle in Minkowski spacetime as the other fundamental interactions are, but instead it is a consequence of the curvature of spacetime itself. Anything that carries energy bends and deforms the spacetime continuum and in turn things will move along the geodesics of this curved spacetime. In the words of Wheeler, “Spacetime tells matter how to move; matter tells spacetime how to curve” [166]. It is an elegant way to describe an interaction which intensity depends only on the source mass and that couples with the same strength to everything. The latter is called *equivalence principle* and it also states that every uniformly accelerated reference frame is locally equivalent to a homogeneous gravitational field.

At low energies or small scales as the ones of typical particles interactions the spacetime curvature is usually very small and asymptotically flat (unless when the background geometry is already non-trivial) and practical calculations can be performed treating spacetime as Minkowskian. However, at cosmological scales or very high energies gravity can easily become the most important interaction. It dictates the formation of stars, black holes, galaxies and the evolution of the entire universe.

But at extremely high energies, on the order of the Planck scale $M_P \equiv 1/\sqrt{8\pi G}$, where G is the Newton’s constant, the General Relativity theory breaks on singularities and infinite curvature. This was sufficient to start a new quest of a more complete theory of gravity,

focused in formulating a quantum description of it, putting gravity in an equal foot with all the other fundamental interactions. It turns out that a theory of a massless spin-2 quantum field satisfies the equivalence principle, general covariance and gives Einstein's field equations in the classical limit [167], and the corresponding particle became known as the *graviton*. However, a theory with gravitons is non-renormalizable beyond the Planck scale and is predictive only as an effective field theory below M_P . A lot of effort has been made towards a full consistent and predictive theory of gravity valid in all energy scales, but we still have no definitive answer.

Although we still don't have a final theory of quantum gravity there is still a lot that can be learned from a semiclassical theory of quantum matter fields in a classical gravitational background. For instance, interesting phenomena like the Hawking radiation [168, 169], which is the thermal emission of particles from black holes that causes it to evaporate, and the Unruh effect [170–172], which arises in non-inertial frames and predicts that accelerating observer in vacuum Minkowski spacetime see a thermal bath with temperature proportional to their acceleration, are found just from consistency of quantum field theory of matter in a classical spacetime background, which should be an accurate description of Nature at energies below the Planck scale. On the cosmological side, one can also apply the semiclassical theory to the inflationary epoch, which is going to be discussed in the Part III, when quantum fluctuations of the inflaton field give rise to the initial conditions of the Universe evolution.

In this chapter it is given only a taste of semiclassical gravity, by showing some main results of the effective field theory of matter in curved spacetime. For a detailed view see [173–178].

5.1 Einstein's gravity

In Einstein's theory of gravity, General Relativity, the effect of gravity is seen as a change of the spacetime geometry and therefore it is constructed using geometrical objects only. The field equations that describe spacetime and the objects that deform and gravitate on it can be obtained from the Einstein-Hilbert action (in this chapter we use the metric signature to be -2):

$$S_{\text{EH}} = - \int d^4x \sqrt{-g} \left[\frac{1}{16\pi G} (R - 2\Lambda) \right], \quad (5.1)$$

where g is the determinant of the spacetime metric $g_{\mu\nu}$, G is the Newton gravitational constant, R is the scalar curvature of spacetime, L_m is the matter Lagrangian and Λ is a cosmological constant.

The scalar curvature is defined as:

$$R = g^{\mu\nu} R_{\mu\nu} = g^{\mu\alpha} g^{\nu\beta} R_{\mu\nu\alpha\beta}, \quad (5.2)$$

where $R_{\mu\nu}$ is the Ricci tensor and $R_{\mu\nu\alpha\beta}$ is a rank-4 tensor called Riemann tensor, which quantifies the 4-dimensional spacetime curvature, and can be written as [166]:

$$R_{\alpha\beta\gamma}^{\sigma} = \frac{\partial \Gamma_{\alpha\gamma}^{\sigma}}{\partial x^{\beta}} - \frac{\partial \Gamma_{\alpha\beta}^{\sigma}}{\partial x^{\gamma}} + \Gamma_{\lambda\beta}^{\sigma} \Gamma_{\alpha\gamma}^{\lambda} - \Gamma_{\lambda\gamma}^{\sigma} \Gamma_{\alpha\beta}^{\lambda}, \quad (5.3)$$

where the quantities $\Gamma_{\alpha\beta}^\gamma$ are known as the Christoffel symbols and are given in terms of the metric as,

$$\Gamma_{\alpha\beta}^\mu = \frac{1}{2}g^{\mu\sigma} \left(\frac{\partial g_{\sigma\beta}}{\partial x^\alpha} + \frac{\partial g_{\sigma\alpha}}{\partial x^\beta} - \frac{\partial g_{\alpha\beta}}{\partial x^\sigma} \right). \quad (5.4)$$

The energy-momentum tensor can be written in terms of the matter action using the definition

$$T_{\mu\nu} \equiv \frac{-2}{\sqrt{-g}} \frac{\delta S_m}{\delta g^{\mu\nu}}. \quad (5.5)$$

The equations of motion of the Einstein-Hilbert action with respect to the metric can be found to be [179]:

$$R_{\mu\nu} - \frac{1}{2}g_{\mu\nu}R = 8\pi GT_{\mu\nu} + \Lambda g_{\mu\nu}. \quad (5.6)$$

which are the Einstein's field equations for gravity. General Relativity is greatly confirmed experimentally. Among its solutions there are black holes, and one was recently imaged [180], gravitational waves, which existence was confirmed in 2017 [181], wormholes and different possible behaviors for the Universe evolution.

Up to now, we have a classical description of gravity plus matter. However, we know that at least the matter fields are quantum, so a natural next step would be to explore what happens when we quantize matter in a curved classical background. In the next sections we show some general results for the effective action in curved spacetime and some of its consequences.

5.2 Matter fields in curved spacetime

The first step we should take to write a semiclassical theory is to correctly incorporate matter fields into a curved background in a way that preserves general covariance. We also want to maintain any symmetries present in the flat spacetime case, locality and renormalizability and it is also reasonable to forbid the introduction of new parameters with the inverse-mass dimension. A first approach would be to consider that matter couples minimally to gravity. In this case, going from flat to curved spacetime requires:

$$\eta_{\mu\nu} \rightarrow g_{\mu\nu}, \quad \partial_\mu \rightarrow \nabla_\mu, \quad d^4x \rightarrow d^4x\sqrt{-g}, \quad (5.7)$$

where ∇_μ is the covariant derivative in terms of Christoffel symbols,

$$\nabla_\mu A_\nu = \partial_\mu A_\nu - \Gamma_{\mu\nu}^\alpha A_\alpha. \quad (5.8)$$

Therefore, the action for a scalar field minimally coupled to gravity becomes:

$$S_0 = \int d^4x\sqrt{-g} \left[\frac{1}{2}g^{\mu\nu}\partial_\mu\varphi\partial_\nu\varphi - \frac{1}{2}m^2\varphi^2 - \frac{\lambda}{4!}\varphi^4 \right]. \quad (5.9)$$

Now, for a Dirac spinor field we have:

$$S_{1/2} = i \int d^4x \sqrt{-g} \left[\bar{\psi} \gamma^\alpha \nabla_\alpha \psi - im \bar{\psi} \psi \right], \quad (5.10)$$

where the γ^α are the γ -matrices in curved spacetime. To define them, we need to introduce the tetrad base \mathbf{e}_a^μ , such that

$$\mathbf{e}_a^\mu \mathbf{e}^{\nu a} = g^{\mu\nu}, \quad \mathbf{e}_\mu^a \mathbf{e}^{\mu b} = \eta^{ab}, \quad (5.11)$$

so that we can write,

$$\gamma^\mu = \mathbf{e}_a^\mu \gamma^a, \quad (5.12)$$

where the γ^a are the usual γ -matrices in flat spacetime and the γ^μ satisfy the Clifford algebra in curved spacetime:

$$\{\gamma^\mu, \gamma^\nu\} = 2g^{\mu\nu}. \quad (5.13)$$

The covariant derivative of a Dirac spinor field is given in terms of the spin-connection ω_μ^{ab} :

$$\nabla_\mu \psi = \partial_\mu \psi + \frac{i}{2} \omega_\mu^{ab} \sigma_{ab} \psi, \quad (5.14)$$

where

$$\sigma_{ab} = \frac{i}{2} [\gamma_a, \gamma_b], \quad \omega_\mu^{ab} = \frac{1}{2} (\mathbf{e}_\alpha^b \partial_\mu \mathbf{e}^{\alpha a} + \Gamma_{\nu\mu}^\alpha \mathbf{e}_\alpha^b \mathbf{e}^{\nu a}) = -\omega_\mu^{ba}. \quad (5.15)$$

For a massless non-Abelian gauge vector field we have,

$$S_1 = \frac{1}{4} \int d^4x \sqrt{-g} G_{\mu\nu}^a G^{a\mu\nu}, \quad (5.16)$$

where

$$G_{\mu\nu}^a = \nabla_\mu A_\nu^a - \nabla_\nu A_\mu^a - gf^{abc} A_\mu^b A_\nu^c = \partial_\mu A_\nu^a - \partial_\nu A_\mu^a - gf^{abc} A_\mu^b A_\nu^c, \quad (5.17)$$

so the gauge symmetry is maintained.

In the case when matter couples non-minimally to gravity through geometrical objects, we have that for spinors and vectors non-minimal terms always requires the introduction of inverse-mass dimension parameters, but for a scalar field we can have the coupling

$$\xi \varphi^2 R, \quad (5.18)$$

where the dimensionless parameter ξ is named non-minimal parameter, and in fact such term is needed to guarantee renormalizability of the theory already at one-loop level.

For the vacuum, or pure gravity, sector besides the Einstein-Hilbert we could also have higher derivatives terms for the metric in the action without violating our conditions:

$$S_{\text{vac}} = S_{\text{EH}} + S_{\text{HD}} \quad (5.19)$$

$$S_{\text{HD}} = \int d^4x \sqrt{-g} \left[a_1 R_{\mu\nu\alpha\beta} R^{\mu\nu\alpha\beta} + a_2 R_{\mu\nu} R^{\mu\nu} + a_3 R^2 + a_4 \square R \right] \quad (5.20)$$

where the constants $a_{1,\dots,4}$ are all dimensionless parameters.

Before showing the quantitative results of loop quantum correction of matter fields in a curved background maybe it is useful to see qualitatively what we should expect. Thinking in terms of Feynman diagrams, we can see that each divergent loop diagram in flat space will give rise to infinitely many diagrams in curved space, as $\sqrt{-g}$ becomes an infinite expansion if we write the metric as a background plus perturbation, $g_{\mu\nu} = \tilde{g}_{\mu\nu} + h_{\mu\nu}$. Thus, in each vertex we can add an infinite number of gravitational external legs. So, keeping in mind that as gravity is not being quantized, the internal propagators in the loops are from matter fields only, for scalars we have:

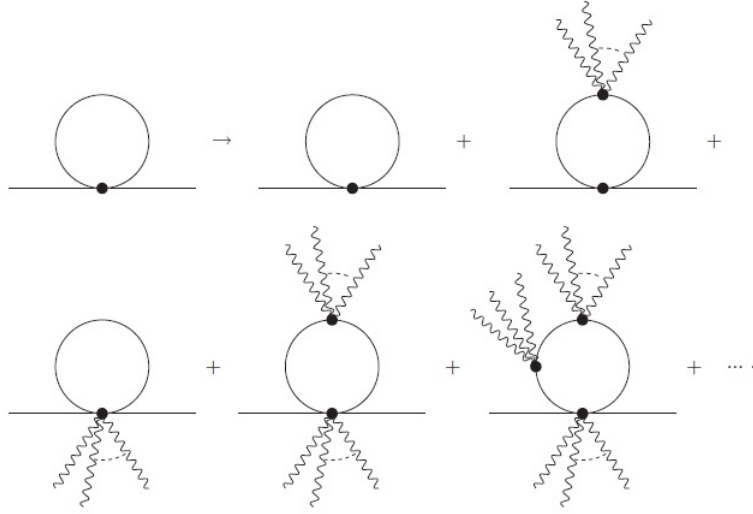


Figure 5.1: One-loop corrections to the mass of a scalar field in curved spacetime. Figure from [13].

We also note that adding vertices with external legs from gravity introduces more propagators in the loop and thus the degree of divergence always decreases. For example, the second diagram in the first line of Figure 5.1 has quadratic divergence, but the divergence degree of the third diagram is logarithmic. This new logarithmic divergence has to be cancelled by introducing counterterms into the action. These counterterms cannot involve derivatives of the scalar field, so it has to be of the form $\sim \varphi^2 \partial \partial h$. The only covariant quantity that can be constructed from this is $\varphi^2 R$, which is precisely the non-minimal coupling. The other divergent diagrams like the first on the second line of Figure 5.1 has divergences similar to the flat spacetime case, and don't require the introduction of additional counterterms.

The matter contribution to the vacuum energy can be ignored in flat spacetime as this vacuum energy is non-interacting, but in curved spacetime this situation changes as we can have gravity interacting with it. Therefore, we have again infinitely many new diagrams, Figure 5.2

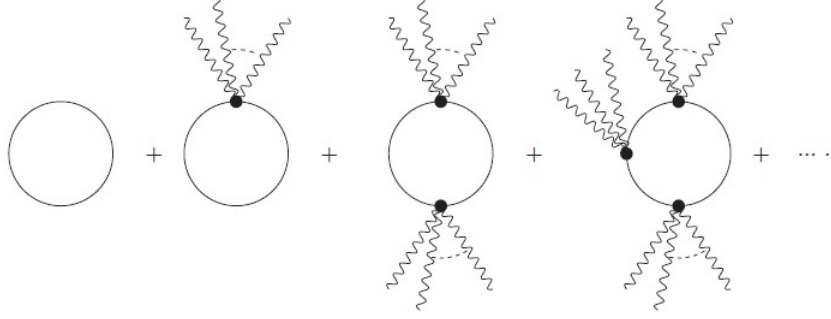


Figure 5.2: One-loop corrections to the vacuum energy from a scalar field in curved spacetime. Figure from [13].

Hence, in order to cancel the new quadratic and logarithmic divergences we need to add new counterterms. They should be constructed with the metric only, and by dimensionality and covariance we see that we need to add higher derivative terms like the ones in Eq. (5.20).

Therefore, we see that the non-minimal coupling and higher derivative terms are indeed necessary to have a renormalizable theory of a scalar field in curved spacetime. We shall see next the quantitative results from calculating the one-loop divergences of the effective action.

5.3 Effective action in curved spacetime

The quantum effective action is defined as [76],

$$e^{i\Gamma[g_{\mu\nu}]} = \int \mathcal{D}\Phi e^{iS[\Phi;g_{\mu\nu}]}, \quad (5.21)$$

where the Φ are the matter fields fluctuations and we set the vacuum expectation value of the matter fields to zero. As gravity is not being quantized, we can write:

$$e^{i\Gamma[g_{\mu\nu}]} = e^{iS_{\text{vac}}[g_{\mu\nu}]} \int \mathcal{D}\Phi e^{iS_m[\Phi;g_{\mu\nu}]}. \quad (5.22)$$

This gives the quantum effective action of vacuum.

The effective action can be expanded in loop-order contributions, $\Gamma = \Gamma^{(1)} + \Gamma^{(2)} + \dots$, and here we will be interested in the one-loop, leading order, contribution. We start with a general action of a massive scalar and spinor fields that have a Yukawa interaction and are charged under the $SU(2)$ gauge group. As we are going to use dimensional regularization later, we write the action in n dimensions:

$$S_{0m} = \int d^n x \sqrt{-g} \left[-\frac{1}{4} G_{0\mu\nu}^a G_0^{a\mu\nu} + \frac{1}{2} g^{\mu\nu} (D_\mu \varphi_0)^a (D_\nu \varphi_0)^a - \frac{1}{2} (m_0^2 - \xi_0 R) \varphi_0^a \varphi_0^a \right. \\ \left. - \frac{1}{4!} \lambda (\varphi_0^a \varphi_0^a)^2 + \bar{\psi}_0^a (i\gamma^\mu(x) D_\mu^{ab} - M_0 \delta^{ab} - i h_0 \epsilon^{acb} \varphi_0^c) \psi_0^b \right]. \quad (5.23)$$

We will omit the $SU(2)$ adjoint index from now on. The renormalized matter action should have the form:

$$S_m = \mu^{n-4} \int d^n x \sqrt{-g} \left[-\frac{1}{4} Z_1'' G_{\mu\nu} G^{\mu\nu} + \frac{1}{2} Z_1 g^{\mu\nu} (D_\mu \varphi)(D_\nu \varphi) - \frac{1}{2} Z_1 Z_2 (m^2 - \xi R) \varphi^2 \right. \\ \left. - \frac{1}{4!} Z_1^2 Z_4 \lambda \varphi^4 + Z_1' \bar{\psi} i \gamma^\mu(x) D_\mu \psi - Z_1' Z_2' M \bar{\psi} \psi - Z_h Z_1' Z_1^{1/2} i h \bar{\psi} \varphi \psi \right], \quad (5.24)$$

where μ is parameter with mass dimension and Z_k depend on the couplings λ , g and h and can be written as:

$$Z_k = 1 + \delta_k. \quad (5.25)$$

The δ_k are called *counterterms* and are introduced to cancel the divergences coming from quantum loop corrections for the matter fields. We call a theory that can be written as Eq. (5.24) as multiplicative renormalizable, and multiplicative renormalizable theories in flat spacetime should remain so in curved spacetime [174]. In particular, due to covariance, the Z_1 , Z_1' and Z_1'' should be the same as in flat spacetime.

In order to find the one-loop counterterms one has to calculate the one-loop contribution to the effective action, which is given by

$$\Gamma^{(1)} = -\frac{i}{2} \text{Tr} \ln \hat{H}_{AB}. \quad (5.26)$$

The operator H_{AB} is the bilinear part of the action Eq. (5.23) in the quantum fields, and can usually be written as [174]

$$\hat{H}_{AB} = \hat{\mathbb{1}}_{AB} g^{\mu\nu} \nabla_\mu \nabla_\nu + 2 \hat{h}_{AB}^\mu \nabla_\mu + \hat{\Pi}_{AB}, \quad (5.27)$$

where the indices A, B run on the space of fields, where the operators \hat{h}_{AB}^μ and $\hat{\Pi}_{AB}$ act on.

To calculate the divergent part of Eq. (5.26) we will make use of Schwinger-de Witt technique and expand \hat{H}_{AB} using heat kernel method [182, 183]. This consists in writting \hat{H}_{AB} as,

$$\frac{i}{2} \text{Tr} \ln \hat{H}_{AB} = -\frac{i}{2} \text{Tr} \int_0^\infty \frac{ds}{s} e^{-is \hat{H}_{AB}}, \quad (5.28)$$

where

$$e^{-is \hat{H}_{AB}} = \hat{U}(x, x'; s) = \hat{U}_0(x, x'; s) \sum_{k=0}^\infty (is)^k \hat{a}_k(x, x'). \quad (5.29)$$

The \hat{a}_k are the Schwinger-de Witt, or heat kernel, coefficients while $\hat{U}_0(x, x'; s)$ has the form

$$\hat{U}_0(x, x'; s) = \frac{1}{(4\pi i s)^{n/2}} \mathcal{D}^{1/2}(x, x') \exp \left(-\frac{\sigma(x, x')}{2is} - im^2 s \right), \quad (5.30)$$

where $\sigma(x, x')$ is the geodesic distance between x and x' and

$$\mathcal{D}(x, x') = \det[-\partial_\mu \partial_\nu \sigma(x, x')], \quad (5.31)$$

is the Van Vleck-Morett determinant. The regularization of the integral in Eq. (5.28) can be done in several ways, and we will choose dimensional regularization. Only the first few heat kernel coefficients are necessary to find the divergences as, in the four-dimensional case, the \hat{a}_0 -coefficient corresponds to the quartic divergence, the \hat{a}_1 to the quadratic divergence and \hat{a}_2 to the most important logarithmic divergences. They are all known and can be found in [175, 184, 185]. For more details, see [186–188] and references therein. Then, the divergent part of the one-loop effective action can be expressed as,

$$\Gamma_{\text{div}}^{(1)} = -\frac{\mu^{n-4}}{(4\pi)^2(n-4)} \int d^n x \sqrt{-g} \text{Tr} \left[\frac{1}{2} \hat{P} \cdot \hat{P} + \frac{1}{12} \hat{S}_{\mu\nu} \hat{S}^{\mu\nu} + \frac{1}{6} \square \hat{P} + \frac{\hat{1}}{180} (R_{\mu\nu\alpha\beta} R^{\mu\nu\alpha\beta} - R_{\mu\nu} R^{\mu\nu} + \square R) \right], \quad (5.32)$$

where

$$\hat{P}_{AB} = \hat{\Pi}_{AB} + \hat{1}_{AB} \frac{R}{6} - \nabla_\mu \hat{h}_{AB} - \hat{h}_{\mu A} \hat{h}_{CB}^\mu, \quad (5.33)$$

$$\hat{S}_{AB\mu\nu} = (\nabla_\nu \nabla_\mu - \nabla_\mu \nabla_\nu) \hat{1}_{AB} + \nabla_\nu \hat{h}_{\mu AB} - \nabla_\mu \hat{h}_{\nu AB} + \hat{h}_{\nu AC} \hat{h}_{\mu CB} - \hat{h}_{\mu AC} \hat{h}_{\nu CB}. \quad (5.34)$$

Thus, we see that the Schwinger-de Witt technique is a powerful tool to calculate divergences of the effective action in curved spacetime, as it preserves general covariance and reduces the problem of finding divergences to multiplication and commutation of matrices.

In order to find \hat{h} and $\hat{\Pi}$ we first follow the background field method to split all the matter fields into its background and quantum fluctuation:

$$\varphi \rightarrow \varphi + \sigma, \quad A_\mu \rightarrow A_\mu + B_\mu, \quad \psi \rightarrow \psi + \chi. \quad (5.35)$$

Then, the bilinear in the quantum fluctuations part of the action Eq. (5.23), plus the gauge fixing term, where we have chosen the diffeomorphism invariant gauge $\nabla_\mu B_\nu^\mu$, is

$$\begin{aligned} S^{(2)} + S_{GF} = \int d^n x \sqrt{-g} \left[-\frac{1}{2} \sigma \square \sigma + \frac{1}{2} B^\mu \left(\delta_\mu^\nu \square - R_\mu^\nu + g^2 \varphi^2 \delta_\mu^\nu \right) B_\nu + g B^\mu (\partial_\mu \sigma \varphi + \partial_\mu \varphi \sigma) \right. \\ \left. - \frac{1}{4} \lambda \sigma^2 \varphi^2 - \frac{1}{2} \sigma (m^2 - \xi R) \sigma + i \bar{\chi} \gamma^\mu \nabla_\mu \chi - i h \bar{\chi} \phi \chi - i h \bar{\chi} \sigma \psi \right. \\ \left. - i h \bar{\psi} \sigma \chi - M \bar{\chi} \chi \right]. \end{aligned} \quad (5.36)$$

With the change of variables,

$$\sigma = i \tilde{\sigma}, \quad \chi = -\frac{1}{2} (\gamma^\nu \nabla_\nu - i M) \eta, \quad (5.37)$$

we can write the Eq. (5.36) as,

$$S^{(2)} + S_{GF} = \frac{1}{2} \int d^n x \sqrt{-g} \begin{pmatrix} \tilde{\sigma} & B^\mu & \bar{\eta} \end{pmatrix} (\hat{H}) \begin{pmatrix} \tilde{\sigma} \\ B_\nu \\ \eta \end{pmatrix}. \quad (5.38)$$

The differential operator \hat{H} has the form of Eq. (5.27), where

$$\hat{h}^\alpha = \begin{pmatrix} 0 & \frac{1}{2}g\delta_\mu^\alpha\varphi & -\frac{1}{2}h\bar{\psi}\gamma^\alpha \\ \frac{i}{2}g\delta_\mu^\alpha\varphi & 0 & \frac{1}{2}g\bar{\psi}\gamma_\mu\gamma^\alpha \\ 0 & 0 & -\frac{1}{2}h\varphi\gamma^\alpha \end{pmatrix}, \quad (5.39)$$

and

$$\hat{\Pi} = \begin{pmatrix} m^2 - \xi R + \frac{1}{2}\lambda\varphi^4 & 2igg^{\nu\alpha}\partial_\alpha\varphi & -h\bar{\psi}M \\ -ig\delta_\mu^\alpha\partial_\alpha\varphi & -R_\mu^\nu + g^2\delta_\mu^\nu\varphi^2 & ig\bar{\psi}\gamma_\mu M \\ 2h\psi & 2ig\gamma^\nu\psi & M^2 - \frac{1}{4}R + ih\varphi M \end{pmatrix}. \quad (5.40)$$

The result of the calculations gives:

$$\Gamma_{\text{div}}^{(1)} = \Gamma_{\text{m,div}}^{(1)} + \Gamma_{\text{vac,div}}^{(1)}, \quad (5.41)$$

with [174],

$$\begin{aligned} \Gamma_{\text{m,div}}^{(1)} = & -\frac{\mu^{n-4}}{\epsilon} \int d^n x \sqrt{-g} \left[\frac{1}{2}(8h^2 - 8g^2)g^{\mu\nu}\partial_\mu\varphi\partial_\nu\varphi + \frac{1}{2}R\varphi^2 \left(\left(\frac{1}{6} - \xi \right) \left(\frac{5}{3}\lambda - 4g^2 \right) \right. \right. \\ & - \frac{4}{3}g^2 + \frac{4}{3}h^2 \Big) + \frac{1}{4!} \left(\frac{11}{3}\lambda^2 - 8g^2\lambda + 72g^4 - 96h^4 \right) \varphi^4 \\ & + \frac{1}{2}\varphi^2 \left(-48h^2M^2 + \left(\frac{5}{3}\lambda - 4g^2 \right) m^2 \right) \\ & + i\bar{\psi} \left(2(h^2 + 2g^2)\gamma^\alpha\nabla_\alpha + 2h(h^2 - 6g^2)\varphi \right. \\ & \left. \left. - 4i(h^2 - 4g^2)M \right) \psi \right], \end{aligned} \quad (5.42)$$

and

$$\begin{aligned} \Gamma_{\text{vac,div}}^{(1)} = & -\frac{\mu^{n-4}}{\epsilon} \int d^n x \sqrt{-g} \left[\left(\frac{1}{120}N_s + \frac{1}{20}N_f + \frac{1}{10}N_v \right) C^2 + \frac{N_s}{2} \left(\xi - \frac{1}{6} \right)^2 R^2 \right. \\ & + \left(N_s m^2 \left(\xi - \frac{1}{6} \right) + \frac{N_f M^2}{3} \right) R + \left(-\frac{1}{360}N_s - \frac{11}{360}N_f \right. \\ & - \frac{31}{180}N_v \Big) E + \left(\frac{1}{180}N_s + \frac{1}{30}N_f - \frac{1}{10}N_v \right) \square R \\ & \left. + \frac{1}{2}N_s m^4 - 2N_f M^4 \right]. \end{aligned} \quad (5.43)$$

In these expression, we defined $\epsilon \equiv (4\pi)^2(n-4)$. We wrote for the vacuum divergence a generalized expression for any number of scalars, N_s , fermions, N_f , and vector bosons, N_v , (N counts the fields, not multiplets) and we presented the result in the Weyl basis $\{C^2, R^2, E\}$, with the Weyl tensor, C , and Euler density in $n = 4$, or topological Gauss-Bonnet term, E :

$$C^2 = E + 2R_{\mu\nu}^2 - \frac{2}{3}R^2, \quad E = R_{\alpha\beta\mu\nu}^2 - 4R_{\mu\nu}^2 + R^2, \quad (5.44)$$

which is related to the Riemann basis $\{R_{\alpha\beta\mu\nu}^2, R_{\mu\nu}^2, R^2\}$ as,

$$R_{\alpha\beta\mu\nu}^2 = -E + 2C^2 + \frac{1}{3}R^2, \quad R_{\mu\nu}^2 = \frac{1}{2}C^2 - \frac{1}{2}E + \frac{1}{3}R^2. \quad (5.45)$$

From Eqs. (5.42) and (5.43) we note that, even if we started without a non-minimal coupling, $\xi = 0$, a non-minimal term $\varphi^2 R$ will still appear as a one-loop divergence, as was already expected, and we must introduce this term in the bare action in order to cancel these divergences. In the vacuum sector we see an emergence of curvature squared divergent terms due to pure matter one-loop corrections, hence we must also start with a bare vacuum action with curvature squared terms to cancel these divergences:

$$S_{0\text{vac}} = \int d^n x \sqrt{-g} \left[\Lambda_0 - \frac{1}{\kappa_0^2} R + a_{01} R^2 + a_{02} C^2 + a_{03} E + a_{04} \square R \right]. \quad (5.46)$$

Therefore, this higher-derivatives terms should be present already in the classical theory, but their effect is tiny compared to the Einstein-Hilbert term, which is enhanced by a factor M_P^2 . It is worth mentioning that, besides granting renormalizability and consistency of the quantum theory, the Weyl tensor (or analogously the Riemann tensor) introduces a ghost degree of freedom into the theory, a massive graviton with opposite sign of the propagator [189]. In fact, it is a general theorem that higher derivatives theories (theories that contain derivatives higher than two) have instabilities and unbounded Hamiltonian [190, 191]. There has been some work in understanding the role of such C^2 ghost and if it can indeed lead to serious problems in quantum field theory, even below the Planck scale¹ [193–202].

Another noteworthy point is that the massless theory of Eq. (5.23) plus Eq. (5.46) with vanishing mass-dimension parameters and $\xi = 1/6$ is invariant under local conformal transformations in four dimensions, with the fields transforming as,

$$g'_{\mu\nu} = g_{\mu\nu} e^{2\sigma(x)}, \quad \varphi' = \varphi e^{-\sigma(x)}, \quad A'_\mu = A_\mu, \quad \psi' = \psi e^{-\frac{3}{2}\sigma(x)}. \quad (5.47)$$

However, the conformal symmetry is broken at one-loop order due to trace anomaly. For more details see [203] and references therein.

¹In fact, the action in Eq. (5.46) is also renormalizable in four dimensions when quantizing the graviton [192], which gives another motivation for studying these ghosts.

5.3.1 Renormalization group equations

From Eqs. (5.42) and (5.43) one can write down the relation between the bare parameters and fields, and the renormalized ones:

$$\begin{aligned}
\varphi_0 &= \mu^{(n-4)/2} Z_1^{1/2} \varphi, \quad Z_1 = 1 + \frac{8}{\epsilon} (h^2 - g^2), \\
\xi_0 &= Z_2 \xi + Z_3, \quad Z_2 = 1 + \frac{1}{\epsilon} \left(-\frac{5}{3} \lambda + 12g^2 - 8h^2 \right), \quad Z_3 = -\frac{1}{6\epsilon} \left(-\frac{5}{3} \lambda + 12g^2 - 8h^2 \right), \\
\psi_0 &= \mu^{(n-4)/2} \bar{Z}_1^{1/2} \psi, \quad \bar{Z}_1 = 1 + \frac{1}{\epsilon} (2h^2 + 24g^2), \\
h_0 &= \mu^{(n-4)/2} Z_h h, \quad Z_h = 1 + \frac{1}{\epsilon} (12g^2 + 8h^2), \\
\lambda_0 &= \mu^{(n-4)} Z_\lambda \lambda, \quad Z_\lambda \lambda = \lambda - \frac{1}{\epsilon} \left(\frac{11}{3} \lambda^2 - 24\lambda g^2 + 72g^4 + 16\lambda h^2 - 96h^4 \right), \\
M_0 &= \tilde{Z}_2 M, \quad \tilde{Z}_2 = 1 + \frac{1}{\epsilon} (12g^2 - 6h^2), \\
m_0^2 &= Z_2 m^2 + \tilde{Z}_3 M^2, \quad \tilde{Z}_3 = \frac{1}{\epsilon} 48h^2.
\end{aligned} \tag{5.48}$$

The β and γ -functions can be calculated as well.

$$\beta_P = \lim_{n \rightarrow 4} \mu \frac{dP}{d\mu}, \quad \gamma_\Phi = \lim_{n \rightarrow 4} \mu \frac{d\Phi}{d\mu}, \tag{5.49}$$

where $P = \{m, M, \xi, h, \lambda, g\}$ and $\Phi = \{\varphi, \psi, A_\mu\}$. The general procedure in curved spacetime can be found in [174, 204], here we only present the results. Using relations in Eq. (5.48) we can write

$$\begin{aligned}
\gamma_\varphi &= -\frac{8}{(4\pi)^2} (h^2 - g^2), \\
\gamma_\psi &= -\frac{1}{(4\pi)^2} (2h^2 + 24g^2), \\
\beta_\xi &= \frac{1}{(4\pi)^2} \left(\frac{5}{3} \lambda - 12h^2 + 8g^2 \right) \left(\xi - \frac{1}{6} \right), \\
\beta_h &= -\frac{1}{(4\pi)^2} (12hg^2 + 8h^3), \\
\beta_\lambda &= +\frac{1}{(4\pi)^2} \left(\frac{11}{3} \lambda^2 - 24\lambda g^2 + 72g^4 + 16\lambda h^2 - 96h^4 \right), \\
\beta_M &= -\frac{1}{(4\pi)^2} (12g^2 - 6h^2) M, \\
\beta_{m^2} &= -\frac{1}{(4\pi)^2} \left(\left(-\frac{5}{3} \lambda + 12g^2 - 8h^2 \right) m^2 + 48h^2 M \right).
\end{aligned} \tag{5.50}$$

for the matter sector, and

$$\begin{aligned}
\beta_{a_1} &= \frac{1}{(4\pi)^2} \frac{N_s}{2} \left(\xi - \frac{1}{6} \right), \\
\beta_{a_2} &= \frac{1}{(4\pi)^2} \left(\frac{1}{120} N_s + \frac{1}{20} N_f + \frac{1}{10} N_v \right), \\
\beta_{a_3} &= \frac{1}{(4\pi)^2} \left(-\frac{1}{360} N_s - \frac{11}{360} N_f - \frac{31}{180} N_v \right), \\
\beta_{a_4} &= \frac{1}{(4\pi)^2} \left(\frac{1}{180} N_s + \frac{1}{30} N_f - \frac{1}{10} N_v \right), \\
\beta_\Lambda &= \frac{1}{(4\pi)^2} \left(\frac{1}{2} N_s m^4 - 2 N_f M^4 \right), \\
\beta_\kappa &= \frac{1}{(4\pi)^2} \left(N_s m^2 \left(\xi - \frac{1}{6} \right) + \frac{N_f M^2}{3} \right),
\end{aligned} \tag{5.51}$$

for the vacuum sector. The β -functions for the coupling and masses of the matter fields are exactly the same as in flat spacetime [205], the new features being the equations for the non-minimal ξ and the vacuum action parameters $\Lambda, \kappa, \beta_{a_1 \dots a_4}$.

The renormalization group equations in curved spacetime follow also the overall μ -dependence of the effective action:

$$\mu \frac{d}{d\mu} \Gamma[g_{\mu\nu}, \Phi, P, n, \mu] = 0, \tag{5.52}$$

which gives, in four dimensions and \overline{MS} renormalization scheme [174],

$$\left[\mu \frac{\partial}{\partial \mu} + \beta_P \frac{\partial}{\partial P} + \int d^4 x \gamma_\Phi \Phi \frac{\delta}{\delta \Phi(x)} \right] \Gamma[g_{\mu\nu}, \Phi, P, \mu] = 0. \tag{5.53}$$

The RG equations can be used to find the one-loop effective potential, as we comment in the next section.

5.4 Effective potential

The effective potential is defined as the zero-order approximation in the derivative expansion for the scalar sector of the effective action [76]:

$$\Gamma[g_{\mu\nu}, \Phi, P, \mu] = \int d^4 x \sqrt{-g} \left[-V_{\text{eff}}(\varphi, g_{\mu\nu}) + \frac{1}{2} Z(\varphi, g_{\mu\nu}) g^{\alpha\beta} \partial_\mu \varphi \partial_\nu \varphi + \dots \right]. \tag{5.54}$$

Therefore, we can write

$$\left[\mu \frac{\partial}{\partial \mu} + \beta_P \frac{\partial}{\partial P} + \int d^4 x \gamma_\Phi \Phi \frac{\delta}{\delta \Phi(x)} \right] V_{\text{eff}}(\varphi, g_{\mu\nu}) = 0. \tag{5.55}$$

At one-loop order the dependence on μ will be only through logarithms like $\ln X/\mu^2$, where the exact form of the mass two dimension parameter X can be found by imposing renormalization conditions.

The effective potential can be expanded in scalar curvature dependence,

$$V_{\text{eff}} = V_0 + RV_1 + R^2V_2 + \dots, \quad (5.56)$$

where V_0 is the flat-space effective potential, RV_1 the first curvature-dependent correction and so on, and we are interested only in the first correction. We can see that both functions separately satisfy Eq. (5.55). We can also use the fact that, in one-loop order, degrees of freedom with different spins give additive contributions to the effective action, and we can further split $V_0 = V_0^{(0)} + V_0^{(1/2)} + V_0^{(1)}$ and the same for V_1 . Hence, each contribution to the effective potential can be calculated separately and summed in the end.

General expressions for the effective potential for different models were found in [206]. Another way of calculating the effective potential in curved spacetime is by using local momentum representation and Riemann normal coordinates [207, 208]. Despite of having more cumbersome calculations, this method gives the same results from Schwinger-de Witt technique, with the advantage that the dependence on the mass dimension parameters in the logarithmic corrections is explicit.

5.4.1 Sterile scalar and massive fermions with Yukawa interaction

The effective potential allows us to estimate observable effects of the quantum corrections, and maybe constrain new physics. As an example, consider the action of a sterile scalar, that is, a scalar which is a singlet under any gauge group, coupled with N copies of a massive fermion field. Barra et. al [209] and Toms [210] have shown that such theory requires odd terms in the potential in order to be renormalizable in four dimensions:

$$S = \int d^4x \sqrt{-g} \left[i\bar{\psi}_i(\gamma^\mu \nabla_\mu + iM + ih\varphi)\delta^{ij}\psi_j + \frac{1}{2}(g^{\mu\nu}\partial_\mu\varphi\partial_\nu\varphi - m^2\varphi^2 + \xi R\varphi^2) - \frac{\lambda}{4!}\varphi^4 - \frac{g}{3!}\varphi^3 - \tau\varphi - fR\varphi \right]. \quad (5.57)$$

It is troublesome to couple such sterile scalar with Standard Model fermions, but ψ_i could be in principle right-handed neutrinos or any beyond the Standard Model massive fermions, while φ could be the inflaton field (see Part III). The one-loop effective potential for this action is

$$V_{\text{eff}}(g_{\mu\nu}, \varphi) = \rho_\Lambda + \frac{1}{2}(m^2 - \xi R)\varphi^2 + V + \frac{\hbar}{2(4\pi)^2} \left[\left(\frac{1}{2}(V'' + m^2)^2 - \left(\xi - \frac{1}{6} \right) R(V'' + m^2) \right) \times \ln \left(\frac{V'' + m^2}{\mu^2} \right) - 2N(M + h\varphi)^4 \ln \left(\frac{(M + h\varphi)^2}{\mu^2} \right) + \frac{N}{3}R(M + h\varphi)^2 \ln \left(\frac{(M + h\varphi)^2}{\mu^2} \right) \right], \quad (5.58)$$

where ρ_Λ is the vacuum energy density, and V is

$$V(\varphi) = \frac{1}{2}m^2\varphi^2 + \frac{\lambda}{4!}\varphi^4 + \frac{g}{3!}\varphi^3 + \tau\varphi + fR\varphi. \quad (5.59)$$

The scalar field has no symmetries that forbids the appearance of the odd terms, and so they are present. In principle one could get rid of one of the terms $g\varphi^3$ or $\tau\varphi$ by field redefinitions, but not both.

It is interesting to analyse the induced gravity, i.e the contribution to the vacuum sector, due to solutions of the φ with the odd terms in the potential within some approximations. One particularly interesting analysis is to see how this odd terms could influence in an inflationary scenario (more details will be given in the Part III). In order to do that, let's consider that the non-minimal coupling $\xi R\varphi^2$ and the quartic self-coupling $\lambda\varphi^4$ of the scalar field are dominating, while the mass, classical odd terms and leading order quantum corrections in the effective potential are small and can be consider as perturbations. In a first approximation, the kinetic term can also be consider small, as long as R is almost constant, which happens during inflation [209]. In this case, the equation of motion for the scalar field becomes,

$$\xi R\varphi - \frac{1}{6}\lambda\varphi^3 - m^2\varphi - \frac{1}{2}g\varphi^2 - \tau - fR = 0. \quad (5.60)$$

As $\frac{m^2}{M_P^2}, |\frac{\tau}{M_P^3}|, |\frac{f}{M_P}|, |\frac{g}{M_P}| \ll \xi, \lambda$, we can write $\varphi = \varphi_0 + \varphi_1$, and at zero-order approximation we have,

$$\varphi_0^2 = \frac{6\xi R}{\lambda}. \quad (5.61)$$

And in first order approximation,

$$\varphi_1 = -m^2 \sqrt{\frac{3}{2\lambda\xi R}} - \frac{3g}{2\lambda} - \frac{\tau}{2\xi R} - \frac{f}{2\xi}. \quad (5.62)$$

Then, substituting $\varphi = \varphi_0 + \varphi_1$ back into the action and keeping only $O^1(m^2, g, \tau, f)$ we arrive at the following induced Lagrangian for gravity:

$$L_{\text{ind}} = -\frac{3m^2\xi}{\lambda}R + \frac{3\xi^2}{2\lambda}R^2 + \sqrt{\frac{6\xi R}{\lambda}} \left[\tau - \left(f + \frac{g\xi}{\lambda} \right) R \right]. \quad (5.63)$$

Therefore, the induced gravity is a non-polynomial function of the scalar curvature R , and it is a consequence of just requiring a renormalized theory of coupled sterile scalar and massive fermions.

We will analyse the inflationary scenario with this correction in the next part, after a brief review of early cosmology and inflation.

Part III

The Standard Model of Cosmology

6

Early Universe

Until the sixties mankind had no idea if the Universe seen around us had a beginning or existed since ever, as the two scenarios would be equally supported by Einstein's theory of gravity, General Relativity. In 1929 Hubble had measured a universe expansion [211], but the results were quite controverse. But in 1964 the picture changed completely. The radio-astronomers Wilson and Penzias detected by chance what is now known as Cosmic Microwave Background Radiation (CMB) [212], a 2.7 K background noise that comes equally from every direction of the sky. This radiation had been already predicted by Gamow and Dicke [213,214] as a primordial radiation resulting from the Universe undergoing an extremely hot and dense phase. This favoured the Big Bang theory, which claimed that the Universe indeed had a beginning, when all its content was once collapsed in a single point, and afterwards it expanded to the cosmological scales. One of the main predictions of the Big Bang theory is that this cosmic background radiation would have a black-body spectrum, what was only verified, with astonishing agreement, by the COBE satellite measurements in 1990 [215].

When we work out General Relativity with the big bang cosmology we arrive at a singularity (infinite curvature) at time $t = 0$. This could mean that the big bang is in fact the beginning of space and time, but it could also mean that General Relativity is just a low-energy description of gravity, and to get trustful results at extremely high energies, such as in the big bang ($\sim M_P$), we need a new theory of gravity that is valid up to this regimes i.e. quantum gravity. In fact, the current most accepted scenario of early universe is that the time immediately before the radiation dominated era is not the beginning of everything, but the end of an inflationary era.

In order to have a consistent cosmological evolution that doesn't evoke fine-tuning of

initial conditions we need our Universe to undergo an epoch of accelerated expansion¹, called inflation, driven by a scalar field, named inflaton. The idea of inflation was envisioned by Guth, Linde, Steinhardt and Starobinsky in the 80's [216–219] and further developed later on. In the inflationary scenario, after inflation ends, the inflaton field decays into the Standard Model particles, in what is called reheating², and the inflaton's quantum fluctuations during inflation generate the initial seeds of perturbations on the matter density field and background metric that later on will grow to form all the structure we see in the Universe. We still don't have a definitive picture of what happened before inflation, or if there was anything at all before (or even if inflation really happened!), but we believe that a quantum gravity theory could shed some light on this dark period.

However, if we only take into account the Standard Model content and gravity, plus an inflationary epoch, we don't get a perfect agreement with the behavior of the Universe at large scales. In 1933, Zwicky [220] calculated the gravitational mass of galaxies within the Coma cluster, through their rotation velocity, and obtained a value around 400 times greater than expected from their luminosity. He then proposed that most of the galaxy matter was dark and gave it the name of *dark matter*. Today we know that we need more matter than the luminous one, not only to fix the rotation curves of galaxies, but to explain the very structure of the Universe the way we see it. It seems that dark matter is a new particle that interacts mostly through gravity, and maybe extremely weakly through the other forces, and it is also non-relativistic since very early times, so it is usually called *cold dark matter*. We still don't know what dark matter really is, its quantum numbers, mass and how it couples with the Standard Model. We only know that it makes around $\sim 80\%$ of the matter density of the Universe although its true nature remains a mystery.

When dark matter is taken into account we are able to have an amazingly accurate description of our Universe evolution [221–225]. After reheating, the observable Universe was a dense plasma of fundamental particles in thermal equilibrium and the temperature was so high that all particles were massless. As the Universe expanded, it cooled down to the electroweak phase transition temperature, ~ 120 GeV, and the particles gained mass through the Higgs mechanism. The quarks are asymptotically free at high energies, but at the QCD phase transition, around 150 MeV, the strong interactions between quarks and gluons became important. After that, quark bound states were able to form and the baryons and mesons became the relevant degrees of freedom.

If the production rate of a given species is smaller than the expansion rate of the Universe this species departs from thermal equilibrium and decouples from the primordial plasma. As the dark matter, if ever in thermal equilibrium, interacts very little with other particles it decoupled relatively early, around 1 MeV³. After that, it started to form gravitational potential wells where later on the baryonic matter were attracted to, cooled down and formed

¹There are other ways to avoid the fine-tuning problems in big bang cosmology, but inflation is the most popular one.

²The name reheating is because during inflation the universe expands so fast that all the other content get negligible energy density and the Universe has to be re-heated after inflation ends.

³The exact value will depend on the dark matter model.

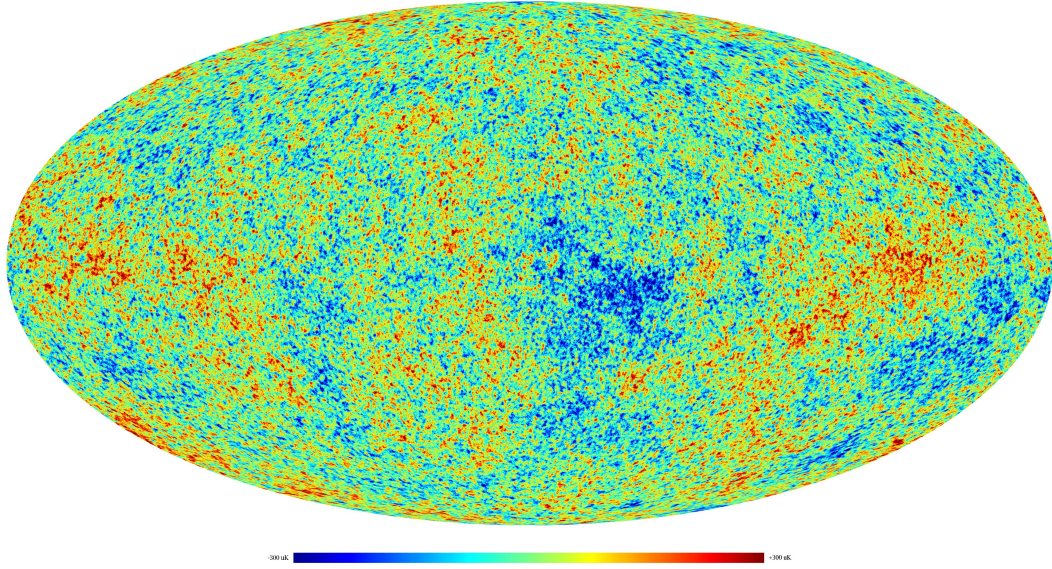


Figure 6.1: Cosmic Microwave Background Radiation measured by Planck satellite. It depicts the temperature variation across the background. Figure of ESA/Planck Collaboration [14]

galaxies and clusters. The neutrinos also decoupled early, at 0.8 MeV, as they only interact through weak force. At energies around 1 eV the reaction $e^- + p^+ \leftrightarrow H + \gamma$ became inefficient to destroy Hydrogen atoms and more atoms started to form. This epoch is called *recombination*. After recombination, most of the electrons were in bound states with protons and neutrons, and the Thomson scattering, $e^- + \gamma \rightarrow e^- + \gamma$, that kept the photons strongly coupled to the plasma becomes inefficient. Thus the photons decoupled, and their last scattering surface traveled freely through the Universe to become what we observe today as the Cosmic Microwave Background Radiation. Figure 6.1 is an image of the CMB measured by the Planck satellite, a picture of the Universe when it was $\sim 400,000$ years old. The red color represent hotter regions. The temperature variations of the CMB are around $\delta T/\bar{T} \sim 10^{-5}$ which reflects the thermal equilibrium state the photons were before decoupling.

After the photons decoupling, light elements began to form, more precisely Hydrogen, Helium, Deuterium, Beryllium and Lithium. Their abundances can be calculated and they match accurately with observations⁴. Afterwards, gravitational instability took place, and baryonic matter fell into dark matter potential wells, collapsed into the first stars, then galaxies and clusters of galaxies.

If there were only dark and baryonic matter in the Universe it would be experiencing a decelerating expansion today. But in 1998 two independent groups measured, using supernovae data, that the Universe expansion is actually accelerating [228, 229]. The fluid that drives this accelerated expansion behaves like a vacuum density, and we usually model it as

⁴Actually, the abundance of primordial Lithium predicted by Λ CDM model is on the order of three times higher when compared to observations, a puzzle there is still lacking an explanation [226, 227]

a cosmological constant in Einstein's equation, which value is extremely small (4×10^{-66} eV in natural units). The attempts to reproduce this value from vacuum contributions of SM particles result in a complete failure, around 100 orders of magnitude higher, and introducing a bare cosmological constant that cancels all this contribution to leave only the observed value requires a huge fine-tuning [230, 231]. There is not yet a fundamental description or explanation for the current accelerated expansion of the Universe, and dark energy is now one of the biggest problems in theoretical physics.

The energy density of our universe today is made of $\sim 4\%$ of baryonic matter, $\sim 25\%$ of dark matter and $\sim 70\%$ of dark energy, so around 95% of the Universe content is still a puzzle in modern Physics [232]. It is embarrassing to see how much we know that we don't know.

In this last part we shall look into early and late times cosmology to see how initial seeds of perturbation can form large scale structure and then show how the cold dark matter model can be modified to better fit the observational data.

6.1 The Friedmann-Lemaître-Robertson-Walker Universe

We are in the era of precision cosmology. It is possible to make large and accurate cosmological observations as never before in our history through cataloging a huge number of galaxies, clusters and supernovae. Such galaxies surveys suggest that our Universe is homogeneous and isotropic at scales above 100 Mpc. Figure 6.2 is a map of the Sloan Digital Sky Survey (SDSS), where we can observe how the galaxy distribution is very similar even in opposite regions of the sky. Furthermore, the homogeneity and isotropy of the Universe at its young age ($\approx 400,000$ years after the Big Bang) can be seen through observations of the Cosmic Microwave Background Radiation (CMB).

Even though this does not mean that our Universe as a whole is homogeneous and isotropic, it does imply that at least a region as large as our present Hubble volume⁵ is. Therefore, we can *a priori* consider all observable universe to be homogeneous and isotropic at large scales. This is called the cosmological principle.

The spacetime metric that satisfies the cosmological principle and describes an homogeneous and isotropic universe is known as the Friedmann-Lemaître-Robertson-Walker (FLRW) metric, and it is given by (in comoving spherical coordinates):

$$ds^2 = -dt^2 + a^2(t) \left(\frac{dr^2}{1 - kr^2} + r^2 d\theta^2 + r^2 \sin^2 \theta d\phi^2 \right). \quad (6.1)$$

It can only depend on a time-dependent function that scales all the three spatial directions, otherwise it would destroy homogeneity and isotropy. This function $a(t)$ is called scale factor and it governs the evolution of the spatial part of the metric through time. The constant k ⁶

⁵Hubble volume, or Hubble sphere, is defined through the characteristic scale $H(t)^{-1}$. The expansion rate of the Universe today is parametrized by H_0 and the radius of the Hubble sphere today is defined as c/H_0 .

⁶ k is in units which the spatial curvature radius equals one.

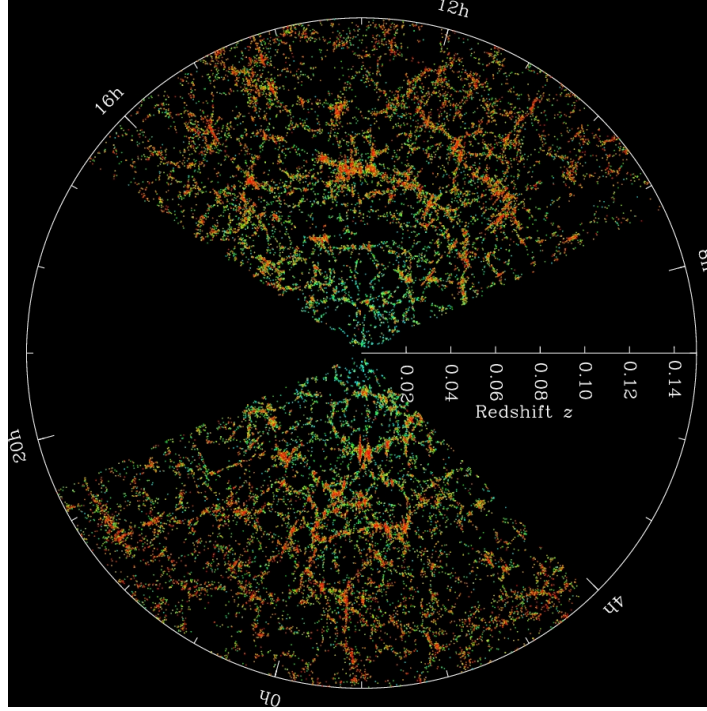


Figure 6.2: SDSS map of the Universe. The Earth is in the middle of the image and each point is a galaxy. Figure from [15].

that appears in the FLRW metric can be 0, +1, -1, where each of this values determines a different spatial curvature i.e. zero, positive and negative, respectively.

The non-vanishing components of the Ricci tensor for the FLRW metric are

$$\begin{aligned} R_{00} &= -3\frac{\ddot{a}}{a}, \\ R_{ij} &= \left[\frac{\ddot{a}}{a} + 2\frac{\dot{a}^2}{a^2} + \frac{2k}{a^2} \right] g_{ij}. \end{aligned} \quad (6.2)$$

and therefore the scalar curvature is

$$R = 6 \left[\frac{\ddot{a}}{a} + \frac{\dot{a}^2}{a^2} + \frac{k}{a^2} \right]. \quad (6.3)$$

6.1.1 Friedmann equations

To proceed with the study of the Universe with the FLRW metric we need also to talk about the matter content. We choose to model matter as a perfect fluid⁷ to assure consistency with the diagonal form of the metric and spatial isotropy. Hence, it follows that the energy-momentum tensor, in comoving coordinates, has the form

$$T_{\nu}^{\mu} = \text{diag}(-\rho, p, p, p,) \quad (6.4)$$

⁷Perfect fluids, or ideal fluids, are completely described by their density and pressure, which are constant throughout space.

where $\rho = \rho(t)$ is the energy density and $p = p(t)$ is the pressure. From the energy-momentum conservation it follows that, for $\nu = 0$:

$$\begin{aligned}\nabla_\mu T_0^\mu &= 0 = \partial_\mu T_0^\mu + \Gamma_{\mu\lambda}^\mu T_0^\lambda - \Gamma_{\mu 0}^\lambda T_\lambda^\mu \\ &= \frac{\partial \rho}{\partial t} + 3 \frac{\dot{a}}{a} (\rho + p) .\end{aligned}\tag{6.5}$$

We can choose a simple equation of state that relates the energy density and pressure of the fluid. In general, perfect fluids types which are interesting in cosmology obey the following equation of state [221]:

$$p = \omega \rho,\tag{6.6}$$

where ω is known as the equation of state parameter.

Then, the Eq. (6.5) becomes,

$$\frac{\dot{\rho}}{\rho} = -3(1 + \omega) \frac{\dot{a}}{a}.\tag{6.7}$$

Assuming that ω is constant we can integrate this last equation, which gives

$$\rho \propto a^{-3(1+\omega)}.\tag{6.8}$$

Different values of ω determine different types of ideal fluids. The *dust* is any agglomerate of collisionless non-relativistic particles, so it has a negligible internal pressure when compared to its energy density, $p_M = 0$. The particles can be baryonic⁸ or dark matter, and a Universe composed mostly of dust is called a *matter dominated* universe. The energy density for this case follows the relation:

$$\rho_M \propto a^{-3}, \quad \omega = 0.\tag{6.9}$$

Hence, we see that the matter density decreases as the Universe expands.

Radiation is the name given for the type of fluid used to describe photons and massive relativistic particles, such as the neutrinos. As we know that the trace of the electromagnetic energy-momentum tensor vanishes [179], $\omega = 1/3$ for radiation and the equation of state becomes $p_R = \frac{1}{3}\rho_R$. In this case, the energy density goes with the scale factor as

$$\rho_R \propto a^{-4}.\tag{6.10}$$

We call *radiation dominated* a universe in which most of its content is radiation.

Another interesting type of fluid is the *vacuum energy*. In this case, $\omega = -1$, $p_\Lambda = -\rho_\Lambda$ which gives the same energy-momentum tensor of a cosmological constant. For this case the energy density remains constant through the Universe expansion,

$$\rho_\Lambda \propto a^0.\tag{6.11}$$

⁸In cosmology *baryonic matter* stands for all Standard Model particles that compose atoms and so all visible matter in the Universe.

Therefore, as the energy densities of dust and radiation decrease as the Universe expands, if there is initially a non-vanishing quantity of vacuum energy, it will eventually predominate the Universe after a long time. If that happens, we say that the Universe is *vacuum dominated*.

In order to find the dynamical equations that describe the evolution of the scale factor $a(t)$ we need to solve the Einstein's equation $R_{\mu\nu} - \frac{1}{2}g_{\mu\nu}R = 8\pi GT_{\mu\nu}$. The 00-component gives the Friedmann equation:

$$\left(\frac{\dot{a}}{a}\right)^2 + \frac{k}{a^2} = \frac{8\pi G}{3}\rho. \quad (6.12)$$

On the other hand, the ii -components, which are all equal due to isotropy, give

$$2\frac{\ddot{a}}{a} + \left(\frac{\dot{a}}{a}\right)^2 + \frac{k}{a^2} = -8\pi Gp. \quad (6.13)$$

The substitution of Eq. (6.12) in Eq. (6.13) results in an equation for the acceleration of the scale factor

$$\frac{\ddot{a}}{a} = -\frac{4\pi G}{3}(\rho + 3p). \quad (6.14)$$

We know that today $\dot{a}(t) > 0$, and if $\rho + 3p$ was always positive in the past, then \ddot{a} was always negative. So, at some past time a must have been zero. This event, called Big Bang, is generally defined as the zero time and in $a = 0$ the FLRW cosmology has a singularity i.e. the curvature becomes infinite.

The expansion rate of the Universe is determined by the Hubble parameter $H \equiv \dot{a}/a$. As we can see, the Hubble parameter is not a constant and in general goes with time as t^{-1} . The Hubble time, or Hubble radius, H^{-1} , defines the time scale of the expansion and the Hubble constant H_0 is the value of the expansion rate today, measured as $H_0 = 67.8 \pm 0.9 \text{ km.s}^{-1}/\text{Mpc}$ from CMB data⁹ [235].

The Friedmann equation can be rewritten as

$$H^2 + \frac{k}{a^2} = \frac{8\pi G}{3}\rho \Rightarrow \frac{k}{H^2 a^2} = \frac{8\pi G}{3H^2}\rho - 1 \equiv \Omega - 1, \quad (6.15)$$

where Ω is called the density parameter and is the ratio between the energy density and the critical density,

$$\Omega \equiv \frac{\rho}{\rho_c}, \quad \rho_c \equiv \frac{3H^2}{8\pi G}. \quad (6.16)$$

As $H^2 a^2 \geq 0$, there is a correspondence between the sign of k and the sign of $\Omega - 1$, given by [221]:

$$\begin{aligned} k = +1 &\Rightarrow \Omega > 1, & \rho > \rho_c, & \text{Closed} \\ k = 0 &\Rightarrow \Omega = 1, & \rho = \rho_c, & \text{Flat} \\ k = -1 &\Rightarrow \Omega < 1, & \rho < \rho_c, & \text{Open} \end{aligned}$$

⁹Actually, we have currently a tension in the measured value of the expansion rate today inferred from the CMB and from local measurements i.e. supernovae, galaxy clusters, weak lensing. The local measurements give $H_0 = 74.03 \pm 1.42 \text{ km.s}^{-1}/\text{Mpc}$ which results in a 4.4σ difference between the two measurements [233, 234]. To the present date there is no clear explanation for such a tension, but it could be an indication of new physics.

Hence, the density parameter tell us which of the three FLRW geometries describe our Universe, so it is of great importance to measure it with precision. Recent observations of the Cosmic Microwave Background Radiation lead to $\Omega = 1.0005 \pm 0.0033$ [235], therefore the spatial slice of our Universe is very flat.

Finally, we can see that the scale factor evolution for a universe dominated by different types of energies (different ω 's) is found from the solution of Friedmann equations. Considering $\rho = \rho_i a^{-3(1+\omega)}$, where ρ_i is a constant, we have that Eq. (6.12) for $k = 0$ results in:

$$\left(\frac{\dot{a}}{a}\right)^2 = \frac{8\pi G}{3} \rho_i a^{-3(1+\omega)} \Rightarrow \dot{a} = \left(\frac{8\pi G}{3} \rho_i\right)^{1/2} a^{1-\frac{3}{2}(1+\omega)}. \quad (6.17)$$

The solution for such equation is

$$a = C_1 t^{\frac{2}{3(1+\omega)}}, \quad C_1 = \text{constant}. \quad (6.18)$$

Therefore, for a matter-dominated universe when $\omega = 0$, $a \propto t^{2/3}$, and for a radiation-dominated universe $\omega = 1/3$ and the scale factor evolves as $a \propto t^{1/2}$. For the case when $\omega = -1$ we go back in Eq. (6.17), that becomes $\dot{a} = \left(\frac{8\pi G}{3} \rho_i\right)^{1/2} a$, which implies $a \propto e^{Ht}$. So, in a vacuum-dominated universe the scale factor grows exponentially. An universe with exponential acceleration is also known as de Sitter universe.

Right after the Big Bang, the Universe was an extremely hot plasma of relativistic fundamental particles, so it behaved as a radiation-dominated universe [221]. As the Universe expanded and cooled down bound states started to form as protons, neutron and eventually the first light atoms. As we saw earlier, the radiation energy density decreases faster with the expansion than the matter energy density, and consequently the Universe became matter-dominated with the scale factor evolving like $a \propto t^{2/3}$. Today the Universe is not matter-dominated anymore, but vacuum-dominated. We call the source of such observed accelerated expansion as dark energy and its true nature is one of the major mysteries in modern Physics. This picture is named the Λ CDM model of cosmology.

The Λ CDM model gives several predictions of how the Universe evolved from its early stages to what we see today, and the agreement with observations is astonishing. For example, the temperature at different stages can be calculated, and combined with our knowledge of particle physics and thermodynamics we get predictions on the formation of light atoms like Hydrogen, Helium, Deuterium and Lithium. The abundance of such primordial atoms predicted by big bang nucleosynthesis (BBN) agrees perfectly with the observed abundance, something that is hardly accomplished by other models or easily destroyed with modifications of Λ CDM.

But despite of its success, the Λ CDM model indeed contains some fine-tuning problems, related to its flatness and CMB homogeneity. Next, we shall see this problems and how the Λ CDM model can be extended in order to solve them.

6.2 Flatness and horizon problems

In Eq. (6.15) we defined the density parameter Ω in terms of the curvature k and Hubble parameter:

$$|\Omega - 1| = \frac{|k|}{a^2 H^2}. \quad (6.19)$$

If the Universe is completely flat, $\Omega \equiv 1$, then it remains flat for all time, but otherwise it evolves. For a matter and radiation-dominated universe the expansion is decelerating (\dot{a} decreases with time) and therefore $(aH)^{-1}$ increases with time. Consequently, the density parameter evolves away from flatness, $|\Omega - 1| > 0$.

The current observed spatial curvature is, however, very small, which implies that at much earlier time it must have been extremely small. For example, to match the present value of $|\Omega - 1|$ it is required that, at the time of BBN, $|\Omega(t_{BBN}) - 1| \lesssim 10^{-16}$. This is known as the flatness problem because such fine-tuning on the initial conditions seems extremely unlikely.

In order to talk about the second fine-tuning problem let's define the *particle horizon* as the maximum physical distance a light signal can travel between two times t_i and t_f :

$$d_h = \int_{t_i}^{t_f} \frac{dt'}{a(t')}. \quad (6.20)$$

This defines the past light cone of a particle at t_f since t_i .

Everything we observe in the Universe today was on our past light cone, in particular the last scattering surface of photons by electrons at recombination time, the CMB. But if we calculate the past light cone in a radiation-dominated universe of particles from the last scattering surface until the singularity we find that this is much smaller than our past light cone:

$$\int_0^{t_{\text{rec}}} \frac{dt'}{a(t')} \ll \int_{t_{\text{rec}}}^{t_0} \frac{dt'}{a(t')}. \quad (6.21)$$

This implies that opposite regions we observe in the CMB (actually, this happens already for separations of $\gtrsim 2^\circ$) didn't have enough time to be in causal contact, e.g. see Figure (6.3) [16]. However, even opposite regions of the CMB have very similar temperature and density distributions. Therefore, the homogeneity we observe in the CMB radiation can only be explained within the Λ CDM model if the Universe was already like this from the very beginning, but this again requires a huge fine-tuning on the initial conditions.

To rescue the Λ CDM model we can use the aid of a period of extremely fast expansion before the radiation era. Such period is called inflation and we shall look into it in more detail in the next section.

6.3 Inflation

Inflation is by definition any epoch during which the scale factor is accelerating:

$$\ddot{a} > 0. \quad (6.22)$$

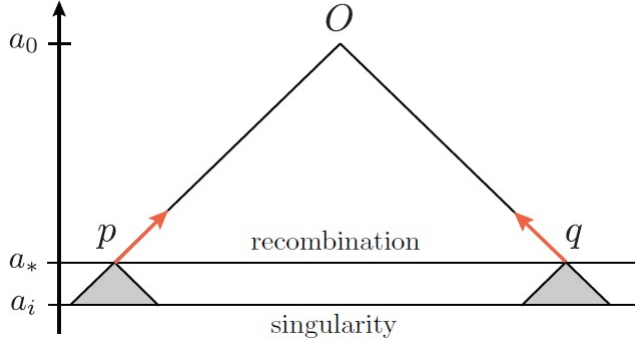


Figure 6.3: The horizon problem in Λ CDM model. All events that we currently observe are on our past light cone. The intersection of our past light cone with the spacelike slice labelled *recombination* corresponds to two opposite points in the observed CMB. Their past light cones don't overlap before they hit the singularity, $a_i = 0$, so the points appear never to have been in causal contact. Figure from [16].

We can write an equivalent condition for inflation in terms of the Hubble length, or more precisely the comoving Hubble length:

$$\frac{d}{dt} \left(\frac{1}{aH} \right) < 0 \quad \Rightarrow \quad -\frac{\dot{H}}{H^2} < 1. \quad (6.23)$$

Therefore, the comoving Hubble length decreases with time and so the observable universe becomes smaller during inflation.

It is easy to see that the first condition of Eq. (6.23) makes the density parameter Eq. (6.15) to evolve towards flatness during an inflationary epoch. Therefore, even if the initial conditions of the Universe favour a non-trivial spatial curvature, eventually it will become flat after a sufficient time of inflation.

An inflationary epoch also solves the horizon problem due to the reduction of the comoving Hubble length during this period. The integral in Eq. (6.20),

$$d_h = \int \frac{da}{a^2 H}, \quad (6.24)$$

is larger at early times, as $(aH)^{-1}$ is decreasing, and therefore the particle horizon can become very large in the past. This allows our present observable Universe to have origin from a region well inside the Hubble radius. This makes all the observable universe to be in causal contact at some time during inflation. In particular, comoving scales (and physical as well), $a\lambda \propto ak^{-1}$, get out of the horizon during inflation and enter back in only at late times, during radiation, matter or vacuum-dominated eras. This whole picture of early inflationary epoch plus Λ CDM model is known as the Standard Model of Cosmology.

An interesting question now would be, if we assume that the inflationary epoch is driven also by a perfect fluid, what type of ideal fluid it should be? From the dynamical equation

for the scale factor acceleration Eq. (6.14), in order to have $\ddot{a} > 0$ we need that

$$\rho + 3p < 0. \quad (6.25)$$

Hence, inflation is driven by a material with negative pressure. The relation implies the equation of state parameter to be:

$$\omega < -\frac{1}{3}. \quad (6.26)$$

In fact, a fluid with negative pressure can be modeled by a scalar field, which in this case is usually referred to as *inflaton*,

$$\mathcal{L} = -\frac{1}{2}\partial_\mu\phi\partial^\mu\phi - V(\phi). \quad (6.27)$$

Then, the energy-momentum tensor is given by

$$T_{\mu\nu} = -\frac{2}{\sqrt{-g}}\frac{\partial\sqrt{-g}\mathcal{L}}{\partial g^{\mu\nu}} = \partial_\mu\phi\partial_\nu\phi - g_{\mu\nu}\left(\frac{1}{2}g^{\alpha\beta}\partial_\alpha\phi\partial_\beta\phi - V(\phi)\right). \quad (6.28)$$

Consistency with FLRW metric implies $\phi = \phi(t)$, hence we have for the energy density $\rho_\phi = -T_0^0$ and pressure $p_\phi\delta_i^j = T_i^j$:

$$\rho_\phi = \frac{1}{2}\dot{\phi}^2 + V(\phi), \quad (6.29)$$

$$p_\phi = \frac{1}{2}\dot{\phi}^2 - V(\phi). \quad (6.30)$$

Therefore, we can write the Friedmann equation (6.12) for this content in a flat space as:

$$H^2 = \frac{8\pi G}{3}\left(\frac{1}{2}\dot{\phi}^2 + V(\phi)\right), \quad (6.31)$$

and the continuity equation (6.5) becomes:

$$\ddot{\phi} + 3H\dot{\phi} = -\frac{dV}{d\phi}. \quad (6.32)$$

Using ρ_ϕ and p_ϕ we see that the condition for inflation is satisfied as long as

$$\dot{\phi}^2 \ll V(\phi). \quad (6.33)$$

The potential of the scalar field is treated here as an arbitrary function, but the hope is to someday obtain it from more fundamental physics. At present time, inflation is just a model and different potentials correspond to different types of inflation.

Due to relation in Eq. (6.33) there is a standard approach to inflation which is to consider an almost flat potential so that the kinetic term of the scalar field is negligible. This is called *slow-roll approximation* because the field rolls slowly down the potential. Within this approximation, Eqs. (6.31) and (6.32) become:

$$H^2 \simeq \frac{8\pi G}{3}V(\phi), \quad (6.34)$$

$$3H\dot{\phi} \simeq -V'(\phi). \quad (6.35)$$

where we have assumed also that

$$\ddot{\phi} < 3H\dot{\phi}. \quad (6.36)$$

We can define the dimensionless parameters, called slow-roll parameters

$$\epsilon(\phi) \equiv 4\pi G \left(\frac{\dot{\phi}}{H} \right)^2, \quad (6.37)$$

$$\eta(\phi) \equiv \frac{\ddot{\phi}}{H\dot{\phi}}, \quad (6.38)$$

and using Eqs. (6.32)-(6.36) we get

$$\epsilon(\phi) \simeq \frac{1}{16\pi G} \left(\frac{V'(\phi)}{V(\phi)} \right)^2 = -\frac{\dot{H}}{H^2}, \quad (6.39)$$

$$\eta(\phi) \simeq \frac{1}{8\pi G} \left(\frac{V''(\phi)}{V(\phi)} \right) = \frac{V''(\phi)}{3H^2}. \quad (6.40)$$

In term of this parameters the slow-roll conditions are:

$$|\epsilon| \ll 1, \quad |\eta(\phi)| \ll 1, \quad (6.41)$$

and inflation ends when $\epsilon \approx 1$.

Another important quantity we need to introduce is the amount of inflation that occurs. This is defined as the number of e-foldings N

$$dN \equiv -Hdt. \quad (6.42)$$

So, the amount of inflation from a time t to its end is given by

$$N = -\int_t^{t_{\text{end}}} Hdt = -\int_{\phi}^{\phi_{\text{end}}} \frac{H}{\dot{\phi}} d\phi = -\sqrt{4\pi G} \int_{\phi}^{\phi_{\text{end}}} \frac{1}{\sqrt{\epsilon(\phi)}} d\phi. \quad (6.43)$$

Within the slow-roll approximation we have

$$N \simeq 8\pi G \int_{\phi_{\text{end}}}^{\phi} \frac{V(\phi)}{V'(\phi)} d\phi. \quad (6.44)$$

In order to solve the flatness and horizon problems we need around $N \simeq 60$ e-folds. The precise value depends on the energy scale of inflation (in which in general $H \sim 10^{11} - 10^{13}$ GeV) and on the details of reheating phase after inflation, when the inflaton field decays in Standard Model particles.

6.3.1 Inflationary observables

We can write correlation functions and power spectra for the perturbations in the matter and metric at the early universe. From these statistical quantities we can build cosmological

observables, and the most important ones that can be related to inflation are the scalar spectral index, n_s , tensor spectral index, n_T and tensor-to-scalar ratio, r :

$$n_s - 1 \equiv \frac{d \ln P_\zeta}{d \ln k}, \quad (6.45)$$

$$n_T \equiv \frac{d \ln P_h}{d \ln k}, \quad (6.46)$$

$$r \equiv \frac{A_T}{A_\zeta}. \quad (6.47)$$

In these expressions P_ζ and P_h are the power spectrum of scalar curvature and tensor perturbations, respectively, and A_ζ and A_T are their amplitudes. These quantities can be related to the inflaton's perturbations by doing general relativistic perturbations.

A general perturbed metric can be written at linear order, using conformal time $d\tau = dt/a$, as:

$$ds^2 = a^2(\tau) [-(1 + 2\phi)d\tau^2 + 2(\partial_i B + B_i)dx^i d\tau + ((1 + 2\psi)\delta_{ij} + 2\partial_i \partial_j E + h_{ij})dx^i dx^j], \quad (6.48)$$

where ϕ , ψ , B and E represent the scalar perturbations of the metric, h_{ij} the tensor sector, responsible for gravitational waves and the vector perturbations decay in an expanding universe, as we show in the next chapter [236]. This perturbed metric is related to a perturbed energy-momentum tensor, δT_ν^μ , by the Einstein's equation:

$$\delta G_\nu^\mu = 8\pi G \delta T_\nu^\mu, \quad (6.49)$$

where $G_{\mu\nu} = R_{\mu\nu} - \frac{1}{2}g_{\mu\nu}R$. This metric has gauge redundancies, which could lead to coordinate (gauge) transformations to be confused with physical perturbations. In order to solve this issue one can either fix a gauge or work with gauge independent variables such as:

$$\Phi \equiv \phi + \frac{1}{a}[a(B - E')]', \quad (6.50)$$

$$\Psi \equiv -\psi - aH(B - E') + \frac{1}{3}\nabla^2 E, \quad (6.51)$$

for the metric, and the uniform density curvature perturbation:

$$\zeta \equiv \psi - \frac{1}{3}\nabla^2 E - aH\frac{\delta\rho}{\rho'}, \quad (6.52)$$

for the matter field described as a perfect fluid, which is going to be the inflaton for the inflationary case, and the primes denote derivation with respect to the conformal time. The tensor perturbations are gauge-invariant by definition. The density curvature perturbation is specially interesting as it doesn't evolve on super-horizon scales, $k \ll H$, for adiabatic perturbations [223]. Therefore, the value of ζ that is computed at horizon crossing during inflation survives unaltered until it enters the horizon again at later times.

The scalar perturbations of the metric are sourced by the perturbations on the inflaton field and the perturbations of the inflaton field, in turn, at very short scales are fundamentally

quantum fluctuations. By quantizing the perturbations φ of inflaton field $\bar{\phi}$ in a de Sitter background one finds that the variance of the inflaton perturbations receives non-zero quantum fluctuations. Hence, one can define the power spectrum $P_\varphi(k)$ of quantum fluctuations, and it turns out to be scale-invariant [223]

$$P_\varphi(k) \equiv \left(\frac{k^3}{2\pi^2} \right) |\varphi_k|^2 = \left(\frac{H}{2\pi} \right)^2. \quad (6.53)$$

In a flat hypersurface, $\psi = 0 = E$ and

$$\zeta = -aH \frac{\delta\rho}{\rho'} = -H \frac{\varphi}{\dot{\phi}}, \quad (6.54)$$

so that the inflaton quantum fluctuations power spectrum is related to the curvature perturbation power spectrum as

$$P_\zeta = \left(\frac{H}{\dot{\phi}} \right)^2 \left(\frac{H}{2\pi} \right)^2. \quad (6.55)$$

If the inflationary background is not exactly de Sitter, as in the case of almost flat inflaton potentials, then P_φ will depart from scale-invariance. Hence, the spectral index n_s measures the deviation of the power spectrum from scale-invariance, and $P_\zeta(k)$ can be parametrized as:

$$P_\zeta = A_\zeta \left(\frac{k}{k_*} \right)^{n_s-1}, \quad (6.56)$$

where k_* is a reference scale and A_ζ is the scalar power spectrum amplitude evaluated at such scale.

The power spectrum from tensor perturbations in de Sitter space is also scale invariant and written as:

$$P_h(k) = \frac{2}{M_P^2} \left(\frac{H}{2\pi} \right)^2 = A_T \left(\frac{k}{k_*} \right)^{n_T}. \quad (6.57)$$

In slow-roll approximation we can write these quantities as [223],

$$P_\zeta(k) \simeq \frac{V}{24\pi^2 M_P^4 \epsilon}, \quad (6.58)$$

$$n_s - 1 = -6\epsilon + 2\eta, \quad (6.59)$$

$$n_T = -2\epsilon, \quad (6.60)$$

$$r = 16\epsilon. \quad (6.61)$$

The temperature fluctuations in the cosmic microwave background radiation are sourced mostly by density scalar perturbations. Therefore, by looking at the CMB power spectrum we can infer the values of A_ζ and n_s , as its shape depends strongly on this initial conditions

and cosmological parameters. The values for n_s and A_ζ (at $k_* = 0.05 \text{ Mpc}^{-1}$) measured by Planck in 2018 are [17]:

$$n_s = 0.9649 \pm 0.0042, \quad (6.62)$$

$$A_\zeta \simeq 2.01 \times 10^{-9}. \quad (6.63)$$

We haven't observed the primordial tensor perturbations yet. Most searches focus on the imprint that tensor modes leave in the polarisation of the CMB. The presence of a gravitational wave background creates an anisotropic stretching of the spacetime which induces a special type of polarisation pattern named *B-modes*. Such a pattern cannot be created by scalar fluctuations and is therefore a unique signature of primordial gravitational waves. To-date we only have an upper bound on r [17]:

$$r < 0.11. \quad (6.64)$$

These three observables are used to constrain different inflationary models. We shall see now two natural models of inflation and their predicted observables.

6.4 Higgs inflation

We saw earlier that general models of inflation require the introduction of a new scalar field called inflaton to drive the inflationary epoch. However, we do have a scalar field in the Standard Model of Particle Physics, the Higgs field, so it may be interesting to see if the Higgs can generate an inflation at early times [237].

In Part II we saw that for a scalar field in curved spacetime to be renormalized it has to couple non-minimally to gravity. Therefore, the action for the Higgs field, in unitary gauge, plus gravity is¹⁰:

$$S = \int d^4x \sqrt{-g} \left[\frac{M_P^2}{2} R + \xi H^2 R - \frac{1}{2} \partial_\mu H \partial^\mu H - \frac{\lambda}{4} \left((v + H)^2 - \frac{\mu^2}{\lambda} \right) \right], \quad (6.65)$$

where ξ is the non-minimal coupling. M_P here is actually slightly corrected by the Higgs vev , but as $v \ll M_P$ we just neglected this correction.

In order to write the action with a canonical curvature term (in Einstein frame) we do a Weyl transformation on the metric:

$$g_{\mu\nu}(x) = \Omega^{-2}(x) \tilde{g}_{\mu\nu}(x), \quad \sqrt{-g} = \Omega^{-4} \sqrt{-\tilde{g}}. \quad (6.66)$$

With this transformation, the Ricci scalar becomes:

$$R = \Omega^2 (\tilde{R} + 6(\tilde{\square} \ln \Omega) - 6\tilde{g}^{\mu\nu} (\partial_\mu \ln \Omega)(\partial_\nu \ln \Omega)), \quad (6.67)$$

¹⁰It was also shown in Part II that the vacuum action induced by scalar field quantum correction includes curvature square terms, but this induced term is small and we shall neglect it for now.

where,

$$(\tilde{\square} \ln \Omega) = \frac{1}{\sqrt{-\tilde{g}}} \partial_\mu (\sqrt{-\tilde{g}} \tilde{g}^{\mu\nu} (\partial_\nu \ln \Omega)). \quad (6.68)$$

Hence, the action becomes:

$$S = \int d^4x \sqrt{-\tilde{g}} \Omega^{-4} \left[\frac{M_P^2}{2} \left(1 + \frac{\xi H^2}{M_P^2} \right) \Omega^2 (\tilde{R} + 6(\tilde{\square} \ln \Omega) - 6\tilde{g}^{\mu\nu} (\partial_\mu \ln \Omega) (\partial_\nu \ln \Omega)) - \frac{1}{2} \Omega^2 \tilde{g}^{\mu\nu} \partial_\mu H \partial_\nu H - U(H) \right]. \quad (6.69)$$

Therefore, to get a canonical Ricci scalar we need:

$$\Omega^2 = 1 + \frac{\xi H^2}{M_P^2}, \quad (6.70)$$

which implies that,

$$(\partial_\mu \ln \Omega) (\partial_\nu \ln \Omega) = \Omega^{-4} \left(\frac{\xi h}{M_P^2} \right)^2 \partial_\mu H \partial_\nu H. \quad (6.71)$$

Putting it back in the action and neglecting the total derivative we get:

$$S = \int d^4x \sqrt{-\tilde{g}} \left[\frac{M_P^2}{2} \tilde{R} - \left(\Omega^{-2} + \frac{6\Omega^{-4}\xi^2 H^2}{M_P^2} \right) \frac{1}{2} \tilde{g}^{\mu\nu} \partial_\mu H \partial_\nu H - \Omega^{-4} U(H) \right]. \quad (6.72)$$

In order to obtain a canonical kinetic term for the scalar part of the action we introduce the field χ that satisfies:

$$\frac{\partial \chi}{\partial H} = \sqrt{\frac{\Omega^2 + 6\xi^2 H^2 / M_P^2}{\Omega^4}}. \quad (6.73)$$

Finally, the action for the Higgs plus gravity in Einstein frame is:

$$S = \int d^4x \sqrt{-\tilde{g}} \left[\frac{M_P^2}{2} \tilde{R} - \partial_\mu \chi \partial^\mu \chi - V(\chi) \right], \quad (6.74)$$

where,

$$V(\chi) = \Omega^{-4}(\chi) \frac{\lambda}{4} \left[(v + H(\chi))^2 - \frac{\mu^2}{\lambda} \right]. \quad (6.75)$$

For small field values $H \simeq \chi$, but for large $H \gg M_P / \sqrt{\xi}$, or $\chi \gg \sqrt{6} M_P$, we have

$$H \simeq \frac{M_P}{\sqrt{\xi}} e^{\frac{\chi}{\sqrt{6} M_P}}, \quad (6.76)$$

so that the potential is, as $v \ll M_P / \sqrt{\xi}$,

$$V(\chi) = \frac{\lambda M_P^4}{4\xi^2} \left(1 - e^{-\sqrt{\frac{2}{3}} \frac{\chi}{M_P}} \right)^2. \quad (6.77)$$

This potential is exponentially flat, and it produces a successful inflationary scenario.

The slow-roll parameters are

$$\epsilon \simeq \frac{4M_P^4}{3\xi^2 H^4}, \quad \eta \simeq -\frac{4M_P^2}{3\xi H^2}. \quad (6.78)$$

and the number of e-folds before the end of inflation is

$$N = \frac{1}{M_P} \int_{H_{\text{end}}}^H \frac{1}{\sqrt{2\epsilon(H')}} \left(\frac{d\chi}{dH'} \right)^2 dH' \simeq \frac{3}{4} \frac{H^2 - H_{\text{end}}^2}{M_P^2/\xi}. \quad (6.79)$$

The slow-roll inflation regime ends when $\epsilon \simeq 1$. This implies that at the end of inflation the field value is approximately:

$$H_{\text{end}} \simeq \left(\frac{4}{3} \right)^{1/4} \frac{M_P}{\sqrt{\xi}}. \quad (6.80)$$

Now, as $H \gg H_{\text{end}}$, H can be written in terms of the number of e-folds as

$$H^2(N) = \frac{4M_P^2}{3\xi} N. \quad (6.81)$$

Using the normalized scalar power spectrum amplitude in Eq. (6.58) and its measured value Eq. (6.63) we can put a constraint on the value of the non-minimal coupling. For $N = 60$,¹¹

$$\xi \simeq 50000\sqrt{\lambda}. \quad (6.82)$$

One interesting feature of Higgs inflation is that as the Higgs coupling to Standard Model is known, in principle it is possible to calculate details of the reheating phase, when the Higgs would decay into SM particles, which is rather arbitrary in other inflationary models [241, 242]. It is also worth mentioning that Higgs inflation scenario is full of subtleties, most related to Higgs potential instability. As inflation happens at very large energies and the Higgs self-coupling λ runs, at such high energies λ can become so small that an inflationary regime would not be possible (as we need $\xi \gg 1$) or even negative, leading to instabilities. For a complete discussion see [243–245] and references therein.

6.5 Starobinsky inflation

Another natural model of inflation was realized in 1980 by Starobinsky [218], and it was one of the first inflationary models. It consists of a R^2 term together with the Einstein-Hilbert action:

$$S = \int d^4x \sqrt{-g} \left(\frac{1}{16\pi G} R + \alpha R^2 \right). \quad (6.83)$$

¹¹Such high value for the non-minimal coupling results on the so called unitarity problem or the naturalness problem of the Higgs inflation scenario, as perturbation theory breaks at the same energy scale of inflationary epoch. For more details see [238–240].

We can treat the integrand as a general $f(R)$ function of the Ricci scalar R :

$$S = \frac{M_P^2}{2} \int d^4x \sqrt{-g} f(R), \quad (6.84)$$

where

$$f(R) = R + \frac{2\alpha}{M_P^2} R^2. \quad (6.85)$$

Now let's introduce a field φ and write the dynamically equivalent action:

$$S = \frac{M_P^2}{2} \int d^4x \sqrt{-g} [f(\varphi) + f'(\varphi)(R - \varphi)]. \quad (6.86)$$

The equation of motion of φ gives:

$$f''(\varphi)(R - \varphi) = 0. \quad (6.87)$$

Therefore, $\varphi = R$ if $f''(\varphi) \neq 0$ and we recover Eq. (6.84). Now, defining $\phi = f'(\varphi)$ and setting

$$U(\phi) = \varphi(\phi)\phi - f(\varphi(\phi)), \quad (6.88)$$

we get

$$S = \frac{M_P^2}{2} \int d^4x \sqrt{-g} [\phi R - U(\phi)]. \quad (6.89)$$

Now we can do the same thing as in the previous section in order to write the action in Einstein frame, but choosing the parameter Ω to be $\Omega(x) = e^{\omega(x)}$. Hence, the action becomes:

$$S = \frac{M_P^2}{2} \int d^4x \sqrt{-\tilde{g}} \Omega^{-4} [\phi \Omega^2 (\tilde{R} - 6\tilde{g}^{\mu\nu} \partial_\mu \omega \partial_\nu \omega) - U(\phi)]. \quad (6.90)$$

We can choose $\Omega^2 = \phi$, and $\Omega^2 = e^{2\omega}$ implies $\omega = \frac{1}{2} \ln \phi$, which gives

$$S = \int d^4x \sqrt{-\tilde{g}} \left[\frac{M_P^2}{2} \tilde{R} - \frac{M_P^2}{2} \frac{6}{4} \tilde{g}^{\mu\nu} \partial_\mu (\ln \phi) \partial_\nu (\ln \phi) - \frac{M_P^2}{2} \Omega^{-4} U(\phi) \right]. \quad (6.91)$$

Now, we rewrite the action in terms of the scalar field χ that canonically normalizes the kinetic term:

$$S = \int d^4x \sqrt{-\tilde{g}} \left[\frac{M_P^2}{2} \tilde{R} - \frac{1}{2} \tilde{g}^{\mu\nu} \partial_\mu \chi \partial_\nu \chi - V(\chi) \right]. \quad (6.92)$$

In order to find how χ depends on ϕ we solve

$$\frac{3}{2} \frac{M_P^2}{\phi^2} \partial_\mu \phi \partial_\nu \phi = \partial_\mu \chi \partial_\nu \chi \quad \Rightarrow \quad \left(\frac{\partial \chi}{\partial \phi} \right)^2 = \frac{3}{2} \frac{M_P^2}{\phi^2}, \quad (6.93)$$

which gives,

$$\chi = \sqrt{\frac{3}{2}} M_P \ln \phi \quad \Rightarrow \quad \phi = e^{\sqrt{\frac{2}{3}} \frac{\chi}{M_P}}, \quad (6.94)$$

and the potential $V(\chi)$ is given by

$$V(\chi) = \frac{M_P^2}{2\phi^2(\chi)} U(\phi(\chi)). \quad (6.95)$$

This is a generic mapping of a $f(R)$ theory to scalar-metric action, and the prescription is valid for any analytic $f(R)$ theory. For the case we had in Eq. (6.85), remembering that we can rewrite Eq. (6.88) as

$$U(\phi) = R(\phi)\phi - f(R(\phi)), \quad (6.96)$$

we have

$$\phi = f'(R) = 1 + \frac{4\alpha}{M_P^2} R \quad \Rightarrow \quad R = \frac{M_P^2}{4\alpha} (\phi - 1), \quad (6.97)$$

and therefore,

$$U(\phi) = \frac{M_P^2}{8\alpha} (\phi - 1)^2. \quad (6.98)$$

Then, the potential $V(\chi)$ is

$$V(\chi) = \frac{M_P^4}{16\alpha} \left(1 - e^{-\sqrt{\frac{2}{3}} \frac{\chi}{M_P}} \right)^2. \quad (6.99)$$

This is the same potential as found before that drives Higgs inflation, and now the normalization of the power spectrum gives $\alpha \approx 2 \times 10^8$. Therefore, we have the same slow-roll parameters and observables:

$$\epsilon = \frac{3}{4N^2}, \quad \eta = -\frac{1}{N}, \quad n_s - 1 = -\frac{2}{N} \left(1 + \frac{9}{4N} \right), \quad r = \frac{12}{N^2}. \quad (6.100)$$

For $N = 60$,

$$n_s = 0.9654, \quad r = 0.0033, \quad (6.101)$$

which is in agreement with Planck measurements. In Figure 6.4 is shown the 68% and 95% confidence level measurements of n_s and r by Planck, together with several models of inflation evaluated at $N = 50$ and $N = 60$. Starobinsky inflation is the green mark, and we can see how well it fits observation.

The Higgs and Starobinsky inflation gives the same expressions for the observables, but they are certainly not the same model. For instance, the reheating phase is completely different in the two cases. The Starobinsky inflation modifies gravity and introduces a new scalar degree of freedom whose coupling to all fields is Planck scale suppressed. Then, the reheating occurs mainly due its decay into the Higgs bosons [246], which afterwards decays in SM particles. In Higgs inflation, however, the Higgs-inflaton field energy is transferred directly to all SM degrees of freedom. This changes the reheating temperature predicted in the two scenarios, which therefore changes the precise number of e-folds that happens after a given mode leaves the horizon until the end of inflation. Therefore, the two models can predict slightly different observables. For more details see [247] and references therein.

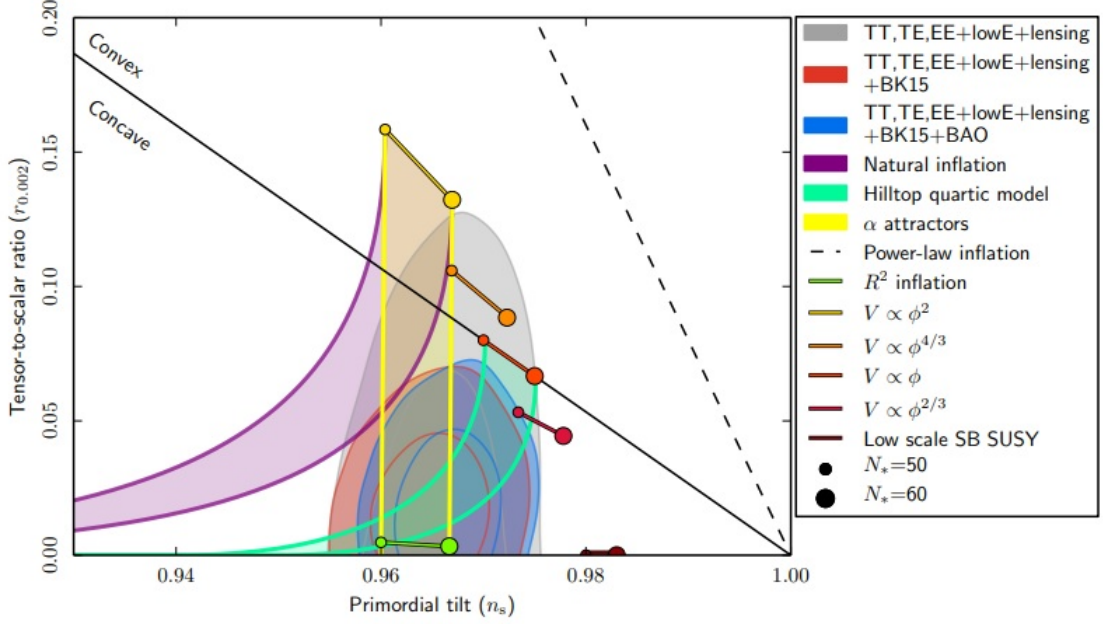


Figure 6.4: The spectral index and tensor-to-scalar ratio measured by Planck using CMB data. The figure also shows several models of inflation, with n_s and r calculated with $N = 50$ and $N = 60$. TT stands for temperature power spectrum from CMB, EE the polarization spectrum and TE the temperature-polarization spectrum, BAO for baryonic acoustic oscillations and BK15 are B-mode polarization data. Figure from [17].

6.6 Starobinsky inflation with sterile scalar coupled to massive fermions

We saw in Part II that for a theory of a sterile scalar field coupled to massive fermions through a Yukawa interaction to be renormalizable, odd terms are required in the scalar field potential:

$$V(\varphi) = \frac{1}{2}m^2\varphi^2 + \frac{\lambda}{4!}\varphi^4 + \frac{g}{3!}\varphi^3 + \tau\varphi + fR\varphi - \xi\varphi^2R. \quad (6.102)$$

This potential, within an inflationary approximation where φ is the inflaton field, induces contributions to the vacuum action that are non-polynomial in the scalar curvature:

$$S = \int d^4x \sqrt{-g} \left[\frac{1}{16\pi G}R - \frac{3m^2\xi}{\lambda}R + \frac{3\xi^2}{2\lambda}R^2 + \sqrt{\frac{6\xi R}{\lambda}} \left(\tau - \left(f + \frac{g\xi}{\lambda} \right) \right) R \right], \quad (6.103)$$

where $[f + g\xi/\lambda] = [M]$, $[\tau] = [M]^3$, and $\frac{m^2}{M_P^2}, |\frac{\tau}{M_P^3}|, |\frac{f}{M_P}|, |\frac{g}{M_P}| \ll 1$. During inflation, $R > 0$ and we need $\lambda > 0$ for stability of the scalar potential, therefore $\xi > 0$. Now, we shall look what these small non-polynomial terms do in Starobinsky inflation. This section is based on preliminary results of [19].

The curvature squared term,

$$\frac{3\xi^2}{2\lambda}R^2, \quad (6.104)$$

can actually drive Starobinsky inflation as long as $\frac{3\xi^2}{2\lambda} \sim 2 \times 10^8$ (see last section).

As,

$$\frac{1}{16\pi G}R - \frac{3m^2\xi}{\lambda}R \approx \frac{1}{16\pi G}R, \quad (6.105)$$

we can write just,

$$S = \frac{M_P^2}{2} \int d^4x \sqrt{-g} \left[R + \frac{\alpha}{M_P^2} R^2 + \frac{2}{M_P^2} \sqrt{\frac{6\xi R}{\lambda}} (\tau - \beta) R \right], \quad (6.106)$$

where we defined,

$$\alpha \equiv \frac{3\xi^2}{\lambda}, \quad \beta \equiv \left(f + \frac{g\xi}{\lambda} \right). \quad (6.107)$$

Hence,

$$S = \frac{M_P^2}{2} \int d^4x \sqrt{-g} f(R). \quad (6.108)$$

Mapping to a scalar-metric action in the same way we did for Starobinsky inflation,

$$S = \frac{M_P^2}{2} \int d^4x \sqrt{-g} [\phi R - V(\phi)], \quad (6.109)$$

where now,

$$\phi = f'(R) = 1 + \frac{2\alpha}{M_P^2}R + \frac{\tau}{M_P^2} \sqrt{\frac{6\xi}{\lambda}} R^{-1/2} - \frac{3\beta}{M_P^2} \sqrt{\frac{6\xi}{\lambda}} R^{1/2}. \quad (6.110)$$

We can write R as:

$$R = R_0 + \Delta R_1, \quad (6.111)$$

where $R_0 \sim O^0(\tau, \beta)$ and $\Delta R_1 \sim O^1(\tau, \beta) \ll R_0$. With this approximation we have,

$$R^{1/2} \approx R_0^{1/2} \left(1 + \frac{\Delta R_1}{2R_0} \right), \quad R^{-1/2} \approx R_0^{-1/2} \left(1 - \frac{\Delta R_1}{2R_0} \right). \quad (6.112)$$

In zero order of the expansion we get,

$$\phi = 1 + \frac{2\alpha}{M_P^2} R_0, \quad (6.113)$$

and in first order, defining $\gamma \equiv \sqrt{\frac{6\xi}{\lambda}}$, we find

$$\Delta R_1 = \frac{3\beta\gamma R_0^{1/2} - \tau\gamma R_0^{-1/2}}{2\alpha - \frac{\tau\gamma}{2} R_0^{-3/2} - \frac{-3\beta\gamma}{2} R_0^{-1/2}} \approx \frac{3\beta\gamma R_0^{1/2} - \tau\gamma R_0^{-1/2}}{2\alpha}, \quad (6.114)$$

as $\tau/\alpha, \beta/\alpha \ll \alpha$, and this gives, from the scalar equation of motion,

$$R(\phi) = V'(\phi) = \frac{M_P^2}{2\alpha}(\phi - 1) + \frac{3\sqrt{2}}{4} \frac{\beta\gamma M_P}{\alpha^{3/2}}(\phi - 1)^{1/2} - \frac{\tau\gamma}{\sqrt{2\alpha}M_P}(\phi - 1)^{-1/2}. \quad (6.115)$$

The integration with respect to ϕ results in the potential:

$$V(\phi) = \frac{M_P^2}{4\alpha}(\phi - 1)^2 + \frac{\sqrt{2}}{2} \frac{\beta\gamma M_P}{\alpha^{3/2}}(\phi - 1)^{3/2} - \frac{2\tau\gamma}{\sqrt{2\alpha}M_P}(\phi - 1)^{1/2}. \quad (6.116)$$

Recalling that we want a action of the form,

$$S = \int d^4x \sqrt{-g} \left[\frac{M_P^2}{2} R - \partial_\mu \chi \partial^\mu \chi - U(\chi) \right], \quad (6.117)$$

we can see that, as the new terms only contribute to the potential, after the Weyl transformation we get the same relation between the field χ with canonically normalized kinetic term and ϕ of the R^2 case:

$$U(\chi) = \frac{M_P^2}{2\phi^2} V(\phi(\chi)), \quad \phi = e^{\sqrt{\frac{2}{3}} \frac{\chi}{M_P}}. \quad (6.118)$$

Therefore the potential becomes,

$$U(\chi) = \frac{M_P^4}{8\alpha} \left(1 - e^{-\sqrt{\frac{2}{3}} \frac{\chi}{M_P}} \right)^2 + \frac{\sqrt{2}}{4} \frac{\beta\gamma M_P^3}{\alpha^{3/2}} e^{-2\sqrt{\frac{2}{3}} \frac{\chi}{M_P}} \left(e^{\sqrt{\frac{2}{3}} \frac{\chi}{M_P}} - 1 \right)^{3/2} - \frac{\tau\gamma M_P}{\sqrt{2\alpha}} e^{-2\sqrt{\frac{2}{3}} \frac{\chi}{M_P}} \left(e^{\sqrt{\frac{2}{3}} \frac{\chi}{M_P}} - 1 \right)^{1/2}, \quad (6.119)$$

or, in terms of the original parameters,

$$U(\chi) = \frac{M_P^4 \lambda}{24\xi^2} \left(1 - e^{-\sqrt{\frac{2}{3}} \frac{\chi}{M_P}} \right)^2 - \frac{\tau M_P}{\sqrt{\xi}} e^{-2\sqrt{\frac{2}{3}} \frac{\chi}{M_P}} \left(e^{\sqrt{\frac{2}{3}} \frac{\chi}{M_P}} - 1 \right)^{1/2} + \frac{1}{6} \left(f + \frac{g\xi}{\lambda} \right) \frac{\lambda M_P^3}{\xi^{5/2}} e^{-2\sqrt{\frac{2}{3}} \frac{\chi}{M_P}} \left(e^{\sqrt{\frac{2}{3}} \frac{\chi}{M_P}} - 1 \right)^{3/2}. \quad (6.120)$$

To get the observables we need:

$$\epsilon = \frac{M_P^2}{2} \left(\frac{U'(\chi)}{U(\chi)} \right)^2, \quad \eta = M_P^2 \frac{U''(\chi)}{U(\chi)}. \quad (6.121)$$

where when dividing by U we should pick only the leading term, the same from R^2 potential:

$$U_0 = \frac{M_P^4}{8\alpha} e^{-2\sqrt{\frac{2}{3}} \frac{\chi}{M_P}} (e^{\sqrt{\frac{2}{3}} \frac{\chi}{M_P}} - 1)^2, \quad (6.122)$$

and in the squared we also keep only to $O^1(\tau, \beta)$ terms. Thus,

$$\epsilon = \frac{4}{3} (e^{\sqrt{\frac{2}{3}} \frac{\chi}{M_P}} - 1)^{-2} + \frac{8\sqrt{2}}{3} \frac{\beta\gamma}{\sqrt{\alpha}M_P} \left[-2(e^{\sqrt{\frac{2}{3}} \frac{\chi}{M_P}} - 1)^{-3/2} + \frac{3}{2} e^{\sqrt{\frac{2}{3}} \frac{\chi}{M_P}} (e^{\sqrt{\frac{2}{3}} \frac{\chi}{M_P}} - 1)^{-5/2} \right] - \frac{16\sqrt{2}}{3} \frac{\tau\gamma\sqrt{\alpha}}{M_P^3} \left[-2(e^{\sqrt{\frac{2}{3}} \frac{\chi}{M_P}} - 1)^{-5/2} + \frac{1}{2} e^{\sqrt{\frac{2}{3}} \frac{\chi}{M_P}} (e^{\sqrt{\frac{2}{3}} \frac{\chi}{M_P}} - 1)^{-7/2} \right], \quad (6.123)$$

$$\begin{aligned}
\eta = & \frac{4}{3} \frac{(2 - e^{\sqrt{\frac{2}{3}} \frac{\chi}{M_P}})}{(e^{\sqrt{\frac{2}{3}} \frac{\chi}{M_P}} - 1)^2} + \frac{4\sqrt{2}}{3} \frac{\beta\gamma}{\sqrt{\alpha}M_P} \left[4(e^{\sqrt{\frac{2}{3}} \frac{\chi}{M_P}} - 1)^{-1/2} - \frac{9}{2} e^{\sqrt{\frac{2}{3}} \frac{\chi}{M_P}} (e^{\sqrt{\frac{2}{3}} \frac{\chi}{M_P}} - 1)^{-3/2} \right. \\
& + \left. \frac{3}{4} e^{2\sqrt{\frac{2}{3}} \frac{\chi}{M_P}} (e^{\sqrt{\frac{2}{3}} \frac{\chi}{M_P}} - 1)^{-5/2} \right] - \frac{8\sqrt{2}}{3} \frac{\tau\gamma\sqrt{\alpha}}{M_P^3} \left[4(e^{\sqrt{\frac{2}{3}} \frac{\chi}{M_P}} - 1)^{-3/2} \right. \\
& - \left. \frac{3}{2} e^{\sqrt{\frac{2}{3}} \frac{\chi}{M_P}} (e^{\sqrt{\frac{2}{3}} \frac{\chi}{M_P}} - 1)^{-5/2} - \frac{1}{4} e^{2\sqrt{\frac{2}{3}} \frac{\chi}{M_P}} (e^{\sqrt{\frac{2}{3}} \frac{\chi}{M_P}} - 1)^{-7/2} \right]. \tag{6.124}
\end{aligned}$$

For large χ values we can take only the leading term in each expression, which gives:

$$\epsilon \simeq \frac{4}{3} e^{-2\sqrt{\frac{2}{3}} \frac{\chi}{M_P}} - \frac{4\sqrt{2}}{3} \frac{\beta\gamma}{\sqrt{\alpha}M_P} e^{-\frac{3}{2}\sqrt{\frac{2}{3}} \frac{\chi}{M_P}} + 8\sqrt{2} \frac{\tau\gamma\sqrt{\alpha}}{M_P^3} e^{-\frac{5}{2}\sqrt{\frac{2}{3}} \frac{\chi}{M_P}}, \tag{6.125}$$

$$\eta \simeq -\frac{4}{3} e^{-\sqrt{\frac{2}{3}} \frac{\chi}{M_P}} + \frac{\sqrt{2}}{3} \frac{\beta\gamma}{\sqrt{\alpha}M_P} e^{-\frac{1}{2}\sqrt{\frac{2}{3}} \frac{\chi}{M_P}} - 6\sqrt{2} \frac{\tau\gamma\sqrt{\alpha}}{M_P^3} e^{-\frac{3}{2}\sqrt{\frac{2}{3}} \frac{\chi}{M_P}}. \tag{6.126}$$

Defining,

$$\sigma \equiv e^{-\sqrt{\frac{2}{3}} \frac{\chi}{M_P}}, \tag{6.127}$$

we can rewrite ϵ and η as,

$$\epsilon = \frac{4}{3} \sigma^2 - \frac{4\sqrt{2}}{3} \frac{\beta\gamma}{\sqrt{\alpha}M_P} \sigma^{3/2} + 8\sqrt{2} \frac{\tau\gamma\sqrt{\alpha}}{M_P^3} \sigma^{5/2}, \tag{6.128}$$

$$\eta = -\frac{4}{3} \sigma + \frac{\sqrt{2}}{3} \frac{\beta\gamma}{\sqrt{\alpha}M_P} \sigma^{1/2} - 6\sqrt{2} \frac{\tau\gamma\sqrt{\alpha}}{M_P^3} \sigma^{3/2}. \tag{6.129}$$

As ϵ can be written as $\epsilon = \epsilon_0 + \delta\epsilon$, where $\epsilon_0 \sim O^0(\tau, \beta)$ and $\delta\epsilon \sim O^1(\tau, \beta)$, to calculate the number of e-folds,

$$N_\chi = \frac{1}{M_P} \int_{\chi_{\text{end}}}^{\chi} \frac{1}{\sqrt{2\epsilon(\chi')}} d\chi', \tag{6.130}$$

we can expand in ϵ :

$$N_\chi = \frac{1}{\sqrt{2}M_P} \int_{\chi_{\text{end}}}^{\chi} \left[\epsilon_0^{-1/2} - \frac{1}{2} \epsilon_0^{-3/2} \delta\epsilon \right] d\chi'. \tag{6.131}$$

Explicitly, we have

$$\begin{aligned}
N_\chi = & -\frac{\sqrt{3}}{2} \int_{\sigma_{\text{end}}}^{\sigma} \left[\left(\frac{4}{3} \right)^{-1/2} \sigma^{-2} + \left(\frac{4}{3} \right)^{-3/2} \frac{2\sqrt{2}}{3} \frac{\beta\gamma}{\sqrt{\alpha}M_P} \sigma^{-5/2} \right. \\
& \left. - \left(\frac{4}{3} \right)^{-3/2} 4\sqrt{2} \frac{\tau\gamma\sqrt{\alpha}}{M_P^3} \sigma^{-3/2} \right] d\sigma, \tag{6.132}
\end{aligned}$$

where

$$d\sigma = -\sqrt{\frac{2}{3}} \frac{1}{M_P} \sigma d\chi. \tag{6.133}$$

After integrating and using that $\chi_{\text{end}} \ll \chi$, where χ is deep in inflationary era, we get a result that does not depend on χ_{end} , similar to the pure R^2 case:

$$N_\chi = \frac{\sqrt{3}}{2} \left(\frac{4}{3}\right)^{-1/2} \left[-e^{\sqrt{\frac{2}{3}} \frac{\chi}{M_P}} - \left(\frac{3}{4}\right) \frac{4\sqrt{2}}{9} \frac{\beta\gamma}{\sqrt{\alpha}M_P} e^{\frac{3}{2}\sqrt{\frac{2}{3}} \frac{\chi}{M_P}} + \left(\frac{3}{4}\right) 8\sqrt{2} \frac{\tau\gamma\sqrt{\alpha}}{M_P^3} e^{\frac{1}{2}\sqrt{\frac{2}{3}} \frac{\chi}{M_P}} \right] \quad (6.134)$$

$$= \frac{3}{4} \left[\sigma^{-1} + \frac{3}{4} \frac{4\sqrt{2}}{9} \frac{\beta\gamma}{\sqrt{\alpha}M_P} \sigma^{-3/2} - \frac{3}{4} 8\sqrt{2} \frac{\tau\gamma\sqrt{\alpha}}{M_P^3} \sigma^{-1/2} \right]. \quad (6.135)$$

In order to find the field χ in terms of the number of e-fold N we can expand on σ in Eq. (6.135), which gives:

$$\sigma = \sigma_0 + \delta\sigma_1 = \frac{3}{4N} + \frac{\sqrt{2}}{3} \frac{\beta\gamma}{\sqrt{\alpha}M_P} \left(\frac{3}{4N}\right)^{1/2} - 6\sqrt{2} \frac{\tau\gamma\sqrt{\alpha}}{M_P^3} \left(\frac{3}{4N}\right)^{3/2}. \quad (6.136)$$

Then, by plugging this result in Eq. (6.128) and Eq. (6.129), and keeping only to $O^1(\tau, \beta)$ terms, we find:

$$\epsilon = \frac{3}{4N^2} - \frac{\sqrt{6}}{6} \frac{\beta\gamma}{\sqrt{\alpha}M_P} \frac{1}{N^{3/2}} - \frac{9\sqrt{6}}{4} \frac{\tau\gamma\sqrt{\alpha}}{M_P^3} \frac{1}{N^{5/2}}, \quad (6.137)$$

$$\eta = -\frac{1}{N} - \frac{\sqrt{6}}{18} \frac{\beta\gamma}{\sqrt{\alpha}M_P} \frac{1}{N^{1/2}} + \frac{3\sqrt{6}}{4} \frac{\tau\gamma\sqrt{\alpha}}{M_P^3} \frac{1}{N^{3/2}}. \quad (6.138)$$

The observables are:

$$n_s - 1 = -6\epsilon + 2\eta, \quad r = 16\epsilon, \quad (6.139)$$

Therefore,

$$n_s - 1 = -\frac{2}{N} \left(1 + \frac{9}{4N}\right) + \frac{\sqrt{6}}{9} \frac{\beta\gamma}{\sqrt{\alpha}M_P} \frac{1}{N^{1/2}} \left(-1 + \frac{9}{N}\right) + \frac{3\sqrt{6}}{2} \frac{\tau\gamma\sqrt{\alpha}}{M_P^3} \frac{1}{N^{3/2}} \left(1 + \frac{9}{N}\right), \quad (6.140)$$

$$r = \frac{12}{N^2} - \frac{8\sqrt{6}}{3} \frac{\beta\gamma}{\sqrt{\alpha}M_P} \frac{1}{N^{3/2}} - 36\sqrt{6} \frac{\tau\gamma\sqrt{\alpha}}{M_P^3} \frac{1}{N^{5/2}}, \quad (6.141)$$

and in terms of the original parameters:

$$n_s - 1 = -\frac{2}{N} \left(1 + \frac{9}{4N}\right) + \frac{2\sqrt{3}}{9M_P} \left(f + \frac{g\xi}{\lambda}\right) \frac{1}{\sqrt{\xi}N} \left(-1 + \frac{9}{N}\right) + 9\sqrt{3} \frac{\tau\xi^{3/2}}{\lambda M_P^3} \frac{1}{N^{3/2}} \left(1 + \frac{9}{N}\right), \quad (6.142)$$

$$r = \frac{12}{N^2} - \frac{16\sqrt{3}}{3M_P} \left(f + \frac{g\xi}{\lambda}\right) \frac{1}{\xi^{1/2}} \frac{1}{N^{3/2}} - 216\sqrt{3} \frac{\tau\xi^{3/2}}{\lambda M_P^3} \frac{1}{N^{5/2}}. \quad (6.143)$$

In order to estimate the values of n_s and r let's recall that τ has mass-dimension three and f, g have mass-dimension one, and the mass scale that dominates in the correction of these parameters is the fermions masses M (see Eq. (5.58)). We should expect that the effect of the non-polynomial terms is larger for heavier fermions, and if we consider this fermions as right-handed neutrinos or some supersymmetric particle we could in principle go to very high values. Considering $\lambda \approx 1$, we have $\xi \approx 1 \times 10^4$, and we can choose $M = 1$ TeV, so that

$$\tau \sim m_f^3 \approx 1 \times 10^9 \text{ GeV}, \quad f = 10^3 \text{ GeV} = g. \quad (6.144)$$

Using that $M_P = 10^{19}$ GeV, with $N = 60$ we find:

$$n_s = 0.9654, \quad r = 0.0033, \quad (6.145)$$

and for $N = 50$:

$$n_s = 0.9582, \quad r = 0.0048, \quad (6.146)$$

which are exactly the same, to this precision, to the R^2 case. The non-polynomial terms start to become non-negligible for $M \sim 10^{15}$ GeV, where for $N = 60$,

$$n_s = 0.9650, \quad r = 0.0031, \quad (6.147)$$

but the effect is still small. The Figure 6.5 shows the potential, Eq. (6.120) for fermions with mass 10^{15} GeV and 10^{16} GeV, compared with Starobinsky inflation. We see that the potential changes, however the perturbation does not destroy the plateau or the minimum. In principle, the non-polynomial terms could change the details of the end of inflation, when $\epsilon \approx 1$, as we can see from the curves that this is the region of major difference. Therefore, we can see that the perturbations of the R^2 inflation are stable against odd terms corrections to the potential, even if induced by very heavy fermions.

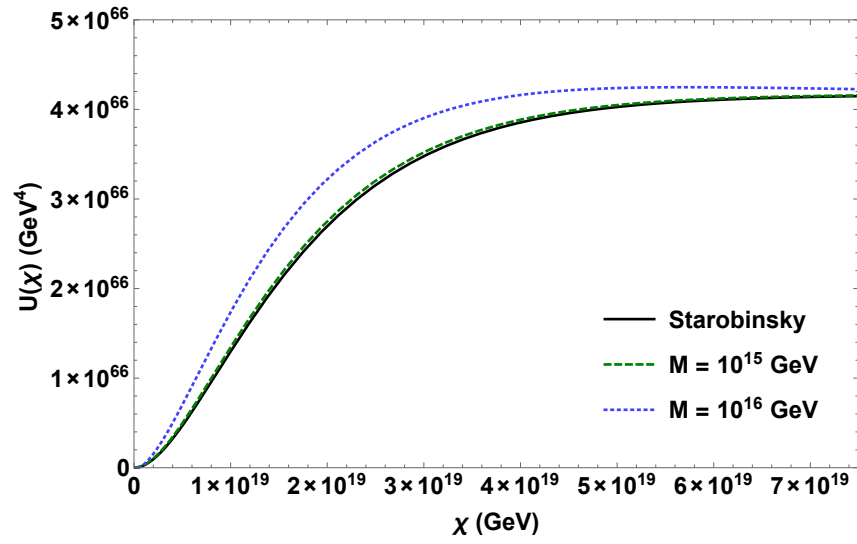


Figure 6.5: The potential $U(\chi)$ of Starobinsky inflation perturbed by non-polynomial terms, induced by scalars coupled to fermions of mass 10^{15} GeV (green, dashed) and 10^{16} GeV (blue dotted), together with the pure R^2 term (black).

7

Large scale structure formation

The universe was very homogeneous and isotropic at the recombination time as observations of the cosmic microwave background indicate. However, we can see clearly inhomogeneities in the Universe today in the form of galaxies and clusters that combine in a structure. The explanation for highly non-linear structure to form from such small initial perturbations lies within gravitational instability: matter is attracted to denser regions, amplifying the already existing inhomogeneities. Even small overdensities of order 10^{-5} , as the one seen in CMB, eventually attract enough matter to form structure.

But to really assure these small perturbations, originated from quantum fluctuations at the inflation era, clustered to the structure we see today one has to study how fast such overdensities grow in an expanding universe. The general way to calculate this evolution is through perturbing the Einstein's equation. But the gravitational instability in the Newtonian limit produces fair results when applied to non-relativistic matter at scales that don't exceed the Hubble horizon, which is sufficient for our purposes.

7.1 Linear perturbation theory

We can approximate matter to behave as a perfect fluid at large scales. This means that at any time t matter will be characterized by its density $\rho(\mathbf{x}, t)$, its entropy per mass unit $S(\mathbf{x}, t)$, the gravitational potential $\phi(\mathbf{x}, t)$ and the 3-velocities vector field $\mathbf{V}(\mathbf{x}, t)$. The set of equations that governs the evolution of such quantities are called hydrodynamical equations:

- Continuity equation

$$\frac{\partial \rho}{\partial t} + \nabla \cdot (\rho \mathbf{V}) = 0; \quad (7.1)$$

- Euler equation

$$\frac{\partial \mathbf{V}}{\partial t} + (\mathbf{V} \cdot \nabla) \mathbf{V} + \frac{\nabla p}{\rho} + \nabla \phi = 0; \quad (7.2)$$

- Entropy conservation

$$\frac{dS(\mathbf{x}, t)}{dt} = \frac{\partial S}{\partial t} + (\mathbf{V} \cdot \nabla) S = 0; \quad (7.3)$$

- Poisson equation

$$\Delta \phi = 4\pi G \rho, \quad (7.4)$$

which together with the equation of state $p = p(\rho, S)$ form a set of seven equations for the seven unknown functions described previously.

In an expanding homogeneous and isotropic universe the matter energy density is a function of time only and the velocities obey Hubble's law

$$\rho = \bar{\rho}(t), \quad \mathbf{V} = \mathbf{V}_0 = H(t)\mathbf{x}. \quad (7.5)$$

Plugging this expressions in the continuity equation results in the familiar equation, Eq. (6.5), $\dot{\bar{\rho}} + 3H\bar{\rho} = 0$. To study the evolution of matter perturbations we add a little perturbation to the matter distribution [236]:

$$\begin{aligned} \rho &= \bar{\rho} + \delta\rho(\mathbf{x}, t), & \mathbf{V} &= \mathbf{V}_0 + \delta\mathbf{v}, & \phi &= \bar{\phi} + \delta\phi, \\ p &= \bar{p} + \delta p = \bar{p} + c_s^2 \delta\rho. \end{aligned} \quad (7.6)$$

where we have ignored entropic perturbations and c_s is propagation velocity of a perturbation in a certain medium, usually called *sound speed*. The linear hydrodynamical equations for small perturbations are

$$\frac{\partial \delta\rho(\mathbf{x}, t)}{\partial t} + \bar{\rho} \nabla \delta\mathbf{v}(\mathbf{x}, t) + \nabla(\delta\rho(\mathbf{x}, t) \cdot \mathbf{V}_0) = 0, \quad (7.7)$$

$$\frac{\partial \delta\mathbf{v}(\mathbf{x}, t)}{\partial t} + (\mathbf{V}_0 \cdot \nabla) \delta\mathbf{v}(\mathbf{x}, t) + (\delta\mathbf{v}(\mathbf{x}, t) \cdot \nabla) \mathbf{V}_0 + \frac{c_s^2}{\bar{\rho}} \nabla \delta\rho(\mathbf{x}, t) + \nabla \delta\phi(\mathbf{x}, t) = 0, \quad (7.8)$$

$$\Delta \delta\phi(\mathbf{x}, t) = 4\pi G \delta\rho(\mathbf{x}, t). \quad (7.9)$$

It is easier to solve this equations in Fourier space, but in order to do a Fourier transform of the quantities we have to remove the explicit dependence on the coordinate \mathbf{x} of \mathbf{V}_0 . To do so it is convenient to use Lagrangian coordinates \mathbf{q} , which are comoving to Hubble flow, instead of the Eulerian coordinates, which are related in the following way:

$$\mathbf{x} = a(t)\mathbf{q}. \quad (7.10)$$

In this new coordinates the time derivative and the gradient become

$$\begin{aligned} \left(\frac{\partial}{\partial t} \right)_{\mathbf{x}} &= \left(\frac{\partial}{\partial t} \right)_{\mathbf{q}} - (\mathbf{V}_0 \cdot \nabla_{\mathbf{x}}), \\ \nabla_{\mathbf{x}} &= \frac{1}{a} \nabla_{\mathbf{q}}. \end{aligned} \quad (7.11)$$

Substituting this relations in eqs. (7.7)-(7.9) and introducing the density contrast of perturbations $\delta \equiv \delta\rho/\bar{\rho}$, we obtain

$$\frac{\partial\delta(\mathbf{q},t)}{\partial t} + \frac{1}{a}\nabla\delta\mathbf{v}(\mathbf{q},t) = 0, \quad (7.12)$$

$$\frac{\partial\delta\mathbf{v}(\mathbf{q},t)}{\partial t} + H\delta\mathbf{v}(\mathbf{q},t) + \frac{c_s^2}{a}\nabla\delta(\mathbf{q},t) + \frac{1}{a}\nabla\delta\phi(\mathbf{q},t) = 0, \quad (7.13)$$

$$\Delta\delta\phi(\mathbf{q},t) = 4\pi G a^2 \bar{\rho}\delta(\mathbf{q},t). \quad (7.14)$$

The derivatives are all with respect to \mathbf{q} and from now on we omit its dependence in the equations. It is also possible to combine these three equations into one second order equation for δ :

$$\ddot{\delta} + 2H\dot{\delta} - \frac{c_s^2}{a^2}\nabla^2\delta - 4\pi G\bar{\rho}\delta = 0. \quad (7.15)$$

This equation describes the matter inhomogeneities in an expanding universe on sub-horizon scales.

7.1.1 Adiabatic perturbations

After a Fourier transformation in δ :

$$\delta(\mathbf{x},t) = \int \delta_{\mathbf{k}} e^{(i\mathbf{k}\mathbf{x})} \frac{d^3k}{(2\pi)^3}, \quad (7.16)$$

the Eq. (7.15), for each Fourier mode, becomes:

$$\ddot{\delta}_{\mathbf{k}} + 2H\dot{\delta}_{\mathbf{k}} + \left(\frac{c_s^2 k^2}{a^2} - 4\pi G\bar{\rho} \right) \delta_{\mathbf{k}} = 0. \quad (7.17)$$

The evolution of each perturbation mode depends strongly on the spatial scale, where the critical wavelength that determines the form of the evolution is named Jeans length,

$$\lambda_J^{\text{ph}} = \frac{2\pi a}{k_J} = c_s \sqrt{\frac{\pi}{G\bar{\rho}}}. \quad (7.18)$$

At scales much smaller than the Jeans length ($\lambda \ll \lambda_J$) the pressure gradient dominates the effect of gravity. If c_s changes adiabatically ($\frac{\dot{c}_s}{c_s} \ll H$), then the solution of Eq. (7.17) has the form

$$\delta_{\mathbf{k}} \propto \frac{1}{\sqrt{c_s a}} e^{\pm i k \int \frac{c_s dt}{a}}. \quad (7.19)$$

So the perturbations oscillate like sound-waves.

At scales much larger than the Jeans length ($\lambda \gg \lambda_J$) gravity dominates, and perturbations experience a power-law growth. To see that, let's consider the case of dark matter. For dark matter $c_s = 0$ at linear level, and we can analyse its evolution at different epochs:

- In a matter-dominated universe we have

$$\ddot{\delta}_{m\mathbf{k}} + 2H\dot{\delta}_{m\mathbf{k}} - 4\pi G\rho_{0m}\delta_{m\mathbf{k}} = 0. \quad (7.20)$$

As $a \propto t^{2/3}$, then $H \propto t^{-1}$ and

$$\ddot{\delta}_{m\mathbf{k}} + \frac{4}{3t}\dot{\delta}_{m\mathbf{k}} - \frac{2}{3t^2}\delta_{m\mathbf{k}} = 0. \quad (7.21)$$

Plugging the ansatz $\delta_{m\mathbf{k}} = t^p$ we find a growing and a decaying solution, and $\delta_{m\mathbf{k}}$ gives:

$$\delta_{m\mathbf{k}}(t) = C_1(k)t^{2/3} + C_2(k)t^{-1}. \quad (7.22)$$

Therefore, the growing modes of dark matter perturbations grow with a in a matter-dominated universe.

- In a radiation-dominated universe the mean density is the sum of the radiation and matter densities:

$$\ddot{\delta}_{m\mathbf{k}} + 2H\dot{\delta}_{m\mathbf{k}} - 4\pi G \sum_i \rho_{0i}\delta_{i\mathbf{k}} = 0. \quad (7.23)$$

Radiation fluctuations on scales smaller than the horizon oscillate as sound waves due to the large radiation pressure and it also doesn't cluster, so $\delta_{rk} = 0$ [236]. Hence,

$$\ddot{\delta}_{m\mathbf{k}} + 2H\dot{\delta}_{m\mathbf{k}} - 4\pi G\rho_{0m}\delta_{m\mathbf{k}} = 0. \quad (7.24)$$

This is the Meszaros equation and can be solved analytically, in principle. But qualitatively, since $\delta_{m\mathbf{k}}$ evolves only on cosmological time scales, $\ddot{\delta}_{m\mathbf{k}} \sim H^2\delta_{m\mathbf{k}} \sim \frac{8\pi G}{3}\rho_{0r}\delta_{m\mathbf{k}} \gg 4\pi G\rho_{0m}\delta_{m\mathbf{k}}$, then we can neglect the last term of Eq. (7.24), and solving the resulting equation we find

$$\delta_{m\mathbf{k}}(t) = B_1(k) + B_2(k)\ln t. \quad (7.25)$$

Hence, the dark matter perturbations grow only logarithmically in a radiation-dominated universe.

Only the growing mode of the perturbations is important at late times because it is due to this mode that the Universe has structure. The evolution of the growing mode can be split into a k independent term $\delta_c(t) \equiv D(z)$, called growth factor, and a redshift independent term $\delta(k, 0)$, $\delta(k, z) = D(z)\delta(k, 0)$, where we can write in general that [248, 249]

$$D(z) = \frac{H(z)}{H_0} \int_z^\infty dz' (1+z') \left(\frac{H_0}{H(z')} \right)^3. \quad (7.26)$$

7.1.2 Vector perturbations

Trivial solutions with $\delta = 0$ and $\delta S = 0$ can correspond to non-trivial solutions to the hydrodynamical equations. In this case Eqs. (7.12)-(7.14) reduce to

$$\nabla \delta \mathbf{v} = 0, \quad \frac{\partial \delta \mathbf{v}}{\partial t} + H \delta \mathbf{v} = 0. \quad (7.27)$$

From the first equation it follows that, for plane waves perturbations, $\delta \mathbf{v} \propto \delta \mathbf{v}_{\mathbf{k}}(t) e^{i\mathbf{k}\mathbf{q}}$, the velocity $\delta \mathbf{v}$ is perpendicular to the wavenumber \mathbf{k} . The solution of the second equation has the form $\delta \mathbf{v}_{\mathbf{k}} \propto 1/a$. Hence, we see that the vector perturbations decrease with the Universe expansion. Therefore, such perturbations could only have significant amplitudes today if they were huge back in the past, so large that they would destroy the isotropy on the observed early universe. There is no place for such high vector perturbations in an inflationary universe, so they don't play a role in the structure formation of the Universe.

7.2 The matter power spectrum

We can characterize the amplitude of density perturbations by its Fourier transform

$$\delta(\mathbf{x}, t) = \int \frac{d^3 k}{(2\pi)^3} \delta(\mathbf{k}, t) e^{i\mathbf{k}\mathbf{x}}, \quad \delta(\mathbf{k}, t) = \int d^3 x \delta(\mathbf{x}, t) e^{-i\mathbf{k}\mathbf{x}}. \quad (7.28)$$

As $\delta(\mathbf{x})$ is real and has zero average (homogeneous universe), we have that $\langle \delta(\mathbf{k}, t) \rangle = 0$ and $\delta(-\mathbf{k}, t) = \delta^*(\mathbf{k}, t)$. The matter power spectrum is defined as:

$$\langle \delta(\mathbf{k}, t) \delta^*(\mathbf{k}', t) \rangle \equiv (2\pi)^3 \delta^3(\mathbf{k} - \mathbf{k}') P(k). \quad (7.29)$$

The statistical properties of the density contrast are encoded in the set of correlation functions [250]

$$\xi_2(\mathbf{x}_1, \mathbf{x}_2) = \langle \delta(\mathbf{x}_1) \delta(\mathbf{x}_2) \rangle, \quad \xi_3(\mathbf{x}_1, \mathbf{x}_2, \mathbf{x}_3) = \langle \delta(\mathbf{x}_1) \delta(\mathbf{x}_2) \delta(\mathbf{x}_3) \rangle, \dots \quad (7.30)$$

where the average is taken over ensembles.

The homogeneity of space implies that the two-point correlation function, ξ_2 , for example, to be invariant under translations. Therefore, it can only be a function of the separation between the points, $\xi_2(\mathbf{x}_1, \mathbf{x}_2) = \xi_2(\mathbf{x}_1 - \mathbf{x}_2)$. On the other hand, isotropy requires $\xi(\mathbf{x})$ to be invariant under rotations as well, so the two-point correlation function must be a function of the modulus of the distance between the two points only, $\xi_2(\mathbf{x}_1, \mathbf{x}_2) = \xi_2(|\mathbf{x}_1 - \mathbf{x}_2|)$.

One can compute the two-point correlation function

$$\xi_2(\mathbf{r}) = \langle \delta(\mathbf{x}) \delta(\mathbf{x} + \mathbf{r}) \rangle, \quad (7.31)$$

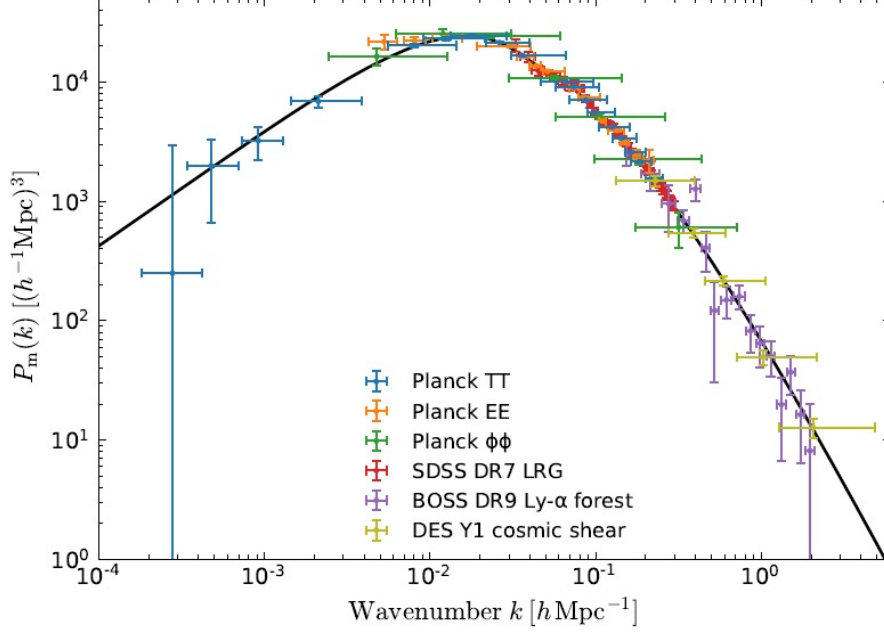


Figure 7.1: Linear matter power spectrum at $z = 0$ inferred from different cosmological probes, together with the Λ CDM prediction in black. We can see how well the Λ CDM model fits observations. Figure from [14].

in terms of the Fourier coefficients as follows:

$$\begin{aligned}
 \xi_2(\mathbf{r}) &= \int \frac{d^3k}{(2\pi)^3} \int \frac{d^3k'}{(2\pi)^3} \langle \delta(\mathbf{k}) \delta^*(\mathbf{k}') \rangle e^{-i\mathbf{k}\mathbf{x}} e^{i\mathbf{k}'(\mathbf{x}+\mathbf{r})} \\
 &= \frac{1}{(2\pi)^6} \int \int d^3k d^3k' (2\pi)^3 \delta^3(\mathbf{k} - \mathbf{k}') P(k) e^{-i\mathbf{x}(\mathbf{k}-\mathbf{k}')} e^{i\mathbf{k}'\mathbf{r}} \\
 &= \frac{1}{(2\pi)^3} \int d^3k P(k) e^{i\mathbf{k}\mathbf{r}} \\
 &= \frac{1}{2\pi^2} \int dk k^2 P(k) \frac{\sin(kr)}{kr}.
 \end{aligned} \tag{7.32}$$

Hence, it follows that the two-point correlation function is the Fourier transform of the power spectrum. Roughly speaking, the two-point correlation function measures the probability of finding an object, e.g. a star, galaxy, cluster, from a distance r of another object, or the spatial distribution of pairs with a giving separation distance.

The power spectrum has dimension of volume but sometimes it is useful to work with a dimensionless quantity defined as

$$\Delta^2(k) = \frac{k^3 P(k)}{2\pi^2}. \tag{7.33}$$

When studying the large scale structure of the Universe we are interested in measuring the matter power spectrum today and understand how it originated from a primordial power

spectrum, established at the time of inflation. As the potential $\phi(\mathbf{k})$ and the density contrast $\delta(\mathbf{k})$ are related by the Poisson equation we can work with the potential instead of the density, and relate the potential today with the primordial one ϕ_p . Schematically, we have that [222]

$$\phi(\mathbf{k}, a) = \phi_p(\mathbf{k}) \times T(k) \times \frac{D(a)}{a}, \quad (7.34)$$

where $T(k)$ is the transfer function. It encodes the evolution of perturbations crossing the horizon and through the transition from radiation-dominated to matter dominated universe. By definition, the transfer function is given by

$$T(k) \equiv \frac{\phi(k, a \gg 1)}{\phi_{\text{LS}}(k, a \gg 1)}, \quad (7.35)$$

where ϕ_{LS} is the large scale potential.

It is also the transfer function that carries the characteristic form of the matter power spectrum. It is possible to calculate the transfer function numerically through evolving Boltzmann equations, and there are open codes like CAMB or CLASS that do the job, but here only a qualitative analysis will be made in order to construct an intuition for the matter power spectrum shape as seen in Figure (7.1). A more complete description can be found on [251].

First, let's consider modes $k < k_{eq}$, where k_{eq} is the wavenumber of the mode which enters the horizon at the radiation-matter equality (transition epoch between a radiation-dominated to a matter-dominated universe). Therefore, these modes enter the horizon only at late times, when the dominant content of the Universe is non-relativistic matter. At this stage the perturbations grow like the scale factor, as gravity dominates at these scales and this favors the growing of perturbations.

The power spectrum at small wavelengths, $k > k_{eq}$, presents more subtleties. Perturbation modes that enter the horizon at the radiation era have their amplitude reduced due to radiation pressure. As the baryons and radiation plasma was tightly coupled before recombination the radiation and baryons perturbations only oscillated instead of growing. This oscillations gave rise to the so called baryonic acoustic oscillations (BAO), whose peak appears as the little wiggles in the power spectrum around 0.1 Mpc^{-1} [222]. As dark matter doesn't couple to radiation it doesn't feel the radiation perturbations, and so we have a logarithmic grow of matter perturbations, as we saw in section (7.1.1). After this logarithmic grow the perturbations start growing with the scale factor $\delta_{\text{cdm}} \propto a$ after the era of radiation-matter equality. Larger modes enter the horizon even earlier in the radiation-dominated era, and its corresponding perturbations experience more logarithmic growth when compared to smaller modes. The transfer function has the form $T(k) \propto \ln(k/k_{eq})$ and the power spectrum $P(k) \propto k^n T^2(k) \propto k^{-3} \ln^2(k/k_{eq})$ ¹. Then, we see that the matter power spectrum, for $k > k_{eq}$, decreases the larger is the mode.

The region in which the matter power spectrum curve stops growing and start decreasing corresponds to modes that enter the horizon at the radiation-matter transition epoch, which happens approximately at $k \sim 10^{-2} \text{ Mpc}^{-1}$.

¹We chose $n = -3$ to consider, for simplicity, a scale-invariant primordial power spectrum, as we saw on last chapter.

7.3 Halo Model

In the previous section we saw how to describe the evolution of perturbations on the dark matter initial density field. These perturbations grow with time and end up forming even denser regions, highly non-linear and no more correctly described by linear perturbation theory. Such regions then stabilize forming objects we call halos.

It is on these dark matter halos that the baryonic matter cools down and forms galaxies. Therefore, understanding the formation of such halos, their properties and how they are distributed in space is of extreme importance, as it is a first step for a larger comprehension of galaxies properties and the structure of the Universe.

In this section we shall review the spherical collapse model of matter, how halos are distributed in the Universe with relation to their mass, and how matter is allocated inside the halos.

7.3.1 Spherical Collapse

As the Universe evolves some regions become denser than the average and therefore start expanding slower than the rest. Consequently, the overdensity $\delta(x)$ in these regions grows until they stop expanding and start collapsing. One simplified way to study the formation of such non-linear objects is to assume that matter collapses spherically. This approximated model was first studied in 1972, by Gunn and Gott [252].

First, let's consider a spherical region with matter in the newtonian regime:

$$\frac{d^2 r}{dt^2} = -\frac{GM}{r^2}, \quad (7.36)$$

where r is the sphere radius and M its mass. Integrating this equation gives a relation for the energy E of the system

$$\frac{1}{2} \left(\frac{dr}{dt} \right)^2 - \frac{GM}{r} = E. \quad (7.37)$$

The first term of the equation is the sphere kinetic energy K and the second one its potential energy U . If we remember that the sphere mass is conserved and given by

$$M_i = V_i \rho_i = \frac{4}{3} \pi r_i^3 \bar{\rho}_i (1 + \delta_i), \quad (7.38)$$

where the i label means an initial time and $\bar{\rho}_i = \bar{\rho}(t_i) \simeq \frac{3H_i^2}{8\pi G}$, we can rewrite the potential energy as:

$$U = -\frac{(H_i r_i)^2}{2} (1 + \delta_i). \quad (7.39)$$

We also know that the sphere velocity expansion initially follows the Hubble law, that is, it is the radius of the sphere times the expansion rate of the Universe $\dot{r}_i = r_i H_i$ so that the kinetic energy is given by

$$K_i = \frac{(r_i H_i)^2}{2}. \quad (7.40)$$

So, we see that the potential energy can be written in terms of the kinetic energy using the relation $U_i = -K_i(1 + \delta_i)$, so that the total energy is

$$E = K_i - K_i(1 + \delta_i) = K_i\delta_i. \quad (7.41)$$

As long as the gravitational potential energy is greater than the kinetic one ($E < 0, \delta_i > 0$), the sphere will expand until a maximum radius r_{\max} and then collapse. The maximum radius can be found if we remember that on this moment, $\dot{r} = 0$ and $K = 0$, that is, $E = U$ in Eq. (7.37)

$$E = -\frac{G}{r_{\max}} \frac{4}{3} \pi r_i^3 \bar{\rho}_i (1 + \delta_i) = -\frac{r_i^3 H_i^2 (1 + \delta_i)}{2r_{\max}}. \quad (7.42)$$

But we have that $K_i = r_i^2 H_i^2 / 2$, therefore

$$E = \frac{r_i}{r_{\max}} K_i (1 + \delta_i). \quad (7.43)$$

It follows from energy conservation that the Eq. (7.41) and Eq. (7.43) imply that,

$$\frac{r_{\max}}{r_i} = \frac{(1 + \delta_i)}{\delta_i}. \quad (7.44)$$

One can see that the larger the initial density, the smaller will be the maximum radius of the sphere before collapsing.

Consider now the radius R of the region at some time after t_i . The region density is $(r_i/r)^3 \equiv (1 + \delta)$. In the spherical collapse model there is a relation between the initial radius r_i and a posteriori comoving radius r . In a Einstein-de Sitter universe ($\Omega_m = 1$) we can write a parametric solution of Eq. (7.37) as a cycloid of the form $r(\theta) = A(1 - \cos \theta)$; $t(\theta) = B(\theta - \sin \theta)$, which results in the relation [253, 254]:

$$\frac{r(z)}{r_i} = \frac{(1 + z)}{(5/3)\delta(z)} \frac{(1 - \cos \theta)}{2}; \quad \frac{1}{1 + z} = \left(\frac{3}{4}\right)^{2/3} \frac{(\theta - \sin \theta)^{2/3}}{(5/3)\delta(z)}, \quad (7.45)$$

$$\Rightarrow \frac{r_i}{r(z)} = \frac{6^{2/3}}{2} \frac{(\theta - \sin \theta)^{2/3}}{(1 - \cos \theta)}. \quad (7.46)$$

The evolution of a spherical region which has an initial overdensity $\delta_i > 0$ parametrized like this starts at $\theta = 0$. At $\theta = \pi$ the region reaches its maximum size $r = r_{\max}$ and at $\theta = 2\pi$ the collapse ceases. At $\theta = \pi$ we have that

$$\frac{r_i}{r(z)} \equiv \frac{r_i}{r_{\max}} = \frac{6^{2/3}}{2} \frac{\pi^{2/3}}{(1 - \cos \pi)} \Rightarrow \left(\frac{r_i}{r_{\max}}\right)^3 = \left(\frac{3\pi}{4}\right)^2 \approx 5.55 = \frac{\rho_{\max}}{\bar{\rho}_{\max}}, \quad (7.47)$$

therefore, when the spherical region expands to its maximum size it has an average density around 5.55 times the average density of the Universe at the same epoch.

In principle one could conclude that by Eq. (7.46) the matter sphere collapses into a radius $r = 0$, but in fact it reaches virial equilibrium for a $r > 0$ into a object we call halo. We can estimate average density of such virialized object as follows: first we know that in virial

equilibrium, by the virial theorem, that $K = -U/2$. From the conservation of energy when the sphere is in its maximum size and in its equilibrium we get

$$E_{\text{vir}} = U_{\text{vir}} + K_{\text{vir}} = \frac{1}{2}U_{\text{vir}} = U_{\text{max}} = E_{\text{max}} \quad \Rightarrow \quad r_{\text{vir}} = \frac{1}{2}r_{\text{max}}, \quad (7.48)$$

where r_{vir} is the virial radius of the halo.

Between the maximum size of the sphere and its collapse the Universe has its density modified by a factor $(1 + z_{\text{max}})^3/(1 + z_{\text{vir}})^3$, as in a EdS universe we have that $\bar{\rho} = \bar{\rho}_i a^{-3}$. Such factor by Eq. (7.46) is $(1 + z_{\text{max}})^3/(1 + z_{\text{vir}})^3 = 2^{2/3.3}$, and therefore the average density of the Universe by the time of the sphere collapse is 1/4 of the Universe density by the maximum sphere size. We also have that the virialized object is eight times denser than it was when it had maximum radius ($r_{\text{vir}} = r_{\text{max}}/2 \Rightarrow (r_i/r_{\text{vir}})^3 = 2^3 (r_i/r_{\text{max}})^3$). Hence, the average density of the sphere in virial equilibrium is:

$$\Delta_{\text{vir}} \equiv 8 \times \frac{\rho_{\text{max}}}{\bar{\rho}_{\text{max}}} \times 4 \times \bar{\rho}_{\text{vir}} = \frac{9\pi^2}{16} \times 32 \times \bar{\rho}_{\text{vir}} \approx 178\bar{\rho}_{\text{vir}}, \quad (7.49)$$

that is, the density of the halo is approximately 178 times the average density of the Universe at the time of the collapse.

It is also possible to obtain an initial critical density δ_{sc} that a region must have in order to collapse into a halo. The second equation of Eq. (7.45) tell us that for a region to collapse at a redshift z it must have had a density of

$$\frac{1}{1+z} = \left(\frac{3}{4}\right)^{2/3} \frac{(2\pi - 0)^{2/3}}{(5/3)\delta_{sc}} \Rightarrow \frac{\delta_{sc}}{1+z} = \frac{3}{5} \left(\frac{3\pi}{2}\right)^{2/3} \approx 1.686. \quad (7.50)$$

Even though it is a simple model, the spherical collapse offers useful results that agree with the observable universe, as for example the minimum density of a region to collapse or, as we shall see in following, to be considered a halo.

7.3.2 Dark matter halos properties

The approach to the problem of structure formation in the Universe by means of the Halo Model begins by assuming that all the matter of the Universe is distributed inside structures called halos. At small scales, the statistics for the mass distribution is given in terms of the spatial distribution of matter inside a halo only, and it is not important how this halos are located throughout space. On the other hand, at larger scales the matter distribution statistics is governed by the spatial distribution of halos, and the inner structure details of each halo can be neglected. This fact, that the matter distribution can be studied in two separate regimes, is the very core of the Halo Model.

Just like we can think about the matter statistical distribution in two separate steps, in the Halo Model we can also separate the physics into two different sectors. In particular, the regime that cannot be described precisely using linear perturbation theory, the small scales, is confined inside halos that can be treated as the virialized objects we saw on last section. Let's now turn to the three ingredients that completely determines the Halo Model.

The average number density of halos

The most important result obtained by the spherical collapse model was the critical density amplitude δ_{sc} , Eq. (7.50) that some region must have in order to gravitationally collapse. Such result does not depend on the details of the region, so we can use it to obtain an approximation for the number density of collapsed objects as a function of the mass and redshift, known as mass function.

Press and Schechter in 1974 modeled the mass function, $n(M, z)$, assuming that it is given by the function, $F(M; z)$, of the fraction of collapsed objects at redshift z and with mass larger than M through the relation [255]:

$$n(M, z)dM = -\frac{\bar{\rho}}{M} \frac{dF}{dM} dM. \quad (7.51)$$

To determine the fraction of collapsed objects $F(M; z)$ we first consider an overdensity $\delta(r, t)$ smoothed by a window function $W(r)$, which is used to do a mean over the fluctuations inside a scale R . Here we will use a top-hat window function, defined as

$$W(r) = \begin{cases} (\frac{4\pi}{3}R^3)^{-1} & |r| \leq R, \\ 0 & |r| > R \end{cases} \quad \int d^3r W(r) = 1.$$

so that

$$\tilde{\delta}(r, t) = \tilde{\delta}(r)D(t) = \int d^3r' \delta(r')W(r' + r)D(t). \quad (7.52)$$

and the mass dependence is through the relation $M = \frac{4\pi}{3}\bar{\rho}(bR)^3$.

If a region with overdensity $\delta(r, z) > \delta_{sc} \approx 1.686(1+z)$ collapses into a halo of mass M , the fraction of objects with mass larger than M is [253]

$$F(M) \equiv \int_{\delta_{sc}}^{\infty} p(\tilde{\delta}(r))d\tilde{\delta} = \frac{1}{\sqrt{2\pi}\sigma_R} \int_{\delta_{sc}}^{\infty} \exp\left(-\frac{\tilde{\delta}^2}{2\sigma_R^2}\right) d\tilde{\delta}, \quad (7.53)$$

where $p(\delta)$ is the probability of some point in space to have an overdensity δ which we will assume to be a Gaussian probability distribution. Therefore, σ_R is the variance in the smoothed density field given by

$$\sigma_R^2 = \frac{1}{2\pi^2} \int P(k)W_F^2(kR)k^2 dk. \quad (7.54)$$

$W_F(kR)$ is the Fourier transform of the top-hat function,

$$W_F(x) = \frac{3(\sin(x) - x \cos(x))}{x^3}. \quad (7.55)$$

Substituting Eq. (7.53) in Eq. (7.51) we get,

$$n(M)dM = -\frac{\bar{\rho}}{M} \frac{d\sigma_R}{dM} \frac{d}{d\sigma_R} \left[\frac{(-1)}{\sqrt{2\pi}\sigma_R} \int_{\delta_{sc}}^{\delta_{sc}/2\sigma_R} \exp\left(-\frac{\tilde{\delta}^2}{2\sigma_R^2}\right) d\tilde{\delta} \right]. \quad (7.56)$$

Using that

$$\frac{d}{dx} \int_a^{b(x)} f(z) dz = f(b(x)) \frac{d}{dx} b(x), \quad \text{if } f(a) = 0, \quad (7.57)$$

we arrive at the following expression for the Press-Schechter mass function:

$$n(M) dM = -\frac{\bar{\rho}}{M} \left(\frac{2}{\pi}\right)^{1/2} \left(\frac{\delta_{sc}}{\sigma_R^2(M)} \frac{d\sigma_R(M)}{dM}\right) \exp\left(-\frac{\delta_{sc}^2}{2\sigma_R^2}\right) dM. \quad (7.58)$$

Is useful to rewrite the last equation in terms of the variable ν , such that,

$$\nu \equiv \frac{\delta_{sc}^2}{\sigma_R^2}; \quad \frac{d\nu}{dM} = -\frac{2\nu}{\sigma_R} \frac{d\sigma_R}{dM}. \quad (7.59)$$

Hence, Eq. (7.58) becomes,

$$\frac{Mn(M)}{\rho} dM = \nu f(\nu) \frac{d\nu}{\nu}; \quad \nu f(\nu) = \left(\frac{\nu}{2\pi}\right)^{1/2} e^{-\frac{\nu}{2}}. \quad (7.60)$$

Despite of being obtained from simple considerations and analitically, the Press-Schechter mass function agrees reasonably with N-body simulations [256]. Inspired by the Press & Schechter formalism, many mass functions [257, 258] were obtained later from numerical simulations of cold dark matter, such as the Jenkins mass function [256], which will be used later

$$\nu f(\nu) = a_1 \exp\left(-\left|\log\left(\frac{\sqrt{\nu}}{\delta_{sc}}\right) + a_2\right|^{a_3}\right), \quad (7.61)$$

where $a_1 \approx 0.315$, $a_2 \approx 0.61$ and $a_3 \approx 3.8$. We should also impose the normalization condition,

$$\int f(\nu) d\nu = 1. \quad (7.62)$$

Halo density profile

Another important ingredient we need in the Halo Model is how the dark matter is distributed inside the halos. Assuming spherical halos, functions of the form:

$$\rho(r, M) = \frac{\rho_s}{(r/r_s)^\alpha (1 + r/r_s)^\beta} \quad \text{and} \quad \rho(r, M) = \frac{\rho_s}{(r/r_s)^\alpha [1 + (r/r_s)^\beta]}, \quad (7.63)$$

have been widely studied in simulations of elliptical galaxies, where ρ_s is the amplitude of the density profile and r_s defines a scale for the halo radius. Choosing $(\alpha, \beta) = (1, 3)$ and $(1, 2)$ in the expression on the left we obtain the Hernquist [259] and Navarro-Frenk-White (NFW) [260, 261] profiles, respectively, while for $(\alpha, \beta) = (3/2, 3/2)$ in the expression of the right gives the M99 [262] density profile.

The NFW density profile is one of the most successful in the description of the density of virialized halos in numerical simulations. In this profile, the average density inside a halo ρ_h

can be estimated as 180 times the average density of the Universe. The expression for the average density in halos then reads [263]:

$$\rho_h = 180\bar{\rho}(z) = \frac{3}{4\pi r_{\text{vir}}^3} \int_0^{r_{\text{vir}}} 4\pi r^2 dr \rho(r) = 3\rho_s \int_0^1 \frac{x^2 dx}{cx(1+cx^2)}, \quad (7.64)$$

where $x = r/r_{\text{vir}}$, $c \equiv r_{\text{vir}}/r_s$, is known as the concentration parameter and r_{vir} is the virial radius. Integrating the last equation gives,

$$\rho_s = \frac{180}{3} \bar{\rho} \frac{c^3}{\ln(1+c) - c/(1+c)}. \quad (7.65)$$

In the NFW profile [264],

$$c = \frac{9}{1+z} \left(\frac{M}{M_*} \right)^{-0.13}, \quad (7.66)$$

where M_* is a characteristic mass scale chosen such that $\nu(M_*, z) = 1$. Here $M_* \approx 2 \times 10^{13} M_\odot$ [250].

It is also useful to introduce the normalized halo density profile,

$$u(\mathbf{r}|M) = \frac{\rho(\mathbf{r}, M)}{M}, \quad \int u(r|M) d^3r = 1, \quad (7.67)$$

and also its Fourier transform

$$u(\mathbf{k}|M) = \frac{\int \rho(\mathbf{r}, M) e^{-i\mathbf{k}\cdot\mathbf{r}} d^3r}{\int \rho(\mathbf{r}, M) d^3r}. \quad (7.68)$$

For spherically symmetric profiles truncated at the virial radius (which is the halo radius), we have:

$$u(k|M) = \int_0^{r_{\text{vir}}} dr 4\pi r^2 \frac{\sin(kr)}{kr} \frac{\rho(r, M)}{M}, \quad \text{and note that} \quad \lim_{k \rightarrow 0} u(k|M) = 1. \quad (7.69)$$

Figure (7.2) shows the Fourier transform of the Navarro-Frenk-White normalized density profile for some different mass values and $z = 0$. We see that, as expected, the larger the mass scale is, the greater will be the suppression on the density profile, as can be verified from Eq. (7.69).

Halo bias

Dark matter halos are biased tracers of the real dark matter distribution as the probability for a halo to form depends a lot on the initial density field. This effect is mostly important at large scales as it directly affects the galaxy distribution. For this reason the halo bias, $b(M)$, is generally modeled from the mass function.

For the Press-Schechter mass function the bias has the form

$$b(M) = 1 + \frac{\nu - 1}{\delta_{sc}}, \quad \nu = \frac{\delta_{sc}^2}{\sigma_R^2}. \quad (7.70)$$

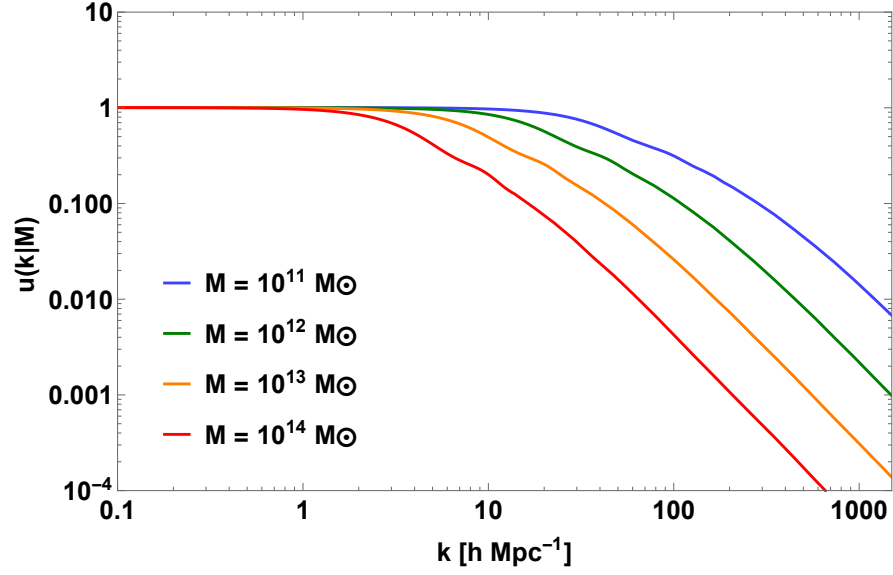


Figure 7.2: Fourier transform of the normalized Navarro-Frenk-White density profile, shown for some different mass values.

Such halo bias was improved by Sheth and Tormen [257] through its own mass function, and later on Tinker et al. using simulations came out with one of the most accurate halo bias, the Tinker bias [265],

$$b(\nu) = 1 + \frac{1}{\delta_{\text{sc}}} \left[q\nu + s(q\nu)^{1-t} - \frac{1}{\sqrt{q}} \frac{1}{1 + s(1-t)(1-t/2)(q\nu)^{-t}} \right], \quad (7.71)$$

where $q = 0.707$, $s = 0.35$ and $t = 0.8$ results in a better agreement with simulations.

Hence, the correlation function between halos can be written in terms of the dark matter correlation function:

$$\xi_{\text{hh}}(\mathbf{r}'_1, \mathbf{r}'_2, M_1, M_2) = b(M_1)b(M_2)\xi_{\text{dm}}(\mathbf{r}'_1, \mathbf{r}'_2). \quad (7.72)$$

7.3.3 Structure formation with halos

In the Halo Model all matter of the Universe is within halos which in turn can be described by its mass and density profile. Therefore, the density at some point \mathbf{r} is obtained by summing up the contributions from each halo [250]:

$$\rho(\mathbf{r}) = \sum_i \rho(\mathbf{r} - \mathbf{x}_i | M), \quad (7.73)$$

where \mathbf{x}_i is the position of the center of the i -th halo of mass M_i . We can rewrite this equation using the normalized density profile $u(k|M)$:

$$\begin{aligned}\rho(\mathbf{r}) &= \sum_i M_i u(\mathbf{r} - \mathbf{x}_i | M) \\ &= \sum_i \int dM \int d^3 r' \delta(M - M_i) \delta^3(\mathbf{r}' - \mathbf{x}_i) M u(\mathbf{r} - \mathbf{r}'),\end{aligned}\quad (7.74)$$

where the last equality follows from the relation $\int \delta(x - y) f(x) dx = f(y)$, and $\delta(x - y)$ is the Dirac delta function.

The density of halos with mass M is:

$$n(M) \equiv \left\langle \sum_i \delta(M - M_i) \delta^3(\mathbf{r}' - \mathbf{x}_i) \right\rangle, \quad (7.75)$$

where $\langle \dots \rangle$ stands for an average over ensembles. Hence, the average density on the point \mathbf{r} is,

$$\begin{aligned}\bar{\rho} = \langle \rho(\mathbf{r}) \rangle &= \left\langle \sum_i \int dM \int d^3 r' \delta(M - M_i) \delta^3(\mathbf{r}' - \mathbf{x}_i) M u(\mathbf{r} - \mathbf{r}') \right\rangle \\ &= \int dM n(M) M \int d^3 r' u(\mathbf{r} - \mathbf{r}') \\ &= \int dM n(M) M.\end{aligned}\quad (7.76)$$

The two-point correlation function can be obtained directly:

$$\begin{aligned}\xi(\mathbf{r}_1, \mathbf{r}_2) &= \langle \delta(\mathbf{r}_1) \delta(\mathbf{r}_2) \rangle \\ &= \left\langle \left(\frac{\rho(\mathbf{r}_1)}{\bar{\rho}} - 1 \right) \left(\frac{\rho(\mathbf{r}_2)}{\bar{\rho}} - 1 \right) \right\rangle = \left\langle \frac{\rho(\mathbf{r}_1) \rho(\mathbf{r}_2)}{\bar{\rho}^2} \right\rangle - 1 \\ &= \frac{1}{\bar{\rho}^2} \left\langle \sum_i M_i u(\mathbf{r}_i - \mathbf{r}_1) \sum_j M_j u(\mathbf{r}_j - \mathbf{r}_2) \right\rangle - 1 \\ &= \frac{1}{\bar{\rho}^2} \left\langle \sum_{i=j} M_i^2 u(\mathbf{r}_i - \mathbf{r}_1) u(\mathbf{r}_i - \mathbf{r}_2) \right\rangle + \\ &\quad + \frac{1}{\bar{\rho}^2} \left\langle \sum_{i \neq j} M_i M_j u(\mathbf{r}_i - \mathbf{r}_1) u(\mathbf{r}_j - \mathbf{r}_2) (1 + \xi_{hh}(\mathbf{r}_i, \mathbf{r}_j)) \right\rangle - 1 \\ &= \frac{1}{\bar{\rho}^2} \left\langle \sum_i \int dM M^2 \delta(M - M_i) \int d^3 r' \delta^3(\mathbf{r}_i - \mathbf{r}') u(\mathbf{r}' - \mathbf{r}_1) u(\mathbf{r}' - \mathbf{r}_2) \right\rangle \\ &\quad + \frac{1}{\bar{\rho}^2} \int dM_1 M_1 \int dM_2 M_2 \int d^3 r'_1 u(\mathbf{r}'_1 - \mathbf{r}_1) \int d^3 r'_2 u(\mathbf{r}'_2 - \mathbf{r}_2) \times \\ &\quad \times \sum_i \sum_j \left\langle \delta(M_1 - M_i) \delta^3(\mathbf{r}_i - \mathbf{r}'_1) \delta(M_2 - M_j) \delta^3(\mathbf{r}_j - \mathbf{r}'_2) \right\rangle - 1.\end{aligned}$$

The second term of this equation contains the average of the product of two number densities per halo mass unity:

$$\left\langle \sum_i \delta(M_1 - M_i) \delta^3(\mathbf{r}_i - \mathbf{r}'_1) \sum_j \delta(M_2 - M_j) \delta^3(\mathbf{r}_j - \mathbf{r}'_2) \right\rangle = \langle n(\mathbf{r}'_1, M_1) n(\mathbf{r}'_2, M_2) \rangle. \quad (7.77)$$

Written in terms of the mass function $n(M)$, the equation becomes

$$\delta n(\mathbf{r}, M) = \frac{n(\mathbf{r}, M) - n(M)}{n(M)} \Rightarrow n(\mathbf{r}, M) = n(M)\delta n(M) + n(M), \quad (7.78)$$

and, as $\langle \delta n(M) \rangle = 0$:

$$\langle n(\mathbf{r}'_1, M_1)n(\mathbf{r}'_2, M_2) \rangle = \langle \delta n(\mathbf{r}'_1, M_1)\delta n(\mathbf{r}'_2, M_2) \rangle n(M_1)n(M_2) + n(M_1)n(M_2). \quad (7.79)$$

Therefore,

$$\begin{aligned} \xi(\mathbf{r}_1, \mathbf{r}_2) &= \frac{1}{\bar{\rho}^2} \int dM M^2 n(M) \int d^3 r' u(\mathbf{r}' - \mathbf{r}_1) u(\mathbf{r}' - \mathbf{r}_2) + \\ &+ \frac{1}{\bar{\rho}^2} \int dM_1 M_1 \int dM_2 M_2 \int d^3 r'_1 u(\mathbf{r}'_1 - \mathbf{r}_1) \int d^3 r'_2 u(\mathbf{r}'_2 - \mathbf{r}_2) \times \\ &\times (\langle \delta n(\mathbf{r}'_1, M_1)\delta n(\mathbf{r}'_2, M_2) \rangle n(M_1)n(M_2) + n(M_1)n(M_2)) - 1. \end{aligned}$$

But the average $\langle \delta n(\mathbf{r}'_1, M_1)\delta n(\mathbf{r}'_2, M_2) \rangle$ is exactly the correlation function between two dark matter halos on the positions \mathbf{r}'_1 and \mathbf{r}'_2 , and of masses M_1 e M_2 , respectively. We shall denote this correlation function as $\xi_{\text{hh}}(\mathbf{r}'_1, \mathbf{r}'_2 | M_1, M_2)$. For the last term we have $(\int dM n(M) M)^2 = \bar{\rho}^2$, as $\int u(r|M) d^3 r = 1$, such that,

$$\begin{aligned} \xi(\mathbf{r}_1, \mathbf{r}_2) &= \frac{1}{\bar{\rho}^2} \int dM M^2 n(M) \int d^3 r' u(\mathbf{r}' - \mathbf{r}_1) u(\mathbf{r}' - \mathbf{r}_2) + \\ &+ \frac{1}{\bar{\rho}^2} \int dM_1 M_1 n(M_1) \int dM_2 M_2 n(M_2) \times \\ &\times \int d^3 r'_1 \int d^3 r'_2 u(\mathbf{r}'_1 - \mathbf{r}_1) u(\mathbf{r}'_2 - \mathbf{r}_2) \xi_{\text{hh}}(\mathbf{r}'_1, \mathbf{r}'_2 | M_1, M_2). \end{aligned}$$

The two points of the correlation function can be in the same halo or in two different ones, so we can split the correlation function into two terms: one that takes into account the contribution of only one halo ($i = j$), $\xi_{1\text{h}}(\mathbf{r}_1, \mathbf{r}_2)$, and other in which two different halos contribute ($i \neq j$), $\xi_{2\text{h}}(\mathbf{r}_1, \mathbf{r}_2)$. Using this, the total two-point correlation function can be written as

$$\xi(\mathbf{r}_1, \mathbf{r}_2) = \xi_{1\text{h}}(\mathbf{r}_1, \mathbf{r}_2) + \xi_{2\text{h}}(\mathbf{r}_1, \mathbf{r}_2), \quad (7.80)$$

where

$$\xi_{1\text{h}}(\mathbf{r}_1 - \mathbf{r}_2) = \int dM \frac{M^2}{\bar{\rho}^2} n(M) \int d^3 r' u(\mathbf{r}' - \mathbf{r}_1) u(\mathbf{r}' - \mathbf{r}_2) \quad (7.81)$$

$$\begin{aligned} \xi_{2\text{h}}(\mathbf{r}_1 - \mathbf{r}_2) &= \int dM_1 \frac{M_1}{\bar{\rho}} n(M_1) \int dM_2 \frac{M_2}{\bar{\rho}} n(M_2) \times \\ &\times \int d^3 r'_1 \int d^3 r'_2 u(\mathbf{r}'_1 - \mathbf{r}_1) u(\mathbf{r}'_2 - \mathbf{r}_2) \xi_{\text{hh}}(\mathbf{r}'_1, \mathbf{r}'_2 | M_1, M_2), \end{aligned} \quad (7.82)$$

As the power spectrum is the Fourier transform of the correlation function, we can also split $P(k)$ into two parts:

$$P_{\text{h}}(k) = P_{1\text{h}}(k) + P_{2\text{h}}(k), \quad (7.83)$$

where

$$P_{1h}(k) = \frac{1}{\bar{\rho}^2} \int dM M^2 n(M) |u(k|M)|^2 \quad (7.84)$$

$$P_{2h}(k) = \frac{1}{\bar{\rho}^2} \int dM_1 M_1 n(M_1) u(k|M_1) \int dM_2 M_2 n(M_2) u(k|M_2) P_{hh}(k|M_1, M_2), \quad (7.85)$$

and $P_{hh}(k|M_1, M_2)$ is the power spectrum of the dark matter halos. At the linear regime, $P_{hh}(k|M_1, M_2) \approx b_1(M_1)b_2(M_2)P_{lin}(k)$, where $P_{lin}(k)$ is the linear power spectrum. The integrals are calculated for typical mass values of observed halos. In general one can consider $10^6 M_\odot \lesssim M \lesssim 10^{15} M_\odot$ [250].

Therefore, we obtained a non-linear dark matter power spectrum which depends only on the linear power spectrum, halo mass function, density profile and halo bias, as dictates the Halo Model. That's why the Halo Model is such a useful semi-analytical tool to explore the Universe structure at the non-linear regime: the linear power spectrum can be easily dealt with linear perturbation theory and the three Halo Model ingredients can be improved with dark matter simulations.

8

Forecasts for Warm Dark Matter from photometric galaxy surveys

The Λ CDM model, with a cosmological constant (Λ) and cold dark matter (CDM) contributing approximately 70% and 25% respectively to the energy density budget, is the best cosmological description of our universe we have to-date. This conclusion comes from a variety of observations from different probes at different epochs. A recent example is the analysis of the first year of data of the Dark Energy Survey using probes from galaxy clustering and weak lensing simultaneously to show the consistency of this model even when combined with data from the cosmic microwave background [266].

However, it is fair to say that the nature of dark matter is still not settled. In fact, some tensions have been found when comparing small scales (few Mpc down to kpc) observations with CDM-only numerical simulations. These tensions can be described by three “problems”: the core-cusp problem, where the inner density profile of a CDM halo in a simulation with dark matter only has a cuspy density profile close to the centre of the halo whereas the measured density of galaxies has a core profile for small radii [267–271]; the missing satellite problem, which arises because one observes less satellite galaxies of our galaxy and M31 than subhalos predicted in CDM simulations [272–274]; and the ‘*too-big-to-fail*’ problem, where halos that are massive enough to form dwarf galaxies in simulations are not actually found in observations, that is, the observed dwarf galaxies are less massive than predicted [275–277]. Hence, in general we observe less structure at small scales than predicted by pure CDM simulations.

While several groups try to explain these tensions through astrophysical processes such as adding baryons in simulations [278], there is also the possibility of changing the nature

of dark matter to obtain a better agreement with observations. For instance, assuming that dark matter is warm instead of cold could in principle ameliorate these tensions. A recent comparison between the warm dark matter (WDM) and baryonic effects in the context of the too-big-to-fail problem can be found in [279].

Regardless of these issues with simulations, the nature of the dark matter is a fundamental question for particle physics and should be investigated using any available probe. The aim of this chapter is to study the possibility of using the angular power spectrum of photometric galaxy surveys to answer the question of whether dark matter is cold or warm.

Warm dark matter behaves very similarly to CDM at large scales but in the early universe it decouples while still mildly relativistic. This gives a thermal velocity to the dark matter particles and consequently a non-negligible free-streaming scale below which perturbations are smoothed out. The tightest constraint on the warm dark matter particle mass comes from Lyman α (Ly α) forest from absorption lines of distant quasars in the intergalactic medium at high redshifts and it reaches a lower bound of $m_{\text{wdm}} \geq 5.3 \text{ keV}$ (at 2σ CL) if warm dark matter is assumed to be a thermal relic [280].

In this chapter we study the sensitivity to the mass of a thermal warm dark matter particle using a Fisher matrix approach considering the galaxy angular power spectrum in photometric surveys as an observable. We will use as examples the Dark Energy Survey (DES) and a Large Synoptic Survey Telescope (LSST)-like surveys. The ongoing DES¹ project is a wide area ($\sim 5,000 \text{ deg}^2$) and relatively deep ($z \sim 1.4$) photometric map of the southern sky and among its goals is the determination of the cosmological parameters using the distribution of galaxies, weak gravitational lensing, cluster number counts and type Ia supernovae. The LSST² is intended to be the largest galaxy survey ever made mapping $30,000 \text{ deg}^2$ of the visible sky for $z \leq 3$ and will be able to perform a variety of studies, including the investigation on the nature of dark energy and dark matter.

One particular challenge we face comes from the fact that the modifications due to warm dark matter in the power spectrum arise at small, nonlinear scales. We adopt a halo model prescription to estimate the power spectrum at these scales. The halo model provides a flexible tool to model nonlinear effects for a given input cosmology. It may be used as a less computationally intensive, albeit less accurate, alternative to full-fledged simulations in exploratory studies such as the present one. However, we will also show results using a numerical fit to warm dark matter simulations.

We find our forecasts to be less restrictive than the Ly α constraints, but these bounds should be pursued anyways in combination with other probes. This chapter is based on [20].

¹www.darkenergysurvey.org

²www.lsst.org

8.1 Warm dark matter and structure formation

8.1.1 Linear regime

Warm dark matter, being lighter than its CDM counterpart, remains relativistic for a longer period during the radiation dominated era and also retains some thermal velocity at decoupling (which gives warm dark matter its name). This gives enough time for warm dark matter particles to diffuse out of perturbations after their decoupling. The effect of this scenario at late times is a suppression on structure formation below a certain scale related to the free-streaming length of the particles, which depends on their mass.

A simple way to estimate the free-streaming length is by computing the comoving length scale that a particle can travel until matter-radiation equality (t_{eq}), as in radiation era matter perturbations don't grow [221]:

$$\lambda_{\text{fs}} = \int_0^{t_{\text{eq}}} \frac{v(t)dt}{a(t)} \approx \int_0^{t_{\text{NR}}} \frac{cdt}{a(t)} + \int_{t_{\text{NR}}}^{t_{\text{eq}}} \frac{v(t)dt}{a(t)}, \quad (8.1)$$

where t_{NR} is the time when WDM particles become non-relativistic.

For WDM made of a two-component fermion, the free-streaming length can be written as [221]:

$$\lambda_{\text{fs}} \approx 0.4 \left(\frac{m_{\text{wdm}}}{\text{keV}} \right)^{-4/3} \left(\frac{\Omega_{\text{wdm}} h^2}{0.135} \right)^{1/3} [h^{-1} \text{Mpc}], \quad (8.2)$$

where m_{wdm} and Ω_{wdm} are the mass and density parameter of the warm dark matter particle, respectively. Here we will assume that all dark matter in the universe is warm, when calculating constraints on its mass.

The free-streaming scale can be qualitatively illuminating but to obtain a more accurate scenario of the WDM physics first we need the transfer function for this type of dark matter. We work here with the [281] fitting formula from Boltzmann code calculations, with revisited parameters [282]:

$$T_{\text{wdm}}(k) = \left[\frac{P_{\text{wdm}}^{\text{lin}}(k)}{P_{\text{cdm}}^{\text{lin}}(k)} \right]^{1/2} = \left[1 + (\alpha k)^{2\mu} \right]^{-5/\mu}, \quad (8.3)$$

where $\mu = 1.12$ and,

$$\alpha = 0.049 \left(\frac{m_{\text{wdm}}}{\text{keV}} \right)^{-1.11} \left(\frac{\Omega_{\text{wdm}}}{0.25} \right)^{0.11} \left(\frac{h}{0.7} \right)^{1.22} [h^{-1} \text{Mpc}]. \quad (8.4)$$

In Figure 8.1 we show the linear power spectrum for warm dark matter. We see that, as expected, the lighter the WDM particle is, the more it will suppress the formation of structure, since it stays relativistic for a longer time.

The characteristic length-scale α in the parametrization of the transfer function is closely related to the free-streaming scale λ_{fs} , and we will define $\lambda_{\text{fs}}^{\text{eff}} \equiv \alpha$ as an effective free-streaming

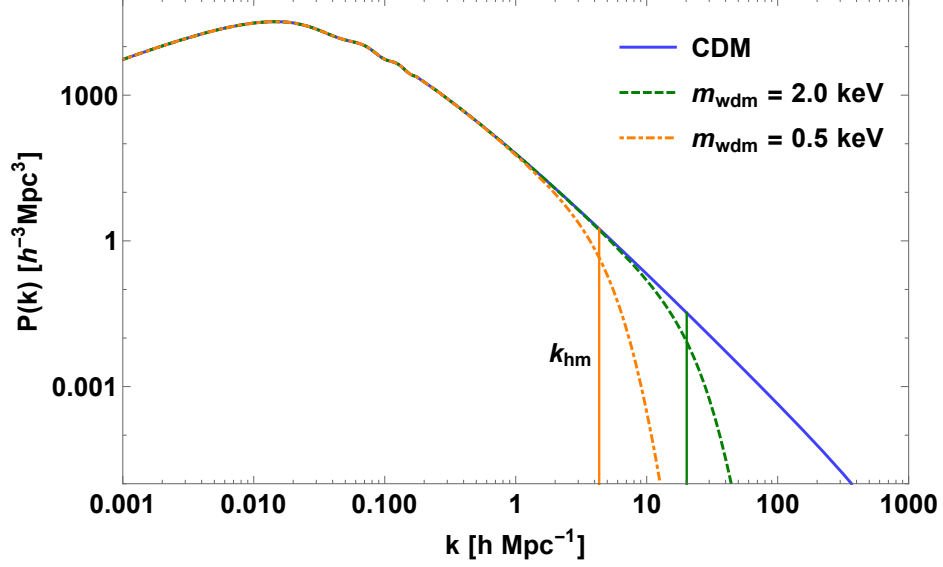


Figure 8.1: Linear matter power spectrum at $z = 0$ for WDM particle masses of $m_{\text{wdm}} = 2.0 \text{ keV}$ (dashed) and $m_{\text{wdm}} = 0.5 \text{ keV}$ (dot-dashed), together with the linear power spectrum for CDM. The vertical lines indicate the half-mode scale for each mass.

scale. This scale can be used to define a free-streaming mass scale given by:

$$M_{\text{fs}}(z) = \frac{4\pi}{3} \bar{\rho}(z) \left(\frac{\lambda_{\text{fs}}^{\text{eff}}}{2} \right)^3, \quad (8.5)$$

where $\bar{\rho}(z)$ is the mean density of the universe at a given redshift. This free-streaming mass defines the mass scale where the suppression of structure formation occurs. Below this scale the initial density perturbation are mostly erased.

Another useful length scale introduced in the literature is the half-mode scale λ_{hm} , which corresponds to the length scale at which the amplitude of the WDM transfer function is suppressed to 1/2 relative to CDM. From Eq. (8.3) we get for the half-mode scale:

$$\lambda_{\text{hm}} = 2\pi \lambda_{\text{fs}}^{\text{eff}} \left(2^{\mu/5} - 1 \right)^{-1/2\mu} \approx 14 \lambda_{\text{fs}}^{\text{eff}}. \quad (8.6)$$

This scale is shown as the vertical lines ($k_{\text{hm}} = 2\pi/\lambda_{\text{hm}}$) of Figure 8.1 for WDM particles of masses $m_{\text{wdm}} = 2.0 \text{ keV}$ and $m_{\text{wdm}} = 0.5 \text{ keV}$. As expected this scale is larger for smaller masses.

The half-mode length scale leads to another mass scale, called the half-mode mass scale:

$$M_{\text{hm}}(z) = \frac{4\pi}{3} \bar{\rho}(z) \left(\frac{\lambda_{\text{hm}}}{2} \right)^3 \approx 2.7 \times 10^3 M_{\text{fs}}(z). \quad (8.7)$$

The half-mode mass scale was found from numerical simulations to be the relevant one where WDM physics first affect the properties of structure formation [283, 284].

8.1.2 Non-linear regime: Halo Model modifications for WDM

At low redshifts, or scales of few kpc, the non-linear effects of gravity become relevant and modify the predictions of the linear theory. In fact, non-linearities tend to increase the power spectrum at small scales due to gravitational clumping. Unfortunately, it was found from numerical simulations that not much information is retained from the linear power spectrum with a small-scale suppression after the nonlinear growth of structure [285]. This effect obviously reduces the sensitivity to the mass of the WDM particle which causes the suppression in the linear power spectrum in the first place.

Therefore, in order to get meaningful results, we have to take into account the non-linear effects of gravity. One approach is by running simulations such as N-body or hydrodynamical simulations, but these are very costly and time-consuming as they require large computers and need to be repeated for each different cosmology. Another strategy available is to make use of semi-analytical models such as the halo model, which gives somewhat accurate results when compared to simulations [286, 287] and enables qualitative insights about structure formation at non-linear scales. However, the Halo Model was constructed and calibrated for cold dark matter, as the halo mass function, density profile and halo bias all come from N-body simulation of CDM. In order to use the halo model for warm dark matter one needs to make some modifications.

There are several proposals to modify the halo model for WDM in the literature, e.g. [288], [289], [290], [291] and [292]. Here we are going to adopt a recent proposal by Schneider [292].

First, one assumes the window function to be a 3D spherical top-hat in Fourier space (so-called sharp-k window function) instead of a top-hat in real space. The motivation to do so comes from Eq. (7.54). If we have a linear power spectrum that decreases more rapidly than k^{-3} for large k , which is the case for warm dark matter, we loose the sensitivity of the variance over the power spectrum at non-linear scales with a top-hat window function. As a consequence, the halo model would not account for the suppression of the power at small scales. But with a sharp-k window function $W_{\text{sk}}(kr) = \Theta(1 - kR)$ Eq. (7.54) becomes,

$$\sigma_{\text{sk}}(R)^2 = \frac{1}{2\pi^2} \int_0^{1/R} P_{\text{wdm}}^{\text{lin}}(k) k^2 dk, \quad (8.8)$$

and now we have a variance that fully captures the WDM suppression. As the relation between radius and mass is not well defined for a sharp-k window function it is useful to impose:

$$M = \frac{4\pi}{3} \bar{\rho}(bR)^3, \quad (8.9)$$

where $b = 2.5$ is fitted from simulations [293].

The NFW profile functional form remains the same:

$$\rho(r, M) = \frac{\rho_s}{(r/r_s)(1 + r/r_s)^2}, \quad \rho_s = \frac{180\bar{\rho}_z}{3} \frac{c^3}{\ln(1+c) - c/(1+c)}, \quad (8.10)$$

but the concentration parameter is modified using a generalization of the CDM case:

$$c_{\text{wdm}}(M) = c_{\text{cdm}}(M) \left(1 + \gamma_1 \frac{M_{\text{hm}}(z)}{M}\right)^{-\gamma_2}, \quad (8.11)$$

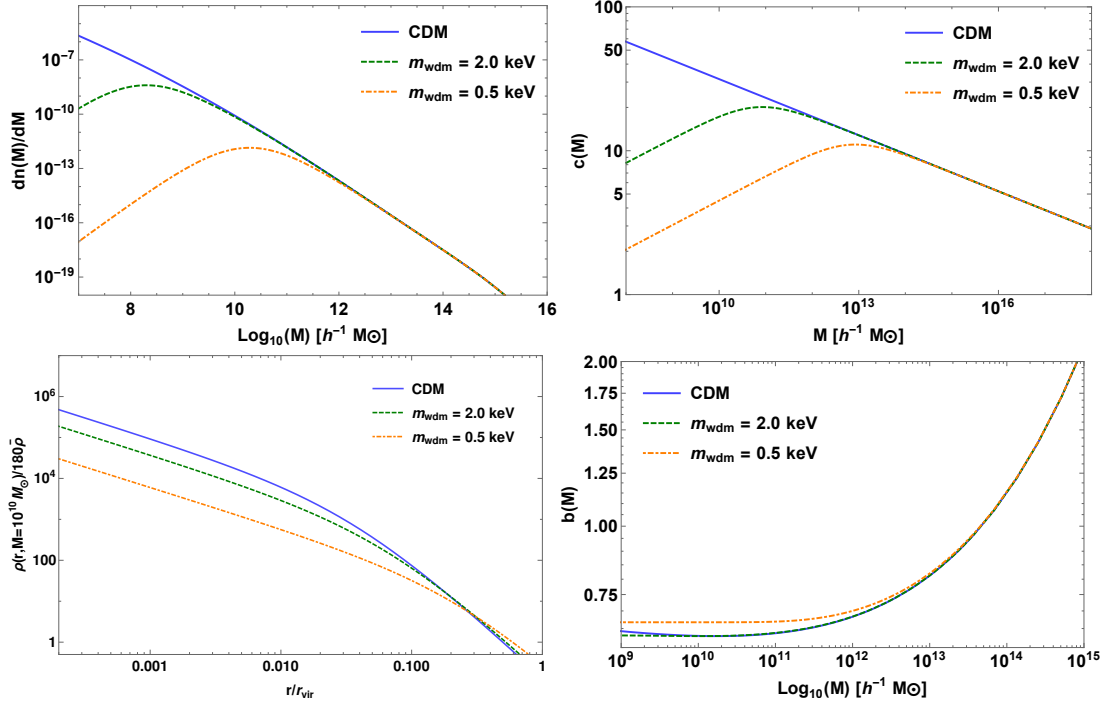


Figure 8.2: Jenkins mass function (first), concentration-mass parameter (second), NFW density profile (third) and Tinker halo bias (fourth) for CDM (solid lines), $m_{\text{wdm}} = 2.0 \text{ keV}$ (dashed) and $m_{\text{wdm}} = 0.5 \text{ keV}$ (dot-dashed).

where the parameters $\gamma_1 = 15$ and $\gamma_2 = 0.3$ are adjusted from N-body simulations [291] and $M_{\text{hm}}(z)$ is defined in Eq. (8.7).

We used the same functional form of the Tinker halo bias $b(\nu)$ in Eq. (7.71) and of the Jenkins mass function in Eq. (7.61), but as ν is different for different m_{wdm} through the variance, these quantities will also depend on the mass of WDM.

For illustration we show the mass function, Eq. (7.61), concentration parameter, Eq. (8.11), NFW profile, Eq. (8.10), and halo bias, Eq. (7.71) with these modifications for different WDM masses in Figure 8.2. As expected, there is a suppression in the number of halos with small masses and it is stronger for lighter WDM particles, and the turnover region is close to the half-mode mass. The concentration inside small halos also gets smoothed in the WDM case, and the inner density of low-mass halos decreases faster for smaller WDM particle masses. This effect is actually the reason for the explanation of the core-cusp problem in WDM.

8.1.3 Non-linear fitting formula for WDM

Another possible way to deal with non-linear effects is to use fitting formulas. A fitting formula for the non-linear power spectrum of WDM was obtained from simulations. Inspired by the linear fit from (Bode et al. 2001), Viel et al [294] suggested a formula for the non-linear suppression with an accuracy compared to simulations of 2% at $z < 3$ and masses

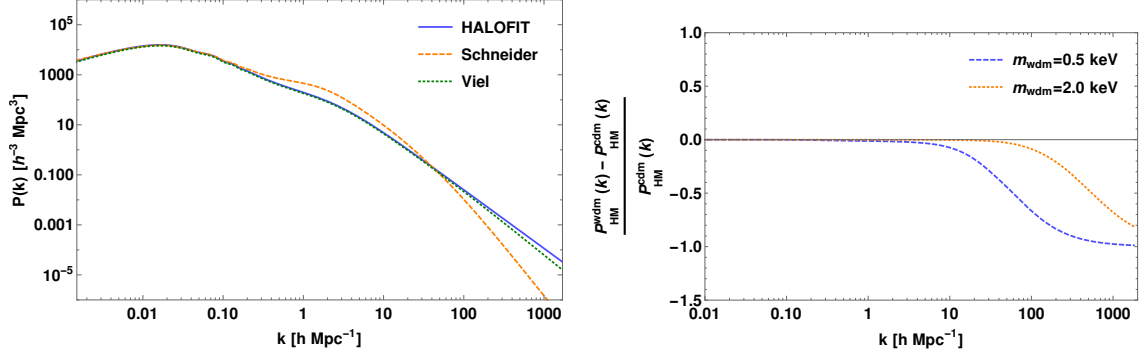


Figure 8.3: Left: Power spectrum from Viel (dotted) and from modified Halo model (dashed) for $m_{\text{wdm}} = 0.5 \text{ keV}$, together with CDM `halofit` (solid line) at $z=0.5$. Right: Difference between non-linear power spectrum from modified halo model for WDM particle masses of $m_{\text{wdm}} = 0.5 \text{ keV}$ (dashed) and $m_{\text{wdm}} = 2.0 \text{ keV}$ (dotted) and CDM at $z=0.5$.

$m_{\text{wdm}} \geq 0.5 \text{ keV}$:

$$P_{\text{wdm}}^{\text{nonlin}}(k, z) = P_{\text{cdm}}^{\text{halofit}}(k) \left\{ 1 + [\beta(z)k]^{\nu l} \right\}^{-s/\nu}, \quad (8.12)$$

$$\beta(z) = 0.0476 \left(\frac{m_{\text{wdm}}}{1 \text{ keV}} \right)^{-1.85} \left(\frac{1+z}{2} \right)^{1.3}, \quad (8.13)$$

where $\nu = 3$, $l = 0.6$ and $s = 0.4$.

In the Figure 8.3 we show the 3D power spectrum for the modified halo model and the non-linear fitting formula, together with the `halofit` [295] for cold dark matter. Comparing with Figure 8.1 one sees that the suppression effect of warm dark matter is much smaller in the non-linear power spectrum than in the linear one. This happens because the linear power spectrum enters in the halo model directly only in the 2-halo term and non-linear effects, which increase the power at small scales, end up by diminishing the WDM imprint. In the right panel of same figure we see the suppression of the non-linear power spectrum within the modified halo model for two different values of the WDM mass.

The halo model predicts a higher suppression of structure at small scales than the non-linear fitting formula from Viel. We opted for an optimistic analysis of the WDM structure and we used the halo model with sharp-k window function to obtain the general constraints for DES and LSST. As we will show in the following section, the use of the Viel non-linear fitting formula results in much weaker constraints for WDM mass.

8.2 Forecasting constraints for WDM particle mass from photometric surveys

We want to estimate constraints on the sensitivity to the warm dark matter particle mass in a DES-like and a LSST-like surveys, which are wide area photometric surveys. This class

of surveys maps galaxies at high redshifts ($z \sim 1\text{--}3$) but with poor radial distances resolution, and hence one measures a 2D projection of the galaxy power spectra at different redshift bins.

8.2.1 Angular power spectrum

In order to write down the angular power spectrum we need first to project the dark matter density field $\delta(\mathbf{x}, z)$ along a given direction of the sky using a radial selection function $\phi(z)$, and then expand it in Fourier modes followed by a spherical harmonics decomposition of the plane waves. This leads to the definition of the angular power spectrum C_ℓ [222]:

$$\langle a_{\ell m} a_{\ell' m'} \rangle \equiv \delta_{\ell\ell'} \delta_{mm'} C_\ell, \quad (8.14)$$

with

$$a_{\ell m} = 4\pi i^\ell \int dz \phi(z) \int \frac{d^3 k}{(2\pi)^3} \delta(\mathbf{k}, z) j_\ell(kr(z)) Y_{\ell m}^*(\hat{\mathbf{k}}), \quad (8.15)$$

where j_ℓ are the spherical Bessel functions of order ℓ , $\phi(z)$ is the normalised selection function and $r(z)$ is the comoving distance to redshift z given by,

$$r(z) = \int_0^z \frac{c}{H(z')} dz', \quad \frac{H(z)}{H_0} = \sqrt{\Omega_m(1+z)^3 + \Omega_\Lambda}. \quad (8.16)$$

If the survey is sliced into n redshift bins i the selection function will be given by a sum in each bin:

$$\phi(z) = \sum_i \phi_i(z) = \sum_i n(z) W_i(z), \quad (8.17)$$

where each $\phi_i(z)$ is written in terms of the number density of galaxies per unit solid angle and per unit redshift $n(z)$ and a window function

$$W_i(z) = \Theta(z - z_{min}^i) \Theta(z_{max}^i - z), \quad (8.18)$$

that selects the i -th redshift bin. However, in the case of photometric surveys, where there are large uncertainties in redshift measurement, we need to include the probability $P(z^{ph}|z)$ of assigning a true redshift z given a measured photometric redshift z^{ph} . The probability function for spectroscopic calibrated galaxies is usually written as a Gaussian distribution [296]:

$$P(z^{ph}|z) = \frac{1}{\sqrt{2\pi}\sigma(z)} \exp \left[-\frac{(z - z^{ph})^2}{2\sigma(z)^2} \right], \quad (8.19)$$

and the selection function for a photometric redshift bin i is given by

$$\phi_i(z) = n(z) \int_{z_{min}^i}^{z_{max}^i} dz^{ph} P(z^{ph}|z). \quad (8.20)$$

For DES [297, 298] the uncertainty in the photometric redshift is described as $\sigma(z) = 0.03(1+z)$ and the galaxy redshift distribution is parametrized as

$$n_{\text{DES}}(z) = A \left(\frac{z}{0.5} \right)^2 \exp \left(-\frac{z}{0.5} \right)^{1.5}. \quad (8.21)$$

For LSST $\sigma(z) = 0.05(1+z)$ and $n(z)$ is given by [299]

$$n_{\text{LSST}}(z) = Bz^2 \exp\left(-\frac{z}{0.5}\right), \quad (8.22)$$

where A and B are normalization constants chosen to guarantee that

$$\int_0^\infty dz \phi(z) = N, \quad (8.23)$$

where N is the total number of objects per unit solid angle of the survey. For DES we use $N = 15 \text{ arcmin}^{-2}$ [300] and for LSST we take $N = 50 \text{ arcmin}^{-2}$ [299].

Since we want to analyse highly non-linear scales we are allowed to use Limber approximation [301] to write the angular power spectrum as:

$$C_\ell = \int dz \frac{\phi(z)^2}{r(z)^2} P_g\left(k = \frac{\ell + 1/2}{r(z)}, z\right), \quad (8.24)$$

where we have introduced the galaxy power spectrum

$$P_g(k, z) = b_g^2 P_{\text{HM}}(k, z), \quad (8.25)$$

where P_{HM} is the halo model 3D matter power spectrum and b_g is the galaxy bias. As we want to give forecasts for a galaxy survey we need to account for the relation between the dark matter and the galaxy distributions, which can be encoded in the galaxy bias. In general this relation can be very complex, but we assume here for simplicity a linear bias model with a redshift-dependent bias.³

In Figure 8.4 the angular power spectra with LSST selection function at $z = 0.5$ for different WDM masses and CDM are shown. In practice we used for the CDM case a $m_{\text{wdm}} = 100 \text{ MeV}$. The difference between the C_ℓ s for CDM and a $m_{\text{wdm}} = 1 \text{ keV}$ WDM is about 0.3% at $\ell = 2000$ at $z = 0$. This difference increases for smaller masses and at higher redshifts where the non-linear effects are less important. In this analysis we will examine both $\ell_{\text{max}} = 1000$ and 2000.

In Figure 8.5 we show for illustration the resulting angular power spectrum for a LSST-like survey for 4 redshift bins for $m_{\text{wdm}} = 0.1 \text{ KeV}$ compared to the ΛCDM case. In this case one can see large differences of around 20% even at $\ell = 500$ for $z = 1.55$.

8.2.2 Fisher matrix analysis

The precision that can be achieved in measurements of cosmological parameters from a given observable is encoded in the Fisher information matrix [306]. In the case of the observable being the angular power spectrum the Fisher matrix can be written as [307]

$$\mathcal{F}_{\alpha\beta} = \sum_{\ell, \ell'} \sum_{i, j} \frac{\partial C_i(\ell)}{\partial p_\alpha} [\langle C_i(\ell), C_j(\ell') \rangle]^{-1} \frac{\partial C_j(\ell')}{\partial p_\beta}, \quad (8.26)$$

³The systematic effects of baryonic feedback such as supernova explosions and radiative cooling have been shown to be at the percent level for the weak lensing C_ℓ even at large values of ℓ [302–305] and we expect it to be of the same order for the angular matter power spectrum.

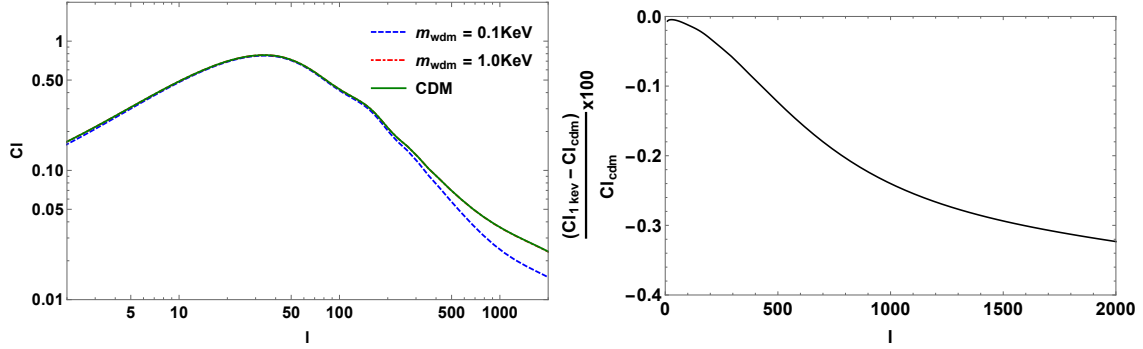


Figure 8.4: Left: C_ℓ s computed for different WDM particle masses at $z=0.5$. Right: percentage difference between C_ℓ s for $m_{\text{wdm}} = 1 \text{ keV}$ and $\text{CDM} = m_{\text{wdm}} = 100 \text{ MeV}$.

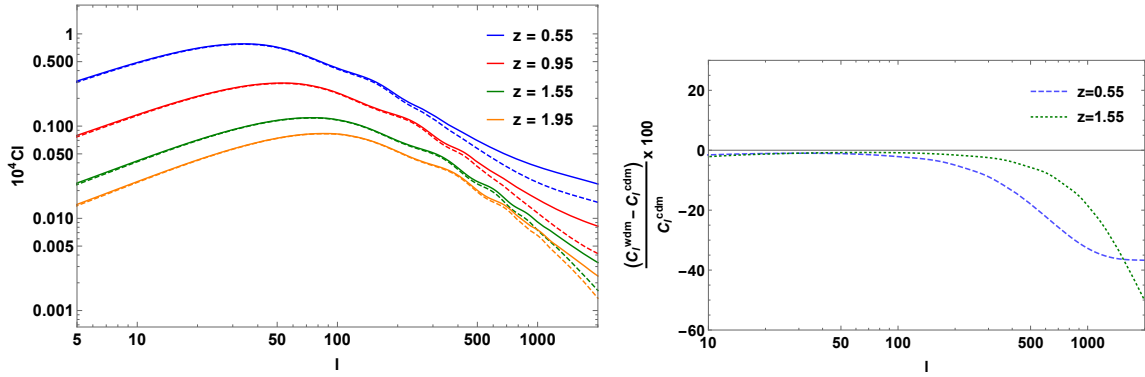


Figure 8.5: Left: C_ℓ s computed at 4 different redshifts for $m_{\text{wdm}} = 0.1 \text{ keV}$ (Dashed lines) and CDM (Solid lines). Right: Percentage difference between C_ℓ s for $m_{\text{wdm}} = 0.1 \text{ keV}$ and CDM at 2 redshifts.

where p_α are the parameters of our analysis and $\langle C_i(\ell), C_j(\ell') \rangle$ is the covariance matrix of the angular power spectrum for redshift bins i and j . The estimated $1\text{-}\sigma$ marginalised uncertainty on a parameter p is then:

$$\sigma_p = \sqrt{(\mathcal{F}^{-1})_{pp}}. \quad (8.27)$$

The parameter set chosen is $p_\alpha = \{m_{\text{wdm}}^{-1}, \Omega_m, b_g\}$. From the recent DES results [308] we know that the parameters that are most constrained by the 2-point statistics of galaxies and weak lensing are Ω_m and σ_8 . Therefore we choose to show our constraints on m_{wdm} against one of these parameters.

We used four redshift bins for DES forecast between $0.6 \leq z \leq 1$ equally spaced with $\Delta z = 0.1$. For LSST we used eight bins also equally spaced with $\Delta z = 0.2$ between $0.4 \leq z \leq 2$. In the following we will marginalize over the galaxy bias in each redshift bin directly in the Fisher matrix framework assuming a fiducial value of $b_g(z) = 1 + 0.84z$, which is estimated from simulations in [309].

We assumed that different bins are uncorrelated and that measurements of C_ℓ s are independent, which results in the following covariance matrix for each redshift bin i [310],

$$\langle C_i(\ell), C_j(\ell') \rangle = \frac{1}{f_{\text{sky}}} \frac{2}{2\ell + 1} C_i(\ell)^2 \delta_{\ell\ell'} \delta_{ij}, \quad (8.28)$$

where the effect of only observing a fraction of the sky, f_{sky} , is well approximated by simply dividing by f_{sky} [311]. For DES we adopt $f_{\text{sky}} = 1/8$ and for LSST $f_{\text{sky}} = 0.485$, according to the area intended to be mapped by the surveys.

The parameters which we aim to constrain are Ω_m and m_{wdm}^{-1} . We chose to work with m_{wdm}^{-1} instead of m_{wdm} to recover our fiducial Λ CDM model in the limit where the parameter related to the mass of dark matter particle goes to zero rather than infinity. This leads to numerical complications when calculating derivatives over m_{wdm}^{-1} (as well for m_{wdm}) as the C_ℓ s become insensitive to small variations close to the fiducial value for the warm dark matter mass. This insensitivity implies that small variations in the mass parameter induce variations in the C_ℓ s that are smaller than numerical noise. We handled this subtlety by calculating the numerical derivative around the fiducial model of an interpolation function constructed with C_ℓ s for various different WDM particle masses at each redshift bin.

For our fiducial Λ CDM model we used $\Omega_m = 0.307$, $\Omega_b = 0.048$, $\Omega_\Lambda = 0.693$, $n_s = 0.968$, $w = -1$, $h = 0.679$ following Planck results [232] and $m_{\text{cdm}} = 100$ MeV. The parameters constraints are shown in Figure 8.6 (for DES-like surveys) and in Figure 8.7 (for LSST-like surveys).

For DES, at 1σ confidence level we found a precision of 0.49% in the measurement of Ω_m ($\sigma(\Omega_m) = 0.0015$). One obtains a sensitivity to an upper limit on the inverse of the WDM mass, which translates into a lower limit in m_{wdm} . In this case we obtain $m_{\text{wdm}} > 126$ eV at 1σ .

For LSST, at 1σ confidence level we found a precision of 0.09% in the measurement of Ω_m ($\sigma(\Omega_m) = 0.0003$). For the WDM particle mass the lower limit found was $m_{\text{wdm}} > 647$ eV also at 1σ . Figure 8.8 shows the 1σ error ellipse for DES and LSST for comparison.

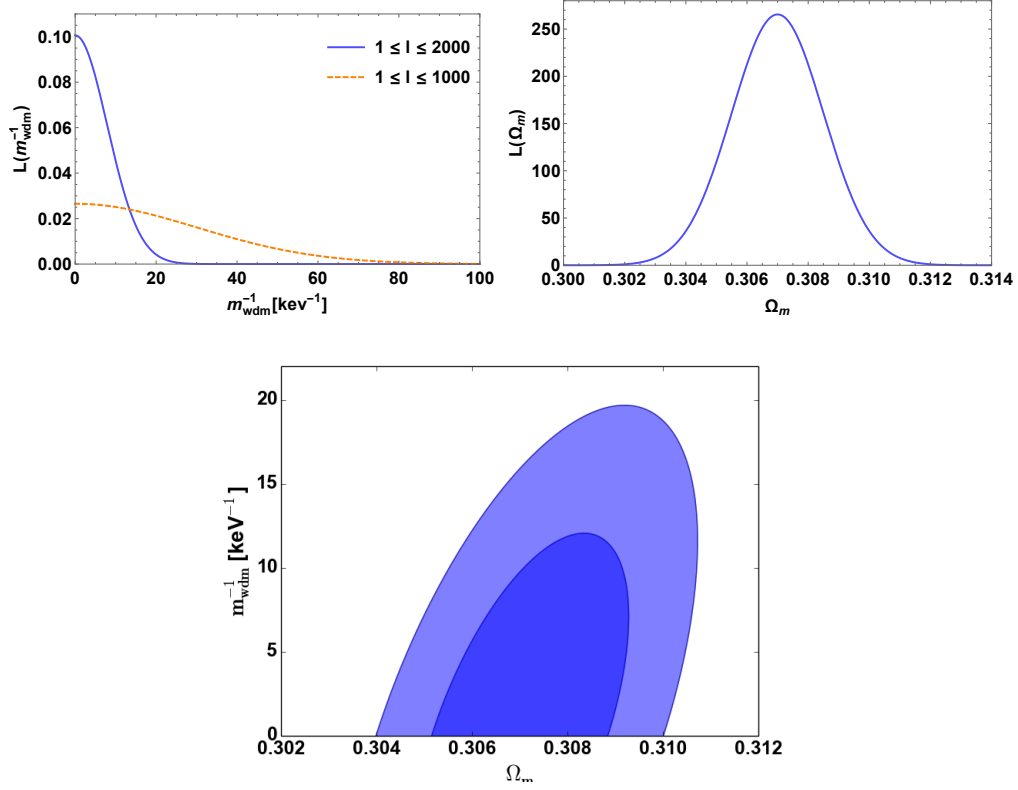


Figure 8.6: Top left: normalized likelihoods of m_{wdm}^{-1} marginalized over Ω_m and b_g . The dashed line shows the probability function for calculations done with l until 1000. We see that decreasing the non-linear regime in the computations has a great impact in error estimation (see Section 8.3). Top right: likelihood of Ω_m with m_{wdm}^{-1} and b_g marginalized. Bottom: the expected error ellipsis for Ω_m and m_{wdm}^{-1} with b_g marginalized. The light blue and dark blue curves represent a 2σ and 1σ confidence region, respectively. All plots are DES forecasts.

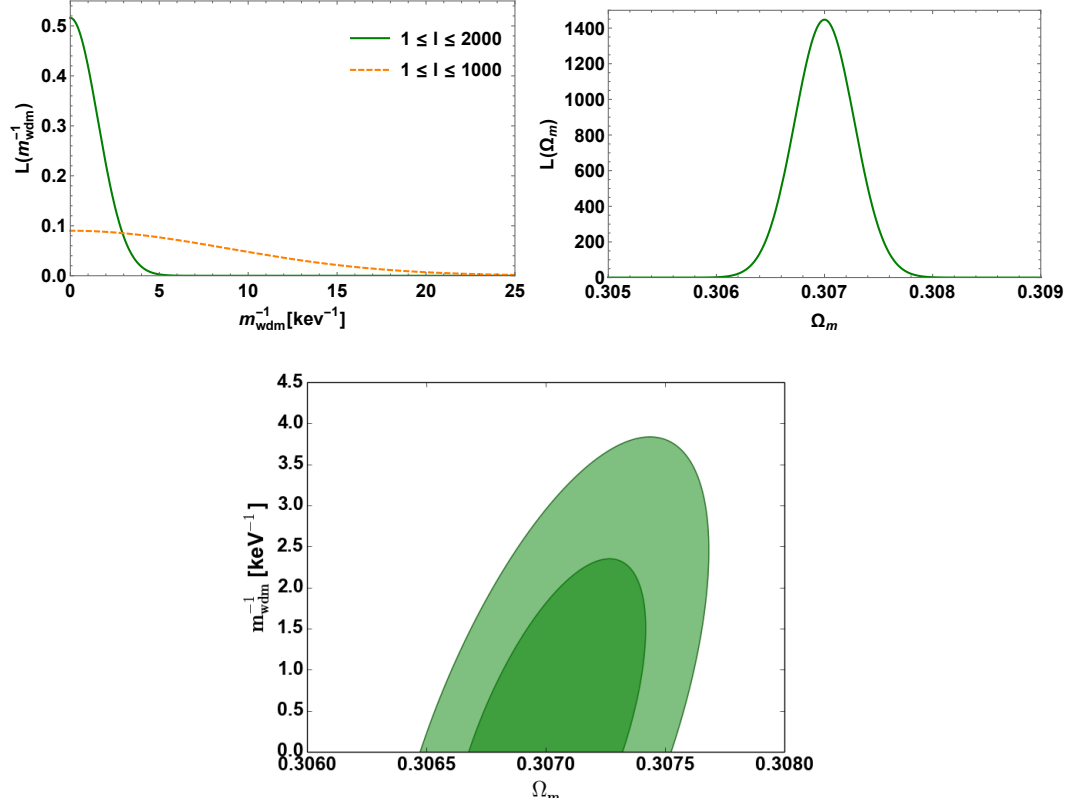


Figure 8.7: Top left: normalized likelihoods of m_{wdm}^{-1} marginalized over Ω_m and b_g . Top right: likelihood of Ω_m with m_{wdm}^{-1} and b_g marginalized. Bottom: the expected error ellipse for Ω_m and m_{wdm}^{-1} with b_g marginalized. The light green and dark green curves represent a 2σ and 1σ confidence region, respectively. All plots are LSST forecasts.

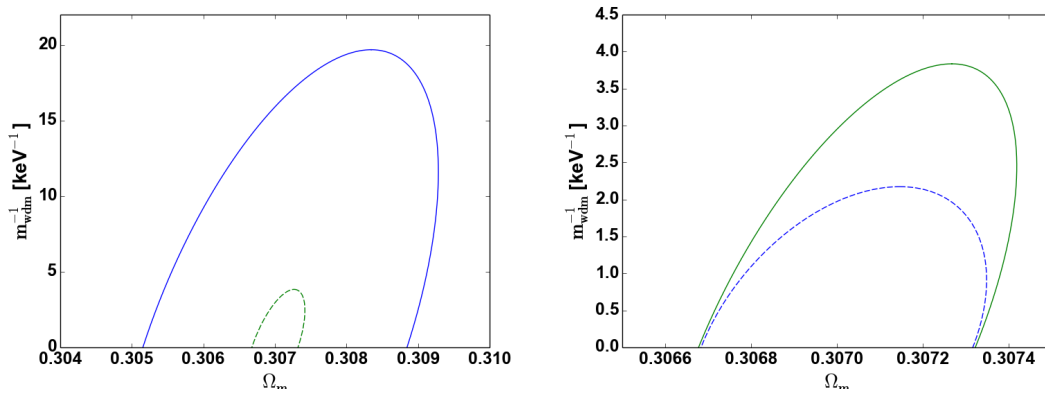


Figure 8.8: Left: Comparison between DES (blue line) and LSST (green dashed) 1σ error ellipse. Right: 1σ error ellipse for LSST (green line) and combined result with shear power spectra from EUCLID (blue dashed).

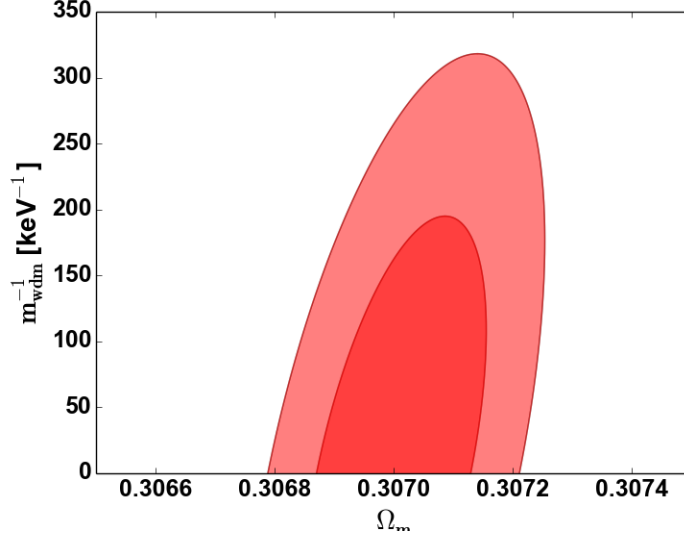


Figure 8.9: 1σ (dark red) and 2σ (light red) error ellipse for LSST using Viel non-linear fitting formula.

As pointed out in the end of Section 8.1 and can be seen from Figure 8.9, we get poor constraints for WDM particle mass when using the non-linear dark matter power spectrum of Viel et al. (2012). At 1σ we could place a lower limit of $m_{\text{wdm}} > 7.8 \text{ eV}$ for the LSST. This justifies why we called the use of the Halo Model an optimistic approach, as otherwise using a best fit from simulations gives barely no constraints on the mass.

8.2.3 Combined result with weak lensing

It is interesting to compare our results with a Fisher matrix forecast for WDM from cosmic shear power spectrum [312]. The effect of deflection of light rays by matter is called gravitational lensing, and when these deflections only cause small modifications on the observed properties of the objects, e.g position, size, shape, we have weak lensing. The observed properties of light sources close to each other in the sky are correlated, and the correlation function of galaxies shapes is called *cosmic shear* [313, 314]. An estimated lower bound of $m_{\text{wdm}} > 935 \text{ eV}$ is obtained from an Euclid-like weak lensing survey where they use multipoles as large as $\ell = 10^4$. This is comparable to our estimate from a LSST-like survey. We should also notice that there is no dependence on the galaxy bias in this case and we assumed a diagonal covariance matrix from weak lensing for simplicity.

The results for the combined 1σ error ellipse for LSST and EUCLID are shown in the right panel of Figure 8.8. For the combined analysis we could place a lower limit of $m_{\text{wdm}} > 1.14 \text{ keV}$ at 1σ and a precision of 0.07% in the measurement of Ω_m ($\sigma(\Omega_m) = 0.0002$).

8.3 Discussion

In this work we made the first estimate of constraints on the WDM particle mass using the galaxy angular power spectrum for a DES and a LSST-like photometric surveys. We used a well-know parametrization of the modified linear power spectrum and a modified Halo Model with a sharp-k window function and a new concentration-mass parameter based on N-body simulations of warm dark matter for the non-linear power spectrum.

We estimated a lower bound of $m_{\text{wdm}} > 126$ eV for DES and $m_{\text{wdm}} > 647$ eV for LSST at 1σ confidence level on the particle mass using the angular power spectrum.

It is interesting to compare our results with a Fisher matrix forecast for WDM from cosmic shear power spectrum [312]. An estimated lower bound of $m_{\text{wdm}} > 645$ eV is obtained from an Euclid-like weak lensing survey where they use multipoles as large as $\ell = 10^4$. This is comparable to our estimate from a LSST-like survey. We should also notice that there is no dependence on the galaxy bias in this case. For the combined probe we found a lower limit of $m_{\text{wdm}} > 1.14$ keV.

Our results degrade rapidly if we leave out very small scales from the analysis. This is expected, since as we showed above the main differences in the power spectrum appear at small scales or large redshifts. We also have results for $\ell < 1000$ shown in the upper left panel of Figure 8.6 and Figure 8.7. In this case the bounds on the mass are reduced to $m_{\text{wdm}} > 33$ eV for DES and $m_{\text{wdm}} > 113$ eV for LSST.

We should recall that there are other ways to modify the halo model to account for WDM. One method worth mentioning is (Schneider et al. 2012), where instead of imposing the normalization condition in Eq. (7.62), one could add another term in the statistics to represent the fraction of dark matter that didn't collapse into halos due to the free-streaming of WDM particles. Then, there would be a correlation function between the dark matter inside and outside halos, which has to be taken into account.

In addition to modifying the halo model, it would also be interesting to consider the halo occupation distribution model (HOD). As in practice we observe galaxies of baryonic matter instead of dark matter, it is relevant to work with a model for the occupation of objects inside halos. This would improve on our naive linear bias model. It would be as well of great importance to correctly include baryonic effects on structure formation, once this scenario is fully understood with the help of simulations.

Our estimated bounds are not competitive with bounds from Ly- α mentioned in the introduction but we think they should be explored anyways with real data and afterwards used in combinations of different probes, including CMB.

9

Conclusions

We have reviewed the theoretical aspects of particle physics, quantum field theory in curved spacetime and cosmology, and showed some new physics searches in these areas.

In Part I we reviewed the parity violation in electroweak theory and treated Atomic Parity Violation using effective field theory to show the possibility to constrain new physics using low energy precision measurements of the Cesium weak charge. We also compared the results with neutrino-nucleus coherent scattering and found that Atomic Parity Violation presented more restrictive bounds on the physics scale, assuming that this new particle, maybe a new heavy neutral mediator, couples with electrons and neutrinos with very similar strength. Concerning light new gauge boson mediator, we parametrized new physics effects in terms of the weak angle, $\sin \theta_W$, using polarized electron scattering experiments. Then, we explored the sensitivity on new measurements of the weak angle by these experiments to find bounds on the kinetic mixing between the Z and Z' as a function of the Z' mass. In the end, we applied the constraints found to models previously proposed in the literature and showed that our findings, in some cases, constitute the strongest limits on the kinetic mixing parameter.

In Part III we applied the results of a renormalizable theory of a sterile scalar coupled to massive fermions through Yukawa interaction to inflation. We found an analogous of the Starobinsky inflation, with perturbations coming from non-polynomial terms induced in the vacuum action by odd terms in the scalar effective potential. We concluded that such perturbations don't change much the Starobinsky scenario unless the fermions have mass close to M_P . Therefore, if very heavy BSM fermions exist and couple with a singlet scalar, they don't harm Starobinsky inflation.

We also have shown, in Part III, the first estimate of constraints on the warm dark matter particle mass using the galaxy angular power spectrum for a DES and a LSST-like photometric

surveys. We treated dark matter through a parametrization of the non-linear matter power spectrum from simulations, and a modified Halo Model with a sharp-k window function and concentration-mass parameter more suited for WDM. The more stringent bound obtained was from the LSST-like survey, where we could place a limit of $m_{\text{wdm}} > 647$ eV at 1σ confidence level for the WDM mass using the angular power spectrum. This limit is comparable to the results from Fisher matrix forecast for WDM from cosmic shear power spectrum from an Euclid-like weak lensing survey. Lastly, we combined the results from the two forecasts, and found the lower limit of $m_{\text{wdm}} > 1.14$ keV.

Bibliography

- [1] J. Erler and M. J. Ramsey-Musolf, “The Weak mixing angle at low energies,” *Phys. Rev.* **D72** (2005) 073003, [arXiv:hep-ph/0409169 \[hep-ph\]](#).
- [2] J. Erler and R. Ferro-Hernández, “Weak Mixing Angle in the Thomson Limit,” *JHEP* **03** (2018) 196, [arXiv:1712.09146 \[hep-ph\]](#).
- [3] C. Bouchiat and C. A. Piketty, “Parity Violation in Atomic Cesium and Alternatives to the Standard Model of Electroweak Interactions,” *Phys. Lett.* **128B** (1983) 73.
- [4] **SLAC E158** Collaboration, P. L. Anthony *et al.*, “Precision measurement of the weak mixing angle in Moller scattering,” *Phys. Rev. Lett.* **95** (2005) 081601, [arXiv:hep-ex/0504049 \[hep-ex\]](#).
- [5] **Qweak** Collaboration, M. T. Gericke, “The Q(weak)(p) experiment: A test for physics beyond the standard model via a precision measurement of the proton weak charge,” *AIP Conf. Proc.* **1149** (2009) no. 1, 237–240.
- [6] **Qweak** Collaboration, D. Androic *et al.*, “Early results from the Q_{weak} experiment,” *EPJ Web Conf.* **66** (2014) 05002, [arXiv:1311.6437 \[nucl-ex\]](#).
- [7] N. Berger *et al.*, “Measuring the weak mixing angle with the P2 experiment at MESA,” *J. Univ. Sci. Tech. China* **46** (2016) no. 6, 481–487, [arXiv:1511.03934 \[physics.ins-det\]](#).
- [8] R. Bucoveanu, M. Gorchtein, and H. Spiesberger, “Precision Measurement of $\sin^2 \theta_w$ at MESA,” *PoS LL2016* (2016) 061, [arXiv:1606.09268 \[hep-ph\]](#).
- [9] **MOLLER** Collaboration, J. Benesch *et al.*, “The MOLLER Experiment: An Ultra-Precise Measurement of the Weak Mixing Angle Using Moller Scattering,” [arXiv:1411.4088 \[nucl-ex\]](#).
- [10] **SoLID** Collaboration, Y. X. Zhao, “Parity Violation in Deep Inelastic Scattering with the SoLID Spectrometer at JLab,” in *22nd International Symposium on Spin Physics (SPIN 2016) Urbana, IL, USA, September 25-30, 2016*. 2017. [arXiv:1701.02780 \[nucl-ex\]](#).
- [11] **CHARM** Collaboration, J. Dorenbosch *et al.*, “Experimental Verification of the Universality of ν_e and ν_μ Coupling to the Neutral Weak Current,” *Phys. Lett.* **B180** (1986) 303–307.

- [12] A. Friedland, M. L. Graesser, I. M. Shoemaker, and L. Vecchi, “Probing Nonstandard Standard Model Backgrounds with LHC Monojets,” *Phys. Lett.* **B714** (2012) 267–275, [arXiv:1111.5331 \[hep-ph\]](#).
- [13] I. L. Shapiro, “Elements of qft in curved spacetime,” (2012).
- [14] **Planck** Collaboration, Y. Akrami *et al.*, “Planck 2018 results. I. Overview and the cosmological legacy of Planck,” [arXiv:1807.06205 \[astro-ph.CO\]](#).
- [15] SDSS, “Science results.” <http://www.sdss.org/science/>.
- [16] D. Baumann, “Cosmology,” *Part III, University of Cambridge, Department of Applied Mathematics and Theoretical Physics* (2015) .
- [17] Y. Akrami, F. Arroja, M. Ashdown, J. Aumont, C. Baccigalupi, M. Ballardini, A. Banday, R. Barreiro, N. Bartolo, S. Basak, *et al.*, “Planck 2018 results. x. constraints on inflation,” *arXiv preprint arXiv:1807.06211* (2018) .
- [18] G. Arcadi, M. Lindner, J. Martins, and F. S. Queiroz, “New physics probes: Atomic parity violation, polarized electron scattering and neutrino-nucleus coherent scattering,” [arXiv:1906.04755 \[hep-ph\]](#).
- [19] J. Martins, A. Romero, F. Sobreira, I. Shapiro, and A. A. Starobinsky, “To be determined,” *To Appear* .
- [20] J. S. Martins, R. Rosenfeld, and F. Sobreira, “Forecasts for Warm Dark Matter from Photometric Galaxy Surveys,” *Mon. Not. Roy. Astron. Soc.* **481** (2018) no. 1, 1290–1299, [arXiv:1803.03132 \[astro-ph.CO\]](#).
- [21] M. F. J. J. Thomson, “Xl. cathode rays,” *The London, Edinburgh, and Dublin Philosophical Magazine and Journal of Science* **44** (1897) no. 269, 293–316. <https://doi.org/10.1080/14786449708621070>.
- [22] E. Rutherford, “LXXIX. the scattering of α and β particles by matter and the structure of the atom,” *The London, Edinburgh, and Dublin Philosophical Magazine and Journal of Science* **21** (1911) no. 125, 669–688.
- [23] E. Fermi, “Tentativo di una teoria dell’emissione dei raggi beta,” *Ric. Sci.* **4** (1933) 491–495.
- [24] C. D. Anderson and S. H. Neddermeyer, “Cloud chamber observations of cosmic rays at 4300 meters elevation and near sea-level,” *Physical Review* **50** (1936) no. 4, 263.
- [25] J. Street and E. Stevenson, “New evidence for the existence of a particle of mass intermediate between the proton and electron,” *Physical Review* **52** (1937) no. 9, 1003.
- [26] H. Yukawa, “On the interaction of elementary particles. i,” *Proceedings of the Physico-Mathematical Society of Japan. 3rd Series* **17** (1935) 48–57.

- [27] P. A. M. Dirac, “The quantum theory of the emission and absorption of radiation,” *Proceedings of the Royal Society of London. Series A, Containing Papers of a Mathematical and Physical Character* **114** (1927) no. 767, 243–265.
- [28] C.-N. Yang and R. L. Mills, “Conservation of isotopic spin and isotopic gauge invariance,” *Physical review* **96** (1954) no. 1, 191.
- [29] A. Salam and J. C. Ward, “On a gauge theory of elementary interactions,” *Il Nuovo Cimento (1955-1965)* **19** (1961) no. 1, 165–170.
- [30] S. L. Glashow, “Partial-symmetries of weak interactions,” *Nuclear Physics* **22** (1961) no. 4, 579–588.
- [31] A. Salam and J. Ward, “Physics letters, 13, 168,” *Physical Review* **136** (1964) 763.
- [32] G. Arnison, A. Astbury, B. Aubert, C. Bacci, G. Bauer, A. Bézaguët, R. Böck, T. Bowcock, M. Calvetti, T. Carroll, *et al.*, “Experimental observation of isolated large transverse energy electrons with associated missing energy at $s = 540$ gev,” *Physics Letters B* **122** (1983) no. 1, 103–116.
- [33] P. Bagnaia *et al.*, “Ua2 kollaboration,” *Phys. lett. B* **129** (1983) 130.
- [34] H. Fritzsch, M. Gell-Mann, and H. Leutwyler, “Advantages of the color octet gluon picture,” *Physics Letters B* **47** (1973) no. 4, 365–368.
- [35] J. R. Oppenheimer, “Note on the theory of the interaction of field and matter,” *Physical Review* **35** (1930) no. 5, 461.
- [36] S.-I. Tomonaga, “On a relativistically invariant formulation of the quantum theory of wave fields,” *Progress of Theoretical Physics* **1** (1946) no. 2, 27–42.
- [37] J. Schwinger, “On quantum-electrodynamics and the magnetic moment of the electron,” *Physical Review* **73** (1948) no. 4, 416.
- [38] J. Schwinger, “Quantum electrodynamics. i. a covariant formulation,” *Physical Review* **74** (1948) no. 10, 1439.
- [39] R. P. Feynman, “Space-time approach to quantum electrodynamics,” *Physical Review* **76** (1949) no. 6, 769.
- [40] R. P. Feynman, “The theory of positrons,” *Physical Review* **76** (1949) no. 6, 749.
- [41] F. J. Dyson, “The radiation theories of tomonaga, schwinger, and feynman,” *Physical Review* **75** (1949) no. 3, 486.
- [42] R. P. Feynman, “Mathematical formulation of the quantum theory of electromagnetic interaction,” *Physical Review* **80** (1950) no. 3, 440.

- [43] D. J. Gross and F. Wilczek, “Ultraviolet behavior of non-abelian gauge theories,” *Physical Review Letters* **30** (1973) no. 26, 1343.
- [44] H. D. Politzer, “Reliable perturbative results for strong interactions?,” *Physical Review Letters* **30** (1973) no. 26, 1346.
- [45] K. G. Wilson, “Confinement of quarks,” *Physical review D* **10** (1974) no. 8, 2445.
- [46] F. Englert and R. Brout, “Broken symmetry and the mass of gauge vector mesons,” *Physical Review Letters* **13** (1964) no. 9, 321.
- [47] P. W. Higgs, “Broken symmetries and the masses of gauge bosons,” *Physical Review Letters* **13** (1964) no. 16, 508.
- [48] S. Weinberg, “A model of leptons,” *Physical review letters* **19** (1967) no. 21, 1264.
- [49] A. Salam, “Elementary particle theory,” in *Prog. Of the Nobel Symposium, 1968, Stockholm, Sweden*, vol. 367. 1968.
- [50] G. ’t Hooft, “Renormalization of massless yang-mills fields,” *Nuclear physics: B* **33** (1971) no. 1, 173–199.
- [51] S. Deser, “General relativity and the divergence problem in quantum field theory,” *Rev. Mod. Phys.* **29** (Jul, 1957) 417–423.
<https://link.aps.org/doi/10.1103/RevModPhys.29.417>.
- [52] G. ’t Hooft and M. Veltman, “One-loop divergencies in the theory of gravitation,” in *Annales de l’IHP Physique théorique*, vol. 20, pp. 69–94. 1974.
- [53] G. ’t Hooft, “Quantum gravity: a fundamental problem and some radical ideas,” *Recent Developments in Gravitation: Cargèse 1978* (1979) 323–345.
- [54] S. Deser, P. Van Nieuwenhuizen, and D. Boulware, “Uniqueness and nonrenormalizability of quantum gravitation,” *General Relativity and Gravitation* (1975) 1–18.
- [55] S. Weinberg, “Ultraviolet divergences in quantum theories of gravitation,” in *General relativity*. 1979.
- [56] M. Martellini, “Renormalizability of quantum gravity with cosmological constant,” *Phys. Rev. Lett.* **51** (Jul, 1983) 152–155.
<https://link.aps.org/doi/10.1103/PhysRevLett.51.152>.
- [57] M. H. Goroff and A. Sagnotti, “The ultraviolet behavior of einstein gravity,” *Nuclear Physics B* **266** (1986) no. 3-4, 709–736.
- [58] S. Chatrchyan, V. Khachatryan, A. M. Sirunyan, A. Tumasyan, W. Adam, E. Aguilo, T. Bergauer, M. Dragicevic, J. Erö, C. Fabjan, *et al.*, “Observation of a new boson at a mass of 125 gev with the cms experiment at the lh,” *Physics Letters B* **716** (2012) no. 1, 30–61.

- [59] G. Aad, T. Abajyan, B. Abbott, J. Abdallah, S. A. Khalek, A. A. Abdelalim, O. Abdinov, R. Aben, B. Abi, M. Abolins, *et al.*, “Observation of a new particle in the search for the standard model higgs boson with the atlas detector at the lhc,” *Physics Letters B* **716** (2012) no. 1, 1–29.
- [60] C. Burgess and G. Moore, *The standard model: A primer*. Cambridge University Press, 2006.
- [61] W. N. Cottingham and D. A. Greenwood, *An introduction to the standard model of particle physics*. Cambridge university press, 2007.
- [62] M. D. Schwartz, *Quantum field theory and the standard model*. Cambridge University Press, 2014.
- [63] M. Robinson, *Symmetry and the standard model*. Springer, 2011.
- [64] S. F. Novaes, “Standard model: An introduction,” *arXiv preprint hep-ph/0001283* (2000) .
- [65] M. Tanabashi, K. Hagiwara, K. Hikasa, K. Nakamura, Y. Sumino, F. Takahashi, J. Tanaka, K. Agashe, G. Aielli, C. Amsler, *et al.*, “Review of particle physics,” *Physical Review D* **98** (2018) no. 3, 030001.
- [66] C. Itzykson and J.-B. Zuber, *Quantum field theory*. Courier Corporation, 2012.
- [67] M. Sher, “Electroweak higgs potential and vacuum stability,” *Physics reports* **179** (1989) no. 5-6, 273–418.
- [68] G. Degrassi, S. Di Vita, J. Elias-Miro, J. R. Espinosa, G. F. Giudice, G. Isidori, and A. Strumia, “Higgs mass and vacuum stability in the standard model at nnlo,” *Journal of High Energy Physics* **2012** (2012) no. 8, 98.
- [69] I. Masina, “Higgs boson and top quark masses as tests of electroweak vacuum stability,” *Physical Review D* **87** (2013) no. 5, 053001.
- [70] D. Buttazzo, G. Degrassi, P. P. Giardino, G. F. Giudice, F. Sala, A. Salvio, and A. Strumia, “Investigating the near-criticality of the higgs boson,” *Journal of High Energy Physics* **2013** (2013) no. 12, 89.
- [71] L. Di Luzio, G. Isidori, and G. Ridolfi, “Stability of the electroweak ground state in the standard model and its extensions,” *Physics Letters B* **753** (2016) 150–160.
- [72] Y. Fukuda, T. Hayakawa, E. Ichihara, K. Inoue, K. Ishihara, H. Ishino, Y. Itow, T. Kajita, J. Kameda, S. Kasuga, *et al.*, “Evidence for oscillation of atmospheric neutrinos,” *Physical Review Letters* **81** (1998) no. 8, 1562.
- [73] I. Esteban, M. Gonzalez-Garcia, M. Maltoni, I. Martinez-Soler, and T. Schwetz, “Updated fit to three neutrino mixing: exploring the accelerator-reactor complementarity,” *Journal of High Energy Physics* **2017** (2017) no. 1, 87.

- [74] M. C. Gonzalez-Garcia, “Neutrino masses and mixing: A little history for a lot of fun,” 2019.
- [75] M. Drewes, “The phenomenology of right handed neutrinos,” *International Journal of Modern Physics E* **22** (Aug, 2013) 1330019.
<http://dx.doi.org/10.1142/S0218301313300191>.
- [76] M. E. Peskin, *An introduction to quantum field theory*. CRC Press, 2018.
- [77] P. Ramond, *Field theory: a modern primer*. Westview press, 1997.
- [78] S. Coleman, *Aspects of symmetry: selected Erice lectures*. Cambridge University Press, 1988.
- [79] C. S. Wu, E. Ambler, R. W. Hayward, D. D. Hoppes, and R. P. Hudson, “Experimental Test of Parity Conservation in Beta Decay,” *Phys. Rev.* **105** (1957) 1413–1414.
- [80] W. Pauli, “Exclusion principle, lorentz group and reflection of space-time and charge,” in *Wolfgang Pauli*, pp. 459–479. Springer, 1988.
- [81] G. Lüders, “On the equivalence of invariance under time-reversal and under particle-antiparticle conjugation for relativistic field theories, dan. mat. fys. medd. 28, 5 (1954); w. pauli,” 1955.
- [82] O. Greenberg, “Why is CPT fundamental?,” *Foundations of Physics* **36** (2006) no. 10, 1535–1553.
- [83] M. A. Bouchiat and C. Bouchiat, “Parity violation in atoms,” *Rept. Prog. Phys.* **60** (1997) 1351–1396.
- [84] M. J. Ramsey-Musolf, “Low-energy parity violation and new physics,” *Phys. Rev.* **C60** (1999) 015501, [arXiv:hep-ph/9903264](https://arxiv.org/abs/hep-ph/9903264) [hep-ph].
- [85] J. L. Rosner, “Atomic parity violation and precision electroweak physics: An Updated analysis,” *Phys. Rev.* **D61** (2000) 016006, [arXiv:hep-ph/9907524](https://arxiv.org/abs/hep-ph/9907524) [hep-ph].
- [86] J. L. Rosner, “Role of present and future atomic parity violation experiments in precision electroweak tests,” *Phys. Rev.* **D65** (2002) 073026, [arXiv:hep-ph/0109239](https://arxiv.org/abs/hep-ph/0109239) [hep-ph].
- [87] J. S. M. Ginges and V. V. Flambaum, “Violations of fundamental symmetries in atoms and tests of unification theories of elementary particles,” *Phys. Rept.* **397** (2004) 63–154, [arXiv:physics/0309054](https://arxiv.org/abs/physics/0309054) [physics].
- [88] A. Derevianko and S. G. Porsev, “Theoretical overview of atomic parity violation,” *Eur. Phys. J.* **A32** (2007) no. 4, 517–523, [arXiv:hep-ph/0608178](https://arxiv.org/abs/hep-ph/0608178) [hep-ph].

- [89] T. D. Lee and C.-N. Yang, “Question of Parity Conservation in Weak Interactions,” *Phys. Rev.* **104** (1956) 254–258.
- [90] R. L. Garwin, L. M. Lederman, and M. Weinrich, “Observations of the Failure of Conservation of Parity and Charge Conjugation in Meson Decays: The Magnetic Moment of the Free Muon,” *Phys. Rev.* **105** (1957) 1415–1417.
- [91] M. A. Bouchiat, J. Guena, L. Hunter, and L. Pottier, “Parity nonconservation in the first order in the weak interaction constant in electron scattering and other effects,” *Sov. Phys. JETP* **36** (1959) 964.
- [92] M. Bouchiat and C. Bouchiat, “I. parity violation induced by weak neutral currents in atomic physics,” *Journal de Physique* **35** (1974) no. 12, 899–927.
- [93] C. Y. Prescott *et al.*, “Parity Nonconservation in Inelastic Electron Scattering,” *Phys. Lett.* **B77** (1978) 347–352. [6.31(1978)].
- [94] L. M. Barkov and M. S. Zolotarev, “Observation of Nonconservation of Parity in Atomic Transitions,” *JETP Lett.* **27** (1978) 357. [6.25(1978)].
- [95] M. A. Bouchiat, J. Guena, L. Hunter, and L. Pottier, “Observation of a Parity Violation in Cesium,” *Phys. Lett.* **117B** (1982) 358. [Erratum: *Phys. Lett.* **121B**, 456(1983)].
- [96] M. Bouchiat and C. Bouchiat, “Weak neutral currents in atomic physics,” *Physics Letters B* **48** (1974) 111–114.
- [97] M. Safronova, D. Budker, D. DeMille, D. F. J. Kimball, A. Derevianko, and C. W. Clark, “Search for new physics with atoms and molecules,” *Reviews of Modern Physics* **90** (2018) no. 2, 025008.
- [98] M. L. Swartz, “Physics with polarized electron beams,” in *Conf. Proc.*, vol. 8708101, pp. 83–131. 1988.
- [99] J. Erler and S. Su, “The Weak Neutral Current,” *Prog. Part. Nucl. Phys.* **71** (2013) 119–149, [arXiv:1303.5522 \[hep-ph\]](#).
- [100] J. Erler, C. J. Horowitz, S. Mantry, and P. A. Souder, “Weak Polarized Electron Scattering,” *Ann. Rev. Nucl. Part. Sci.* **64** (2014) 269–298, [arXiv:1401.6199 \[hep-ph\]](#).
- [101] H. Davoudiasl, H.-S. Lee, and W. J. Marciano, “Muon Anomaly and Dark Parity Violation,” *Phys. Rev. Lett.* **109** (2012) 031802, [arXiv:1205.2709 \[hep-ph\]](#).
- [102] **Particle Data Group** Collaboration, M. Tanabashi *et al.*, “Review of Particle Physics,” *Phys. Rev.* **D98** (2018) no. 3, 030001.

- [103] D. Akimov, J. Albert, P. An, C. Awe, P. Barbeau, B. Becker, V. Belov, A. Brown, A. Bolozdynya, B. Cabrera-Palmer, *et al.*, “Observation of coherent elastic neutrino-nucleus scattering,” *Science* **357** (2017) no. 6356, 1123–1126.
- [104] J. Erler, A. Kurylov, and M. J. Ramsey-Musolf, “The Weak charge of the proton and new physics,” *Phys. Rev.* **D68** (2003) 016006, [arXiv:hep-ph/0302149](#) [[hep-ph](#)].
- [105] C. Bouchiat and P. Fayet, “Constraints on the parity-violating couplings of a new gauge boson,” *Phys. Lett.* **B608** (2005) 87–94, [arXiv:hep-ph/0410260](#) [[hep-ph](#)].
- [106] **COHERENT** Collaboration, D. Akimov *et al.*, “The COHERENT Experiment at the Spallation Neutron Source,” [arXiv:1509.08702](#) [[physics.ins-det](#)].
- [107] **COHERENT** Collaboration, D. Akimov *et al.*, “Observation of Coherent Elastic Neutrino-Nucleus Scattering,” *Science* **357** (2017) no. 6356, 1123–1126, [arXiv:1708.01294](#) [[nucl-ex](#)].
- [108] **COHERENT** Collaboration, D. Akimov *et al.*, “COHERENT 2018 at the Spallation Neutron Source,” [arXiv:1803.09183](#) [[physics.ins-det](#)].
- [109] K. Scholberg, “Prospects for measuring coherent neutrino-nucleus elastic scattering at a stopped-pion neutrino source,” *Phys. Rev.* **D73** (2006) 033005, [arXiv:hep-ex/0511042](#) [[hep-ex](#)].
- [110] J. Liao and D. Marfatia, “COHERENT constraints on nonstandard neutrino interactions,” *Phys. Lett.* **B775** (2017) 54–57, [arXiv:1708.04255](#) [[hep-ph](#)].
- [111] P. deNiverville, M. Pospelov, and A. Ritz, “Light new physics in coherent neutrino-nucleus scattering experiments,” *Phys. Rev.* **D92** (2015) no. 9, 095005, [arXiv:1505.07805](#) [[hep-ph](#)].
- [112] M. Abdullah, J. B. Dent, B. Dutta, G. L. Kane, S. Liao, and L. E. Strigari, “Coherent elastic neutrino nucleus scattering as a probe of a Z' through kinetic and mass mixing effects,” *Phys. Rev.* **D98** (2018) no. 1, 015005, [arXiv:1803.01224](#) [[hep-ph](#)].
- [113] J. Billard, J. Johnston, and B. J. Kavanagh, “Prospects for exploring New Physics in Coherent Elastic Neutrino-Nucleus Scattering,” *JCAP* **1811** (2018) no. 11, 016, [arXiv:1805.01798](#) [[hep-ph](#)].
- [114] B. C. Cañas, E. A. Garcés, O. G. Miranda, and A. Parada, “Future perspectives for a weak mixing angle measurement in coherent elastic neutrino nucleus scattering experiments,” *Phys. Lett.* **B784** (2018) 159–162, [arXiv:1806.01310](#) [[hep-ph](#)].
- [115] D. Aristizabal Sierra, V. De Romeri, and N. Rojas, “COHERENT analysis of neutrino generalized interactions,” *Phys. Rev.* **D98** (2018) 075018, [arXiv:1806.07424](#) [[hep-ph](#)].

- [116] Y. Farzan, M. Lindner, W. Rodejohann, and X.-J. Xu, “Probing neutrino coupling to a light scalar with coherent neutrino scattering,” *JHEP* **05** (2018) 066, [arXiv:1802.05171 \[hep-ph\]](#).
- [117] I. Bischer, W. Rodejohann, and X.-J. Xu, “Loop-induced Neutrino Non-Standard Interactions,” *JHEP* **10** (2018) 096, [arXiv:1807.08102 \[hep-ph\]](#).
- [118] V. Brdar, W. Rodejohann, and X.-J. Xu, “Producing a new Fermion in Coherent Elastic Neutrino-Nucleus Scattering: from Neutrino Mass to Dark Matter,” *JHEP* **12** (2018) 024, [arXiv:1810.03626 \[hep-ph\]](#).
- [119] P. B. Denton, Y. Farzan, and I. M. Shoemaker, “Testing large non-standard neutrino interactions with arbitrary mediator mass after COHERENT data,” *JHEP* **07** (2018) 037, [arXiv:1804.03660 \[hep-ph\]](#).
- [120] O. G. Miranda, G. Sanchez Garcia, and O. Sanders, “Testing new physics with future COHERENT experiments,” [arXiv:1902.09036 \[hep-ph\]](#).
- [121] O. G. Miranda, D. K. Papoulias, M. Tórtola, and J. W. F. Valle, “Probing neutrino transition magnetic moments with coherent elastic neutrino-nucleus scattering,” [arXiv:1905.03750 \[hep-ph\]](#).
- [122] D. Aristizabal Sierra, V. De Romeri, and N. Rojas, “CP violating effects in coherent elastic neutrino-nucleus scattering processes,” [arXiv:1906.01156 \[hep-ph\]](#).
- [123] J. B. Dent, B. Dutta, S. Liao, J. L. Newstead, L. E. Strigari, and J. W. Walker, “Probing light mediators at ultralow threshold energies with coherent elastic neutrino-nucleus scattering,” *Phys. Rev.* **D96** (2017) no. 9, 095007, [arXiv:1612.06350 \[hep-ph\]](#).
- [124] J. B. Dent, B. Dutta, S. Liao, J. L. Newstead, L. E. Strigari, and J. W. Walker, “Accelerator and reactor complementarity in coherent neutrino-nucleus scattering,” *Phys. Rev.* **D97** (2018) no. 3, 035009, [arXiv:1711.03521 \[hep-ph\]](#).
- [125] J. Hakenmuller *et al.*, “Neutron-induced background in the CONUS experiment,” [arXiv:1903.09269 \[physics.ins-det\]](#).
- [126] E. Derman and W. J. Marciano, “Parity Violating Asymmetries in Polarized Electron Scattering,” *Annals Phys.* **121** (1979) 147.
- [127] H. Davoudiasl, H.-S. Lee, and W. J. Marciano, “‘Dark’ Z implications for Parity Violation, Rare Meson Decays, and Higgs Physics,” *Phys. Rev.* **D85** (2012) 115019, [arXiv:1203.2947 \[hep-ph\]](#).
- [128] K. Kumar, S. Mantry, W. Marciano, and P. Souder, “Low-energy measurements of the weak mixing angle,” *Annual Review of Nuclear and Particle Science* **63** (2013) 237–267.

- [129] D. Armstrong, T. Averett, J. Bowman, R. Carlini, *et al.*, “The qweak experiment: a search for new physics at the tev scale via a measurement of the proton’s weak charge,” *arXiv preprint arXiv:1202.1255* (2001) .
- [130] J. Mammei *et al.*, “The moller experiment,” *arXiv preprint arXiv:1208.1260* (2012) .
- [131] P. Souder, “Parity-violating pvdis with solid,” in *AIP Conference Proceedings*, vol. 1441, pp. 123–125, AIP. 2012.
- [132] H. Davoudiasl, H.-S. Lee, and W. J. Marciano, “Dark Side of Higgs Diphoton Decays and Muon g-2,” *Phys. Rev.* **D86** (2012) 095009, [arXiv:1208.2973 \[hep-ph\]](#).
- [133] H. Davoudiasl, H.-S. Lee, I. Lewis, and W. J. Marciano, “Higgs Decays as a Window into the Dark Sector,” *Phys. Rev.* **D88** (2013) no. 1, 015022, [arXiv:1304.4935 \[hep-ph\]](#).
- [134] M. D. Campos, D. Cogollo, M. Lindner, T. Melo, F. S. Queiroz, and W. Rodejohann, “Neutrino Masses and Absence of Flavor Changing Interactions in the 2HDM from Gauge Principles,” *JHEP* **08** (2017) 092, [arXiv:1705.05388 \[hep-ph\]](#).
- [135] **BaBar** Collaboration, J. McKenna, “Search for Low-Mass Dark Sector New Physics States at BABAR,” *J. Phys. Conf. Ser.* **1137** (2018) no. 1, 012041.
- [136] P. Ko, Y. Omura, and C. Yu, “A Resolution of the Flavor Problem of Two Higgs Doublet Models with an Extra $U(1)_H$ Symmetry for Higgs Flavor,” *Phys. Lett.* **B717** (2012) 202–206, [arXiv:1204.4588 \[hep-ph\]](#).
- [137] J. Heeck, “Unbroken B-L symmetry,” *Phys. Lett.* **B739** (2014) 256–262, [arXiv:1408.6845 \[hep-ph\]](#).
- [138] M. Carena, A. Daleo, B. A. Dobrescu, and T. M. P. Tait, “ Z' gauge bosons at the Tevatron,” *Phys. Rev.* **D70** (2004) 093009, [arXiv:hep-ph/0408098 \[hep-ph\]](#).
- [139] P. V. Dong, D. T. Huong, F. S. Queiroz, and N. T. Thuy, “Phenomenology of the 3-3-1-1 model,” *Phys. Rev.* **D90** (2014) no. 7, 075021, [arXiv:1405.2591 \[hep-ph\]](#).
- [140] D. A. Camargo, L. Delle Rose, S. Moretti, and F. S. Queiroz, “Collider bounds on 2-Higgs doublet models with $U(1)_X$ gauge symmetries,” *Phys. Lett.* **B793** (2019) 150–160, [arXiv:1805.08231 \[hep-ph\]](#).
- [141] F. Pisano and V. Pleitez, “An $SU(3) \times U(1)$ model for electroweak interactions,” *Phys. Rev.* **D46** (1992) 410–417, [arXiv:hep-ph/9206242 \[hep-ph\]](#).
- [142] R. Foot, H. N. Long, and T. A. Tran, “ $SU(3)_L \otimes U(1)_N$ and $SU(4)_L \otimes U(1)_N$ gauge models with right-handed neutrinos,” *Phys. Rev.* **D50** (1994) no. 1, R34–R38, [arXiv:hep-ph/9402243 \[hep-ph\]](#).

- [143] H. N. Long, N. V. Hop, L. T. Hue, and N. T. T. Van, “Constraining heavy neutral gauge boson Z' in the 3 - 3 - 1 models by weak charge data of Cesium and proton,” *Nucl. Phys.* **B943** (2019) 114629, [arXiv:1812.08669 \[hep-ph\]](#).
- [144] Y. A. Coutinho, V. Salustino Guimarães, and A. A. Nepomuceno, “Bounds on Z' from 3-3-1 model at the LHC energies,” *Phys. Rev.* **D87** (2013) no. 11, 115014, [arXiv:1304.7907 \[hep-ph\]](#).
- [145] Q.-H. Cao and D.-M. Zhang, “Collider Phenomenology of the 3-3-1 Model,” [arXiv:1611.09337 \[hep-ph\]](#).
- [146] F. S. Queiroz, C. Siqueira, and J. W. F. Valle, “Constraining Flavor Changing Interactions from LHC Run-2 Dilepton Bounds with Vector Mediators,” *Phys. Lett.* **B763** (2016) 269–274, [arXiv:1608.07295 \[hep-ph\]](#).
- [147] G. Arcadi, C. P. Ferreira, F. Goertz, M. M. Guzzo, F. S. Queiroz, and A. C. O. Santos, “Lepton Flavor Violation Induced by Dark Matter,” *Phys. Rev.* **D97** (2018) no. 7, 075022, [arXiv:1712.02373 \[hep-ph\]](#).
- [148] C. Kelso, H. N. Long, R. Martinez, and F. S. Queiroz, “Connection of $g - 2_\mu$, electroweak, dark matter, and collider constraints on 331 models,” *Phys. Rev.* **D90** (2014) no. 11, 113011, [arXiv:1408.6203 \[hep-ph\]](#).
- [149] J. S. Borges and R. O. Ramos, “Symmetry breaking patterns of the 3-3-1 model at finite temperature,” *Eur. Phys. J.* **C76** (2016) no. 6, 344, [arXiv:1602.08165 \[hep-ph\]](#).
- [150] F. F. Deppisch, C. Hati, S. Patra, U. Sarkar, and J. W. F. Valle, “331 Models and Grand Unification: From Minimal SU(5) to Minimal SU(6),” *Phys. Lett.* **B762** (2016) 432–440, [arXiv:1608.05334 \[hep-ph\]](#).
- [151] M. Lindner, M. Platscher, and F. S. Queiroz, “A Call for New Physics : The Muon Anomalous Magnetic Moment and Lepton Flavor Violation,” *Phys. Rept.* **731** (2018) 1–82, [arXiv:1610.06587 \[hep-ph\]](#).
- [152] A. C. O. Santos and P. Vasconcelos, “Lower Mass Bound on the W' mass via Neutrinoless Double Beta Decay in a 3-3-1 Model,” *Adv. High Energy Phys.* **2018** (2018) 9132381, [arXiv:1708.03955 \[hep-ph\]](#).
- [153] A. E. Cárcamo Hernández, H. N. Long, and V. V. Vien, “The first $\Delta(27)$ flavor 3-3-1 model with low scale seesaw mechanism,” *Eur. Phys. J.* **C78** (2018) no. 10, 804, [arXiv:1803.01636 \[hep-ph\]](#).
- [154] F. F. Freitas, C. A. de S. Pires, and P. Vasconcelos, “Resonant production of Z' and signature of right-handed neutrinos within a 3-3-1 model,” *Phys. Rev.* **D98** (2018) no. 3, 035005, [arXiv:1805.09082 \[hep-ph\]](#).

- [155] D. A. Camargo, A. G. Dias, T. B. de Melo, and F. S. Queiroz, “Neutrino Masses in a Two Higgs Doublet Model with a $U(1)$ Gauge Symmetry,” *JHEP* **04** (2019) 129, [arXiv:1811.05488 \[hep-ph\]](#).
- [156] C.-H. Chen and T. Nomura, “Penguin $b \rightarrow s\ell'^+\ell'^-$ and B -meson anomalies in a gauged $L_\mu - L_\tau$,” *Phys. Lett.* **B777** (2018) 420–427, [arXiv:1707.03249 \[hep-ph\]](#).
- [157] S. Baek, “Dark matter contribution to $b \rightarrow s\mu^+\mu^-$ anomaly in local $U(1)_{L_\mu-L_\tau}$ model,” *Phys. Lett.* **B781** (2018) 376–382, [arXiv:1707.04573 \[hep-ph\]](#).
- [158] G. Arcadi, T. Hugle, and F. S. Queiroz, “The Dark $L_\mu - L_\tau$ Rises via Kinetic Mixing,” *Phys. Lett.* **B784** (2018) 151–158, [arXiv:1803.05723 \[hep-ph\]](#).
- [159] P. Foldenauer, “Light dark matter in a gauged $U(1)_{L_\mu-L_\tau}$ model,” *Phys. Rev.* **D99** (2019) no. 3, 035007, [arXiv:1808.03647 \[hep-ph\]](#).
- [160] P. Ko, T. Nomura, and C. Yu, “ $b \rightarrow s\mu^+\mu^-$ anomalies and related phenomenology in $U(1)_{B_3-x_\mu L_\mu-x_\tau L_\tau}$ flavor gauge models,” *JHEP* **04** (2019) 102, [arXiv:1902.06107 \[hep-ph\]](#).
- [161] M. Escudero, D. Hooper, G. Krnjaic, and M. Pierre, “Cosmology with a very light $L_\mu - L_\tau$ gauge boson,” *JHEP* **03** (2019) 071, [arXiv:1901.02010 \[hep-ph\]](#).
- [162] A. Biswas and A. Shaw, “Reconciling dark matter, $R_{K^{(*)}}$ anomalies and $(g-2)_\mu$ in an $L_\mu - L_\tau$ scenario,” *JHEP* **05** (2019) 165, [arXiv:1903.08745 \[hep-ph\]](#).
- [163] W. Altmannshofer, S. Gori, M. Pospelov, and I. Yavin, “Neutrino Trident Production: A Powerful Probe of New Physics with Neutrino Beams,” *Phys. Rev. Lett.* **113** (2014) 091801, [arXiv:1406.2332 \[hep-ph\]](#).
- [164] W. Altmannshofer, S. Gori, S. Profumo, and F. S. Queiroz, “Explaining dark matter and B decay anomalies with an $L_\mu - L_\tau$ model,” *JHEP* **12** (2016) 106, [arXiv:1609.04026 \[hep-ph\]](#).
- [165] A. Einstein, “Die feldgleichungen der gravitation,” *Sitzung der physikalische-mathematischen Klasse* **25** (1915) 844–847.
- [166] C. W. Misner, K. S. Thorne, and J. A. Wheeler, *Gravitation*. Princeton University Press, 2017.
- [167] S. Weinberg, “Photons and gravitons in perturbation theory: Derivation of maxwell’s and einstein’s equations,” *Physical Review* **138** (1965) no. 4B, B988.
- [168] S. W. Hawking, “Black hole explosions?,” *Nature* **248** (1974) no. 5443, 30.
- [169] S. W. Hawking, “Particle creation by black holes,” *Communications in mathematical physics* **43** (1975) no. 3, 199–220.

- [170] S. A. Fulling, “Nonuniqueness of canonical field quantization in riemannian space-time,” *Physical Review D* **7** (1973) no. 10, 2850.
- [171] P. C. Davies, “Scalar production in schwarzschild and rindler metrics,” *Journal of Physics A: Mathematical and General* **8** (1975) no. 4, 609.
- [172] W. G. Unruh, “Notes on black-hole evaporation,” *Physical Review D* **14** (1976) no. 4, 870.
- [173] N. D. Birrell, N. D. Birrell, P. Davies, and P. Davies, *Quantum fields in curved space*. No. 7. Cambridge university press, 1984.
- [174] I. L. Buchbinder, S. D. Odintsov, and I. L. Shapiro, *Effective action in quantum gravity*. 1992.
- [175] B. S. DeWitt, “Quantum field theory in curved spacetime,” *Physics Reports* **19** (1975) no. 6, 295–357.
- [176] I. L. Shapiro, “Effective action of vacuum: the semiclassical approach,” *Classical and Quantum Gravity* **25** (2008) no. 10, 103001.
- [177] V. Frolov and I. Novikov, *Black hole physics: basic concepts and new developments*, vol. 96. Springer Science & Business Media, 2012.
- [178] V. Mukhanov and S. Winitzki, *Introduction to quantum effects in gravity*. Cambridge University Press, 2007.
- [179] L. D. Landau, *The classical theory of fields*, vol. 2. Elsevier, 2013.
- [180] **Event Horizon Telescope** Collaboration, K. Akiyama *et al.*, “First M87 Event Horizon Telescope Results. I. The Shadow of the Supermassive Black Hole,” *Astrophys. J.* **875** (2019) no. 1, L1, [arXiv:1906.11238 \[astro-ph.GA\]](#).
- [181] **LIGO Scientific, Virgo** Collaboration, B. P. Abbott *et al.*, “GW170817: Observation of Gravitational Waves from a Binary Neutron Star Inspiral,” *Phys. Rev. Lett.* **119** (2017) no. 16, 161101, [arXiv:1710.05832 \[gr-qc\]](#).
- [182] B. DeWitt, “Dynamical theory of groups and fields (gordon & brach, new york, 1965),” *Phys. Rev* **162** (1967) 1195.
- [183] B. S. DeWitt, “The global approach to quantum field theory. vol. 1, 2,” *Int. ser. monogr. phys.* **114** (2003) 1–1042.
- [184] E. Fradkin and A. A. Tseytlin, “Renormalizable asymptotically free quantum theory of gravity,” *Nuclear Physics B* **201** (1982) no. 3, 469–491.
- [185] E. V. Gorbar and I. L. Shapiro, “Renormalization group and decoupling in curved space, ii. the standard model and beyond,” *Journal of High Energy Physics* **2003** (2003) no. 06, 004.

- [186] I. G. Avramidi, *Heat kernel and quantum gravity*, vol. 64. Springer Science & Business Media, 2000.
- [187] A. Barvinsky and G. Vilkovisky, “The generalized schwinger-dewitt technique in gauge theories and quantum gravity,” *Physics Reports* **119** (1985) no. 1, 1–74.
- [188] I. G. Avramidi, “Covariant methods for the calculation of the effective action in quantum field theory and investigation of higher-derivative quantum gravity,” *arXiv preprint hep-th/9510140* (1995) .
- [189] K. Stelle, “Classical gravity with higher derivatives,” *General Relativity and Gravitation* **9** (1978) no. 4, 353–371.
- [190] M. Ostrogradsky, “Mémoires sur les équations différentielles, relatives au problème des isopérimètres,” *Mem. Acad. St. Petersburg* **6** (1850) 385–517.
- [191] R. P. Woodard, “The theorem of Ostrogradsky,” *arXiv preprint arXiv:1506.02210* (2015) .
- [192] K. Stelle, “Renormalization of higher-derivative quantum gravity,” *Physical Review D* **16** (1977) no. 4, 953.
- [193] D. Johnston, “Sedentary ghost poles in higher derivative gravity,” *Nuclear Physics B* **297** (1988) no. 4, 721–732.
- [194] T.-j. Chen, M. Fasiello, E. A. Lim, and A. J. Tolley, “Higher derivative theories with constraints: exorcising ostrogradski’s ghost,” *Journal of Cosmology and Astroparticle Physics* **2013** (2013) no. 02, 042.
- [195] A. V. Smilga, “Benign vs. malicious ghosts in higher-derivative theories,” *Nuclear Physics B* **706** (2005) no. 3, 598–614.
- [196] L. Modesto and I. L. Shapiro, “Superrenormalizable quantum gravity with complex ghosts,” *Physics Letters B* **755** (2016) 279–284.
- [197] P. Peter, F. d. O. Salles, and I. L. Shapiro, “On the ghost-induced instability on de sitter background,” *Physical Review D* **97** (2018) no. 6, 064044.
- [198] F. d. O. Salles and I. L. Shapiro, “Do we have unitary and (super) renormalizable quantum gravity below the planck scale?,” *Physical Review D* **89** (2014) no. 8, 084054.
- [199] M. Asorey, L. Rachwal, and I. Shapiro, “Unitary issues in some higher derivative field theories,” *Galaxies* **6** (2018) no. 1, 23.
- [200] S. W. Hawking and T. Hertog, “Living with ghosts,” *Physical Review D* **65** (2002) no. 10, 103515.
- [201] P. Creminelli, A. Nicolis, M. Papucci, and E. Trincherini, “Ghosts in massive gravity,” *Journal of High Energy Physics* **2005** (2005) no. 09, 003.

- [202] G. de Berredo-Peixoto and I. L. Shapiro, “Higher derivative quantum gravity with gauss-bonnet term,” *Physical Review D* **71** (2005) no. 6, 064005.
- [203] I. L. Shapiro, “Local conformal symmetry and its fate at quantum level,” *arXiv preprint hep-th/0610168* (2006) .
- [204] G. Vilkovisky, “Effective action in quantum gravity,” *Classical and Quantum Gravity* **9** (1992) no. 4, 895.
- [205] T. Cheng, E. Eichten, and L.-F. Li, “Higgs phenomena in asymptotically free gauge theories,” *Physical Review D* **9** (1974) no. 8, 2259.
- [206] I. Buchbinder and S. Odintsov, “Effective potential and phase transitions induced by curvature in gauge theories in curved spacetime,” *Classical and Quantum Gravity* **2** (1985) no. 5, 721.
- [207] A. Z. Petrov, *Einstein spaces*. Elsevier, 2016.
- [208] T. Bunch and L. Parker, “Feynman propagator in curved spacetime: A momentum-space representation,” *Physical Review D* **20** (1979) no. 10, 2499.
- [209] V. F. Barra, I. L. Buchbinder, J. G. Joaquim, A. R. Rodrigues, and I. L. Shapiro, “Renormalization of yukawa model with sterile scalar in curved spacetime,” *The European Physical Journal C* **79** (May, 2019) 458.
<https://doi.org/10.1140/epjc/s10052-019-6917-y>.
- [210] D. J. Toms, “Gauged yukawa model in curved spacetime,” *Physical Review D* **98** (2018) no. 2, 025015.
- [211] E. Hubble, “A relation between distance and radial velocity among extra-galactic nebulae,” *Proceedings of the national academy of sciences* **15** (1929) no. 3, 168–173.
- [212] A. A. Penzias and R. W. Wilson, “A measurement of excess antenna temperature at 4080 mc/s.,” *The Astrophysical Journal* **142** (1965) 419–421.
- [213] G. Gamow, “The origin of elements and the separation of galaxies,” *Phys. Rev.* **74** (Aug, 1948) 505–506. <https://link.aps.org/doi/10.1103/PhysRev.74.505.2>.
- [214] R. H. Dicke, P. J. E. Peebles, P. G. Roll, and D. T. Wilkinson, “Cosmic black-body radiation.,” *The Astrophysical Journal* **142** (1965) 414–419.
- [215] J. C. Mather, E. S. Cheng, J. Eplee, R. E., R. B. Isaacman, S. S. Meyer, R. A. Shafer, R. Weiss, E. L. Wright, C. L. Bennett, N. W. Boggess, E. Dwek, S. Gulkis, M. G. Hauser, M. Janssen, T. Kelsall, P. M. Lubin, J. Moseley, S. H., T. L. Murdock, R. F. Silverberg, G. F. Smoot, and D. T. Wilkinson, “A Preliminary Measurement of the Cosmic Microwave Background Spectrum by the Cosmic Background Explorer (COBE) Satellite,” **354** (May, 1990) L37.

- [216] A. H. Guth, “Inflationary universe: A possible solution to the horizon and flatness problems,” *Physical Review D* **23** (1981) no. 2, 347.
- [217] A. D. Linde, “Chaotic inflation,” *Physics Letters B* **129** (1983) no. 3-4, 177–181.
- [218] A. A. Starobinsky, “A new type of isotropic cosmological models without singularity,” *Physics Letters B* **91** (1980) no. 1, 99–102.
- [219] P. J. Steinhardt, “Natural inflation,” *The very early universe* (1982) 251.
- [220] F. Zwicky, “The redshift of extragalactic nebulae,” *Helv. Phys. Acta* **6** (1933) no. 110, 138.
- [221] E. W. Kolb and M. S. Turner, “The early universe,” *Front. Phys., Vol. 69*, **1** (1990) .
- [222] S. Dodelson, *Modern cosmology*. Academic press, 2003.
- [223] D. H. Lyth and A. R. Liddle, *The primordial density perturbation: Cosmology, inflation and the origin of structure*. Cambridge University Press, 2009.
- [224] T. Padmanabhan, *Cosmology and astrophysics through problems*. Cambridge university press, 1996.
- [225] S. Weinberg, *Cosmology*. Oxford university press, 2008.
- [226] B. D. Fields, “The primordial lithium problem,” *Annual Review of Nuclear and Particle Science* **61** (Nov, 2011) 47–68.
<http://dx.doi.org/10.1146/annurev-nucl-102010-130445>.
- [227] V. Singh, J. Lahiri, D. Bhowmick, and D. N. Basu, “Big-bang nucleosynthesis and primordial lithium abundance problem,” *Journal of Experimental and Theoretical Physics* **128** (May, 2019) 707–712. <https://doi.org/10.1134/S1063776119040058>.
- [228] A. G. Riess, A. V. Filippenko, P. Challis, A. Clocchiatti, A. Diercks, P. M. Garnavich, R. L. Gilliland, C. J. Hogan, S. Jha, R. P. Kirshner, *et al.*, “Observational evidence from supernovae for an accelerating universe and a cosmological constant,” *The Astronomical Journal* **116** (1998) no. 3, 1009.
- [229] S. Perlmutter, G. Aldering, G. Goldhaber, R. Knop, P. Nugent, P. Castro, S. Deustua, S. Fabbro, A. Goobar, D. Groom, *et al.*, “Measurements of ω and λ from 42 high-redshift supernovae,” *The Astrophysical Journal* **517** (1999) no. 2, 565.
- [230] S. Weinberg, “The cosmological constant problem,” *Reviews of modern physics* **61** (1989) no. 1, 1.
- [231] S. M. Carroll, “The cosmological constant,” *Living reviews in relativity* **4** (2001) no. 1, 1.

- [232] P. A. Ade, N. Aghanim, M. Arnaud, M. Ashdown, J. Aumont, C. Baccigalupi, A. Banday, R. Barreiro, J. Bartlett, N. Bartolo, *et al.*, “Planck 2015 results: Xiii. cosmological parameters,” *Astronomy and Astrophysics* **594** (2016) .
- [233] A. G. Riess, S. Casertano, W. Yuan, L. M. Macri, and D. Scolnic, “Large Magellanic Cloud Cepheid Standards Provide a 1% Foundation for the Determination of the Hubble Constant and Stronger Evidence for Physics beyond Λ CDM,” *Astrophys. J.* **876** (2019) no. 1, 85, [arXiv:1903.07603 \[astro-ph.CO\]](#) .
- [234] W. L. Freedman *et al.*, “The Carnegie-Chicago Hubble Program. VIII. An Independent Determination of the Hubble Constant Based on the Tip of the Red Giant Branch,” [arXiv:1907.05922 \[astro-ph.CO\]](#) .
- [235] N. Aghanim, Y. Akrami, M. Ashdown, J. Aumont, C. Baccigalupi, M. Ballardini, A. Banday, R. Barreiro, N. Bartolo, S. Basak, *et al.*, “Planck 2018 results. vi. cosmological parameters,” *arXiv preprint arXiv:1807.06209* (2018) .
- [236] V. Mukhanov, *Physical foundations of cosmology*. Cambridge University Press, 2005.
- [237] F. Bezrukov and M. Shaposhnikov, “The standard model higgs boson as the inflaton,” *Physics Letters B* **659** (2008) no. 3, 703–706.
- [238] C. Burgess, H. M. Lee, and M. Trott, “Power-counting and the validity of the classical approximation during inflation,” *Journal of High Energy Physics* **2009** (Sep, 2009) 103–103. <http://dx.doi.org/10.1088/1126-6708/2009/09/103>.
- [239] J. L. F. Barb  n and J. R. Espinosa, “On the naturalness of higgs inflation,” *Physical Review D* **79** (Apr, 2009) . <http://dx.doi.org/10.1103/PhysRevD.79.081302>.
- [240] C. P. Burgess, H. M. Lee, and M. Trott, “On higgs inflation and naturalness,” *Journal of High Energy Physics* **2010** (Jul, 2010) . [http://dx.doi.org/10.1007/JHEP07\(2010\)007](http://dx.doi.org/10.1007/JHEP07(2010)007).
- [241] K. Kohri and H. Matsui, “Higgs vacuum metastability in primordial inflation, preheating, and reheating,” *Physical Review D* **94** (2016) no. 10, 103509.
- [242] H. M. Sadjadi and P. Goodarzi, “Reheating in non-minimal derivative coupling model,” *Journal of Cosmology and Astroparticle Physics* **2013** (2013) no. 02, 038.
- [243] F. Bezrukov, J. Rubio, and M. Shaposhnikov, “Living beyond the edge: Higgs inflation and vacuum metastability,” *Physical Review D* **92** (2015) no. 8, 083512.
- [244] J. Kearney, H. Yoo, and K. M. Zurek, “Is a higgs vacuum instability fatal for high-scale inflation?,” *Physical Review D* **91** (2015) no. 12, 123537.
- [245] T. Markkanen, A. Rajantie, and S. Stopyra, “Cosmological aspects of higgs vacuum metastability,” *arXiv preprint arXiv:1809.06923* (2018) .

- [246] J. García-Bellido, D. G. Figueroa, and J. Rubio, “Preheating in the standard model with the higgs inflaton coupled to gravity,” *Phys. Rev. D* **79** (Mar, 2009) 063531. <https://link.aps.org/doi/10.1103/PhysRevD.79.063531>.
- [247] F. Bezrukov and D. Gorbunov, “Distinguishing between R2-inflation and higgs-inflation,” *Physics Letters B* **713** (2012) no. 4-5, 365–368.
- [248] O. Lahav, P. B. Lilje, J. R. Primack, and M. J. Rees, “Dynamical effects of the cosmological constant,” *Monthly Notices of the Royal Astronomical Society* **251** (1991) no. 1, 128–136.
- [249] S. M. Carroll, W. H. Press, and E. L. Turner, “The cosmological constant,” *Annual review of astronomy and astrophysics* **30** (1992) 499–542.
- [250] A. Cooray and R. Sheth, “Halo models of large scale structure,” *Physics Reports* **372** (2002) no. 1, 1–129.
- [251] D. J. Eisenstein and W. Hu, “Baryonic features in the matter transfer function,” *The Astrophysical Journal* **496** (1998) no. 2, 605.
- [252] J. E. Gunn and J. R. Gott III, “On the infall of matter into clusters of galaxies and some effects on their evolution,” *The Astrophysical Journal* **176** (1972) 1.
- [253] T. Padmanabhan, *Structure formation in the universe*. Cambridge university press, 1993.
- [254] P. J. E. Peebles, *The large-scale structure of the universe*. Princeton university press, 1980.
- [255] W. H. Press and P. Schechter, “Formation of galaxies and clusters of galaxies by self-similar gravitational condensation,” *The Astrophysical Journal* **187** (1974) 425–438.
- [256] A. Jenkins, C. Frenk, S. D. White, J. Colberg, S. Cole, A. E. Evrard, H. Couchman, and N. Yoshida, “The mass function of dark matter haloes,” *Monthly Notices of the Royal Astronomical Society* **321** (2001) no. 2, 372–384.
- [257] R. K. Sheth, H. Mo, and G. Tormen, “Ellipsoidal collapse and an improved model for the number and spatial distribution of dark matter haloes,” *Monthly Notices of the Royal Astronomical Society* **323** (2001) no. 1, 1–12.
- [258] J. Tinker, A. V. Kravtsov, A. Klypin, K. Abazajian, M. Warren, G. Yepes, S. Gottlöber, and D. E. Holz, “Toward a halo mass function for precision cosmology: the limits of universality,” *The Astrophysical Journal* **688** (2008) no. 2, 709.
- [259] L. Hernquist, “An analytical model for spherical galaxies and bulges,” *The Astrophysical Journal* **356** (1990) 359–364.

- [260] J. Navarro and S. D. White, “The structure of cold dark matter halos,” in *SYMPOSIUM-INTERNATIONAL ASTRONOMICAL UNION*, vol. 171, pp. 255–258, KLUWER ACADEMIC PUBLISHERS GROUP. 1996.
- [261] J. F. Navarro, C. S. Frenk, and S. D. White, “A universal density profile from hierarchical clustering,” *The Astrophysical Journal* **490** (1997) no. 2, 493.
- [262] B. Moore, T. Quinn, F. Governato, J. Stadel, and G. Lake, “Cold collapse and the core catastrophe,” *Monthly Notices of the Royal Astronomical Society* **310** (1999) no. 4, 1147–1152.
- [263] P. Schneider, *Extragalactic astronomy and cosmology: an introduction*. Springer, 2014.
- [264] J. S. Bullock, T. S. Kolatt, Y. Sigad, R. S. Somerville, A. V. Kravtsov, A. A. Klypin, J. R. Primack, and A. Dekel, “Profiles of dark haloes: evolution, scatter and environment,” *Monthly Notices of the Royal Astronomical Society* **321** (2001) no. 3, 559–575.
- [265] J. L. Tinker, B. E. Robertson, A. V. Kravtsov, A. Klypin, M. S. Warren, G. Yepes, and S. Gottlöber, “The large-scale bias of dark matter halos: Numerical calibration and model tests,” *The Astrophysical Journal* **724** (2010) no. 2, 878.
- [266] **DES** Collaboration, T. M. C. Abbott *et al.*, “Dark Energy Survey Year 1 Results: Cosmological Constraints from Galaxy Clustering and Weak Lensing,” [arXiv:1708.01530](https://arxiv.org/abs/1708.01530) [[astro-ph.CO](https://arxiv.org/archive/astro)].
- [267] J. Diemand, B. Moore, and J. Stadel, “Convergence and scatter of cluster density profiles,” *Monthly Notices of the Royal Astronomical Society* **353** (2004) no. 2, 624–632.
- [268] P. Salucci, A. Lapi, C. Tonini, G. Gentile, I. Yegorova, and U. Klein, “The universal rotation curve of spiral galaxies–ii. the dark matter distribution out to the virial radius,” *Monthly Notices of the Royal Astronomical Society* **378** (2007) no. 1, 41–47.
- [269] R. Swaters, R. Sancisi, T. Van Albada, and J. Van Der Hulst, “The rotation curves shapes of late-type dwarf galaxies,” *Astronomy & Astrophysics* **493** (2009) no. 3, 871–892.
- [270] W. De Blok, “The core-cusp problem,” *Advances in Astronomy* **2010** (2010) .
- [271] S.-H. Oh, W. De Blok, E. Brinks, F. Walter, and R. C. Kennicutt Jr, “Dark and luminous matter in things dwarf galaxies,” *The Astronomical Journal* **141** (2011) no. 6, 193.
- [272] A. Klypin, A. V. Kravtsov, O. Valenzuela, and F. Prada, “Where are the missing galactic satellites?,” *The Astrophysical Journal* **522** (1999) no. 1, 82.

- [273] B. Moore, S. Ghigna, F. Governato, G. Lake, T. Quinn, J. Stadel, and P. Tozzi, “Dark matter substructure within galactic halos,” *The Astrophysical Journal Letters* **524** (1999) no. 1, L19.
- [274] J. S. Bullock, “Notes on the missing satellites problem,” *Local Group Cosmology* **20** (2013) 95.
- [275] A. V. Tikhonov and A. Klypin, “The emptiness of voids: yet another overabundance problem for the λ cold dark matter model,” *Monthly Notices of the Royal Astronomical Society* **395** (2009) no. 4, 1915–1924.
- [276] P. Peebles and A. Nusser, “Nearby galaxies as pointers to a better theory of cosmic evolution,” *Nature* **465** (2010) no. 7298, 565–569.
- [277] S. Garrison-Kimmel, M. Boylan-Kolchin, J. S. Bullock, and E. N. Kirby, “Too big to fail in the local group,” *Monthly Notices of the Royal Astronomical Society* **444** (2014) no. 1, 222–236.
- [278] A. Fattahi, J. F. Navarro, T. Sawala, C. S. Frenk, L. V. Sales, K. Oman, M. Schaller, and J. Wang, “The cold dark matter content of Galactic dwarf spheroidals: no cores, no failures, no problem,” *ArXiv e-prints* (July, 2016) , [arXiv:1607.06479](#).
- [279] M. R. Lovell, V. Gonzalez-Perez, S. Bose, A. Boyarsky, S. Cole, C. S. Frenk, and O. Ruchayskiy, “Addressing the too big to fail problem with baryon physics and sterile neutrino dark matter,” **468** (July, 2017) 2836–2849, [arXiv:1611.00005](#).
- [280] V. Iršič, M. Viel, M. G. Haehnelt, J. S. Bolton, S. Cristiani, G. Cupani, T.-S. Kim, T. A. Berg, S. López, S. Ellison, *et al.*, “New constraints on the free-streaming of warm dark matter from intermediate and small scale lyman- α forest data,” *arXiv preprint arXiv:1702.01764* (2017) .
- [281] P. Bode, J. P. Ostriker, and N. Turok, “Halo formation in warm dark matter models,” *The Astrophysical Journal* **556** (2001) no. 1, 93.
- [282] M. Viel, J. Lesgourgues, M. G. Haehnelt, S. Matarrese, and A. Riotto, “Constraining warm dark matter candidates including sterile neutrinos and light gravitinos with wmap and the lyman- α forest,” *Physical Review D* **71** (2005) no. 6, 063534.
- [283] P. Colín, O. Valenzuela, and V. Avila-Reese, “On the structure of dark matter halos at the damping scale of the power spectrum with and without relict velocities,” *The Astrophysical Journal* **673** (2008) no. 1, 203.
- [284] N. Menci, F. Fiore, and A. Lamastra, “Galaxy formation in warm dark matter cosmology,” *Monthly Notices of the Royal Astronomical Society* **421** (2012) no. 3, 2384–2394.

- [285] M. Leo, C. M. Baugh, B. Li, and S. Pascoli, “Nonlinear growth of structure in cosmologies with damped matter fluctuations,” *ArXiv e-prints* (Dec., 2017) , [arXiv:1712.02742](#).
- [286] E. Massara, F. Villaescusa-Navarro, and M. Viel, “The halo model in a massive neutrino cosmology,” *Journal of Cosmology and Astroparticle Physics* **2014** (2014) no. 12, 053.
- [287] M. White, “The redshift-space power spectrum in the halo model,” *Monthly Notices of the Royal Astronomical Society* **321** (2001) no. 1, 1–3.
- [288] R. E. Smith and K. Markovic, “Testing the warm dark matter paradigm with large-scale structures,” *Physical Review D* **84** (2011) no. 6, 063507.
- [289] R. M. Dunstan, K. N. Abazajian, E. Polisensky, and M. Ricotti, “The halo model of large scale structure for warm dark matter,” *arXiv preprint arXiv:1109.6291* (2011) .
- [290] D. J. Marsh, “WarmAndFuzzy: the halo model beyond CDM,” *arXiv preprint arXiv:1605.05973* (2016) .
- [291] A. Schneider, R. E. Smith, A. V. Macciò, and B. Moore, “Non-linear evolution of cosmological structures in warm dark matter models,” *Monthly Notices of the Royal Astronomical Society* **424** (2012) no. 1, 684–698.
- [292] A. Schneider, “Structure formation with suppressed small-scale perturbations,” *arXiv preprint arXiv:1412.2133* (2014) .
- [293] A. J. Benson, A. Farahi, S. Cole, L. A. Moustakas, A. Jenkins, M. Lovell, R. Kennedy, J. Helly, and C. Frenk, “Dark matter halo merger histories beyond cold dark matter–i. methods and application to warm dark matter,” *Monthly Notices of the Royal Astronomical Society* **428** (2012) no. 2, 1774–1789.
- [294] M. Viel, K. Markovič, M. Baldi, and J. Weller, “The non-linear matter power spectrum in warm dark matter cosmologies,” *Monthly Notices of the Royal Astronomical Society* **421** (2012) no. 1, 50–62.
- [295] R. Takahashi, M. Sato, T. Nishimichi, A. Taruya, and M. Oguri, “Revising the halofit model for the nonlinear matter power spectrum,” *The Astrophysical Journal* **761** (2012) no. 2, 152.
- [296] Z. Ma, W. Hu, and D. Huterer, “Effects of photometric redshift uncertainties on weak-lensing tomography,” *The Astrophysical Journal* **636** (2006) no. 1, 21.
- [297] F. Sobreira, F. de Simoni, R. Rosenfeld, L. da Costa, M. Maia, and M. Makler, “Cosmological forecasts from photometric measurements of the angular correlation function,” *Physical Review D* **84** (2011) no. 10, 103001.

- [298] M. Crocce, A. Cabré, and E. Gaztañaga, “Modelling the angular correlation function and its full covariance in photometric galaxy surveys,” *Monthly Notices of the Royal Astronomical Society* **414** (2011) no. 1, 329–349.
- [299] P. A. Abell, D. L. Burke, M. Hamuy, M. Nordby, T. S. Axelrod, D. Monet, B. Vrsnak, P. Thorman, D. Ballantyne, J. D. Simon, *et al.*, “Lsst science book, version 2.0,” tech. rep., 2009.
- [300] T. Abbott, F. B. Abdalla, J. Aleksić, S. Allam, A. Amara, D. Bacon, E. Balbinot, M. Banerji, K. Bechtol, A. Benoit-Lévy, *et al.*, “The dark energy survey: more than dark energy—an overview,” *Monthly Notices of the Royal Astronomical Society* **460** (2016) no. 2, 1270–1299.
- [301] M. LoVerde and N. Afshordi, “Extended limber approximation,” *Physical Review D* **78** (2008) no. 12, 123506.
- [302] W.-P. Lin, Y. Jing, S. Mao, L. Gao, and I. McCarthy, “The influence of baryons on the mass distribution of dark matter halos,” *The Astrophysical Journal* **651** (2006) no. 2, 636.
- [303] E. Semboloni, H. Hoekstra, J. Schaye, M. P. van Daalen, and I. G. McCarthy, “Quantifying the effect of baryon physics on weak lensing tomography,” *Monthly Notices of the Royal Astronomical Society* **417** (2011) no. 3, 2020–2035.
- [304] L. Casarini, S. A. Bonometto, S. Borgani, K. Dolag, G. Murante, M. Mezzetti, L. Tornatore, and G. La Vacca, “Tomographic weak-lensing shear spectra from large n-body and hydrodynamical simulations,” *Astronomy & Astrophysics* **542** (2012) A126.
- [305] A. Mead, J. Peacock, C. Heymans, S. Joudaki, and A. Heavens, “An accurate halo model for fitting non-linear cosmological power spectra and baryonic feedback models,” *Monthly Notices of the Royal Astronomical Society* **454** (2015) no. 2, 1958–1975.
- [306] L. Amendola and S. Tsujikawa, *Dark energy: theory and observations*. Cambridge University Press, 2010.
- [307] M. Tegmark, “Measuring cosmological parameters with galaxy surveys,” *Physical Review Letters* **79** (1997) no. 20, 3806.
- [308] T. Abbott, F. Abdalla, A. Alarcon, J. Aleksić, S. Allam, S. Allen, A. Amara, J. Annis, J. Asorey, S. Avila, *et al.*, “Dark energy survey year 1 results: cosmological constraints from galaxy clustering and weak lensing,” *arXiv preprint arXiv:1708.01530* (2017) .
- [309] D. H. Weinberg, R. Davé, N. Katz, and L. Hernquist, “Galaxy clustering and galaxy bias in a Λ CDM universe,” *The Astrophysical Journal* **601** (2004) no. 1, 1.

- [310] G. Hinshaw, D. Spergel, L. Verde, R. Hill, S. Meyer, C. Barnes, C. Bennett, M. Halpern, N. Jarosik, A. Kogut, *et al.*, “First-year wilkinson microwave anisotropy probe (WMAP) observations: The angular power spectrum,” *The Astrophysical Journal Supplement Series* **148** (2003) no. 1, 135.
- [311] A. J. Ross, W. J. Percival, M. Crocce, A. Cabré, and E. Gaztañaga, “[Measuring redshift-space distortions using photometric surveys](#),” *Monthly Notices of the Royal Astronomical Society* **415** (May, 2011) 2193–2204.
<http://dx.doi.org/10.1111/j.1365-2966.2011.18843.x>.
- [312] K. Markovic, S. Bridle, A. Slosar, and J. Weller, “Constraining warm dark matter with cosmic shear power spectra,” *Journal of Cosmology and Astroparticle Physics* **2011** (2011) no. 01, 022.
- [313] S. Dodelson, *Gravitational Lensing*. Cambridge University Press, 2017.
- [314] R. Mandelbaum, “Weak lensing for precision cosmology,” *Annual Review of Astronomy and Astrophysics* **56** (2018) no. 1, 393–433,
<https://doi.org/10.1146/annurev-astro-081817-051928>.